



University of Cyprus
Faculty of Pure and Applied Sciences
Department of Biological Sciences

*Laboratory of Cell Biology and Molecular Embryology
(Assistant Professor Paris A. Skourides)*

**THE ROLE OF CALPAIN2 DURING
VERTEBRATE EMBRYONIC DEVELOPMENT**

*PhD THESIS
NEOPHYTOS CHRISTODOULOU*

NICOSIA, JUNE 2015

Abstract

Calpains are a family of calcium-dependent intracellular cysteine proteases that regulate several physiological processes through limited cleavage of different substrates. The role of Calpain2 in embryogenesis is not clear with conflicting evidence from a number of mouse knockouts. Here we report the temporal and spatial expression of Calpain2 in *Xenopus laevis* embryos and address its role in *Xenopus* development. We show that Calpain2 is expressed maternally with elevated expression in neural tissues and that Calpain2 activity is spatially and temporally regulated. We further show that Calpain2 is activated in response to Wnt/Ca²⁺ pathway in a Dishevelled depended manner during *Xenopus* development. Using a Calpain inhibitor, a dominant negative and a morpholino oligonucleotide we demonstrate that Calpain2 is necessary for proper morphogenesis. Specifically Calpain2 is implicated in Convergent Extension both in mesodermal and neural tissues and its downregulation results in defective blastopore and neural tube closure. These phenotypes are attributed to loss of tissue polarity and blockage of mediolateral intercalation as shown by Keller (mesodermal) explants. Furthermore, we identify Calpain2 as a novel regulator of Apical Constriction. Specifically we show that Calpain2 downregulation results in rostral Neural Tube Defects due to defective Apical Constriction of neuroepithelial cells. We further demonstrate that Calpain2 function is necessary in Apical Constriction driven organogenesis showing that Calpain2 is implicated in Apical Constriction independently of the tissue context. Using high resolution live imaging we demonstrate that Apical Constriction during *Xenopus* neural tube closure is a stepwise process driven by cell autonomous and asynchronous contraction pulses followed by stabilization steps. In addition our data suggest that contraction events are triggered by cell autonomous Ca²⁺ flashes and are driven by a transient contractile apical pool of actin. In addition we provide evidence that the cell autonomy and asynchrony of contraction are required for the correct spatial distribution of Apical Constriction and as a result are critical for tissue morphogenesis. Finally we show that Calpain2 is specifically required for the stabilization step during Apical Constriction but is dispensable during contraction.

Table of Contents

<i>List of Figures</i>	1
II. List of movies	3
1. Introduction	6
1.1 Calpains	6
1.2 Structure of Calpain2	8
1.3 Regulation of Calpain2 function	9
1.3.1 Activation of Calpains	9
1.3.2 Inhibition of Calpains	10
1.4 Calpain <i>in vitro</i> and <i>in vivo</i> functions	11
1.4.1 <i>In Vitro</i> studies	11
1.4.2 <i>In vivo</i> Studies	12
1.5 <i>Xenopus laevis</i>	13
1.5.1 Oogenesis-Fertilization	14
1.5.2 Cleavage stages	15
1.5.3 Gastrulation	16
1.5.4 Neurulation	19
1.6 Neural Tube Closure	21
1.7 Convergent extension	22
1.7.1 Mesenchyme Convergent Extension: a case of intercalation driven by mediolaterally polarized protrusion activity?	23
1.7.2 Convergent Extension: a case of cell-cell adhesions remodeling	26
1.7.3 Convergent extension driven by polarized junction remodeling and polarized protrusions	30
1.8 Apical Constriction	34
1.8.1 Mechanisms driving Apical Constriction induced cell shape changes.	38
I) Apical surface narrowing	38
II) Apicobasal axis elongation	44
1.8.2 Cell-cell adhesions and mechanical coupling during Apical Constriction driven morphogenesis.	49
1.9 Calcium signaling in morphogenesis	50
1.9.1 Mechanisms of Calcium signaling	51
1.9.2 Structure and regulation of Gap junctions	52
2. Methodology	55
2.1 Frogs	55
2.2 Ovulation	55
2.3 Collecting eggs	55
2.4 In-vitro Fertilization	55
2.5 Dejelling embryos	56
2.5 DNA constructs and morpholino oligonucleotide	56
2.6 Microinjections	57
2.7 RNA and cDNA synthesis	58
2.8 RT PCR	58
2.9 Mutagenesis	58

2.10 Mesoderm Convergent Extension assay	59
2.11 Neural Convergent Extension assay	59
2.12 Mesoderm migration	59
2.13 Whole mount in-situ hybridization	59
2.14 Immunofluorescence	60
2.15 Western Blot	61
2.16 Casein Zymography	61
3. Results	62
3.1 Calpain2 function during <i>Xenopus</i> development	62
3.1.1 Expression pattern of Calpain2 during <i>Xenopus</i> development	62
3.1.2 Calpain2 localization in <i>Xenopus</i> embryos	64
3.1.3 Blockage of Calpains function with a Calpain specific inhibitor	65
3.1.4 Blockage of Calpain2 function with a dominant negative construct	67
3.1.5 Downregulation of Calpain2 with a specific Calpain2 specific Morpholino induce similar phenotypes with CI3 treatment	68
3.1.6 Calpain2 function during gastrulation	71
I. Blockage of Calpain2 function does not affect mesoderm specification	71
II. Calpain2 function is necessary for mesoderm convergent extension and affects mesoderm migration	72
3.1.7 Calpain2 function during Neurulation	74
I. Calpain2 downregulation leads to defective Neural Tube Closure without affecting neural markers expression.	74
II. Calpain2 function is necessary for neural folds elevation and anterior Neural Tube Closure	76
III. Calpain2 is implicated in neural convergent extension	77
3.1.8 Elucidating the involvement of Calpain2 in Convergent Extension	80
3.1.9 Calpain2 function is necessary for Apical Constriction during <i>Xenopus</i> Development	82
I. Calpain2 function is indispensable for anterior Neural Tube Closure through its involvement in Apical Constriction	82
II. Calpain2 temporal and spatial localization is in agreement with a role in Apical Constriction	84
III. Calpain2 regulates Apical Constriction independently of tissue context	85
IV. Calpain2 downregulation affects Apical Constriction but does not affect apicobasal polarity	87
V. Calpain2 function is necessary for Shroom3, Lulu and GEF-H1 induced AC	88
3.1.10 Calpain2 activation mechanisms in <i>Xenopus</i>	90
3.2 Live imaging of actin and Calcium dynamics during Neural Tube Closure	93
3.2.1 AC is driven by pulsed contraction of a transient apical contractile actin network	93
3.2.2 Mediolateral junction shrinkage contributes to apical cell surface area reduction during Neural Tube Closure	97
3.2.3 Asynchronous and Cell autonomous Calcium flashes are generated during Apical Constriction	99
3.2.4 The asynchrony and the autonomy of the calcium flashes are necessary for proper morphogenesis	103
3.2.5 Restriction of Calcium flashes via gap junction regulation	105
3.2.6 Calpain2 function is necessary for the stabilization step during Apical Constriction	106
4. Discussion	109
4.1 Calpain2 expression	109
4.3 Calpain2 function during <i>Xenopus</i> morphogenesis	110
4.4 Mechanism of Calpain2 involvement in convergent extension and Apical Constriction	111
4.5 Regulation of Calpain2 activity during embryogenesis	111
4.6 The molecular mechanism controlling Calpain2 function in convergent extension	113
4.7 Molecular mechanism for Calpain2 involvement in Apical Constriction	115
4.8 Mechanisms driving apical cell surface reduction during Neural Tube Closure	116

Proposed model for Apical Constriction in neuroepithelial cells	116
4.9 Calcium flashes trigger cell autonomous contraction pulses	117
4.10 The asynchrony and autonomy of contraction pulses are both necessary for proper Apical Constriction driven morphogenesis	118
4.11 Future Perspectives	119
I) The role of Ca ²⁺ flashes in Apical Constriction	119
II) Exploring the mechanism leading to GAP junction closure in Apically Constricting cells	120
III) How does the mechanical interplay between cells regulate Apical Constriction patterning	121
References	123
ANNEXES	136
I. Abbreviations	136
II. Publications	136
III. Book contribution	136

List of Figures

Figure 1. Calpain family.....	7
Figure 2. Calpain2 domain architecture.	8
Figure 3. Crystal structure of Calpain2..	9
Figure 4. Mechanism of Calpain2 activation via calcium.	10
Figure 5. Crystal structure of Calpain-Calpastatin interaction.	11
Figure 6. <i>Xenopus laevis</i> developmental stages.	14
Figure 7. Stages of <i>Xenopus</i> oogenesis	15
Figure 8. Reorganization of the <i>Xenopus</i> egg cytoplasm by cortical rotation.....	15
Figure 9. Cleavages of a frog egg.....	16
Figure 10. <i>Xenopus</i> gastrulation.....	17
Figure 11. Lateral and mediolateral interclation drive the thinning and the elongation of mesoderm during gastrulation.	18
Figure 12. Radial intercalation during epiboly.....	19
Figure 13. Primary neurulation(neural tube closure).....	20
Figure 14. Cross section of a tailbud embryo.....	21
Figure 15. Neural Tube Defects	22
Figure 16. Convergent extension movements elongate the anterior-posterior.....	23
Figure 17. Keller explant.....	24
Figure 18. Polarized protrusive activity drives Convergent Extension in mesoderm mesenchymal cells.....	25
Figure 19. PCP signalling and cell polarity during Convergent extension.	26
Figure 20. Polarized junction remodelling drives convergent extension during <i>Drosophila</i> GBE.	27
Figure 21. Model of the E-Cad-Dependent MyoII Flow Initiation and Oscillatory Behavior during Germ Band Extension.....	28
Figure 22. Multicellular Rosette Formation in Intercalating Cells.....	29
Figure 23. Mediolateral intercalation mediated by septin-dependent cortical actomyosin activity.	31
Figure 24. Epithelial Rosettes, cell division, single cell intercalation and T1-process drive mediolateral intercalation within the Neural Plate.	32
Figure 25. Cells of the Neural Plate exhibit polarized basal protrusive activity and basolateral cell elongation.	33
Figure 26. Apical Constriction induced cell shape changes.	34
Figure 27. Apical Constriction drives the invagination of bottle cells in <i>Xenopus</i>	35
Figure 28. Apical Constriction during <i>Drosophila</i> ventral furrow formation.	35
Figure 29. Dorsal-view illustration of the four stages of Dorsal Closure.....	36
Figure 30. Apical Constriction and wound healing.....	36
Figure 31. Cell shape changes of neuroepithelial cells undergoing Apical Constriction.....	37
Figure 32. Modes of actomyosin contraction.	39
Figure 33. Predominant model for Apical Constriction of neuroepithelial cells.....	40
Figure 34. Induction of Apical Constriction alters the distribution of myosin II in MDCK cells.	40
Figure 35. Mediolateral orientation of apical actomyosin network in the chicken neuroepithelium.	41
Figure 36. Apical Constriction during ventral furrow formation is driven by pulsed contractions of a medioapical actomyosin network.....	42

Figure 37. Ratchet model of apical constriction.....	42
Figure 38. Radial Cell Polarity(RCP) coordinates Myo-II stabilization and F-actin assembly to facilitate Apical Constriction.....	43
Figure 39. Cell shape changes occurring in ectoderm cells during neurulation in the newt embryo.	45
Figure 40. Polarized microtubule polymerization in neuroepithelial cells undergoing Apical Constriction.	45
Figure 41. Basal cytoplasmic flow along microtubules induce apicobasal axis elongation.	46
Figure 42. Summary and model of the cytoskeletal mechanisms of <i>Xenopus</i> bottle cell formation.	47
Figure 43. Model for the Role of Microtubule Dynamics during DRhoGEF2- Mediated Cellular Shape Change.	48
Figure 44. Model of apical membrane dynamics during bottle cell Apical Constriction.	48
Figure 45. Calcium waves regulate Convergent extension.	51
Figure 46. Schematic diagram of cellular Calcium sources.	52
Figure 47. Structure of Gap junctions	53
Figure 48. Regulation of Gap junction by intracellular Calcium.	54
Figure 49. Temporal expression of Calpain2 during <i>Xenopus</i> development	62
Figure 50. Spatiotemporal expression pattern of Calpain2 during <i>Xenopus</i> development.	63
Figure 51. Localization of exogenous Calpain2.	64
Figure 53. Quantification of phenotypes induced after treatment of embryos with CI3.....	67
Figure 54. Calpain2 dominant negative induces phenotype similar to the phenotype induced by CI3.	68
Figure 55. Characterization of Calpain2 MO.	69
Figure 56. Phenotypes induced after downregulation of Calpain2 with Calpain2 MO.	70
Figure 58. Calpain2 function is indispensable for Convergent Extension and is implicated in mesoderm migration.	73
Figure 59. Downregulation of Calpain2 by MO affects cell movements during Neural Tube Closure.....	75
Figure 60. Calpain2 downregulation results in defective neural fold formation and anterior Neural Tube Defects.....	77
Figure 61. Downregulation of Calpain2 expression by MO inhibits neural Convergent Extension.	79
Figure 62. Radial intercalation is unaffected in Keller explants treated with CI3.	80
Figure 63. Inhibition of Calpains affects the morphology and motility of mesodermal cells.	82
Figure 64. Calpain2 function is not necessary for neural tube primary cilia formation.	83
Figure 65. Calpain2 downregulation leads to defective Apical Constriction.	84
Figure 66. Calpain2 localization in neuroepithelial cells pre and post Apical Constriction.	85
Figure 67. Calpain2 regulates Apical Constriction independently of tissue context.....	87
Figure 69. Calpain2 function is necessary for ectopically induced Apical Constriction.	89
Figure 70. Calpain2 is activated after increase of intracellular Calcium in <i>Xenopus</i> embryos.....	90
Figure 71. Calpain2 acts downstream of the Wnt/Ca ²⁺ pathway.	91
Figure 72. Calpain2 activity is dependent on Dishevelled.	92
Figure 73. Dynamics of apical actin network during Apical Constriction of neuroepithelial cells.	94
Figure 74. Pulsed contractions followed by stabilization steps drive ectopically induced Apical Constriction.	95

Figure 75. Contraction pulses of neuroepithelial cells undergoing Apical Constriction are cell autonomous and asynchronous.....	96
Figure 76. The apical actin network in neuroepithelial cells is contractile.....	96
Figure 77. Two distinct processes contribute to apical surface reduction during Neural Tube Closure.....	98
Figure 78. Cell autonomous Calcium flashes take place during neurulation and their frequency correlates with the speed of Neural Tube Closure.....	100
Figure 79. Calcium flashes precede contraction pulses.....	102
Figure 80. Elevation of intracellular Calcium levels leads to increase Apical Constriction rate and results in continuous rather than pulsed constriction.....	104
Figure 81. The autonomy and the asynchrony of contraction pulses are both necessary for proper morphogenesis.....	104
Figure 82. Cells undergoing Apical Constriction fail to transmit Calcium waves.....	106
Figure 83. Calpain2 function in Lulu induced Apical Constriction.....	107
Figure 85. Calpain2 activity is necessary for the stabilization step during Apical Constriction.....	108

II. List of movies

1. Time-lapse movies of dissociated activin-treated control (left) and CI3-treated (right) caps, plated into fibronectin-coated cover slips and left to spread. A field of cells was randomly chosen, and images were captured at 5 min intervals for 100 minutes. CI3-treated cells moved significantly slower than controls.
2. Time-lapse movie of a MO-injected embryo (right) compared to control (left) at neurula stage. The morphant was injected with 30ng MO at 1 out of 2 blastomeres at 2-cell stage (the injected side is on the left in the movie). Neural tube closure is significantly delayed in the MO-injected side.
3. Time-lapse movie of 30ng MO-injected embryo (left) and an embryo in which the same amount of MO was co-injected with 300pg Calpain2R mRNA (right). The injected sites are the left in both embryos. The severe delay in neural plate movement caused by MO injection is successfully rescued by Calpain2R.
4. Time-lapse movie of control DMZ explant excised at stage 10.5 was filmed for 11 minutes. Membrane GFP (green) was used as lineage tracer.
5. Time-lapse movie of CI3-treated DMZ explants excised at stage 10.5 were filmed for 11 minutes. Membrane GFP (green) was used as lineage tracer. Cells in CI3-treated explants show alteration in morphology, orientation and motility compared with control explant in movie 4.
6. Time lapse recording of neural tube closure of a representative embryo expressing utr-GFP. Frames were acquired at 20second intervals.

7. Time lapse recording of a neurula embryo expressing utr-GFP. Contraction pulse initiation is indicated (red color). Majority of contraction pulses are cell autonomous and asynchronous. Frames were acquired at 20 second intervals.
8. Time lapse recording of a representative neuropithelial cell expressing utr-GFP. Quantification of surface area and apical utr-GFP intensity over time (left) shows that apical actin accumulation coincides with contraction pulses. Frames were acquired at 20 second intervals.
9. Time lapse recording of a neurula embryo expressing utr-GFP. Contraction pulses driven by apical actin are indicated by the red arrowheads. Shrinkage of mediolateral junction is indicated with purple arrowheads. Frames were acquired at 20 second intervals.
10. Time lapse recording showing the anterior neural tube closure of a stage 16 embryo expressing mem-GFP (green) + GECO RED (red). Frames were acquired at 10 second intervals. Asynchronous cell autonomous calcium flashes are taking place during neural tube closure. (Left: merged, Right: GECO-RED)
11. Time lapse recording of a representative neuropithelial cell expressing GECO-RED (intensity coded) + mem-GFP (green). 3 Calcium flashes occur during this time period. Quantification of the apical cell surface area over time shows that cell surface area reduction (contraction pulse) occurs after each calcium flash (red bullets in graph).
12. Time lapse recording of ectodermal cells of a control gastrula embryo expressing Lulu-GFP (purple) + GECO RED (intensity coded). Frames were acquired at 10 second intervals. Calcium flashes are taking place in cells indicated using white arrowheads. After each calcium flash, the apical cell surface shrinks.
13. Time lapse recording of ectodermal cells expressing Lulu-GFP in control and Thapsigargin (THA) treated stage 9 embryos. Frames were acquired at 10 second intervals. Imaging begun 15 minutes after THA treatment.
14. Time lapse recording of ectodermal cells expressing Lulu-GFP (left window, red) + GECO RED (right window, intensity coded) in THA treated stage 9 embryos. Frames were acquired at 10 second intervals. Cells undergo AC without generation of calcium flashes.
15. Time lapse recording of ectodermal cells expressing Lulu-GFP (purple) and GECO-RED (intensity coded) from stage 11.5 embryos. Frames were acquired at 10 second intervals. At the beginning of the movie, cell autonomous calcium flashes are generated in Lulu-GFP positive cells. When a Calcium wave is generated, it is propagated by control cells

but fails to generate intracellular calcium increase in Lulu expressing cells. Calcium flashes are indicated using white arrowheads.

16. Time lapse recording of cells expressing mem-cherry (red) + Lulu GFP (green) in control (left) and CI3 treated (right) embryos. Images were taken at 1 minute intervals. Lulu induced Apical Constriction is affected in CI3 treated embryos.
17. Time lapse recording of a CI3 treated gastrula stage embryo expressing Lulu GFP (green) and GECO-RED (red). Frames were acquired at 10 second intervals. Appearance of Calcium flashes is not affected in the presence of the Calpain inhibitor.

1. Introduction

1.1 Calpains

Calpains are a family of calcium-dependent intracellular cysteine proteases. Calpain family proteases have been present throughout evolution. Calpain family members are present in all eukaryotes, some bacteria but not archaea (Ono and Sorimachi, 2012). Calpains display limited proteolytic activity, cleaving substrates to transform their structure and function (Sorimachi et al., 2010). Deregulation of specific Calpain activities have been implicated in numerous pathological conditions, including cancer, Alzheimer's disease, type 2 diabetes and muscular dystrophy (Huang and Wang, 2001). Mammalian Calpain family consists of 16 genes encoding 15 proteins with proteolytic activity and two regulatory subunits (**Figure1**). Calpain2 family is further subdivided into typical and atypical Calpains. Typical Calpains consist of the domains I, II, III and IV while atypical Calpains family proteins miss one or more of these domains. (**Figure1**). Typical Calpains 1, 2 and 9 form functional heterodimers with the small regulatory domain (Calpain4) through domain IV. Among the 15 members of the Calpain family, the two conventional ubiquitous isoforms Calpain1 (or μ -Calpain) and Calpain2 (or m-Calpain) are the most studied (Ono and Sorimachi, 2012). They are both heterodimers composed of a large catalytic subunit of 80kDa and a common regulatory subunit of 30 kDa (Calpain4) that dissociates upon activation. Calpain1 and Calpain2 share 61% of sequence identity and are very similar in substrate specificity and subcellular localization but they require different Ca^{2+} concentrations for their activity, $\sim 10\text{-}50\mu\text{M}$ and $>500\mu\text{M}$ respectively (Goll et al., 2003). These concentrations are considerably higher than physiological intracellular concentrations of Ca^{2+} (usually $< 1\mu\text{M}$), suggesting the presence of regulatory mechanisms that may lower this requirement. Indeed Calpain2 binds to phospholipids (particularly phosphoinositide biphosphate, PIP_2) (Leloup et al., 2010) and thus localizes at the membrane close to its substrates/cofactors and calcium channels. In this thesis, we will emphasize on the function and regulation of Calpain2.

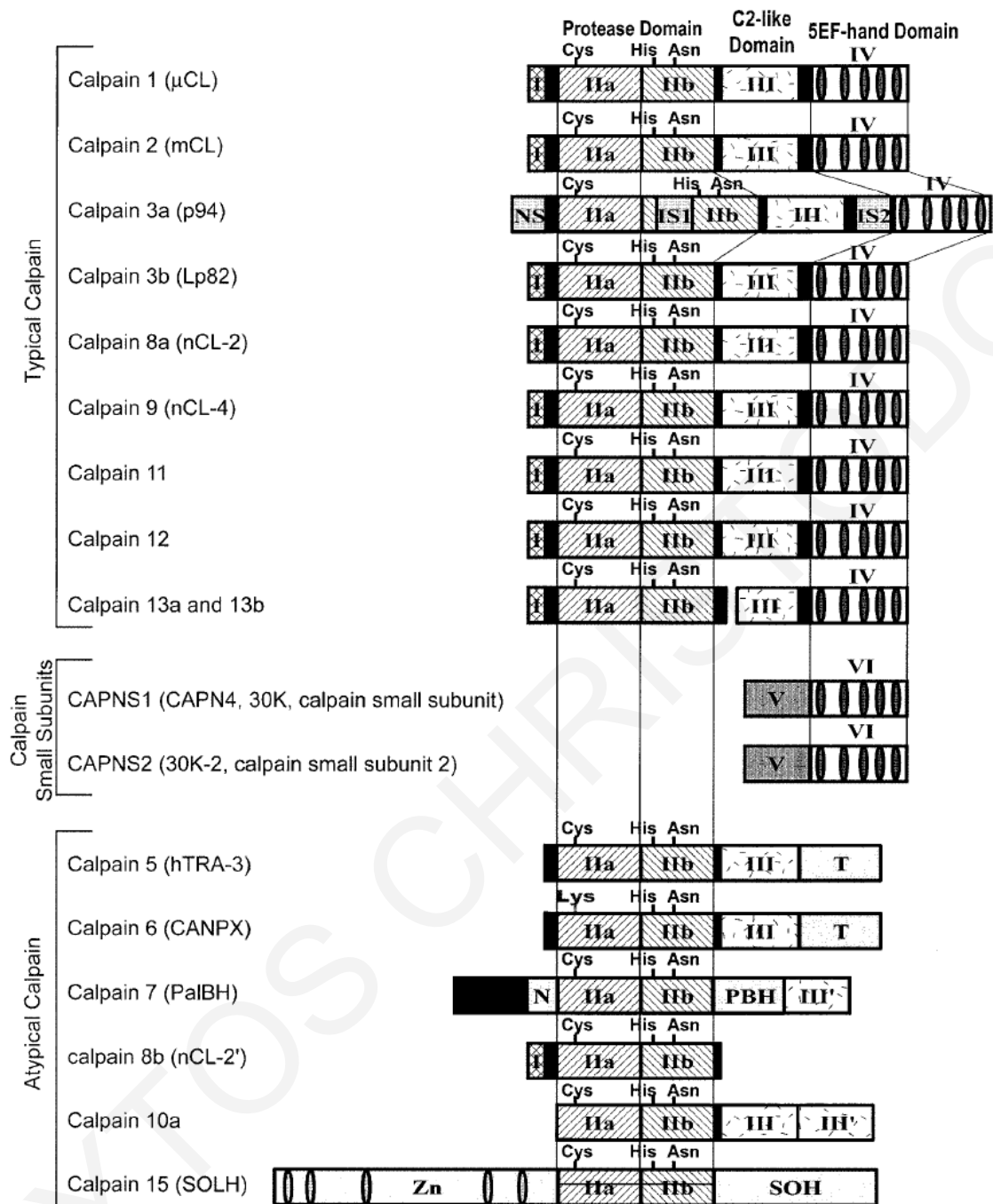


Figure 1. Calpain family.

Adapted from (Suzuki et al., 2004).

1.2 Structure of Calpain2

Calpain2 is composed of a large catalytic subunit of 80kDa and a small regulatory subunit of 30kDa that dissociates upon activation. The large catalytic subunit consist of domains I, II, III and IV. The regulatory subunit is composed of domains V and VI. (**Figure 2,3**) (Franco and Huttenlocher, 2005; Suzuki et al., 2004).

Domain I: The N-terminal domain I is a single α -helix and interacts with the VI domain of the regulatory subunit promoting stabilization of the interaction (Franco and Huttenlocher, 2005)

Domain II: Domain II is the protease domain. The active site residue Cys-105 is forming a catalytic triad with His-262 and Asn-286 which is characteristic of cysteine proteases such as papains and cathepsins. Domain II is composed of two subdomains with the substrate binding cleft in-between (**Figure 3**). The active site residue Cys-105 is found in subdomain IIA and His-262 and Asn-286 are found in subdomain IIB (Goll et al., 2003; Strobl et al., 2000) (**Figure 3**). Therefore, these residues cannot form a catalytic triad when the protein is inactive.

Domain III: Domain III is a C2 like domain. It has been shown that domain III can bind to phospholipids in a calcium depended manner (Franco and Huttenlocher, 2005; Tompa et al., 2001) and targets Calpain2 at the membrane after its activation (Shao et al., 2006).

Domain IV: This domain bears 5 EF-hand Ca^{2+} binding sites. The fifth EF-hand site of domain IV contributes to the dimerization with the regulatory subunit with interaction with the fifth EF-hand of domain VI of the regulatory subunit (**Figure 2,3**) (Blanchard et al., 1997; Hosfield et al., 1999).

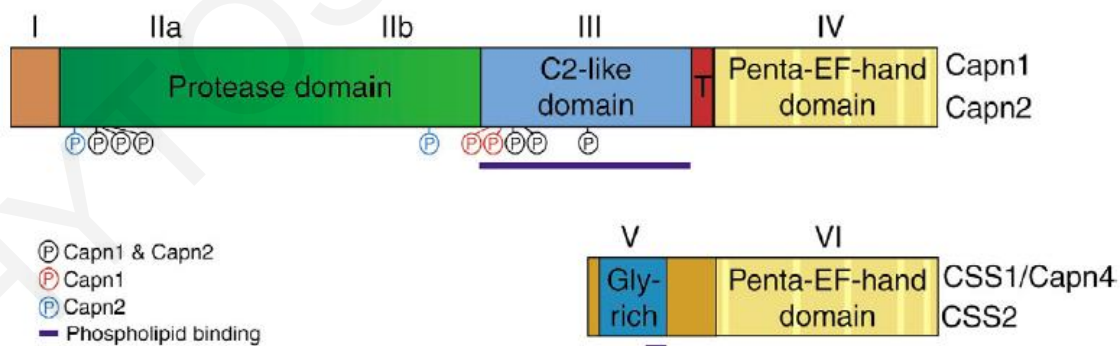


Figure 2. Calpain2 domain architecture. Adapted from (Franco and Huttenlocher, 2005)

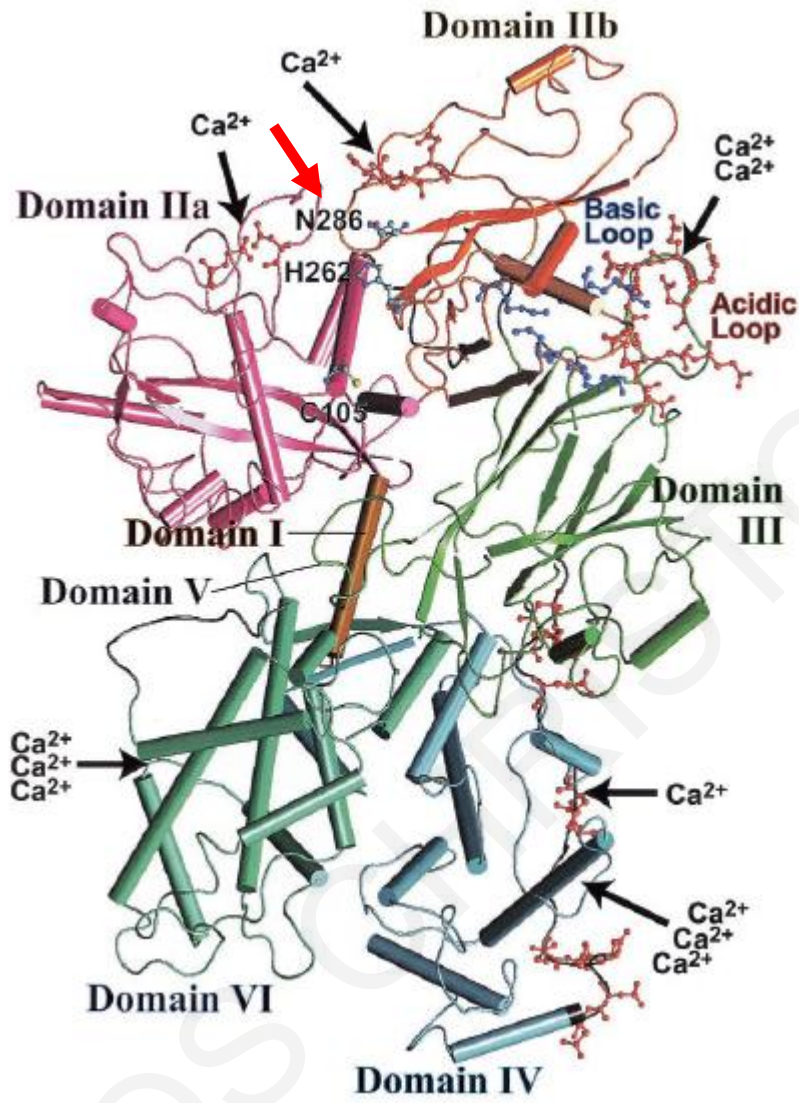


Figure 3. Crystal structure of Calpain2. Active site (red arrow). Adapted from (Suzuki et al., 2004).

1.3 Regulation of Calpain2 function

1.3.1 Activation of Calpains

Calpain activity is highly regulated by several mechanisms. Activation after calcium binding is the best studied mechanism of Calpain activation. Calcium binding induces conformational changes on Calpain2 heterodimer which lead to the activation of the protease. Specifically, in the inactive conformation, subdomain IIa and IIb are far away and the catalytic triad can not form. In addition there tryptophan 288 between Domains IIa and IIb, does not permit the formation of the catalytic triad. This inactive conformation of domainII is stabilized by the interaction of domain I of the large subunit with domain VI of the small subunit and the interaction between subdomain

I Ib and III of the large subunit (Moldoveanu et al., 2002; Reverter et al., 2001; Strobl et al., 2000). These interactions generate constraints to hold the protease domain open. There are at least 3 different calcium binding sites in Calpain-2. The first site is at the EF-hands of domain IV and VI. The second is found at an acidic loop of domain III and the third is found at domain II (Moldoveanu et al., 2002). Binding of calcium to domain IV and domain VI induces the release of domain I from domain VI. In addition, binding of calcium at the acidic loop of domain III induces the release of domain IIb from domain III. These two events release constraints generated by domain interactions. Next, autolysis of domain I releases the regulatory subunit (Moldoveanu et al., 2002). Subsequently, the protease domain binds two calcium atoms, one at domain IIa and one at the domain IIb (Nakagawa et al., 2001). This induces conformational changes at the protease domain and the catalytic triad is formed (Figure 4).

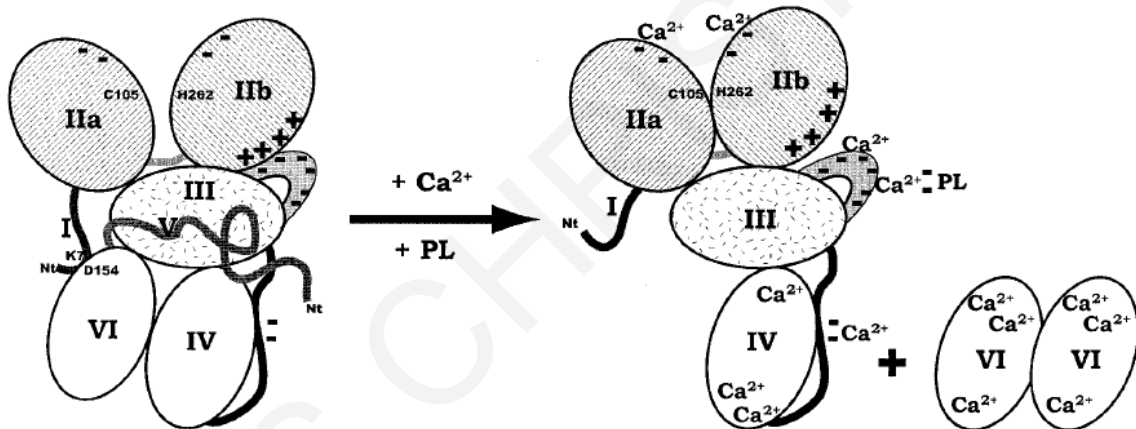


Figure 4. Mechanism of Calpain2 activation via calcium. Adapted from (Suzuki et al., 2004).

However the calcium levels needed *in-vitro* for Calpain2 activation are not normally found in cells. Therefore, it is believed that additional mechanisms contribute to Calpain activation by lowering calcium requirement. Binding of phospholipid, through domain III has been shown to contribute to Calpain activation. Protein interactions and phosphorylation have also been shown to contribute to Calpain activation (Franco and Huttenlocher, 2005).

1.3.2 Inhibition of Calpains

Calpain activity is negatively regulated by the endogenous Calpain inhibitor Calpastatin. Calpastatin consists of a non-inhibitory region and 4 inhibitory repeats. Each inhibitory repeat consists of regions A, B and C. Calpastatin binds preferentially to calcium-bound Calpain molecules; therefore Calpastatin interacts with heterodimeric molecules. Two independent

studies have shown that Calpastatin recognizes Ca^{2+} induced conformation of Calpain2. Specifically Calpastatin binds on Calpain2 through regions A,B and C. Regions A and C bind to domain IV of the large subunit and domain VI of the regulatory subunit respectively Region B binds to DII-III and masks the active site cleft (**Figure 5**). Calpastatin binding on Calpain2 blocks Calpain2 activity as both sides of the active site cleft are masked (Hanna et al., 2008; Moldoveanu et al., 2008).

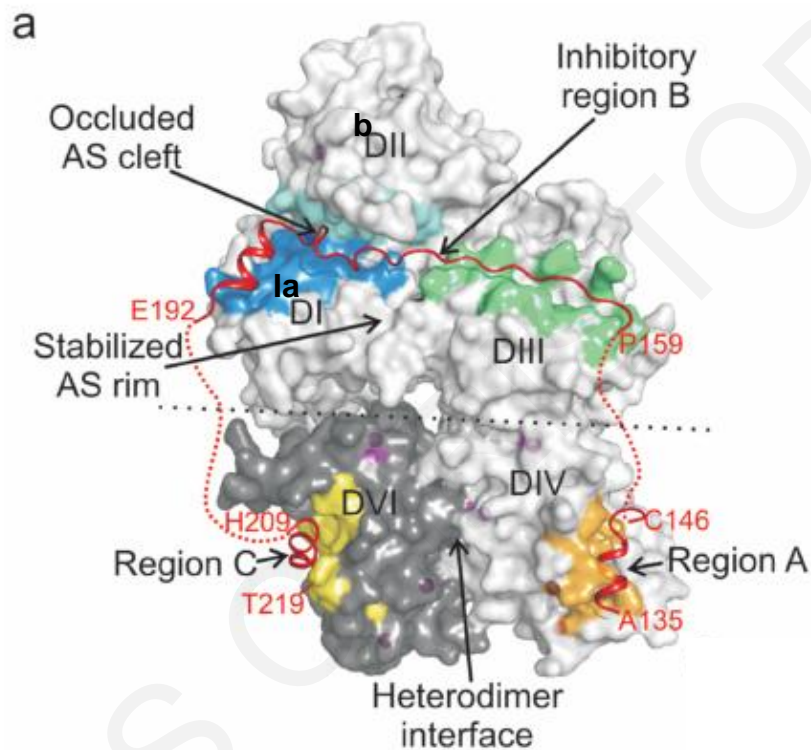


Figure 5. Crystal structure of Calpain-Calpastatin interaction. Adapted from (Moldoveanu et al., 2008).

1.4 Calpain *in vitro* and *in vivo* functions

1.4.1 *In Vitro* studies

The role of Calpains has been extensively investigated *in vitro*. Calpains have been implicated in cell migration, cell adhesion, cytoskeleton remodeling and signal transduction through limited proteolysis of specific substrates. Studies using Calpain inhibitor showed that Calpain's function is necessary for integrin mediated cell migration (Huttenlocher et al., 1997). These data were confirmed by a study in *Capn4* $-/-$ fibroblasts. *Capn4* $-/-$ fibroblasts had decreased cell migration rates due to defects in actin cytoskeleton formation (Dourdin et al., 2001). Moreover, it has been demonstrated that Calpains regulate focal adhesion dynamics through cleavage of focal adhesion proteins (FAK, Vinculin, Paxillin, Talin, Integrins), suggesting that Calpain is implicated in cell

motility through regulation of focal adhesion dynamics (Bhatt et al., 2002; Chan et al., 2010; Cortesio et al., 2011; Franco et al., 2004; Pfaff et al., 1999; Serrano and Devine, 2004). In addition to its role in cell-Extracellular Matrix adhesion Calpain has been implicated in cell-cell adhesion through cleavage of substrates such as E-cadherin, N-cadherin and β -catenin (Benetti et al., 2005; Jang et al., 2009; Rios-Doria et al., 2003). The data from Cpn4 $-/-$ fibroblast suggested that Calpain regulate actin cytoskeleton formation. Several studies have shown that Calpains cleave several actin regulators such as cortactin, filamin, α -actinin and MARCKS (Dedieu et al., 2003; O'Connell et al., 2009; Perrin et al., 2006; Selliah et al., 1996). Furthermore, Calpains are implicated in signal transduction by cleavage of signal transduction molecules such as Rhoa, Src, Tiam, EGFRs and Integrins (Kulkarni et al., 2002; Oda et al., 1993; Pfaff et al., 1999; Stoscheck et al., 1988; Woodcock et al., 2009). Numerous studies answer the question on how Calpain affect cellular processes. Another question is how Calpains are activated, which are the signaling pathways regulating Calpain activation? Several molecules induce elevation of intracellular calcium, such as Wnt5a, TRPM7 and GPCRs. These molecules have been shown to act upstream of Calpains (Li and Iyengar, 2002; Su et al., 2006; Yang et al., 2011). In conclusion, Calpain2 is acting downstream of pathways which are inducing elevation of intracellular calcium and regulates cell adhesion, cytoskeleton and signal transduction via limited proteolysis of specific substrate.

1.4.2 *In vivo* Studies

Despite the numerous *in vitro* studies regarding the cellular functions of Calpains, the study of Calpain's function *in vivo* is still in its infancy. While knockout of Calpain1 resulted in fertile mice with a reduction in platelet aggregation (Azam et al., 2001), disruption of Calpain2 gene in mice led to early embryonic lethality prior to the implantation stage and lack of embryos beyond the 8-cell stage, suggesting that Calpain2 activity is essential for cell viability (Dutt et al., 2006). This is also consistent with another study showing that mice deficient for the regulatory subunit Calpain4, in which the function of both Calpains was lost, also died prior to the implantation stage (Zimmerman et al., 2000). Interestingly, in a separate study after disruption of Calpain4 gene, mice survived to mid-gestation by which time they died due to a failure in heart morphogenesis (Arthur et al., 2000). However, a later study showed that Calpain2 was in fact only required in extraembryonic tissues during mouse development since a fetus-specific conditional Calpain2 knockout resulted in nearly half of the mice surviving to adulthood without any significant abnormalities (Takano et al., 2011). In another study using mice overexpressing

the Calpain endogenous inhibitor Calpastatin in the skin it was demonstrated that Calpains are implicated in wound healing (Nassar et al., 2012). Calpain2 is expressed maternally in mouse, in agreement with a role in early development. Calpain2 mRNA is ubiquitously expressed with elevated expression in the tissues that will give rise to the central nervous system, mesodermal and heart tissues (Raynaud et al., 2008). In *Xenopus*, the Calpain2 gene has been identified and sequenced (Klein et al., 2002) but its role in morphogenesis has not been examined. In contrast Calpain8 function during *Xenopus* embryogenesis has been studied and suggested to be involved in convergent extension movements (Cao et al., 2001) and in neural crest migration (Cousin et al., 2011). In zebrafish, blockage of Calpain2 functions lead to reduced invasion of glioblastoma cells in brain microenvironment. This study shows that Calpain2 function is necessary for proper migration in 3D environment in agreement with studies showing that Calpain2 function is indispensable for migration in 2D environments. From the above studies it has been suggested that Calpain2 is important for proper embryogenesis, but the specific functions of Calpain2 in embryogenesis have not been determined due to discrepancies from mice knock out studies.

1.5 *Xenopus laevis*

Amphibians have been widely used over the past century for the understanding of molecular and cellular events during embryogenesis. *Xenopus laevis*, the African clawed frog is an excellent model system for several reasons. Like other amphibians are tetrapods, therefore they share all the features of land-dwelling organisms. *Xenopus laevis* females lay large number of eggs with a simple hormone injection. The embryos can be fertilized *in vitro* by addition of sperm into the oocytes (Beck and Slack, 2001) (Sive et al., 2010). *Xenopus* embryos are large (1-1.4mm), robust and they undergo external development in a simple salt solution (Beck and Slack, 2001). The development of *Xenopus laevis* embryos is relatively rapid; as they go from fertilization to a free swimming tadpole in 4 days (**Figure 6**). *Xenopus* embryos have the ability to heal well, making tissue-explants experiments possible. In addition, gain of function and loss of function experiments can be carried out using *Xenopus* embryos. Gain of function experiments can be performed by overexpression of injected mRNA encoding a protein of interest. Loss of function experiments are carried out using dominant negative forms of a protein, antisense RNA (Harland and Weintraub, 1985), oligonucleotides (Baker et al., 1990) and morpholino oligos which have become one of the most widely used methods for gene knock-down in *Xenopus* and other model systems (Heasman, 2002; Heasman et al., 2000; Kenwrick et al., 2004; Nutt et al., 2001). The well defined fate maps of *Xenopus* allow targeted gene manipulation in the tissue of interest.

Moreover recently the development of CRISPR/Cas(Blitz et al., 2013; Nakayama et al., 2013) and TALENs (Lei et al., 2012; Nakajima and Yaoita, 2015) technologies allow the generation of knock out *Xenopus* embryos. All the above features allow for micromanipulation, microinjection, microdissection, labeling of the *Xenopus* embryo and genetic manipulations making *Xenopus laevis* an excellent organism for studying molecular and cellular events during embryogenesis

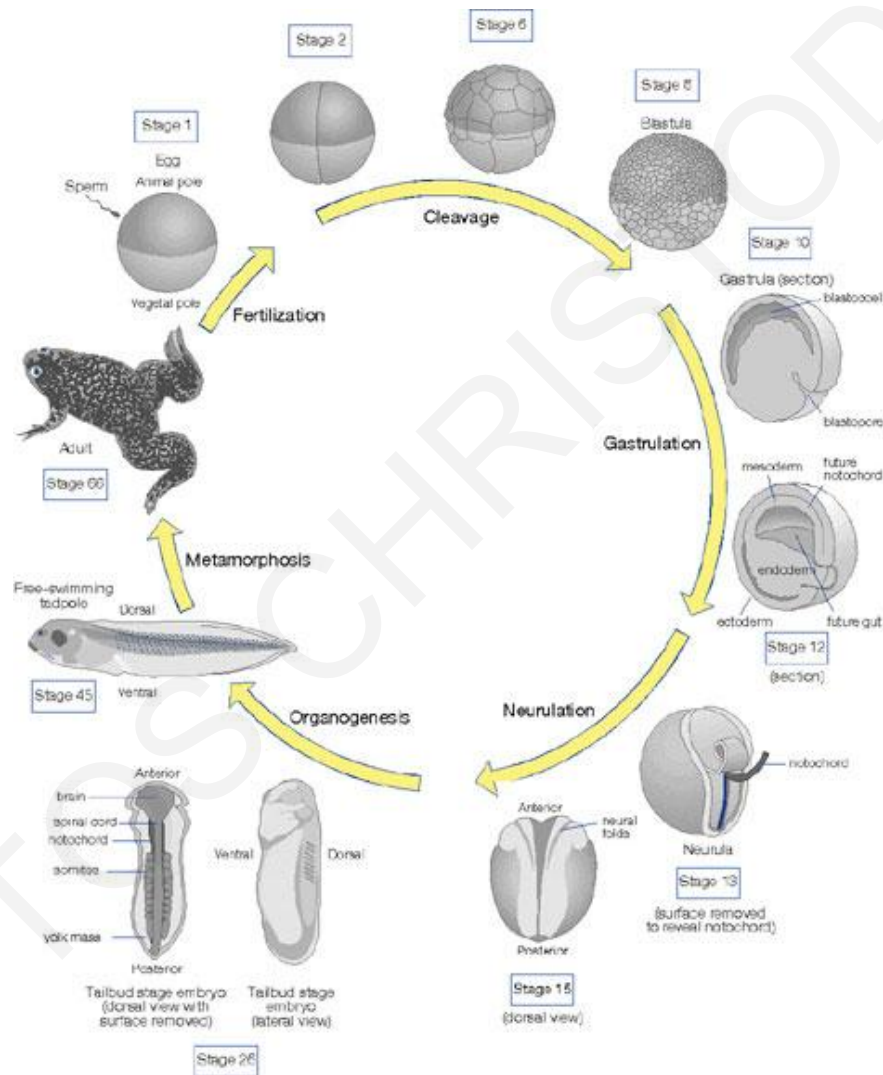


Figure 6. *Xenopus laevis* developmental stages. Adapted from(Staveley, 2007).

1.5.1 Oogenesis-Fertilization

During oogenesis, the animal – vegetal (A-V) polarity of the oocyte is established by the restriction of RNAs to either the animal (darker top half) or the vegetal (lighter bottom half) pole (Figure 7). This creates a radially-symmetrical egg (Smith JC, 2003). The second axis to be formed is the dorsal-ventral axis which is determined by the site of sperm entry. Sperm entry at

the animal hemisphere induces a cytoplasmic rearrangement called cortical rotation. During cortical rotation the cortical cytoplasm rotates 30°, inducing the translocation of material located in the vegetal pole to the prospective dorsal site of the embryo at the animal pole (Gerhart et al., 1989; Gilbert, 2006; Smith JC, 2003) (**Figure 8**).

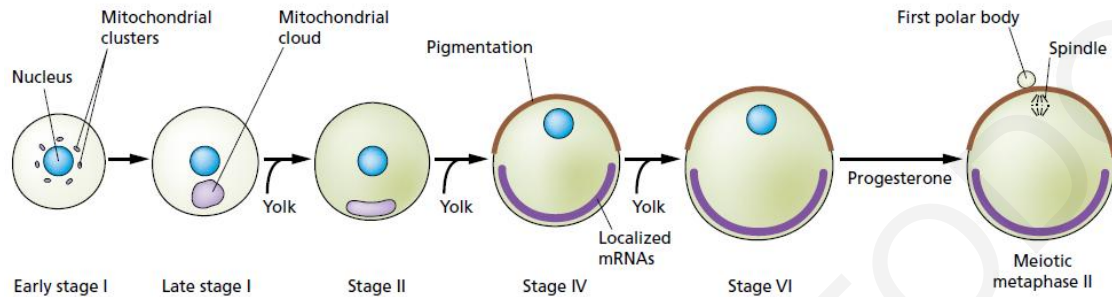


Figure 7. Stages of *Xenopus* oogenesis

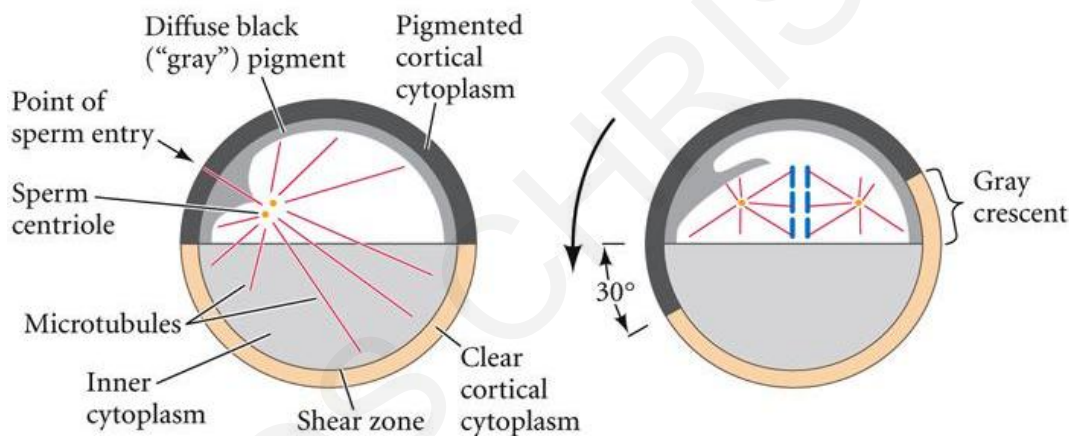


Figure 8. Reorganization of the *Xenopus* egg cytoplasm by cortical rotation.

On the left is a schematic cross section of an egg midway through the first cleavage cycle, before cortical rotation has occurred. On the right, is a schematic showing an egg about 80% of the way into the first cleavage. The cortical cytoplasm rotates 30 degrees relative to the internal cytoplasm. Gastrulation will begin in the gray crescent, the region opposite the point of sperm entry. Adopted from reference Adapted from (Gilbert, 2006).

1.5.2 Cleavage stages

The first cleavage occurs approximately 90 minutes after fertilization and is observed along the A-V axis (Figure 9A). This divides the embryo into right and left halves. The second cleavage is also along the A-V axis and separates the dorsal and ventral site of the embryo. The third cleavage is equatorial separating the animal and vegetal halves. (Gilbert, 2006; Heasman, 2006b) (Figure 9B-H). The next cleavages occur every 20 minutes with no G- phases. In the absence of G-phase the size of the cells (termed blastomeres) decreases and only the blastomere number increases. At the 128-cell stage a fluid-filled cavity, the blastocoel, develops at the animal

hemisphere and the embryo is then referred to as a blastula (Gilbert, 2006) (Figure 9H). After the twelfth cell cycle, zygotic transcription is activated. This is termed the mid-blastula transition (MBT) and it prepares the embryo for gastrulation (Gilbert, 2006; Winklbauer, 2009).

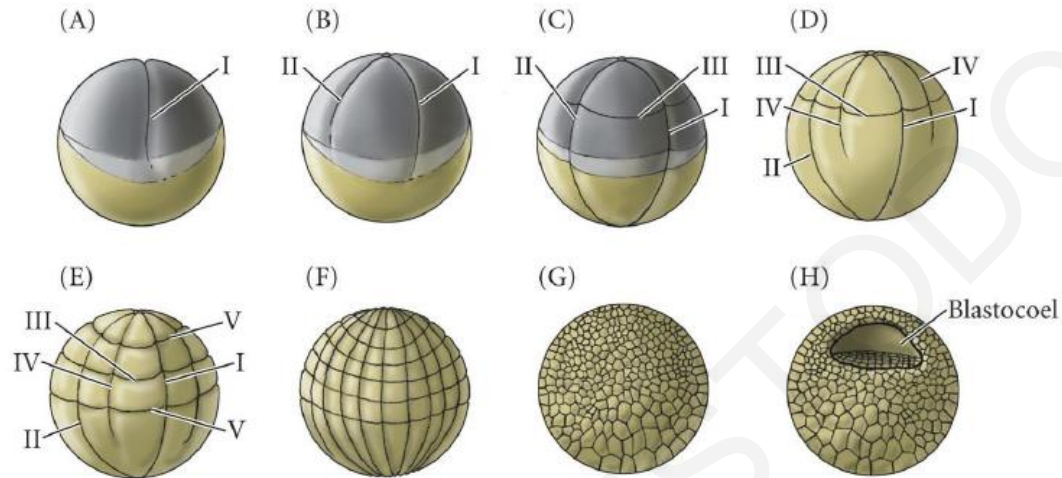


Figure 9. Cleavages of a frog egg.

(A,B) Second cleavage occurs in the animal hemisphere before the first cleavage is completed due to impediment from the vegetal yolk. (C) The third cleavage is equatorial towards the animal pole. (D-H) The vegetal hemisphere ultimately contains fewer and larger blastomeres than the animal pole. H depicts a cross-section through a mid-blastula stage embryo. Adapted from(Gilbert, 2006)

1.5.3 Gastrulation

Gastrulation is the embryonic period during which the single layered blastula is transformed into the three layered embryo (gastrula) with distinguishable layers of endoderm, mesoderm and ectoderm(Leptin, 2005). The three germ layers are shaped into a characteristic body plan and the anteroposterior (A/P) and dorsoventral (D/V) axes are set by the end of gastrulation (Heasman, 2006a). Gastrulation is comprised of a combination of signaling events, cell shape changes and cell movements. Gastrulation begins at the future dorsal site (marginal zone) when prospective endodermal cells invaginate and form the blastopore lip. These cells line the early archenteron. Next, the head mesoderm involutes at the blastopore lip and migrates on the inner surface of the blastocoel roof towards the animal pole. As they involute, mesodermal cells also converge toward the dorsal midline (convergence) and at the same time elongate along the future anterior–posterior axis (extension). Simultaneously the animal cap cells undergo epiboly completely surrounding the surface of the embryo until a ventral blastopore lip forms (**Figure 10**). All these movements contribute to blastopore closure (**Figure 10**) (Gilbert, 2006). Each one of the above events is governed by one morphogenetic movement. Invagination of the prospective endodermal

cells is governed by **Apical Constriction** and is necessary just for the initiation of blastopore closure (Hardin and Keller, 1988; Keller, 1981). Head mesoderm movement towards the blastocoel roof is governed by integrin depended **cell migration** (Alfandari et al., 1996; Davidson et al., 2002b; Winklbauer et al., 1996). The elongation of the mesoderm along the A/P axis is governed by directed **cell migration** and **Convergent Extension** (radial and mediolateral intercalation of cells leading to thinning and elongation of mesoderm) (**Figure 11**) (Keller et al., 2003; Wallingford et al., 2002). The expansion of the ectoderm around the endoderm is governed by Epiboly, during which ectodermal cells of the deep layer intercalate radially resulting in the thinning and the expansion of the ectoderm (**Figure 12**) (Keller et al., 2003; Keller, 1980; Marsden and DeSimone, 2001). Failure of **cell migration**, or/and **Convergent Extension**, or/and **epiboly** results in defective blastopore closure.

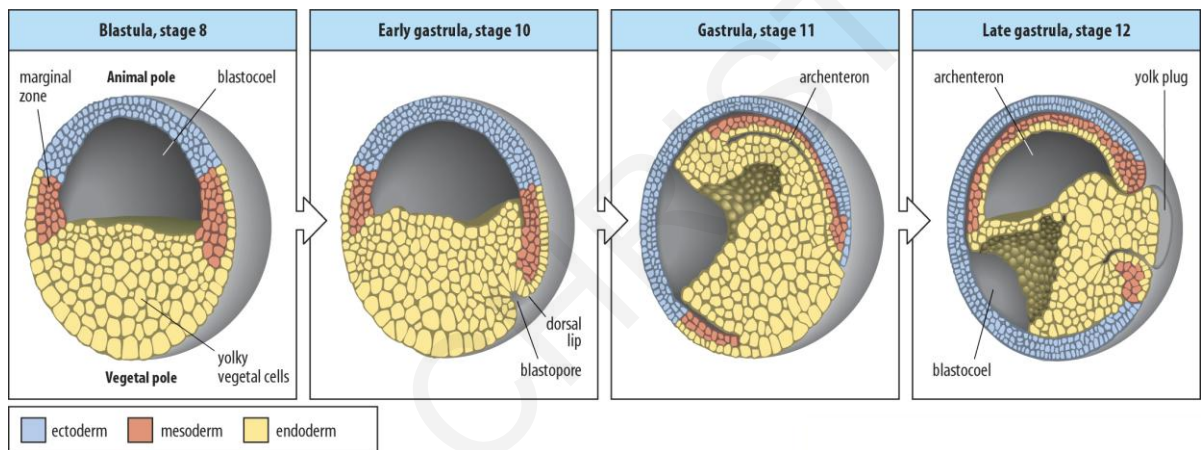


Figure 10. *Xenopus* gastrulation.

Stage 10: Early gastrulation. The bottle cells of the margin move inward to form the dorsal lip of the blastopore, and the mesodermal precursors involute under the roof of the blastocoels. Stage 11: Mid-gastrulation. The archenteron forms and displaces the blastocoel and the cells migrate down toward the vegetal region. Stage 12: Toward the end of gastrulation, the embryo becomes surrounded by ectoderm, the endoderm has been internalized and the mesodermal cells have been positioned between the ectoderm and the endoderm.

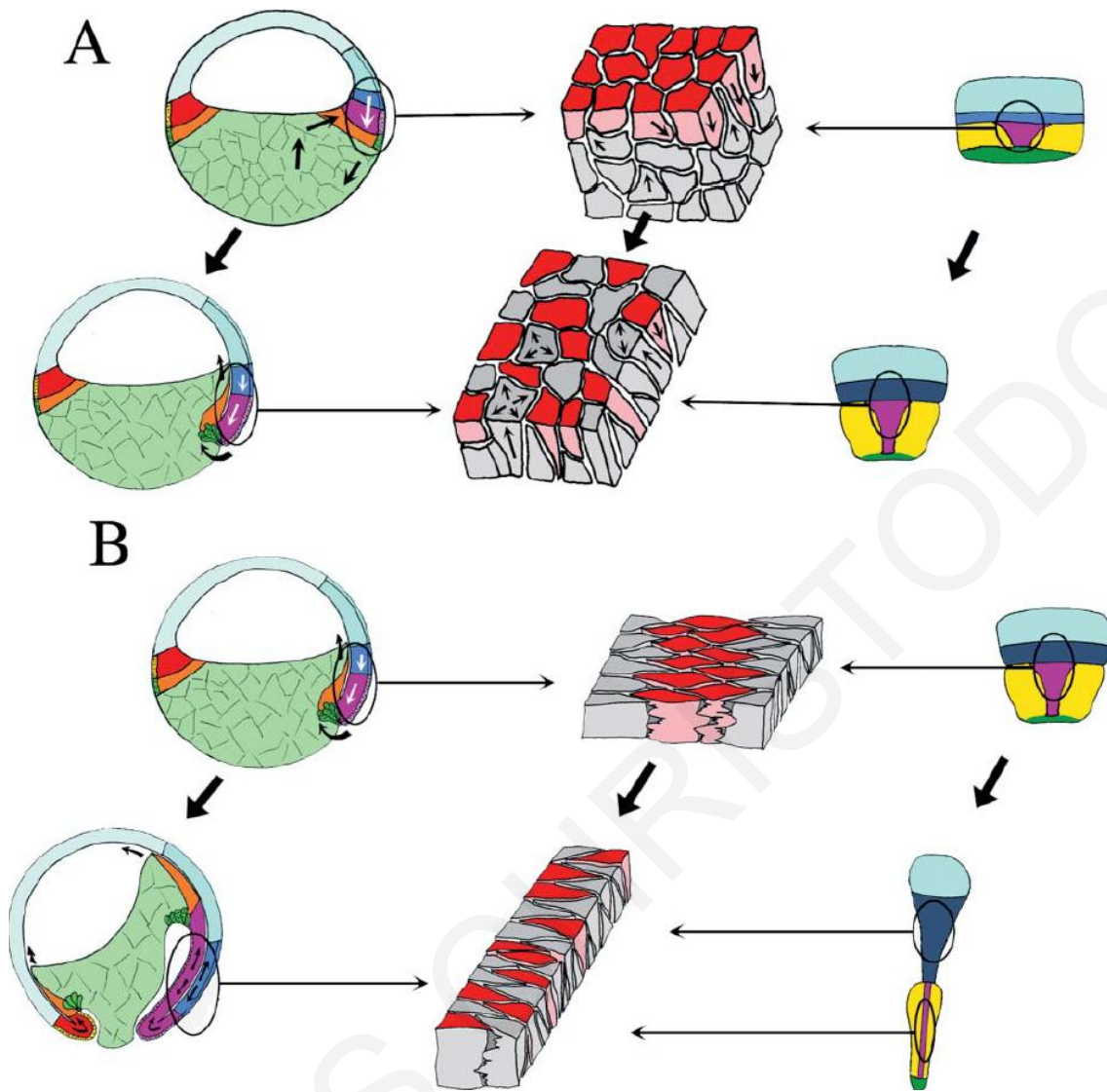


Figure 11. Lateral and mediolateral intercalation drive the thinning and the elongation of mesoderm during gastrulation.

Early in gastrulation, the dorsal deep mesoderm and posterior neural tissue undergoes a thinning and extension (white arrows, left panel, A) that is driven by radial intercalation of convergence and extension also occur independent of other tissues multiple layers of deep cells for form fewer layers of greater area(center panel, A). From the midgastrula stage onward, these same tissues undergo convergence and extension (black arrows, bottom left panel), which is driven by mediolateral cell intercalation(middle panel, B).These movements of thinning and extension and convergent and extension also occur independent of other tissues in explants (right panel, A, B). Adapted from (Keller et al., 2003).

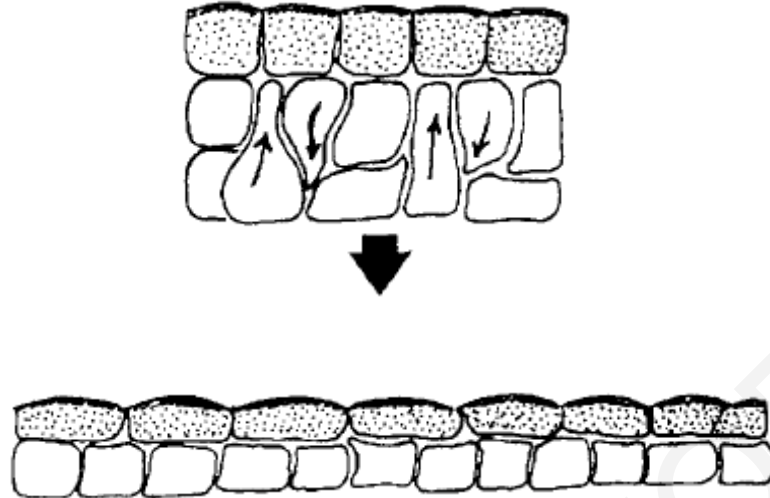


Figure 12. Radial intercalation during epiboly.

Radial intercalation of deep mesenchymal ectodermal cells results in the thinning and spreading of the ectoderm. Adapted from (Keller et al., 2003)

1.5.4 Neurulation

Neurulation is the embryonic period during which the neural tube forms through coordinated morphogenetic movements. Neural tube will give rise to the central nervous system (CNS), the brain anteriorly and the spinal cord posteriorly. At the start of neurulation the prospective CNS starts as a thickened flat sheet of cells, the neural plate (Suzuki et al., 2012). At the two lateral regions of the neural plate is the epidermis and below the neural plate tissue is the notochord. Neurulation is initiated when the underlying dorsal mesoderm signals to the overlying ectoderm to elongate into columnar neural plate cells. During neurulation neural plate narrows and lengthens while it bends forming the neural groove at neural plate midline (**Figure 13 A**). Subsequently, the lateral edges of the neural plate elevate, and move medially where they fuse to form the neural tube (**Figure 13B,C**) (Gilbert, 2006). Neural crest cells, delaminate and migrate away from the neural tube and give rise to a large array of cell types such as melanocytes, cartilage and certain neurons which are also created during neurulation (**Figure 13D**) (Gilbert, 2006). The above events describe the **primary neurulation** in *Xenopus*. **Secondary neurulation** is completed at tailbud stage when the neural tube of the tail is formed (Gilbert, 2006). At tailbud stages the major body parts are in place (**Figure 14**) and organogenesis takes place until a free swimming tadpole is formed.

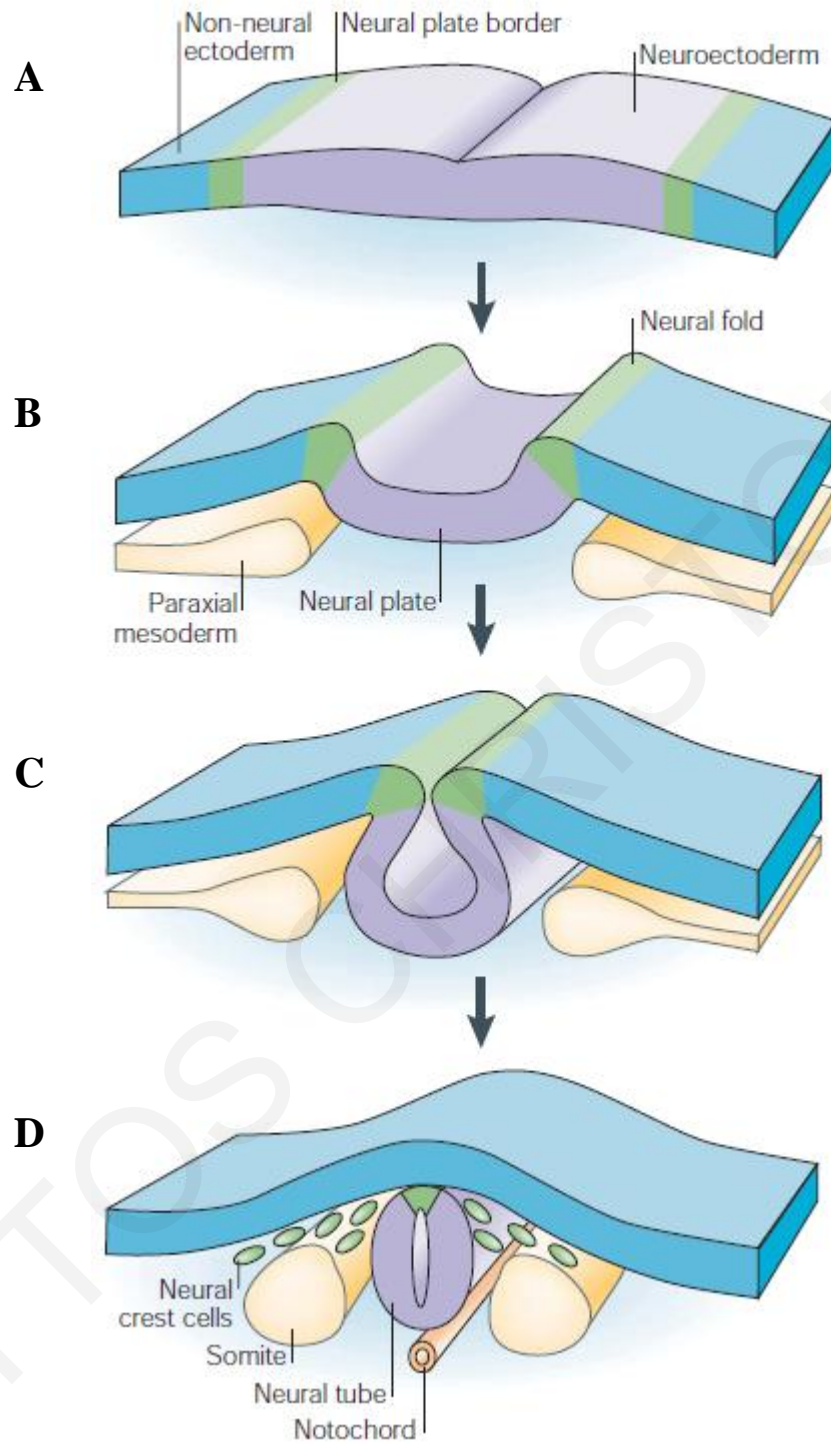


Figure 13. Primary neurulation (neural tube closure). Adapted from (Gammill and Bronner-Fraser, 2003).

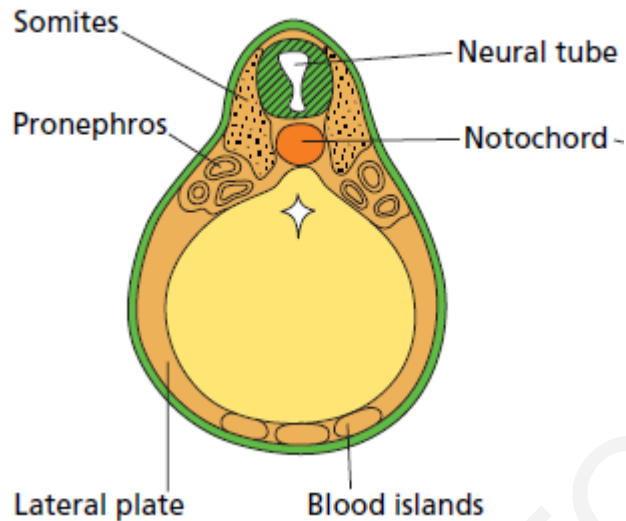


Figure 14. Cross section of a tailbud embryo. Adapted from (Slack, 2006).

1.6 Neural Tube Closure

Neural tube closure (NTC) is one of the most fundamental events during vertebrate development and is responsible for the development of the CNS in vertebrates. Failure of this process results in Neural Tube Defects (NTDs) which are one of the most common human birth defects. NTDs are present in 1 to 1000 human births (Copp et al., 2003). Experimentation using animal models has revealed that failure of NTC is due to either defects in cell fate or in morphogenetic movements (Wallingford, 2005). The process of NTC is a dynamic process governed by intrinsic and extrinsic forces. Intrinsic forces include cell rearrangements and cell shape changes within the neural plate resulting in the lengthening of the neural plate, the elevation of the lateral edges of the neural plate (neural folds), their medial movement and finally their fusion for the formation of the neural tube (Figure 13). The intrinsic forces are governed by two distinct morphogenetic processes, **Convergent Extension (CE)** and **Apical Constriction (AC)**. In addition to these morphogenetic movements oriented cell divisions and programmed cell death are necessary for NTC (Kieserman and Wallingford, 2009). **CE** is responsible for the lengthening and narrowing of the neural plate. **AC** is responsible for the bending of the neural plate, the formation of the neural groove, the elevation of neural folds, their bending and their fusion (Wallingford, 2005). Failure of each one of these process results in failure of NTC, albeit with differences with respect to the precise region that is affected. For example failure of AC results mainly in failure of rostral NTDs (exencephaly or anencephaly) and secondarily in caudally restricted spina bifida (meningomyelocele). Defective CE is linked with craniorachischisis and spina bifida (Suzuki et al., 2012; Wallingford et al., 2013) (**Figure 15**). Interestingly, individual genes have been linked

only with CE or only with AC (Wallingford, 2005). However some genes like Dishevelled (Kinoshita et al., 2008; Wallingford and Harland, 2002) and Shroom3 (Haigo et al., 2003; McGreevy et al., 2015; Simoes Sde et al., 2014) are implicated in both processes showing that the two processes are regulated via common pathways. The extrinsic forces contributing to NTC are the medial migration of the epidermis and the inductive and mechanical contribution from the underlying mesoderm (Suzuki et al., 2012; Wallingford, 2005).

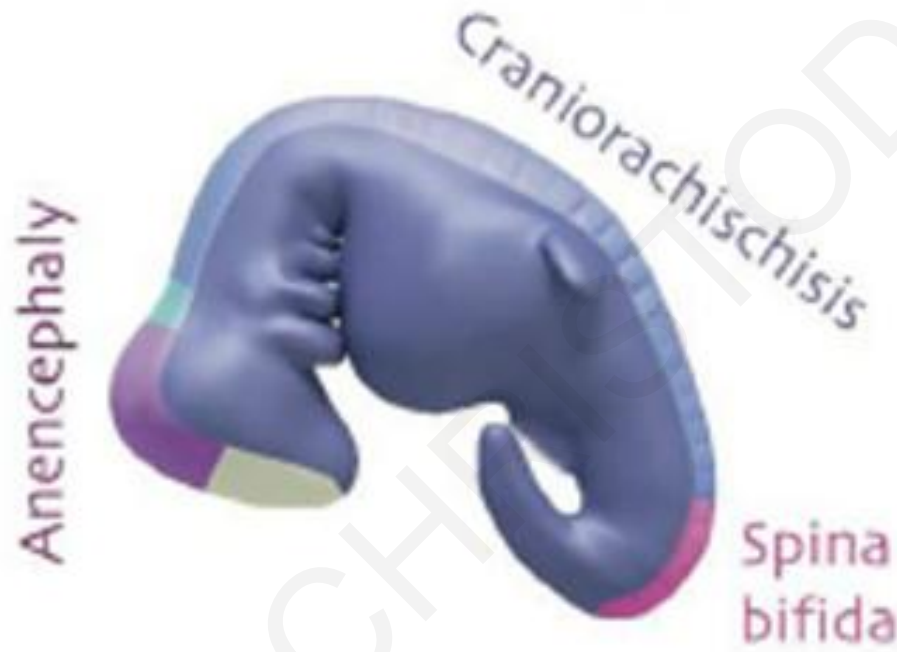


Figure 15. Neural Tube Defects Adapted from (Walingford et al., 2013).

1.7 Convergent extension

Convergent extension (CE) is the morphogenetic movement that results in the thinning and the elongation of tissues through polarized collective cell movements. (Figure 11)(Keller, 2002; Tada and Heisenberg, 2012). CE contributes to blastopore and NTC during gastrulation and neurulation respectively and is the major force driving the elongation of the A/P axis (Wallingford et al., 2002; Wallingford and Harland, 2001) (Figure 16). Moreover, CE contributes to the formation of organs such as the kidney (Castelli et al., 2013). Defective CE in mesodermal tissues results in failure or delay of blastopore closure and shorter A/P axis. Defective CE in the neural tissues results in NTDs and shorter A/P axis.

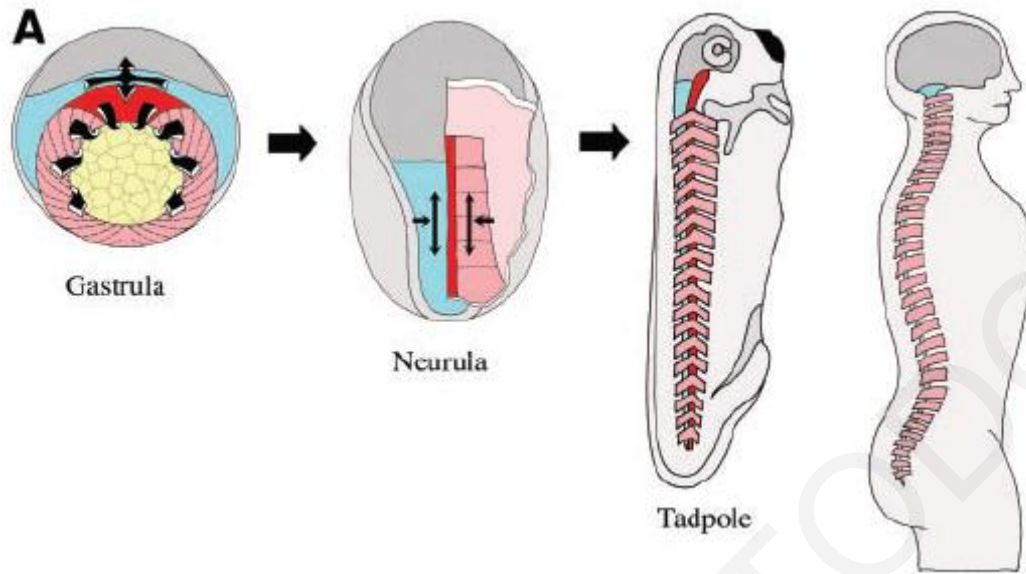


Figure 16. Convergent extension movements elongate the anterior-posterior.

The notochordal (red) and somitic (pink) tissues turn inside and converge (narrow) and extend (lengthens) in the gastrula and neurula stages of the frog embryo. The overlying presumptive hindbrain and spinal cord (blue) tissues converge and extend coordinately but on the outside of the embryo. These movements push the head away from the tail and elongate the body axis of the tadpole. Similar movements elongate the body axis of mammals. Adapted from (Keller, 2002).

CE is conserved among different organisms and tissues driving the narrowing and elongation of mesenchyme as well as of epithelial tissues (Tada and Heisenberg, 2012). During CE oriented exchanges of neighboring cells alter tissue geometry. Cell intercalation is oriented mediolaterally leading to elongation of the A/P axis. Intercalation in different tissues seems to be governed by distinct mechanisms or is the result of different mechanisms cooperation (Tada and Heisenberg, 2012). Polarization of cells is indispensable for proper intercalation during CE. This polarization is governed by the planar cell polarity (PCP) pathway (Wang et al., 2006) as it will be discussed in the next paragraphs.

1.7.1 Mesenchyme Convergent Extension: a case of intercalation driven by mediolaterally polarized protrusion activity?

The first mechanical insight about CE came out after pioneering experiment from Keller. With the use of embryonic explants (Keller explants, **Figure 17**) and live imaging, Keller found that during CE of the mesenchyme chordamesoderm tissue cells show mediolateral (M/L) driven intercalation. This polarized movement results in the elongation and narrowing of the chordamesoderm tissue (**Figure 11**). The movement depends on polarized protrusive activity. Before M/L intercalation, protrusive activity occurs in all directions but when intercalation

begins, protrusions are mediolaterally oriented (Keller et al., 2000; Wallingford et al., 2002). M/L protrusions attach to adjacent cells and crawl on adjacent cells. The tractive foci formed by these protrusions depend on pulsed actomyosin contractions (Kim and Davidson, 2011). This results to the elongation of cells along their M/L axis and drives M/L intercalation (**Figure 18**) and tissue elongation and narrowing (**Figure 11**) (Keller et al., 2000; Wallingford et al., 2002). The same mechanism drives neural CE in *Xenopus*. Neural cells intercalate by mediolaterally oriented protrusions or they can be induced by signals generated by the midline and intercalate using monopolar, medially polarized protrusions (Elul and Keller, 2000). Experiments in *Xenopus* have shown that the non canonical Wnt/PCP pathway and the Wnt/Ca²⁺ but not the canonical Wnt pathway are implicated in CE (Wallingford et al., 2002). As Wallingford et al. elegantly showed, disruption of the Wnt/PCP using a Dishevelled dominant negative blocked CE. These defects in CE were attributed to loss of protrusions polarity during intercalation (**Figure 19**) (Wallingford et al., 2000). M/L intercalation and CE in *Xenopus* also depends on myosin activity, as actomyosin contraction pulses are observed during cell intercalation and are necessary for the maintenance of the tractive foci (Kim and Davidson, 2011). Moreover mesoderm CE depends on cell-cell and cell-Extracellular Matrix (ECM) adhesion. At the same time intercalating cells bind to ECM through integrins and to their neighboring cells through cadherins. These cell behaviors and their regulation by the PCP pathway is conserved among different organisms (Tada and Heisenberg, 2012).

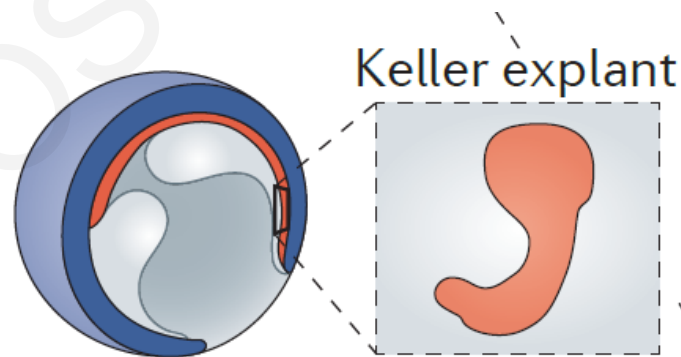


Figure 17. Keller explant

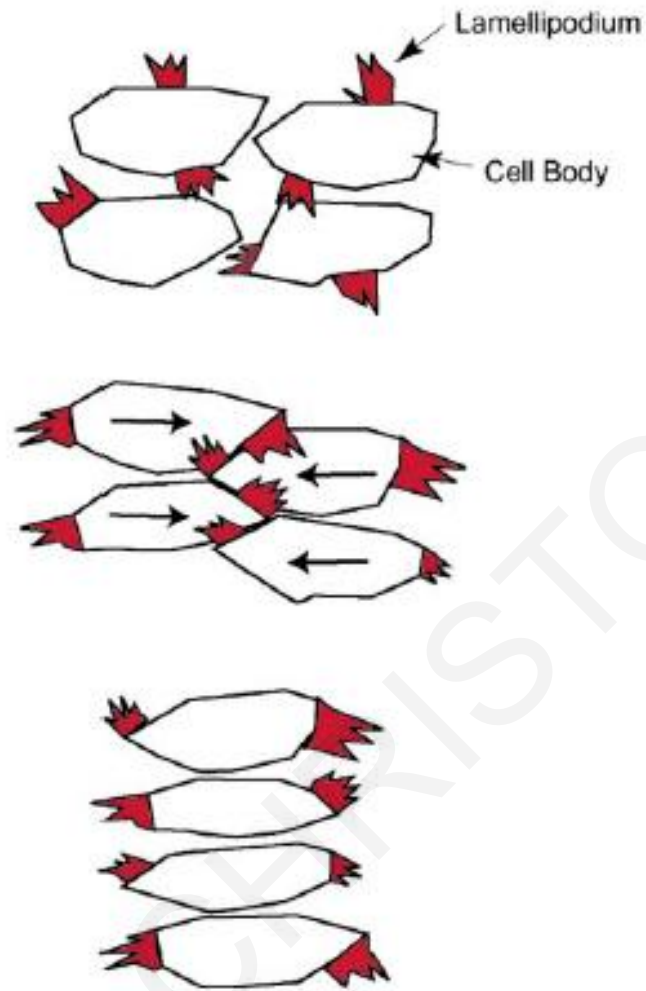


Figure 18. Polarized protrusive activity drives Convergent Extension in mesoderm mesenchymal cells.

Prior to the onset of gastrulation, cells extend and retract lamellipodia randomly. As convergent extension begins, cells align mediolaterally, and stabilize lamellipodia at their medial and lateral ends. The stable lamellipodia attach to mediolaterally neighboring cells and exert traction, pulling the cells between one another. Adapted from (Wallingford et al., 2002).

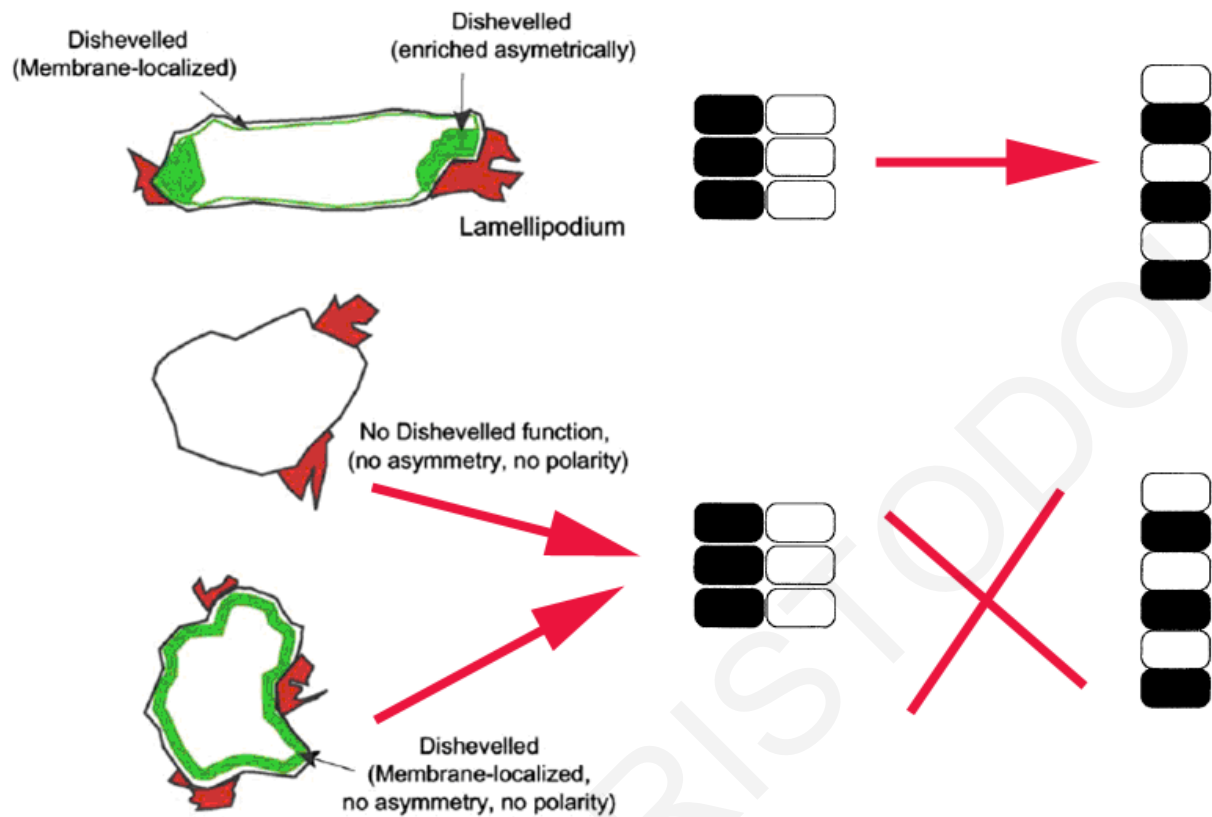


Figure 19. PCP signalling and cell polarity during Convergent extension.

PCP signaling controls polarity of protrusions which is necessary for proper Convergent extension. Both over activation and blockage of PCP pathway disrupt polarity of protrusions and result in defective Convergent extension. Adapted from (Wallingford et al., 2002)

1.7.2 Convergent Extension: a case of cell-cell adhesions remodeling

In epithelial tissues, neighboring cells adhere to one another via adherens and tight junctions.

Therefore CE in epithelial tissues places unique demands. During epithelial intercalation cells must maintain their adhesion and at the same time retain their adhesion. Therefore M/L intercalation in epithelial is not driven by crawling of cells through polarized protrusions but is driven by active rearrangement of cell-cell adhesions and cell intercalation from top to bottom. During *Drosophila* development Germband narrows along its D/V axis and extends at its A/P in a process called Germband extension (GBE) (Irvine and Wieschaus, 1994). Bertet et al. demonstrated that planar polarized junctional myosin activity is necessary for planar polarized junction remodeling and CE (Bertet et al., 2004). Adhesion proteins such as E-cadherin show enriched A-P localization during GBE (Blankenship et al., 2006), generating anisotropy of cortical tension along the apical cell junctions which is necessary for GBE (Rauzi et al., 2008). At the beginning of GBE tetrads of cells form around type 1 junctions. In type 1 junctions (or v-junctions according to (Rauzi et al., 2008)) adjacent cells along the A-P axis are in contact while

cells found in the D-V axis are not in contract (**Figure 20A**). As GBE precedes type 1 junctions significantly shrink leading to configuration where the 4 cells share equal contacts. This new configuration is named type2 junctions. Subsequently type 3 junctions are built perpendicular to type 1 junctions leading to neighbor exchange and cell intercalation (**Figure 20 A**). These events lead to the elongation and narrowing of the tissue (**Figure 20B**). This process is called T1-T3 transition and is regulated by planar polarized activity of myosin (**Figure 20C**). The planar polarized function of myosin is regulated by tension in a positive feedback loop (Fernandez-Gonzalez et al., 2009) and is enhanced by polarized flow of medial actomyosin towards v-junctions for shrinkage of v-junctions (Rauzi et al., 2010; Sawyer et al., 2011). This polarized myosin flow is directed by PCP polarized fluctuations of E-cadherin levels which are triggered by polarized endocytosis of E-Cadherin (Levayer and Lecuit, 2013) (**Figure 21**).

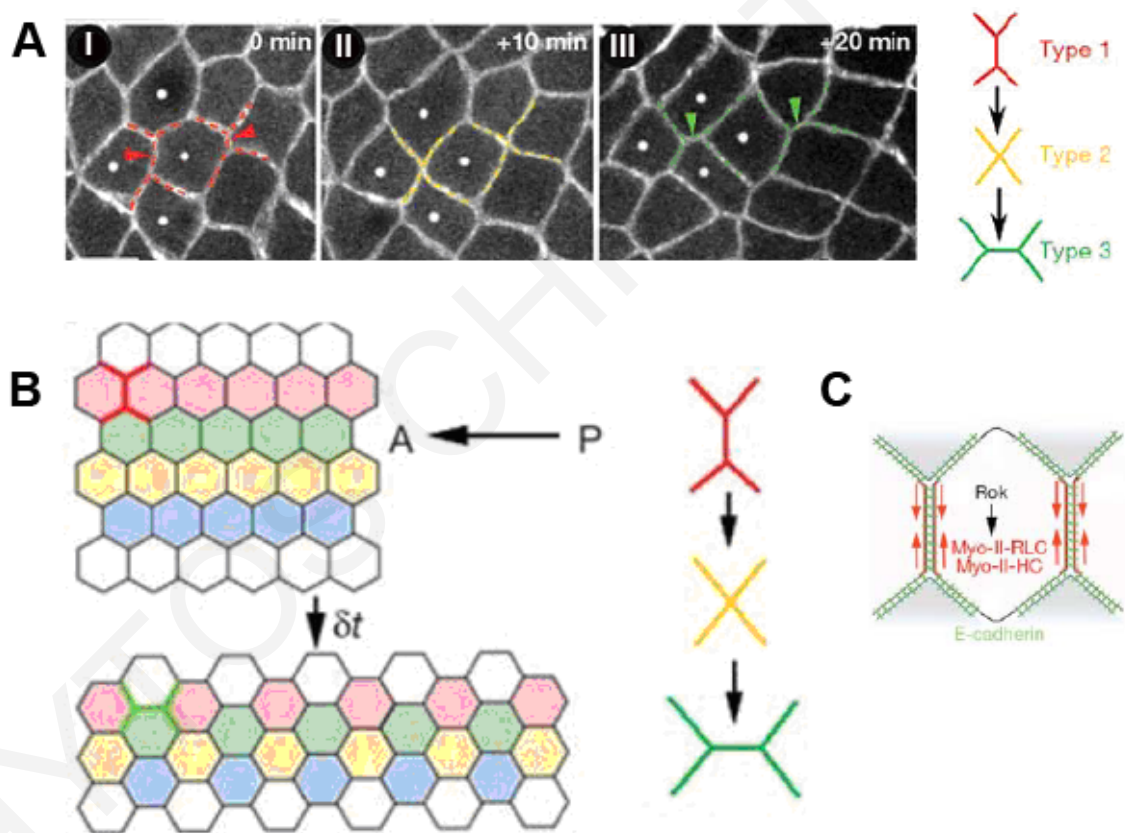


Figure 20. Polarized junction remodelling drives convergent extension during *Drosophila* GBE.

(A) Cell contacts in the type 1 configuration (red dashed line in I) progress towards the type 2 (yellow dashed line in II) and to the type 3 configuration (green dashed line in III). (B) Model: planar cell intercalation depends on the polarized remodeling of junctions along the A/P axis. This process is controlled by the polarized recruitment of myosin II (Myo-II) in a subset of cell junctions (C), thereby forcing polarized junction remodeling. Adapted from (Bertet et al., 2004).

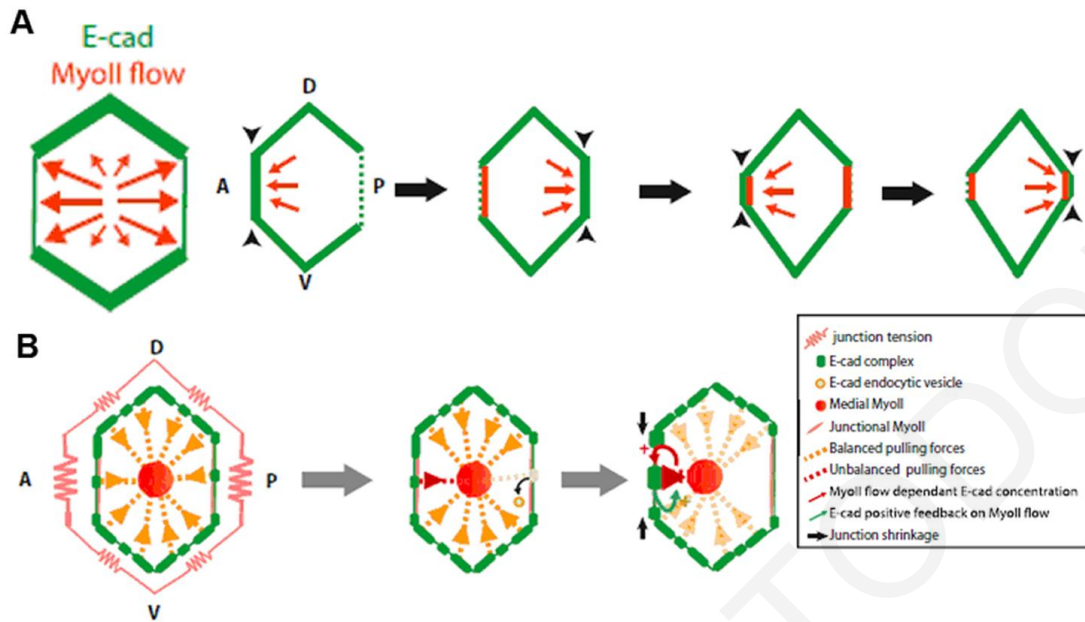


Figure 21. Model of the E-Cad-Dependent MyoII Flow Initiation and Oscillatory Behavior during Germ Band Extension.

(A) MyoII flows alternate anterior and posterior directions (orange arrows) and correlate with imbalances of E-cad integrated intensity (green lines) between facing DV junctions. Each flow induces junction shrinkage (black arrowheads) and local deposition of MyoII in the junction plane (orange lines). (B) Model of MyoII flow initiation. Medial MyoII pulls on junctions through its anchoring to E-cad complexes (orange dashed lines). Junction tension is set by the junctional pool of MyoII (pink lines). E-cad endocytosis breaks anchoring points, thereby generating an imbalance of medial MyoII pulling forces (red dashed line) and initiating flow toward the facing junction. Flow initiation increases E-cad concentration in the facing junction, which feeds back positively on E-cad asymmetry and MyoII flow. A, anterior; P, posterior; D, dorsal; V, ventral. Adapted from (Levayer and Lecuit, 2013).

Another mechanism which contributes to epithelial M/L intercalation during CE is multicellular rosette formation and resolution. When two or more T1 junctions shrink simultaneously through polarized myosin contraction, multicellular rosettes are formed (Blankenship et al., 2006). Subsequently rosettes dissolved via formation of new junctions which are parallel to the A/P axis. These cell movements and neighbor-cell exchange result in the narrowing of the D/V axis and the elongation of the A/P axis (**Figure 22**) (Blankenship et al., 2006). Polarized junction remodeling is a conserved mechanism regulating M/L intercalation during CE. Both T1-T3 transitions and multicellular rosettes formation have been identified during CE of vertebrate epithelial tissues. T1 transitions have been imaged during CE in chicken and mouse embryos neuroepithelium (Nishimura et al., 2012; Williams et al., 2014). Moreover rosette formation and resolution has been documented during CE in mouse and chicken neural plates (McGreevy et al., 2015; Williams et al., 2014), as well as during kidney tubule formation in mouse and *Xenopus* embryos (Karner et al., 2009; Lienkamp et al., 2012) and in the cochlea of mammalian inner ear (Chacon-Heszele et al., 2012; Wang et al., 2005).

Despite the necessity for planar polarized activity of myosin and Rho kinase (Simoes Sde et al., 2014) it has been shown that PCP pathway signaling is not necessary for T1 transition and rosette formation and resolution during *Drosophila* GBE (Zallen and Wieschaus, 2004), while A/P patterning is indispensable for CE in this tissue (Irvine and Wieschaus, 1994). In contrast PCP signaling is necessary for junction remodeling driven CE in all vertebrate tissues (Lienkamp et al., 2012; McGreevy et al., 2015; Wang et al., 2005; Williams et al., 2014), regulating the planar localization of key molecules (McGreevy et al., 2015; Nishimura et al., 2012). This is in agreement with the role of PCP signaling as described in CE driven by polarized protrusions (Wallingford et al., 2000).

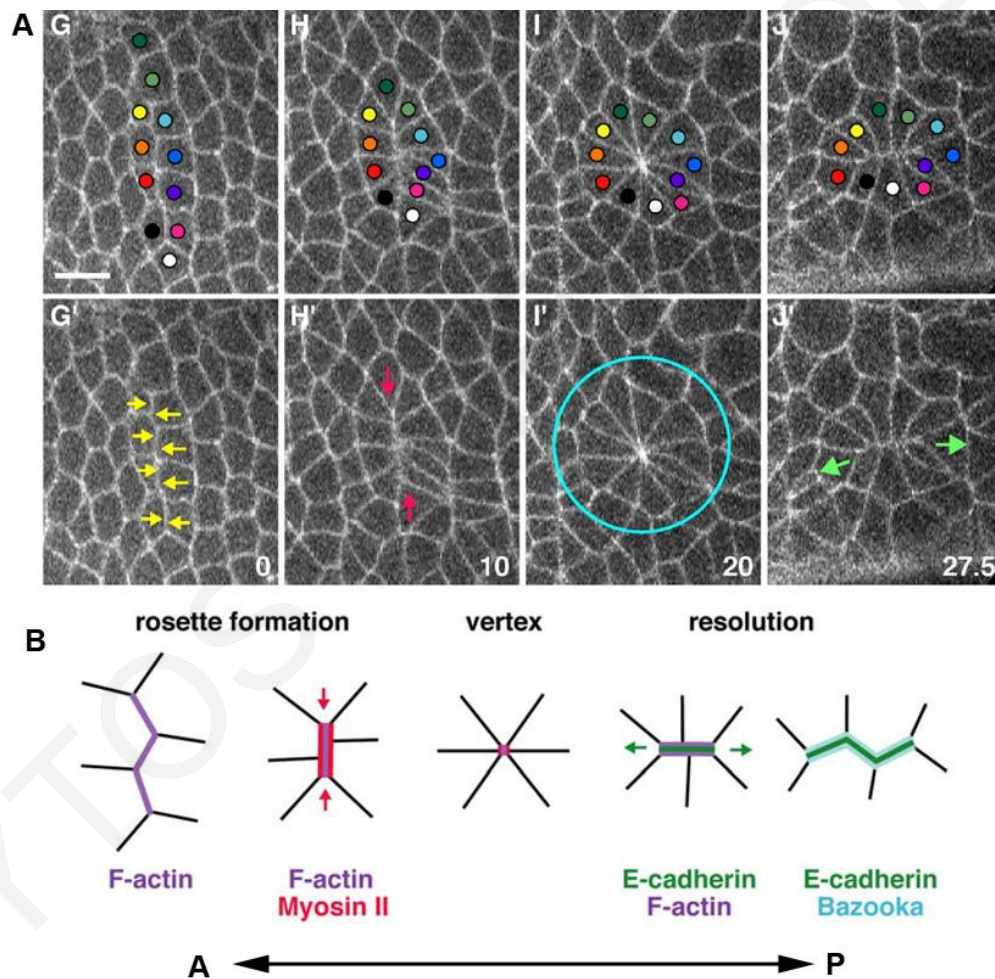


Figure 22. Multicellular Rosette Formation in Intercalating Cells.

(A) Time-lapse images of a single rosette. During rosette formation, two columns of cells initially align (edges that will contract are indicated by yellow arrows). Adjacent pairs of cells constrict their shared interfaces in concert during rosette formation (the direction of convergence is indicated by red arrows). Multiple cells come into simultaneous contact at a high-order vertex (the 11-cell rosette is indicated by a blue circle). This apparently symmetric structure resolves in a strictly directional fashion during rosette resolution (the direction of extension is indicated by green arrows). (B) Model of rosette formation and resolution. Adapted from (Blankenship et al., 2006)

1.7.3 Convergent extension driven by polarized junction remodeling and polarized protrusions

Two distinct mechanisms regulating M/L intercalation and CE are conserved among different organisms. Polarized protrusive activity drives M/L intercalation through the cell-cell traction model (Keller et al., 2000). Polarized junction remodeling drives M/L intercalation either through T1 transitions or through cellular rosettes formation and resolution (Bertet et al., 2004; Blankenship et al., 2006). Two recent studies have shown that these two mechanisms can coexist in the same tissue and are both contributing to CE. In the first study, Shindo and Wallingford studied the behavior of cell-cell junctions during *Xenopus* mesoderm CE (Shindo and Wallingford, 2014). In this study, it has been demonstrated that myosin localization and activity in mesoderm mesenchyme tissue is planar polarized along the junctions which are parallel to the M-L axis (v-junctions). The polarized localization of myosin is governed by Septins. In addition, myosin contractility leads to shrinkage of v-junctions and induced M/L cell intercalation (**Figure 23**). Loss of polarized myosin activity and defective PCP pathway lead to failure of CE (Shindo and Wallingford, 2014). In the same tissue M/L intercalation is driven by polarized protrusive activity which is regulated downstream of the PCP pathway (**Figure 18**). Therefore mesoderm CE in *Xenopus* needs both polarized protrusion activity and polarized junction remodeling.

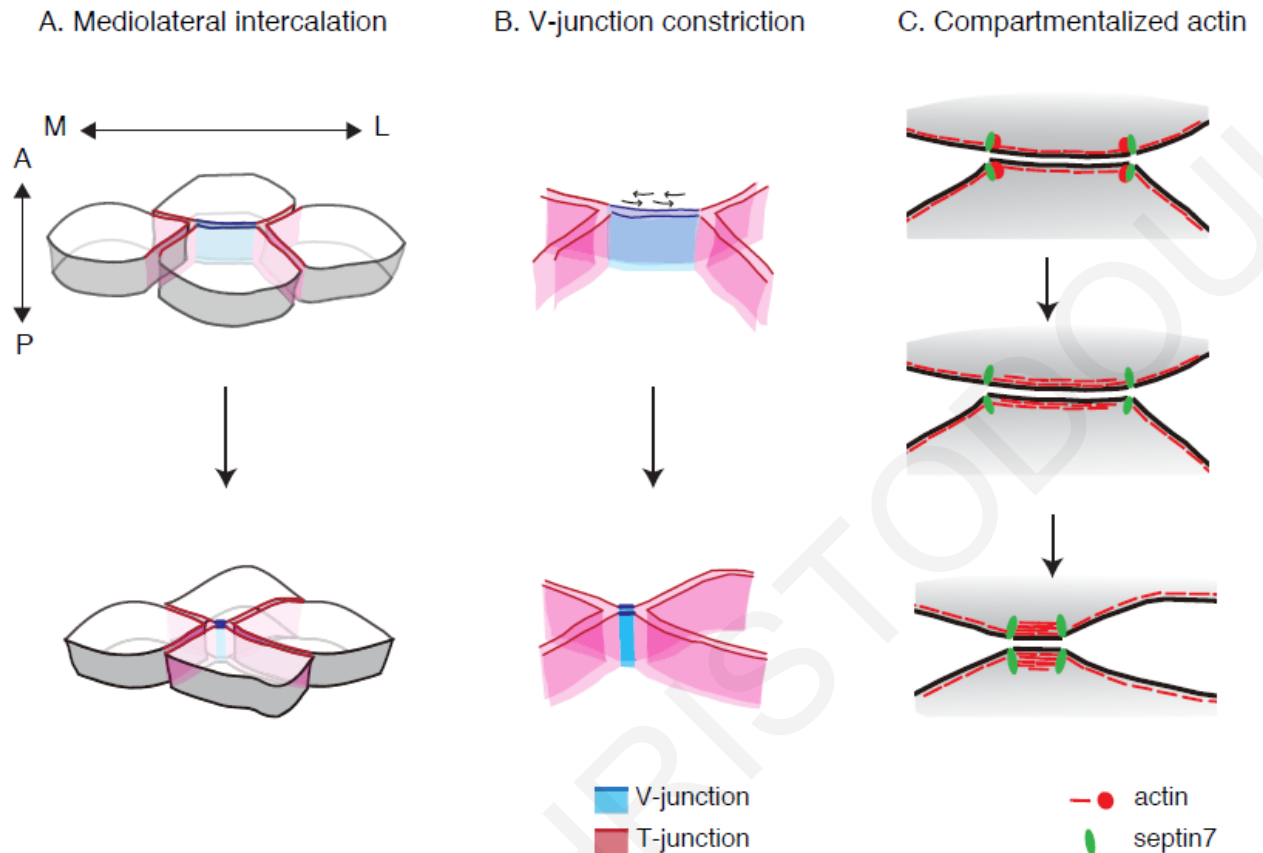


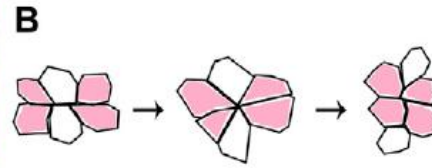
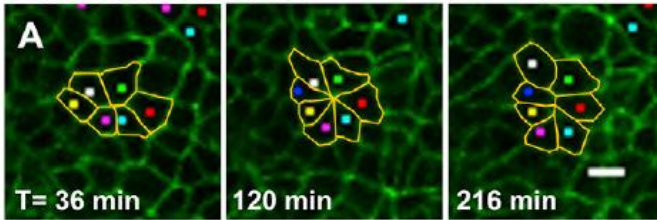
Figure 23. Medirolateral intercalation mediated by septin-dependent cortical actomyosin activity.

(A) Cell behavior during M/L intercalation. The v-junction is colored blue, and t-junctions are colored red. (B) Cortex dynamics during M/L intercalation. Actomyosin activity shrinks the v-junction. (C) Schematic diagram of v-junction shortening by spatially restricted actomyosin activation. septin7 and actin accumulate at vertices, and actomyosin is activated inside v-junctions compartmentalized by septin7, resulting in shrinkage of the v-junction due to spatially restricted-actomyosin activation. Adapted from (Shindo and Wallingford, 2014).

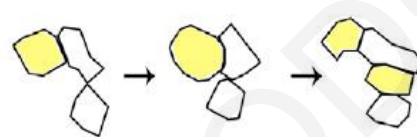
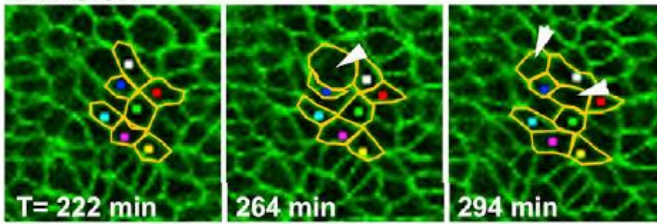
In a second study, Williams et al. studied cell behavior during CE in the mouse neural plate. During mouse NTC, M/L intercalation was driven by rosette resolution, polarized divisions, single cells intercalation and T1 process (**Figure 24**) (Williams et al., 2014). While polarized junction remodeling was observed at the apical cell ends, at the same time polarized protrusive activity and M/L cell elongation was taking place at the basal end of the cells (**Figure 25**) (Williams et al., 2014). The forces generated by both apical junction remodeling and M/L intercalation through protrusive activity at the basal ends were necessary for CE. Apical boundary rearrangement and biased basolateral protrusive activity are dependent on PCP signaling (Williams et al., 2014).

In conclusion, the data from these two studies indicate that polarized junction remodeling and protrusive activity contribute to M/L intercalation during CE.

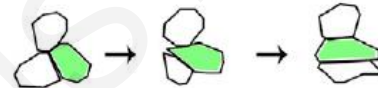
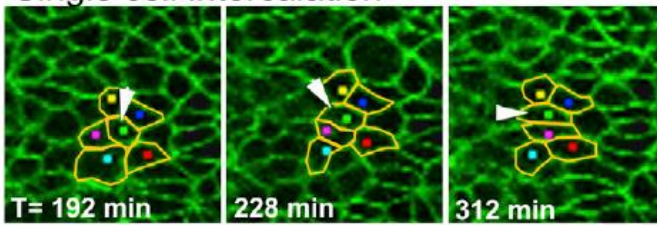
Rosette Resolution



Division



Single cell intercalation



T1 process

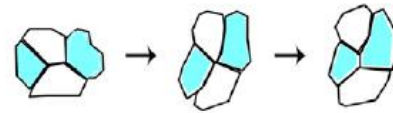
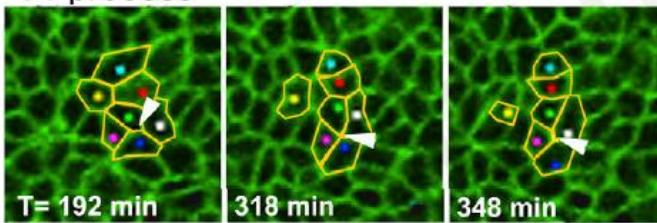


Figure 24. Epithelial Rosettes, cell division, single cell intercalation and T1-process drive mediolateral intercalation within the Neural Plate.

(A) Snapshots from time-lapse movies. Each series represents one type of neighbor exchange observed in the neural epithelium, as indicated by yellow outlines and arrowheads. Anterior is up (B) Schematic summary of each type of neighbor exchange. White cells represent an adjacent cell pair that is separated. Adapted from (Williams et al., 2014).

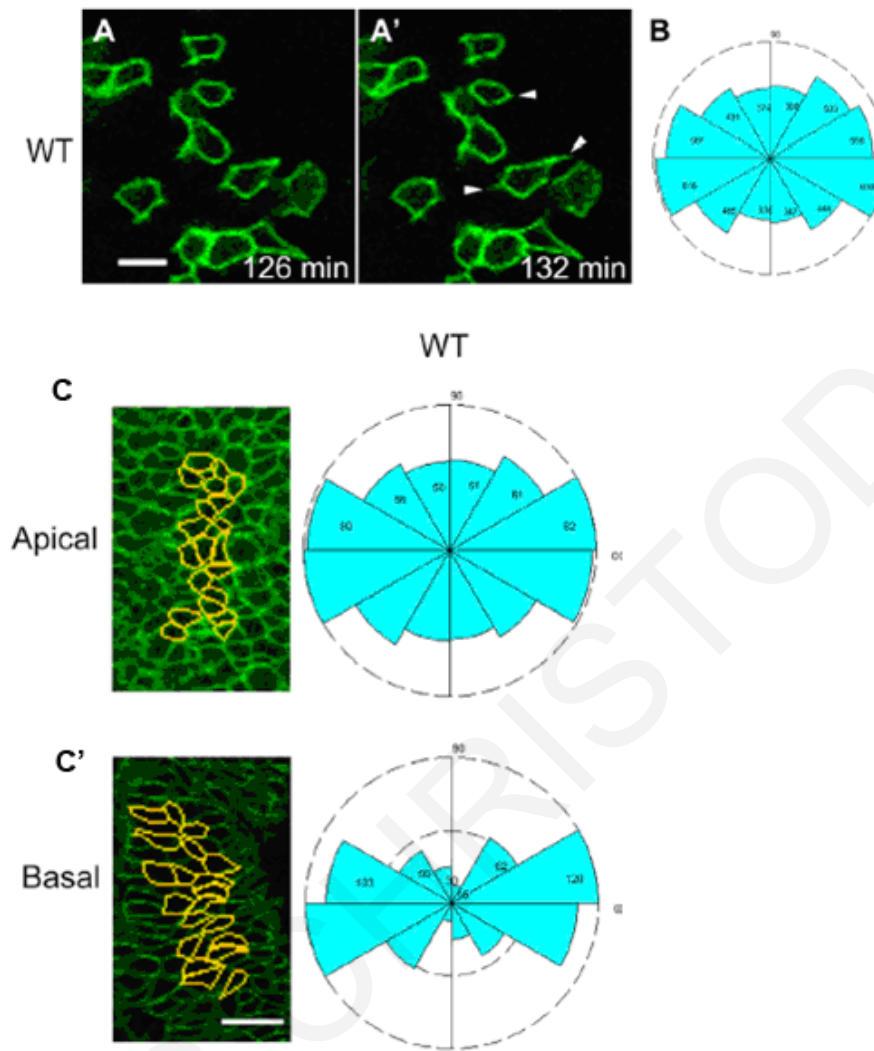


Figure 25. Cells of the Neural Plate exhibit polarized basal protrusive activity and basolateral cell elongation. (A) Still shots from time-lapse movies from neural plates. Arrowheads indicate protrusions that have appeared in subsequent (4 or 6 min) time frames. Anterior is up. (B) Rose diagram indicate the direction of protrusions made by neural plate cells within the indicated embryo type. (C) Cell shape and orientation of the apical and basal ends of neural plate cells Yellow outlines indicate cells measured, and rose diagrams indicate the orientation of major cell axes. Anterior is up and corresponds to 90° in diagrams. Scale bars, 20 μm. Adapted from (Williams et al., 2014).

1.8 Apical Constriction

Apical constriction (AC) induces cell shape changes which are generating forces for the remodeling of flat epithelial tissues during morphogenesis (Martin and Goldstein, 2014; Sawyer et al., 2010). AC is defined by shrinkage of the apical cell surface, a phenomenon which is often coupled to apicobasal axis elongation. Therefore cell shape changes during AC, in many examples, drive the conversion of columnar cells to wedge shaped cells with the cell volume remaining constant (Martin and Goldstein, 2014; Sawyer et al., 2010) (**Figure 26**).

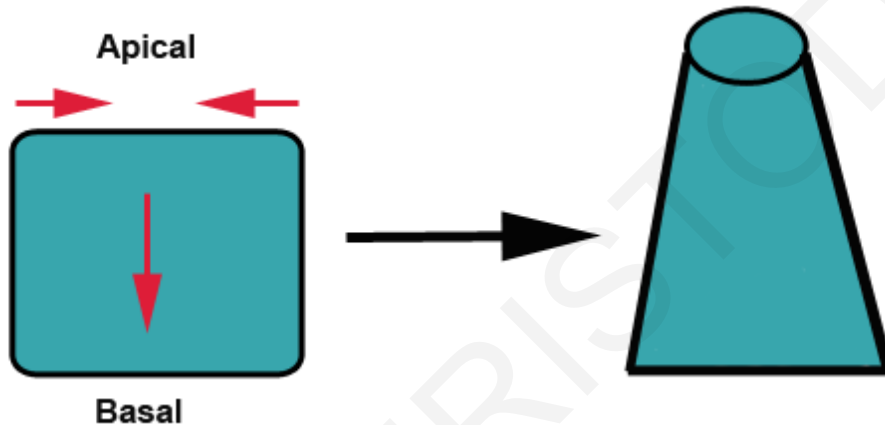


Figure 26. Apical Constriction induced cell shape changes.

Cell shape changes driven by AC have various consequences depending on the physiological context. AC generates the forces for the bending and folding of tissues. In addition, AC contributes to the formation of tubes.

Some examples of AC driven morphogenetic movements will be analyzed in the next paragraphs. AC drives the invagination of *Xenopus* bottle cells during gastrulation, a process which is necessary for the initiation of mesoderm involution (Sawyer et al., 2010) (**Figure 27**).

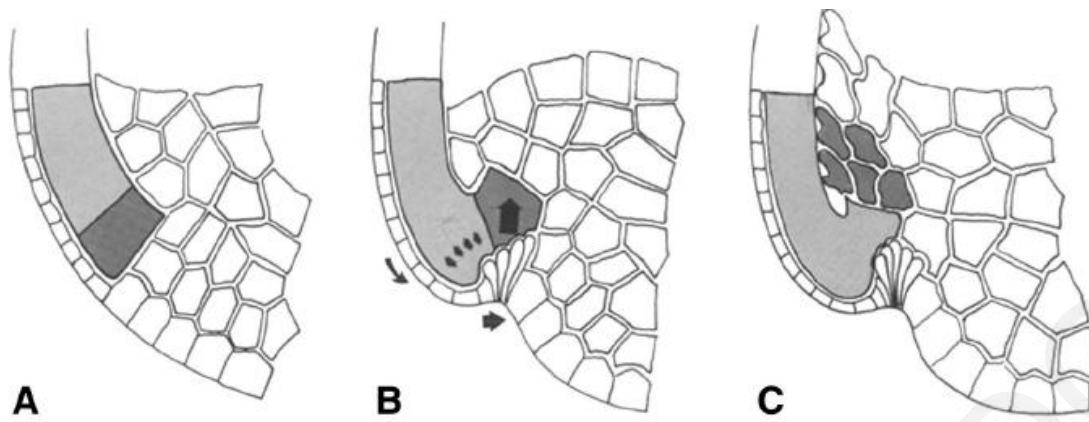


Figure 27. Apical Constriction drives the invagination of bottle cells in *Xenopus*.

Schematic diagrams of bottle cell formation. All images approximate midsagittal views. (A) Prior to gastrulation, the prospective anterior mesoderm (darker shading) and posterior mesoderm (lighter shading) comprise the deep marginal zone. (B) The bottle cells have undergone AC. Arrows indicate movements hypothesized to result. (C) This causes reorientation of the vegetal edge of the marginal zone (anterior mesoderm) such that it is now leading the movement into the blastocoel

In addition, AC has a central role during *Drosophila* gastrulation driving ventral furrow formation. (Figure 28)(Sawyer et al., 2010).

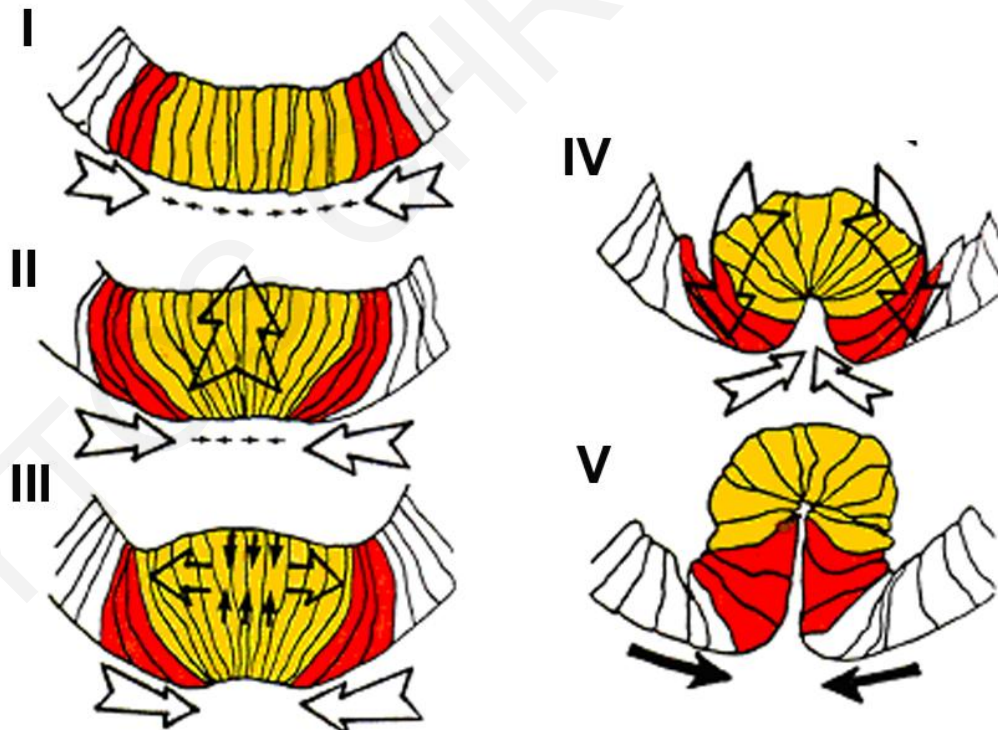


Figure 28. Apical Constriction during *Drosophila* ventral furrow formation.

Cells that apically constrict are colored yellow. Adjacent cells in the ventral plate that develop flattened apical surfaces but do not constrict apically are colored red-orange. Small arrows outside or within cells represent the presumed vectors of forces within these cells as a result of AC or cell elongation or shortening. Larger arrows indicate cumulative forces predicted from the combined forces of individual cells. Adapted from (Sawyer et al., 2010).

During Dorsal Closure in *Drosophila*, epithelial sheets migrate from each site of the embryo to close a hole which is transiently filled with the extraembryonic amnioserosa epithelium (**Figure 29**). Several studies have shown that active AC of amnioserosa epithelial cells is indispensable for dorsal closure (Solon et al., 2009).

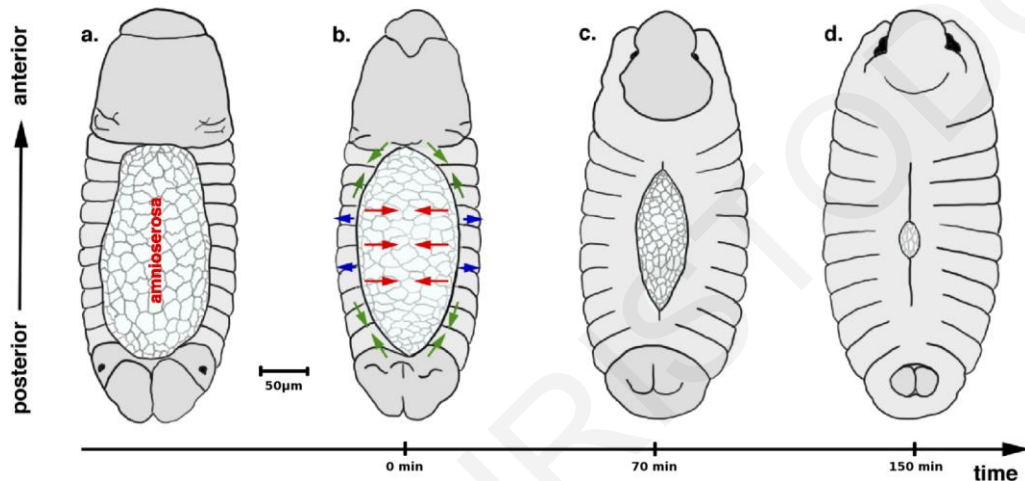


Figure 29. Dorsal-view illustration of the four stages of Dorsal Closure.

(a) initiation/early phase, (b) convergence of epithelial sheets/slow phase, (c) zippering/fast phase and (d) termination. Arrows indicate tissue-level forces: amnioserosa-driven pulling (red), actomyosin cable tension (green) and lateral epidermis pulling (blue).

AC has also been implicated in wound healing. Closure of superficial wounds in *Xenopus* resembles *Drosophila*'s dorsal closure as **Figure 30** shows. Davidson et al have shown that contraction of the deep cells generates the force for wound closure (Davidson et al., 2002a).

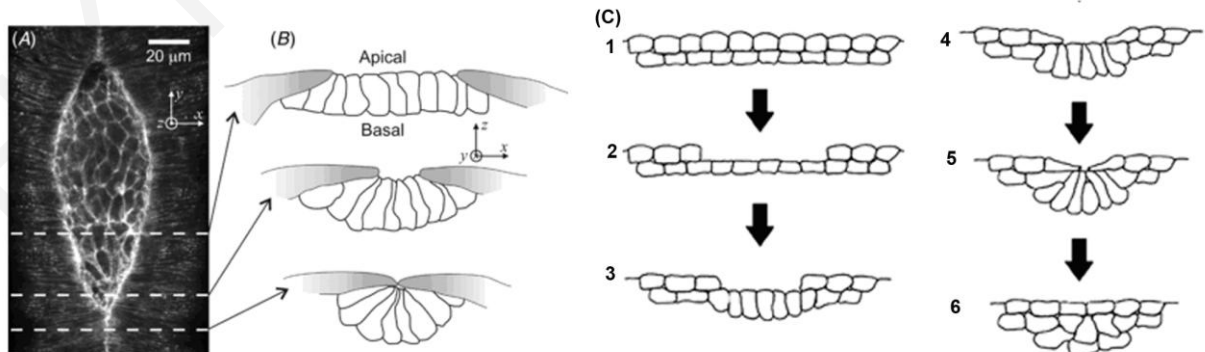


Figure 30. Apical Constriction and wound healing.

Dorsal (A) and sagittal (B) view of *Drosophila* Dorsal Closure. (C) Sagittal view of wounded *Xenopus* animal cap cells. Deep cells undergo AC generating forces contributing to wound healing. Adapted from (Davidson et al., 2002a).

Importantly, AC is implicated in vertebrate's NTC. AC induced cell shape changes in the neuroepithelial cells generate forces for the bending of the neural plate and the formation of the neural tube. During AC neuroepithelial cells narrow their apical surface and elongate their apicobasal axis (Suzuki et al., 2012) (**Figure 31A**). In *Xenopus* embryos these two cell shape changes occur at the same time (Lee et al., 2007) (**Figure 31B,C**). In other vertebrate animals, cell elongation precedes AC (Schoenwolf and Franks, 1984). Defective of neuroepithelial cells results in Neural Tube Defects (NTDs), in most cases anterior NTDs (Suzuki et al., 2012).

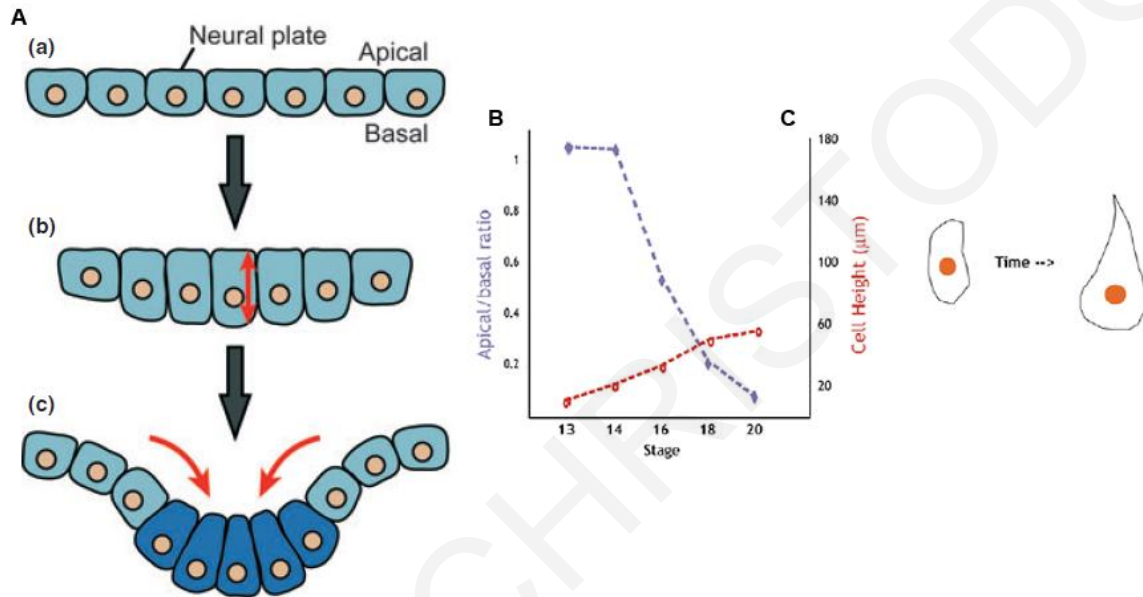


Figure 31. Cell shape changes of neuroepithelial cells undergoing Apical Constriction.

(A) The process of cell shape change. (a) Prior to neurulation, the shape of the neuroepithelial cell is cuboidal. (b) Cell elongation. The neuroepithelial cells first elongate along apicobasal axis to become columnar. (c) AC. After cell elongation starts, cell apices are constricted and minimized, causing cells to adopt wedge or bottle-like shapes from columnar ones. Adapted from (Suzuki et al., 2012). (B) Graph illustrating changes in AC (blue; ratio of apical surface to basal surface measured from cross-sections) and apicobasal cell elongation (red; cell height) of *Xenopus* neuroepithelial cells during NTC (stages 14-19). (C) Schematic illustrating the change in neural epithelial cell shape during NTC. Adapted from (Lee et al., 2007).

Moreover AC has a fundamental role during organogenesis. Specifically several studies have demonstrated that AC is necessary during eye development (Borges et al., 2011; Plageman et al., 2011; Plageman et al., 2010). In addition AC drives the formation of tubular organs such as the gut (Chung et al., 2010). Finally, AC is involved in the formation of all placodes by generating forces for tissue invagination (Llimargas and Casanova, 2010).

1.8.1 Mechanisms driving Apical Constriction induced cell shape changes.

The two main cell shape changes induced by AC is apical surface contraction and apicobasal axis elongation (Sawyer et al., 2010). Apical surface narrowing seems to be consistent from invertebrates to vertebrates while apicobasal elongation is found in most of the cases documented(Sawyer et al., 2010). Are the mechanisms driving these cell shape changes conserved between different organisms? In the next paragraphs we'll try to answer this question.

1) Apical surface narrowing

Contraction of actin filaments by the motor protein myosin (actomyosin complex) is a conserved mechanism driving apical surface constriction in different organisms. The forces generated by the contraction of the actomyosin complex are exerted on the apical cortex through linkage of actin filament with sites of cell-cell adhesion(Martin and Goldstein, 2014). Although the machinery driving apical surface constriction is conserved in different organisms and tissues its organization varies among different organisms and tissues (Martin, 2010). The actomyosin complex can be organized as a bundle or as a meshwork. In actomyosin bundles, actin filaments are aligned with myosin forming a cable. Actomyosin cables can adopt the repeated organization of the muscle sarcomere or can exist with no obvious polarity (**Figure 32A,B**). In actomyosin meshworks, actin filaments and myosin are intertwined in a mesh, forming a two dimensional meshwork (**Figure 32C**). Sliding of myosin on actin filaments generates contractile forces driving the contraction of actomyosin cables and meshworks (**Figure 32A-C**) (Martin, 2010).

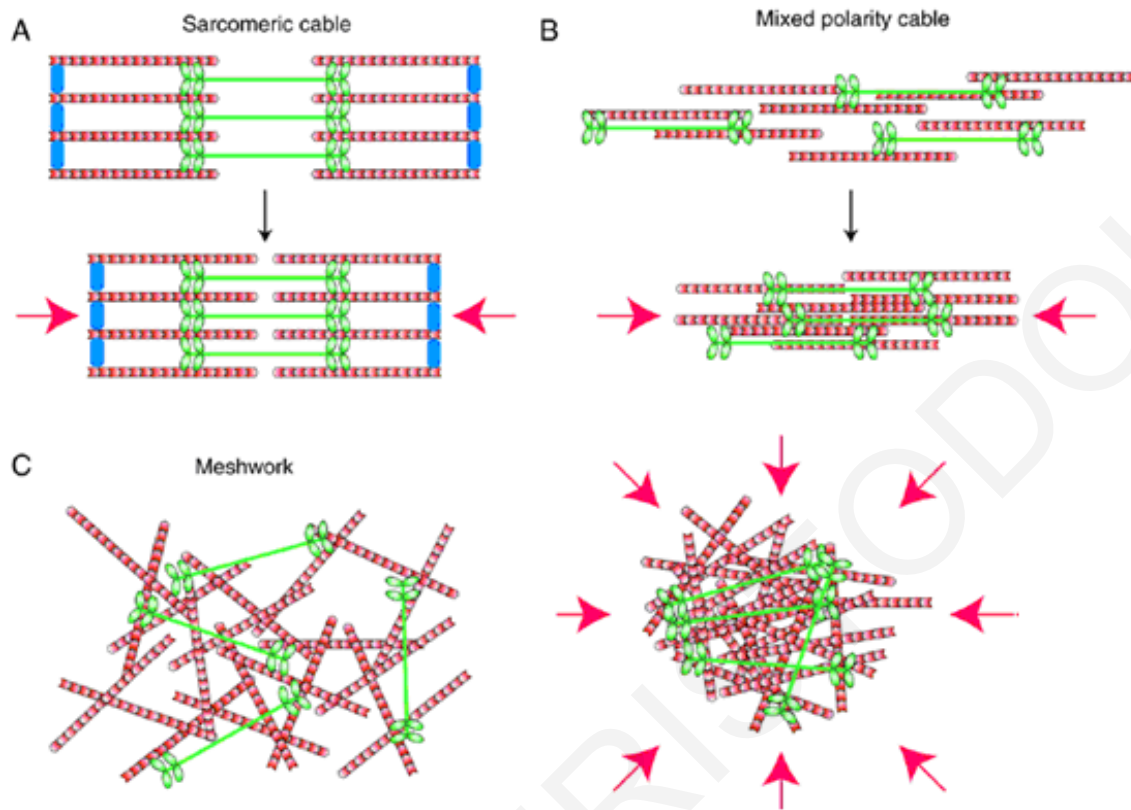


Figure 32. Modes of actomyosin contraction.

(A) Sarcomeric cable contraction. Actin filaments (red) are assembled into arrays with the barbed ends facing away from myosin II minifilaments (green). In regions lacking myosin II, α -actinin (blue) cross-links actin filaments into bundles. The sarcomeric unit is repeated to generate a cable composed of multiple contractile units that can shorten and generate linear tension. (B) Mixed polarity cable contraction. Cables of unbranched filaments with little or no organization of filament polarity contract along the length of the cable. (C) Meshwork contraction. A two-dimensional actin filament meshwork is contracted by myosin II to generate planar tensile forces. Adapted from (Martin, 2010).

During AC in vertebrate's neuroepithelial cells, the actomyosin complex is organized as a circumferential cable which is directly linked with cell-cell adhesions (**Figure 33A**). This cable shortens and thickens as neurulation progresses and neuroepithelial cells constrict their apical surfaces (**Figure 33B**) (Baker and Schroeder, 1967; Burnside, 1971; Schroeder, 1970). Shroom3, an actin binding protein, has been implicated in AC. Shroom3 knock out mice show anterior NTDs phenotypes (Hildebrand and Soriano, 1999). Expression of Shroom3 in polarized epithelial cells induces AC and promotes the formation of circumferential actomyosin complex with sarcomeric organization (**Figure 34**) (Haigo et al., 2003; Hildebrand, 2005). In addition other regulators of AC such as Lulu, regulate the formation of the circumferential actomyosin complex (Chu et al., 2013; Nakajima and Tanoue, 2010). Knockdown of Lulu in MDCK epithelial cell line disrupts the circumferential actomyosin (Nakajima and Tanoue, 2011). These results support the

purse string model for AC during vertebrate NTC. According to the purse string model, contraction of the circumferential actomyosin complex drives AC (**Figure 33B**). In some cases this circumferential actomyosin complex can be polarized. During chicken neurulation the actomyosin complex is planar polarized, possibly generating polarized forces responsible for the polarized folding of the neuroepithelium (**Figure 35A**)(Nishimura et al., 2012). This polarization is depended on the PCP pathway through Celsr1 add Dishevelled (**Figure 35B**). PCP pathway drives the planar polarized localization of Rho-GEF and ROCK, leading to planar polarized activation of myosin(**Figure 35B,C**) (Nishimura et al., 2012).

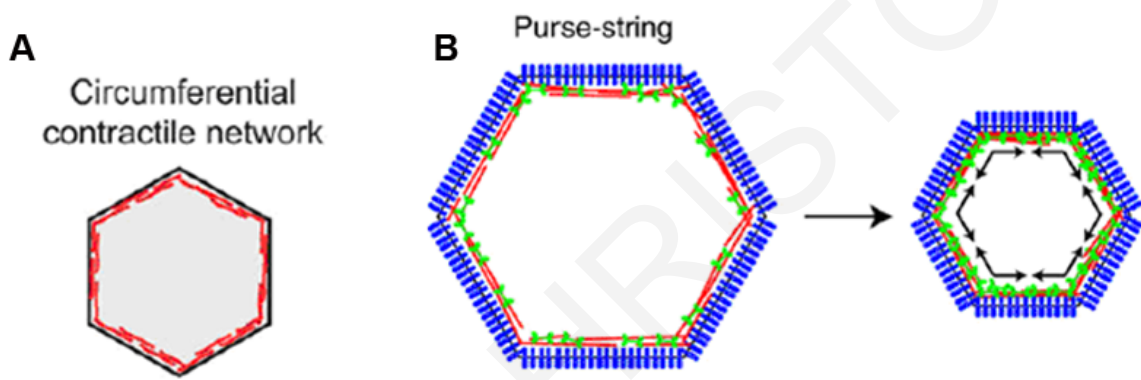


Figure 33. Predominant model for Apical Constriction of neuroepithelial cells.

(A) A circumferential actomyosin complex is present in neuroepithelial cells. (B) The purse-string model of AC. Contractile force generated by myosin-II driven actin filament sliding within the circumferential cable constricts the cell apex. Forces are generated parallel to the cell surface. Adapted from (Martin, 2010).

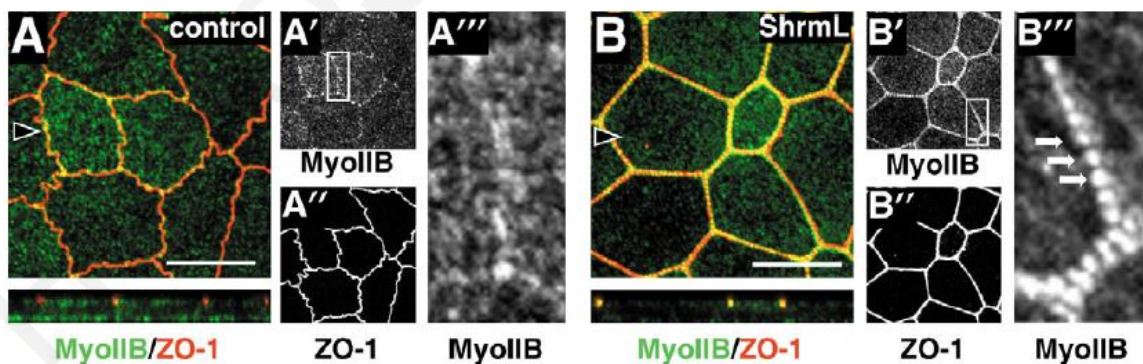


Figure 34. Induction of Apical Constriction alters the distribution of myosin II in MDCK cells.

Control (A) and ShrmL expressing (B) Cells stained for non-muscle myosin II-B (green) and ZO-1 (red). Boxed areas in A' and B' are shown enlarged in A''' and B'''. Lower panels represent X-Z projections of the entire apical-basal axis. Arrowheads denote where X-Z sections were generated. Arrows denote the regularly spaced distribution of non-muscle myosin II-B. Adapted from (Hildebrand, 2005)

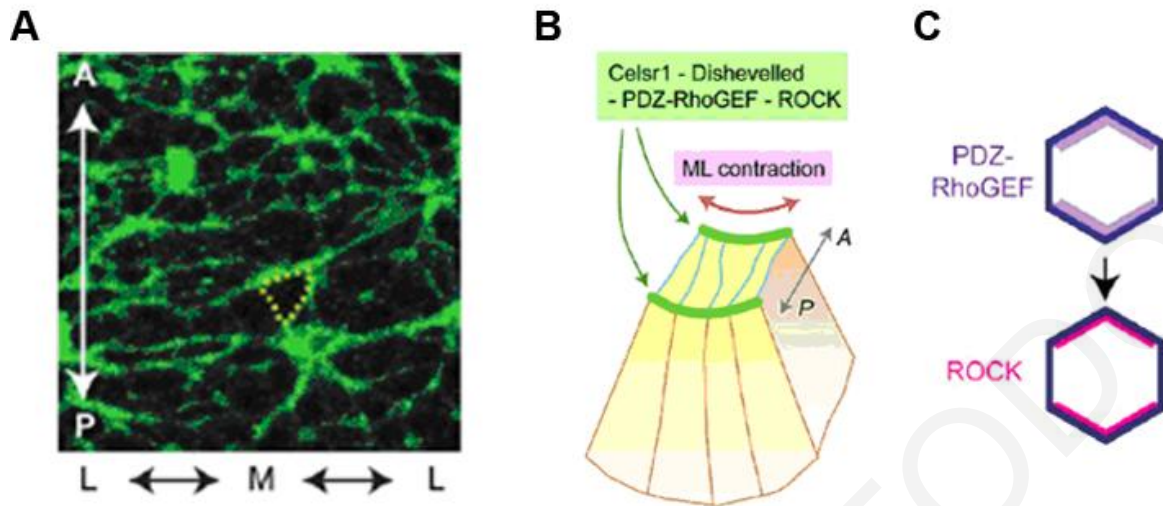


Figure 35. Mediolateral orientation of apical actomyosin network in the chicken neuroepithelium.

(A) Neural plate was stained for pMLC. Phosphorylated myosin is enriched at junctions oriented parallel to the mediolateral junctions. (B,C) PCP dependent activation of the actomyosin at mediolateral junctions. PCP signaling molecules (Dishevelled and Celsr1) are localized at mediolateral junction regulating the polarized activation of ROCK and Rho-GEF. Adapted from (Nishimura et al., 2012)

While studies in vertebrates demonstrated the presence of circumferential actomyosin cables during AC, actomyosin complex during *Drosophila* ventral furrow formation is medioapically localized. Martin et al. demonstrated that AC of ventral furrow cells is pulsed. Repeated constriction pulses are followed by stabilization steps in which cell surface remains the same (**Figure 36A, B(I)**) (Martin et al., 2009). Pulses are asynchronous and have stochastic pattern within the tissue (Martin et al., 2009). Constriction pulses are correlated with increase of medioapical actomyosin complex rather than an increase of the circumferential actomyosin (**Figure 36B(II), C**) (Martin et al., 2009). Contraction of this medioapical actomyosin complex generates the force for apical area shrinkage through linkage with discrete apical cell-cell junctions (**Figure 37**). Roh-Johnson et al. demonstrated that during internalization of endodermal precursor cells in *C. elegans* AC is triggered by dynamic engagement of medioapical actomyosin complex with apical cell-cell contacts (Roh-Johnson et al., 2012). All the above data support a ratchet like mechanism of AC during which contractile forces of the medioapical actomyosin are exerted on discrete cell-cell adhesions. Subsequently, a stabilization step follows during which a cortical actomyosin network provides the tension necessary for apical cell shape stabilization (**Figure 37**) (Martin, 2010). The polarized activation of actomyosin at the medial apex and the connection between actomyosin and junctional complexes are regulated by Radial Cell Polarity of Rho, Rock, Dia and E-cadherin (**Figure 38**) (Mason et al., 2013).

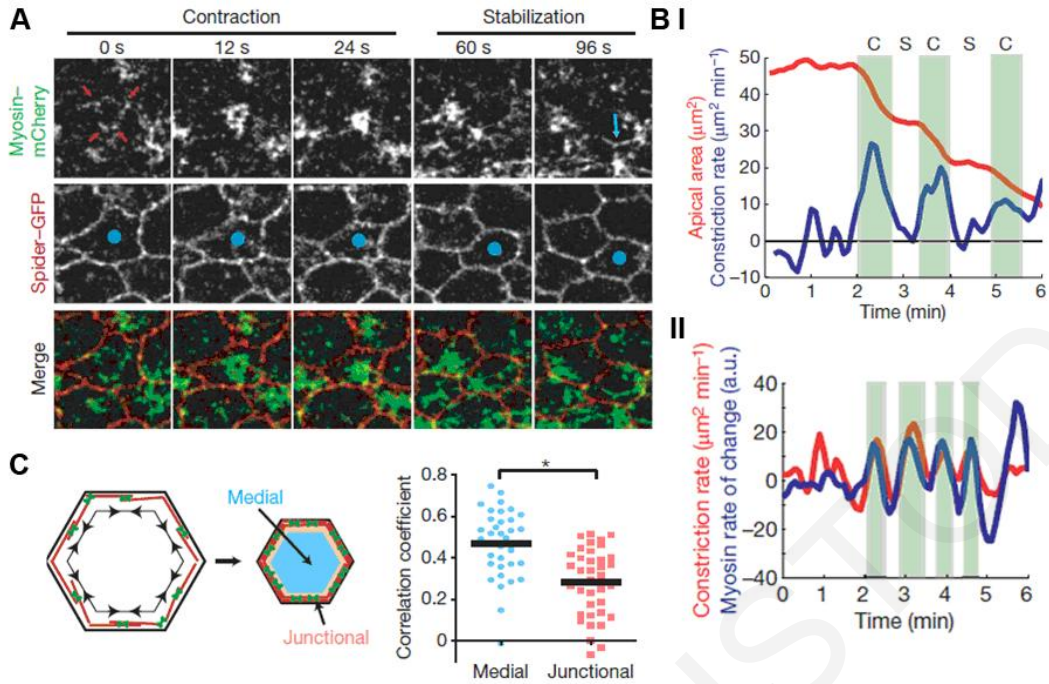


Figure 36. Apical Constriction during ventral furrow formation is driven by pulsed contractions of a medioapical actomyosin network.

(A) Single channel and merged timelapse images of Myosin-mCherry (green) and Spider-GFP (red). Red arrows indicate spots that will coalesce. Blue arrow indicates myosin fiber that appears between contractions. (B) Apical area and myosin intensity vs. time (I) and constriction rate and rate in change of myosin intensity vs. time (II) for an individual cell. C, contraction. S, stabilization. (C) Constriction rate is most highly correlated with medial myosin rather than junctional myosin. The diagram (left) illustrates the purse-string model for contraction in which we expect actin and myosin to become concentrated in the junctional region upon constriction. Data points represent correlation coefficients (r -values) for individual cells and the black bar indicates the mean. Adapted from (Martin et al., 2009).

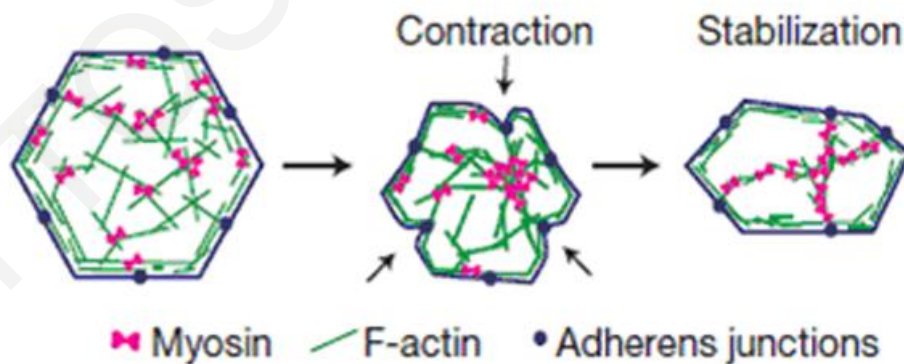


Figure 37. Ratchet model of Apical Constriction.

Myosin (red) contracts an apical actin network (green) that is coupled to adherens junctions (blue) driving constriction. Contractions are pulsed, interrupted by a phase in which the constricted state of the cell is stabilized. Adapted from (Martin et al., 2009).

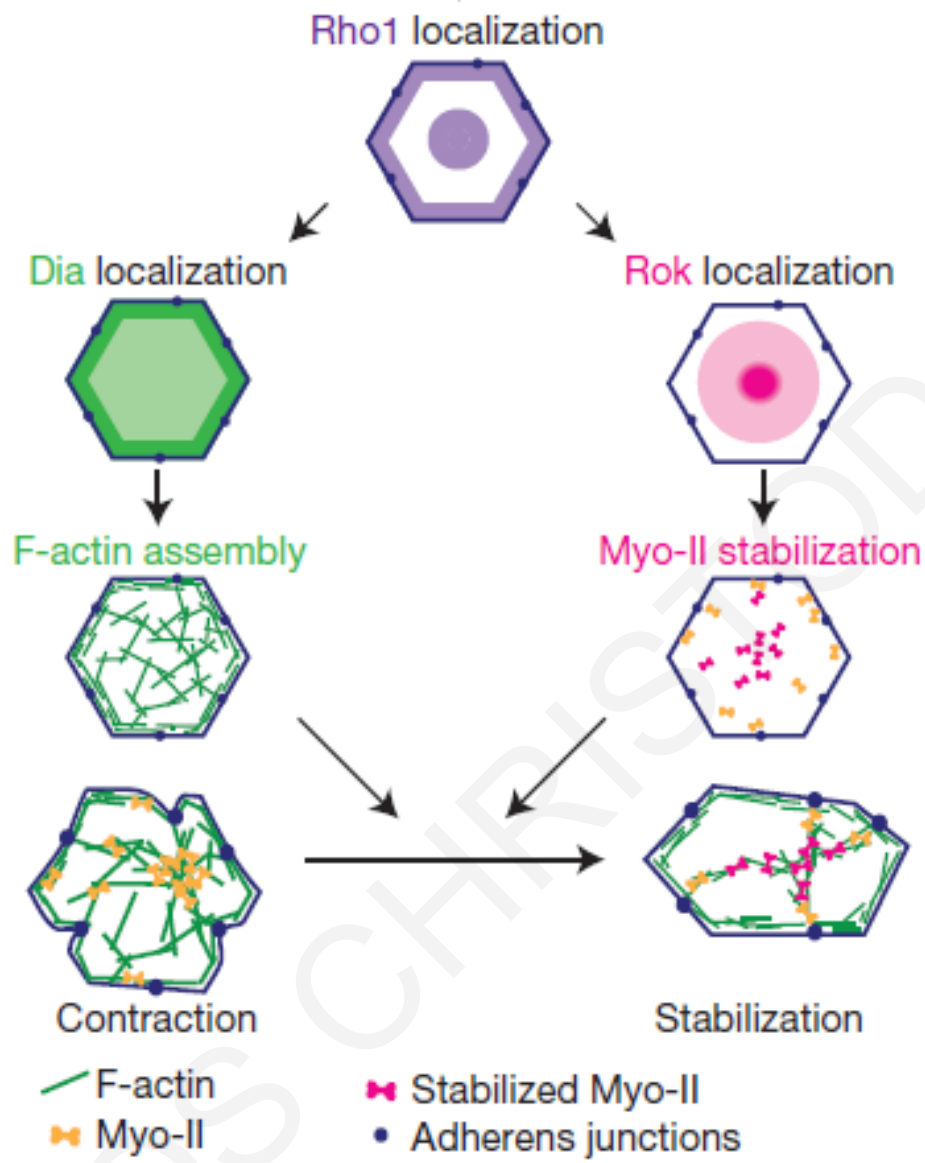


Figure 38. Radial Cell Polarity(RCP) coordinates Myo-II stabilization and F-actin assembly to facilitate Apical Constriction.

II) Apicobasal axis elongation

During vertebrate's NTC neuroepithelial cells elongate along their apicobasal axis (**Figure 39**)(Burnside, 1971). Apicobasal axis elongation is also observed in other tissues and models (Lee and Harland, 2007; Sawyer et al., 2010). In mouse and chicken embryos apicobasal elongation of neuroepithelial cells precede apical surface narrowing while in *Xenopus* it is taking place simultaneously with AC(Suzuki et al., 2012). In flat neuroepithelial cells microtubules are randomly oriented while in elongated cells microtubules are assembled parallel to the apicobasal axis of the cells (Burnside, 1971; Lee et al., 2007) (**Figure 40A**). In addition, during AC of neuroepithelial cells in *Xenopus* γ -tubulin is distributed apically (Lee et al., 2007) (**Figure 40B**). This suggests that polarized polymerization of microtubules from the apical surface to the basal end of the cell drives the apicobasal cell axis elongation. Burnside performed a detailed EM study of microtubules during AC of neuroepithelial cell. Burnside documented several apicobasal microtubules lying next to cytoplasmic vesicles and suggested that microtubules contribute to cell elongation by transport of cytoplasmic material to the basal end of the cell (**Figure 41**). In agreement with the above, during ventral furrow formation in *Drosophila*, hydrodynamic flow of the cytoplasm towards the basal end of the cell was correlated with cell elongation. Treatment of embryos with colchicine resulted in reduced flow velocity, suggesting that microtubules are necessary for this basal flow of the cytoplasm (He et al., 2014).

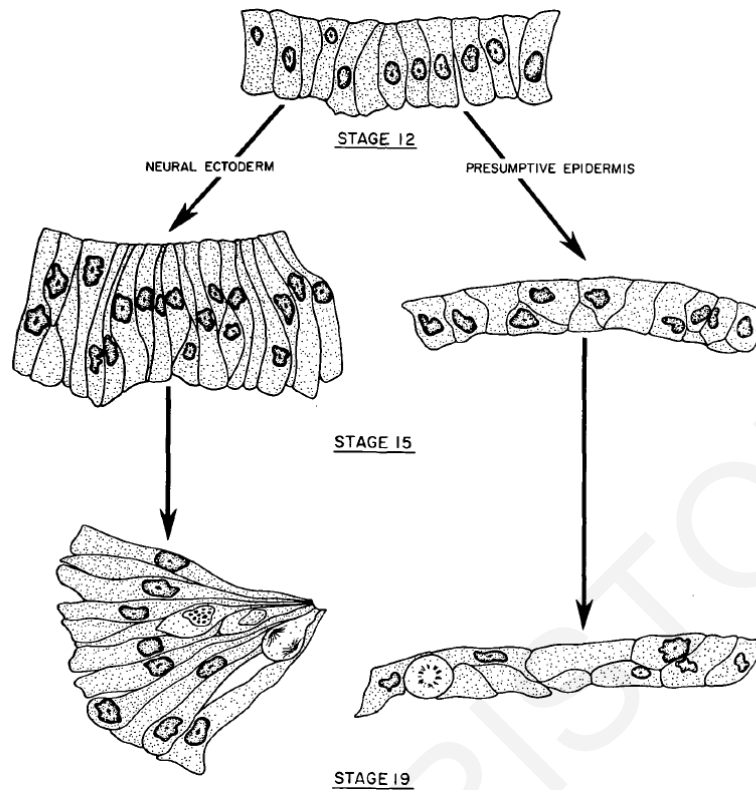


Figure 39. Cell shape changes occurring in ectoderm cells during neurulation in the newt embryo.

At the end of gastrulation the entire ectoderm is composed of a low columnar epithelium. As neurulation proceeds, the presumptive neural cells elongate to form the high columnar epithelium of the placode like neural plate and then constrict apically to form wedge shaped cells as the plate rolls up to form the neural tube. The presumptive epidermal cells flatten throughout the course of neurulation. Adapted from (Burnside, 1971)

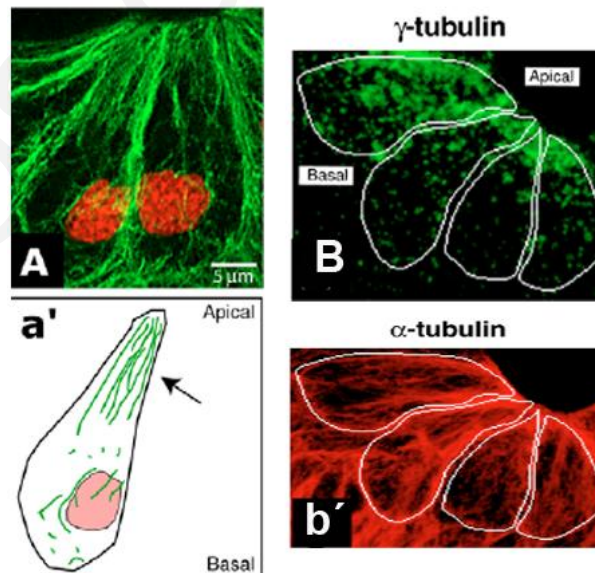


Figure 40. Polarized microtubule polymerization in neuroepithelial cells undergoing Apical Constriction.

(A) High magnification view of microtubules in neuroepithelial cells (green, anti-tubulin; red, propidium iodide, nuclei). (a') Schematic of a cell shown in A. Arrow indicates parallel MT arrays. (B) High-magnification image showing elongating neural epithelial cells stained for γ -tubulin (white lines indicate cell outline). (b') α -tubulin staining for cells shown in A. Adapted from (Lee et al., 2007).

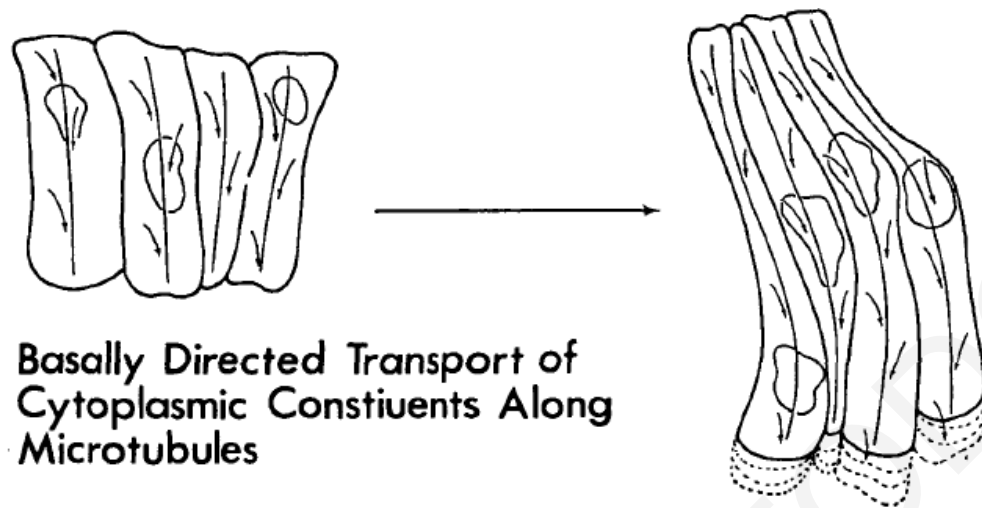


Figure 41. Basal cytoplasmic flow along microtubules induce apicobasal axis elongation.
Adapted from (Burnside, 1971)

In contrast with the above studies, Lee and Harland showed that microtubules are only necessary for apical surface constriction but not for apicobasal axis elongation in *Xenopus* bottle cells. Treatment of *Xenopus* embryos with nocodazole resulted in defective apical surface shrinkage of bottle cells but it didn't affect apicobasal elongation (Lee and Harland, 2007) (**Figure 42**). In addition, disruption of the actomyosin contractility blocked both apical surface narrowing and apicobasal elongation in these cells (Lee and Harland, 2007) (**Figure 42**). Consistent with the above data, Gelbart et al. showed that cell elongation during ventral furrow formation is driven by a volume conservation mechanism and AC induced basal movement of the cytoplasm (Gelbart et al., 2012). In both *Xenopus* bottles cells and ventral furrow formation, blockage of apical surface constriction results in defective apicobasal axis elongation. From these data it is suggested that contraction of the actomyosin complex is necessary for both apical surface constriction and apicobasal axis elongation and that microtubule polymerization is probably necessary for the transport of molecules and factors required for AC to the apical region of the cell. Consistent with the role of microtubules in transport of factors to the apical surface of the cell during AC, is the fact that disruption of microtubules during eye development in *Drosophila* results in defective apical actomyosin complex and failure of apical surface shrinkage (Corrigall et al., 2007). Moreover, the Rho activator RhoGEF, has been shown to bind to microtubule plus ends in *Drosophila* S2 cells (Rogers et al., 2004), suggesting that apical transport of RhoGEF at the apical cell surface results in spatially restricted activation of Rho at the apical cell surface,

which is necessary for the activation of myosin, driving apical actomyosin contraction (**Figure 43**). Endocytosis is also indispensable for AC for the removal of excess membrane. Depolymerization of microtubules, results in defective endocytosis and therefore defective Apical surface constriction(Lee and Harland, 2010). Therefore microtubules are involved in apical surface shrinkage through their role in the transport of endocytic membrane vesicles towards the basal area of the cell (**Figure 44**). From all the above, we can conclude that there are two mechanisms for cell elongation during AC. In the first mechanism, the polarized polymerization of microtubules is necessary for cell elongation probably driving the basal transport of the cytoplasm. In the second mechanism, microtubules are dispensable for cell elongation which is driven by AC induced basal movement of the cytoplasm. In addition, microtubules have two distinct roles during AC, again depending on context. Microtubules are required for the basal movement of cytoplasmic and endocytic membrane vesicles or they are required for the transport of factors necessary for apical surface narrowing towards the cell apex. In some cases, such as in vertebrate's neuroepithelial cells, microtubules have dual function as their depolymerization blocks both cell elongation (basal movement of vesicles) and AC (apical transport of molecules) in these cells.

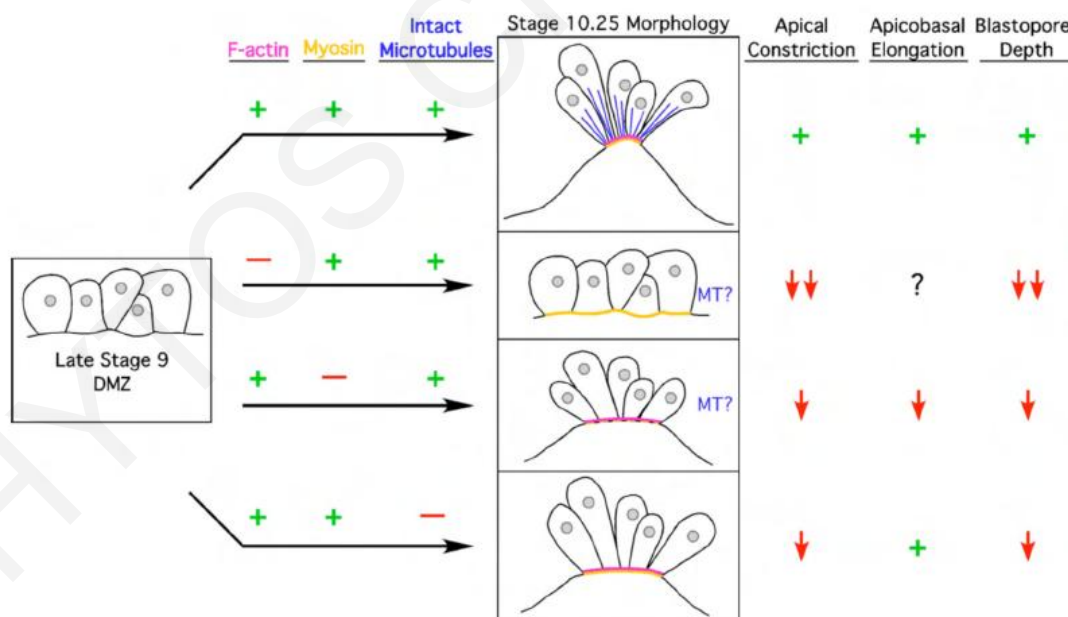


Figure 42. Summary and model of the cytoskeletal mechanisms of *Xenopus* bottle cell formation.

The actomyosin complex is indispensable for apical surface shrinkage while microtubule network is dispensable for apicobasal axis elongation and necessary for apical surface shrinkage. Adapted from (Lee and Harland, 2007).

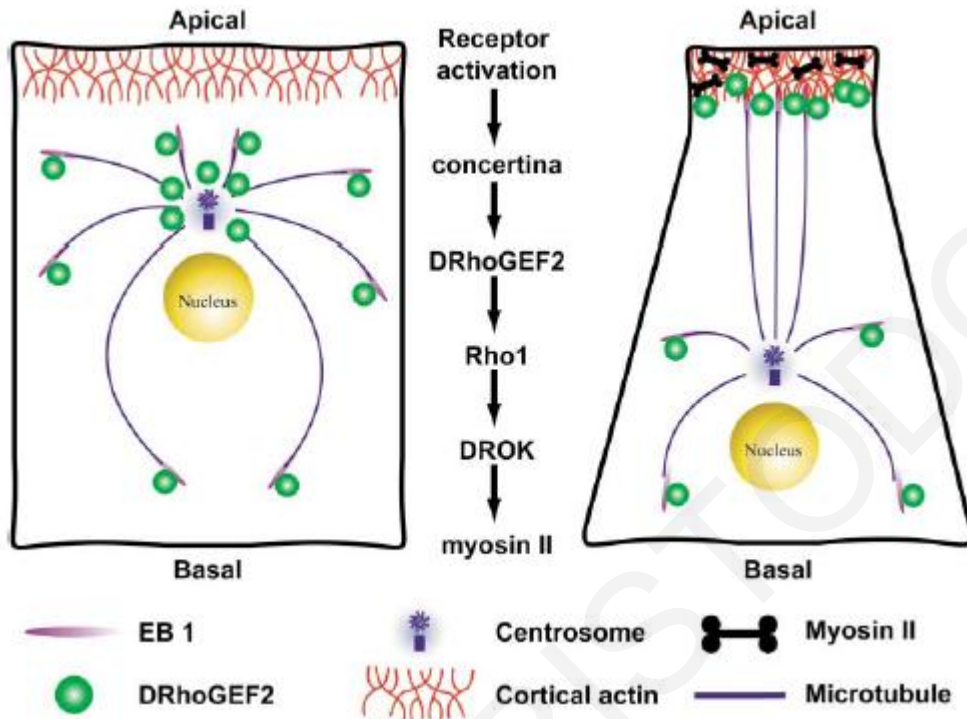


Figure 43. Model for the Role of Microtubule Dynamics during DRhoGEF2- Mediated Cellular Shape Change.

Adapted from (Rogers et al., 2004)

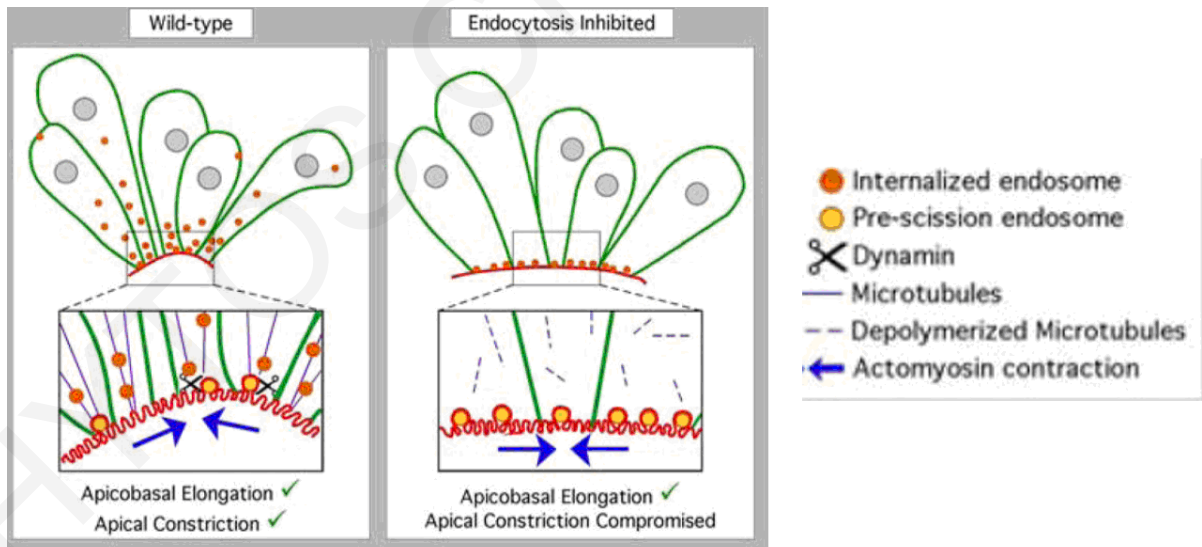


Figure 44. Model of apical membrane dynamics during bottle cell Apical Constriction.

Intact microtubules are needed for endocytosis and apical surface contraction but not apicobasal axis elongation during AC of *Xenopus* bottle cells Adopted from (Lee and Harland, 2010).

1.8.2 Cell-cell adhesions and mechanical coupling during Apical Constriction driven morphogenesis.

Cell-Cell junctions contribute to tissue integrity and organization. In addition, cell-cell adhesions are responsible for the mechanical coupling of cells. Mechanical cell coupling is indispensable for tissue wide morphogenetic movements driven by cell shape changes (Gomez et al., 2011; Leckband et al., 2011). For a cell to apically constrict, the forces generated by the actomyosin complex are exerted on intercellular adhesions (Martin and Goldstein, 2014). Indeed disruption of adhesion complexes in invertebrates or in vertebrates leads to defective AC and morphogenesis (Martin et al., 2010; Morita et al., 2010; Nandadasa et al., 2009). In addition the loss of the connection between the actomyosin complex and cell-cell adhesion complexes lead to defective AC. Examples of these molecules are the afadin homologue Canoe in *Drosophila* (Sawyer et al., 2009) and Vinculin, MARCKS, and ENA/VASP in vertebrates (Chen et al., 1996; Menzies et al., 2004; Roffers-Agarwal et al., 2008; Xu et al., 1998; Zolessi and Arruti, 2001). The last years, cell-cell adhesion molecules have also been implicated in mechanotransduction. Actin regulator molecules such as Vinculin and ENA/VASP are recruited to cell-cell junctions in a tension depended manner (Gomez et al., 2011; Leckband et al., 2011; Leerberg et al., 2014). Loss of these molecules such as Vinculin which is implicated in mechanotrasduction, leads to phenotypes correlated with AC (Menzies et al., 2004; Roffers-Agarwal et al., 2008; Xu et al., 1998).

Solon et al. using live imaging and computational modeling during *Drosophila* dorsal closure elegantly demonstrated that amnioserosa cells are mechanically coupled during AC and this mechanical interaction controls constriction pulses (Solon et al., 2009). Neighboring cells either contract in phase or out of phase. In addition this study proposed a model of forced depended AC. Elimination of tissue tension with laser ablation of cells blocked constriction pulses of neighboring cells. The force generated by the stretching of a cell by its neighbor's constriction was inducing the delayed constriction of the cells (Solon et al., 2009). The data from this study show the importance of mechanical coupling of cells during AC morphogenesis. In addition this study highlights the presence of a mechanotransduction mechanism which is necessary for the coordination of AC driven tissue morphogenesis.

1.9 Calcium signaling in morphogenesis

Calcium signaling (through the Wnt/Ca²⁺ pathway or in the form of calcium waves) has been implicated in morphogenetic movements and cell shape changes during embryogenesis. In *Xenopus* calcium signaling is necessary for CE movements during gastrulation and neurulation (Kuhl et al., 2000a; Kuhl et al., 2000b; Sheldahl et al., 1999; Slusarski et al., 1997a; Slusarski et al., 1997b). In addition, calcium waves have been detected during *Xenopus* mesoderm CE. Blockage of these waves resulted in defective CE (Wallingford et al., 2001) (**Figure 45**). Different molecules that are calcium regulated have been shown to influence these movements and a cross-talk between calcium signaling and the PCP pathway has been identified at different levels (Elul and Keller, 2000; Elul et al., 1997; Ezin et al., 2003; Sheldahl et al., 2003; Shih and Keller, 1992). Use of pharmacological inhibitors in *Xenopus*, chick and rat embryos, showed that calcium is necessary for neural fold formation and NTC in vertebrates (Ferreira and Hilfer, 1993; Moran and Rice, 1976; Nagele et al., 1991; Smedley and Stanisstreet, 1986). These results suggest a role of calcium signaling in AC. Studies in *Drosophila*, have implicated intracellular calcium with AC induced cell shape changes. In the first study, a calcium wave was generated after wounding in *Drosophila* pupals and intracellular calcium increase was correlated with AC of cells next to the wound. This cell shape change was necessary for proper wound healing (Antunes et al., 2013). In the second study, intracellular calcium was linked with AC of amnioserosa cells during dorsal closure. Hunter et al. have shown that intracellular calcium fluxes are correlated with AC of amnioserosa cells. Moreover this study demonstrated that mechanically gated calcium channels are necessary for dorsal closure as blockage of their function results in defective dorsal closure (Hunter et al., 2014). The latter links intracellular calcium dynamics with the tension based mechanism for AC that has been proposed previously (Solon et al., 2009). In the cases of vertebrate NTC, *Drosophila* wound healing and dorsal closure, intracellular calcium is necessary for the proper formation of the actomyosin complex (Antunes et al., 2013; Ferreira and Hilfer, 1993; Hunter et al., 2014; Moran and Rice, 1976; Nagele et al., 1991; Smedley and Stanisstreet, 1986). Despite the correlation of calcium with NTC, in vertebrates, there isn't a study correlating directly intracellular calcium levels with AC of neuroepithelial cells. In addition, the pattern of intracellular calcium levels has not been studied in any organisms during AC driven morphogenesis.

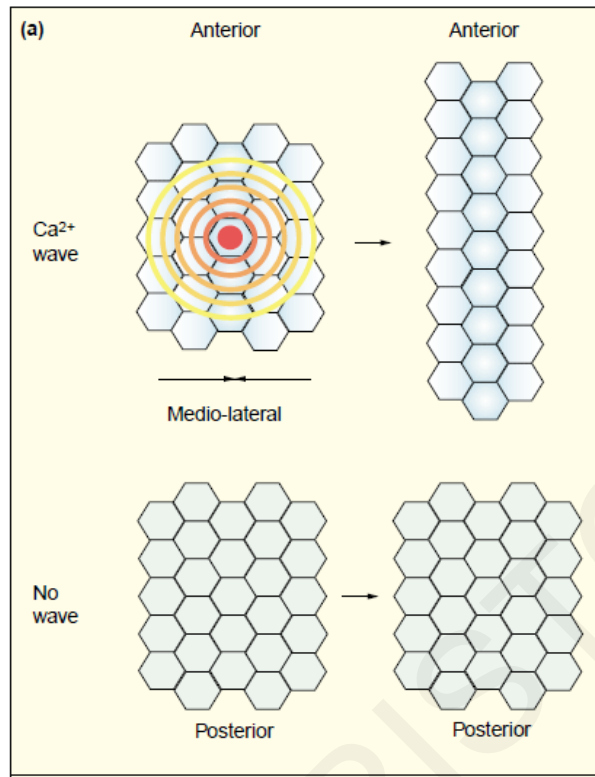


Figure 45. Calcium waves regulate Convergent extension.

Convergent extension and waves of Ca^{2+} signaling. In the presence of intercellular Ca^{2+} waves, dorsal mesoderm cells within Keller explants are able to undergo convergent extension. However, when Ca^{2+} waves are abolished with pharmacological agents, convergent extension movements fail to occur. Adapted from (Tada and Concha, 2001).

1.9.1 Mechanisms of Calcium signaling

G-proteins coupled and tyrosine kinase-linked receptors act upstream of calcium signaling. The activation of these receptors results in the generation of diacylglycerol inositol-1,4,5-triphosphate (IP_3). Diacylglycerol activates PKC and IP_3 induce the release of calcium from intracellular stores through IP_3R and RYR channels, therefore driving intracellular calcium elevation. Increase of intracellular calcium generates a positive feedback loop for further release of calcium from intracellular stores. In addition, increase of intracellular calcium is controlled by membrane calcium channels such as voltage operated channels (CaV. L-Type, T-Type), receptor operated channels (NMDA), second messenger operated channels (SOCs) and transient receptor potential (TRP) channels (**Figure 46**) (Markova and Lenne, 2012; Slusarski and Pelegri, 2007). For intercellular transmission of calcium signaling, calcium waves are generated. Calcium waves are generated when calcium and IP_3 are diffused through gap junctions to adjacent cells. Then IP_3 and calcium positive feedback loop lead to intracellular calcium release from the adjacent cell (Markova and Lenne, 2012) (**Figure 46**). Another mechanism for calcium wave propagation is

the entry of calcium entry from stretch activated calcium channels found in cell membrane. Opening of stretch activated channels results in calcium influx from the extracellular environment. Increase of intracellular calcium results in contraction of the actomyosin complex. Contraction of the actomyosin complex results in the stretching of neighboring cells membrane and opening of their stretch activated calcium channels (Jaffe, 2008) (**Figure 46**).

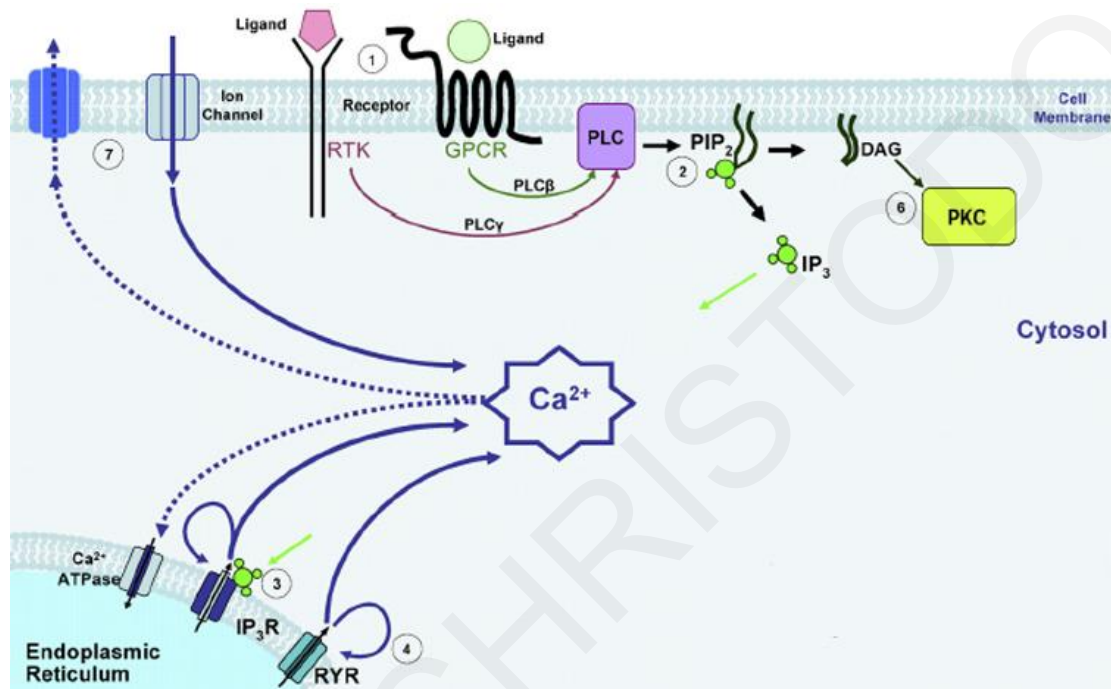


Figure 46. Schematic diagram of cellular Calcium sources.

(1) Stimulation of the cells with agonists and growth factors leads to the activation of GPCR and RTK. (2) This leads to activation of PLC isoforms, which catalyze the hydrolysis of PIP $_2$ giving rise to IP $_3$ and DAG. (3) IP $_3$ binds to its receptor (IP $_3$ R) on the ER and triggers Calcium release from the store. (4) One aspect of CICR involves Calcium binding to the high affinity Calcium activation sites on IP $_3$ R and RyR inducing the channels to open. (5) Intracellular Calcium is rapidly bound by Calcium binding proteins, which leads to their activation. (6) DAG is another second messenger which activates PKC among other targets. (7) Clearance of cytoplasmic Calcium, shown by dashed lines, occurs by Calcium extrusion via plasmalemmal pumps and Na $^+$ /Ca $^{2+}$ exchange as well as by uptake into intracellular stores, such as the endoplasmic reticulum. GPCR, G-protein-coupled receptor; RTK, receptor protein tyrosine kinase; PLC, phosphoinositide-specific phospholipase C; PIP $_2$, membrane phosphatidylinositol-4,5-bisphosphate; PKC, protein kinase C; DAG, diacylglycerol; IP $_3$, inositol-1,4,5- trisphosphate; IP $_3$ R, IP $_3$ receptor; ER, endoplasmic reticulum; RYR, ryanodine receptor; CaMK II, Ca $^{2+}$ /calmodulin-dependent kinase II; CICR, Calcium-induced Calcium release; NFAT, nuclear factor of activated T cells. Adapted from (Slusarski and Pelegri, 2007).

1.9.2 Structure and regulation of Gap junctions

Gap junctions are channels that allow the direct exchange of cytoplasmic material between adjacent cells. Gap junctions are formed when two hexameric connexin hemichannels are docked head to head (Oshima, 2014) (**Figure 47**). Gap junctions have a central role in calcium wave propagation as described above. Gap junction can exist in the open or the closed conformation (Oshima, 2014) (**Figure 47**). The conformation of gap junction is regulated by several factors such as connexin phosphorylation and intracellular calcium (Oshima, 2014; Zou et al., 2014).

Intracellular calcium can modulate gap junction conformation either directly or indirectly by activation of calmodulin (Oshima, 2014; Zou et al., 2014). Elevation of calcium concentration results in closure of Gap junctions (**Figure 48 A,B**) (Dakin et al., 2005; Muller et al., 2002; Suzuki et al., 2004). Dakin et al have shown that elevation of bulk intracellular calcium was not able to block gap junction communication in human fibroblast. This study proposed that calcium influx through specific calcium channels on the membrane results in spatial increase of calcium activity near the plasma membrane and closure of gap junctions (**Figure 48C**) (Dakin et al., 2005; Spray, 2005). Activation of calmodulin by calcium induces the interaction of calmodulin with the cytoplasmic loop of connexins. This interaction blocks the cytoplasmic opening of gap junctions (Zou et al., 2014).

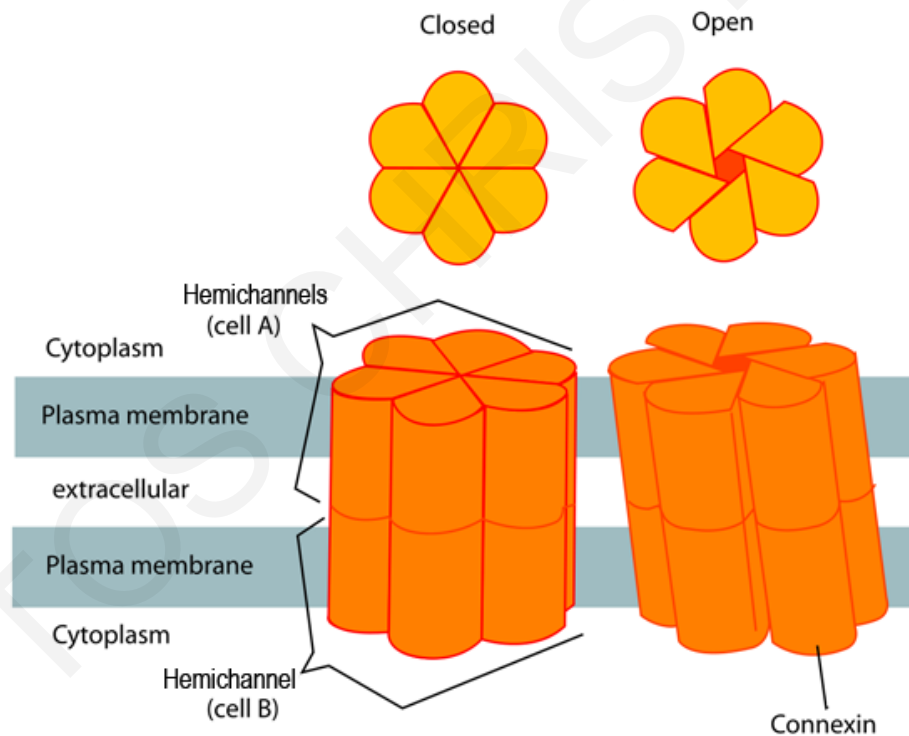


Figure 47. Structure of Gap junctions

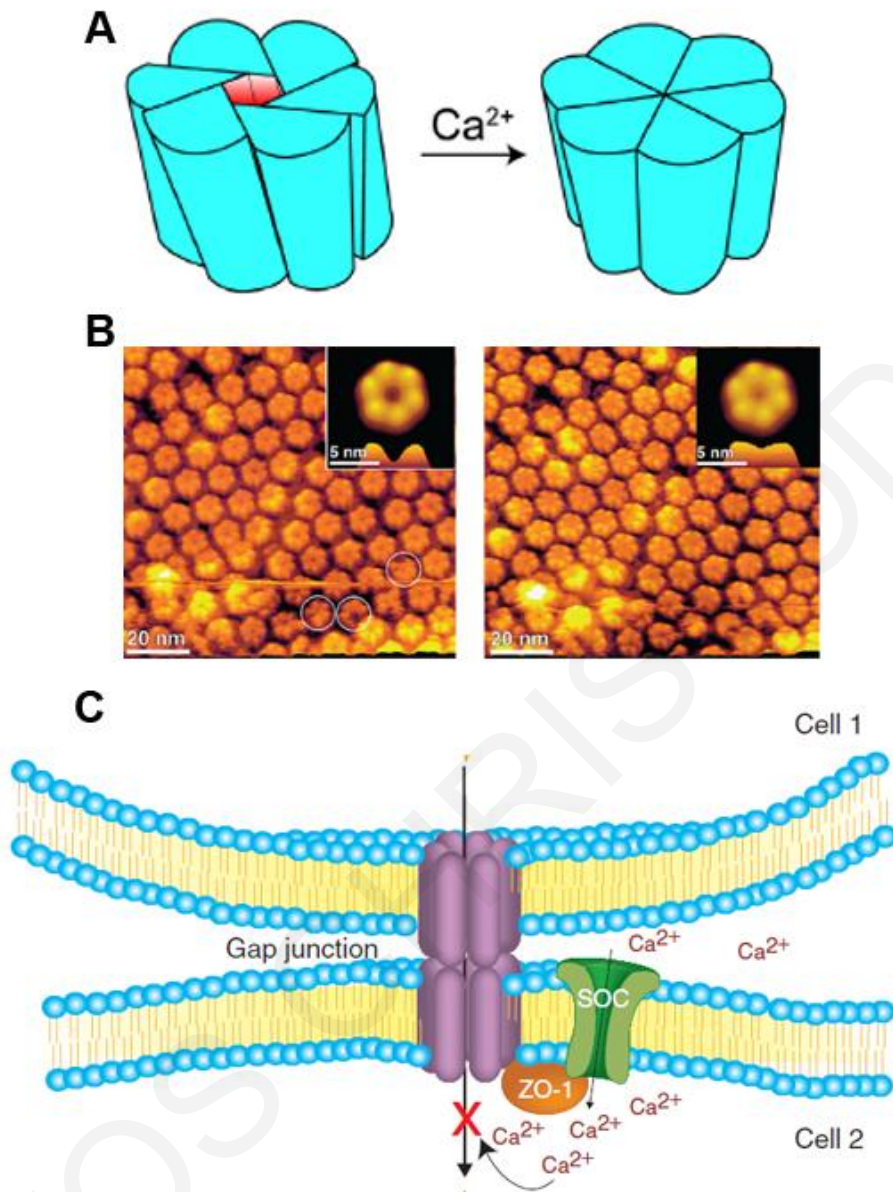


Figure 48. Regulation of Gap junction by intracellular Calcium.

(A) Calcium induces the gating transitions of the gap junction channel between open and closed configurations. (B) Atomic Force Microscopy topograph showing the extracellular connexon surface imaged in a calcium-free buffer solution. (left) and in the presence of 0.5 mmol/L calcium. (C) Calcium entry through the Store Operated Channels increases Calcium concentration to very high levels in close proximity to the gap junction, thereby directly or indirectly closing the intercellular channels. Adapted from (Oshima, 2014) and (Spray, 2005).

2. Methodology

2.1 Frogs

Adult frogs were obtained from several international suppliers, such as NASCO (United States) and *Xenopus express* (France/UK). New frogs were kept separately from the older ones and a recovery/resting period of two weeks was allowed after receiving each new shipment of frogs. This resting period was crucial and helped to increase the quality of oocytes obtained and used for the experiments (Sive et al., 2010).

2.2 Ovulation

Ovulation was induced by administering an injection of 600-750 IU of human Chorionic Gonadotropin (hCG; Chorulon/Sigma) into the dorsal lymph sac of the female frog. Using a fine needle (26 gauge, Fisher) attached to a 1-ml syringe, the injection was performed posteriorly, at the level of the hind limb near the lateral line “stitch”. The “primed” frogs were kept at 18-20 °C and started laying eggs approximately 12 hours after injection (Sive et al., 2010).

2.3 Collecting eggs

The primed female frog was held using the proper method (Sive et al., 2010) and simultaneous lateral and vertical pressure was applied by massaging the belly in order to release the eggs which were collected in the sac near the cloaca. One thumb was kept over a clean, glass petri dish (90cm) containing 0.33X MMR (Ubbels et al., 1983). Egg collection was carried out every hour for the first 2-3 hours of laying and then more often as the day progressed. Females usually laid eggs for about 8 hours. A maximum of 6-8 collections are expected from a frog in 1 day. Each batch of oocytes obtained from the female frog was kept in a separate glass petri dish.

2.4 In-vitro Fertilization

Fertilization was performed immediately after laying and time of fertilization was noted. Before *in vitro* fertilization, excess 0.3xMMR buffer was removed from the petri dish containing the eggs using a plastic pipette (3ml). A small piece of testis was cut and macerated using forceps and mixed with the eggs in order to evenly distribute the sperm throughout the eggs. The eggs were left for roughly 20 minutes in order for fertilization to occur. The eggs should rotate within their viteline membrane so that the animal hemisphere (pigmented half) would face upwards (Ubbels et al., 1983).

2.5 Dejelling embryos

In order to manipulate *Xenopus* embryos, the thick jelly membranes surrounding the embryos must first be removed. In order to achieve this, embryos were gently swirled in a solution of 2% cysteine in 0.3X MMR at pH 8 for 2-3 min (Sive et al., 2010). When the embryos began packing closely together and the jelly coats could be seen floating in the buffer, the cysteine was promptly removed and the fertilized eggs were rinsed at least 10 times in an excess of 0.33X MMR. After dejelling, the embryos were placed in a clean dish either in 0.1X MMR or 4% Ficoll in 0.33X MMR (if the embryos were going to be used for microinjection procedures) and the dead embryos were removed (Ubbels et al., 1983).

2.5 DNA constructs and morpholino oligonucleotide

All plasmids were constructed using standard molecular biology techniques and their sequence was verified by DNA sequencing. Briefly, HA-tagged Calpain2 construct used in rescued experiments (Calpain2R) was generated by polymerase chain reaction (PCR) using *Xenopus* Calpain2 Pcmv-sport6 vector (Imágenes) as a template and Calpain2resF and Calpain2HAR as primers. Calpain2resF primer was designed starting from the ATG (and thus lacking the 5'UTR region recognized by the morpholino) and it also includes silent mutations in the coding sequence (Shown in bold in Table 1). Calpain2HAR primer includes the sequence encoding for a C-terminal HA tag. The PCR product was then cloned into the *NotI* and *XhoI* sites of pCS108 vector. HA-tagged Calpain2 construct (including 5'UTR) used for testing the morpholino effectiveness was generated as described above, using Calpain2surF and Calpain2HAR as primers. A second HA tag was inserted in both Calpain2R and Calpain2 constructs by site directed mutagenesis using Calpain2insHAF and Calpain2insHAR primers. To create the Calpain2 dominant negative construct (Calpain2C105S) the mutation C105S was introduced by site directed mutagenesis, using Calpain2R pCS108 as a template and Calpain2C105SF and Calpain2C105SR as primers. Calpain2 antisense morpholino (MO) was obtained from Gene Tools. The sequence of Calpain2 MO is GTCTGTGCGGCGACCCCGCTCATGTC. The MO was designed to anneal to a region of Calpain2 mRNA that is not conserved among the other members of the Calpains family. All primers used are listed in **Table 1**.

Capn2resF	AAGCGGCCGCATGAGCGGAGTCGCAGACAGACTT GCT AAG
Capn2surrF	AAGCGGCCGCACCGACATGAGCGGGGTCC
Capn2HAR	AACTCGAGTCAAGCGTAATCTGGAACATCGTATGGGTA GAT CAC AGT CAG GGA AAG CCA AG
Capn2insHAF	'5CTTGCTTTCCCTGACTGTGATCGGAGGCGGATATCCT TATGACGTGCCTGACTATGCCGGATCTTACCCATACGAT GTTCCAGATTAC' 3
Capn2insHAR	GTAATCTGGAACATCGTATGGGTAAGATCCGGCATAGT CAGGCACGTCATAAGGATATCCGCCTCCGATCACAGTC AGGGAAAGCCAAG
Capn2C105SF	GGAGCCCTGGGTGACAGCTGGCTTCTTGACAG
Capn2C105SR	CTGCAAGAAGCCAGCTGTCCACCCAGGGCTCC
Capn2RTF	GGACCATTTGTTGACCTGCTG
Capn2RTR	AGTGTCCATCTTGAGCGGC
Capn2insituF	ACCTTGAATTCCGACCATTTGTTGACCTGCTG
Capn2insituR	AGATGCGGCCGCAGTGTCCATCTTGAGCGGC

Table1

2.6 Microinjections

For microinjections, dejellied embryos were placed in a solution of 4% Ficoll in 0.33x MMR. Ficoll collapses the vitelline space, reduces the pressure on the embryo and therefore prevents leakage due to the microinjection procedure. The embryos were injected using a glass capillary pulled needle, forceps, a Singer Instruments MK1 micromanipulator and Harvard Apparatus pressure injector. Embryos were microinjected with capped mRNA which was *in vitro* transcribed using mMessage machine kits (Ambion) or/and with the Calpain2 antisense Morpholino oligonucleotide (MO). Injection volumes were kept below 10nl per blastomere (for 2-8 cells stage embryos) (Smith and Harland, 1991a). For most experiments, injections were made at the 2 cell stage or at the 4-cell stage, into the dorsal blastomeres (lighter) to target neural tissues. Embryos were staged according to Nieuwkoop and Faber (Nieuwkoop, 1994). After injections, embryos were reared for 2 hours or until stage 8 in 4% Ficoll in 0.33x MMR and then washed and maintained in 0.1x MMR alone. For all experiments we injected Calpain2 morpholino at 20-35ng per blastomere and mRNAs at various amounts. Embryos were allowed to develop to the appropriate stage and then imaged live, dissected, or fixed in 1x MEMFA (Sive et al., 2010) for 1-2 hours at room temperature (RT). Fixed embryos were either used immediately or serially dehydrated in methanol and stored at -20°C.

2.7 RNA and cDNA synthesis

Embryos were placed in an autoclaved 1.5 ml capped centrifuge tube (~5 per tube). 500 µl TRIzol reagent (Invitrogen) was added, and embryos were homogenized by pipetting up and down until the sample was uniform. The sample was allowed to incubate for 10min at RT. Tubes were then centrifuged at 14K rpm for 10min at 4°C. The supernatant (RNA) was removed and placed into a new autoclaved 1.5ml tube. An equal volume (as supernatant) of chloroform was added, the tubes were vortexed for 15sec and allowed to incubate at RT for 3min. Tubes were then spun in a 4°C microfuge at 12k rpm for 15min. The top phase (RNA; clear layer - not the pink layer) was placed into a new autoclaved tube. 500 µl of isopropanol was added and the tubes were allowed to stand for 10min at RT, spun at 12K for 10min at 4°C, the supernatant was decanted and the pellet was washed with 500 µl RNAase-free 70% ethanol and RNA was recovered by centrifugation at 9Krpm for 5min at 4°C. The supernatant was removed and the pellet was allowed to dry before being resuspended in 30 µl of sterile water. cDNA was then synthesized from RNA using the SuperScriptIII First strand synthesis kit from Invitrogen.

2.8 RT PCR

For RT-PCR, cDNA was synthesised using the same method mentioned above for different developmental stages and different tissues. The PCR was carried out using specific primer pairs. The PCR products were run on a 1-1.5% agarose gel and images were captured using UVP iBox imaging system.

2.9 Mutagenesis

Mutagenic primer design: Both primers were designed such that they both contained the desired mutation and annealed to the same sequence on opposite strands of the plasmid. The primers were between 25-45 bases, the melting temperatures (T_m) was $\geq 78^\circ\text{C}$, the GC content over 40% and the mutated sequence was located in the middle of the primers. Calpain2 C105S primers are listed in Table1. Procedure: In a PCR tube we added: 125ng of each primer 22.5µl Accuprime (Invitrogen) polymerase mix and 100ng HA-Calpain2 plasmid DNA. The cycling conditions were: 95°C for 1 min, 18 cycles of 95°C for 50 sec, 60°C for 50 sec and 68°C for 7.5min (1.5min per Kb of plasmid), 1 cycle at 68°C for 10 min. The PCR was immediately cooled to 37°C, 1µl of Dpn1(10U/µl) restriction enzyme was added and the reaction incubated for 1 hour. 2µl of the PCR reaction was then used for transformation.

2.10 Mesoderm Convergent Extension assay

For mesoderm CE elongation assays, animal caps were dissected at stage 8 and cultured on agarose-coated petri dishes in 0.5x MMR containing gentamycin and activin protein (10ng/ml) (Piccolo et al., 1996) until sibling embryos completed neurulation. The caps were then fixed in 1xMEMFA and images were captured using a Zeiss LumarV12 fluorescent stereomicroscope.

2.11 Neural Convergent Extension assay

For animal cap assay, 500 pg of XBF2 (Mariani and Harland, 1998) were injected in the animal pole of one cell stage embryos. Animal caps were cut at stage 9 and cultured to stage 20 in DFA medium. To assess neural convergent extension in the neural plate explants, embryos were cultured until stage 12-12.5 and explants were prepared as previously described (Borchers et al., 2006). Following explants elongation, ΔL was calculated as previously described (Borchers et al., 2006).

2.12 Mesoderm migration

Animal caps were dissected at stage 9 and dissociated in CMFM (Ca^{2+} and Mg^{2+} free medium) and then treated with activin protein (1 U/ml in 1xCMFM) for 1 hour. The dissociated cells were subsequently plated in $\frac{1}{2}$ MMR solution in the absence or presence of 25 μM CI3 into fibronectin-coated chambered coverslips. Coverslips were coated with 0.1 mg/ml fibronectin (Sigma, diluted to the appropriate concentration with PBS) for 2 hours at room temperature. For the migration assay, cells were analyzed in the following manner: a field of cells was randomly chosen, and images were captured at 5 min intervals for at least 100 minutes. The velocity of single cells was measured with AxioVision Software 4.8.2 .

2.13 Whole mount in-situ hybridization

Whole-mount in situ hybridization of *Xenopus* embryos was performed according to Harland (1991) (Smith and Harland, 1991b). The basic ISH steps are as follows:

Digoxigenin labelled probe preparation. Antisense (3' to 5') Digoxigenin -labeled RNA probes were synthesized by *in vitro* transcription (IVT) from linearized plasmid templates using bacteriophage RNA polymerases (T3, T7 or SP6) and a ribonucleotide mixture in which the UTPs are labeled with Digoxigenin (DIG-11-UTP). To test the success of the IVT 3-5 μl of the probe was run on a 1% TAE agarose gel (RNase free). The probe was then stored at -80° until use.

Day1 of ISH: The embryos were first transferred to 4ml glass vials and rehydrated through a methanol series (100% methanol, 75% methanol in PBTw, 50% methanol in PBTw, 25% methanol in PBTw and 100% PBTw). Next the embryos were permeabilized by incubation at room temperature for 5 min in 10µg/ml Proteinase K, washed 2X5min in 0.1 M Triethanolamine pH7-8 (TEO), 2X5min in TEO with acetic anhydride and then post fixed in 4% PFA (paraformaldehyde) for 20 min at RT. Embryos were then incubated for 5-6 hours in Prehybridization solution at 60-65°C and incubated overnight at 60-65°C in hybridization solution containing the probe. Probes used: Calpain2, Sox2, Chrd, Xbra.

Day2 of ISH: Post-hybridization washes in SSC, RNase step at 37°C, block (in order to prevent unspecific binding) and antibody (Ab) incubation (Anti-DIG- AP fab fragments. 1:2000) at 4°C overnight or 4hour at RT followed by a brief wash in 1xMAB (Maleic acid buffer) and then overnight wash in 1xMAB at 4°C .

Day3-4 of ISH: Post-antibody washes with MAB solution (5x1 hour washes for overnight Ab incubation and 3-4 10min washes for 4hr RT Ab incubations) and washes in Alkaline phosphatase (AP) buffer which contained levamisole to inhibit endogenous phosphatases (2x10min washes). Visualization of the probe using BM purple. Color development varied depending on the probe used. To stop the color reaction, the embryos were washed in MAB and fixed overnight in 1xMEMFA at RT. Embryos were then bleached. Bright field images were captured on a Zeiss LumarV12 fluorescent stereomicroscope.

2.14 Immunofluorescence

Stored embryos were rehydrated by serial washes. Embryos were then permeabilized in PBDT for several hours at RT. The permeabilization step can be omitted for epidermal staining. Embryos were then blocked in PBDT + 1% normal goat serum for 1 hour at RT. Primary antibodies diluted in block solution were then added (**Table 2**), and embryos were incubated for 4 hours at RT or overnight at 4°C. The next day, embryos were washed 4x10min in PBDT. Embryos were then incubated in secondary antibodies (**Table 2**) at RT for 2 hours and then washed 4x10 minutes in PBDT again. Embryos were then post-fixed in MEMFA for 15-30 minutes at RT, washed in 1xPBS, imaged immediately or dehydrated in methanol and cleared in a 2:1 mixture of BB:BA (Benzyl benzoate: Benzyl alcohol). The embryos were imaged on a Zeiss LSM 710 laser scanning confocal microscope and Zen 2010 software or a Zeiss Axio Imager Z1 using a Zeiss AxioCam MR3, the Axiovision software 4.7.

Antibodies	Dilutions (in block solution)
Acetylated α -tubulin (sc-23950, Santa Cruz)	1:500
Zo-1 rabbit (Invitrogen)	1:500
HA rabbit (sc- Santa Cruz)	1:500
HA mouse (sc- Santa Cruz)	1:500
α PKC rabbit (Invitrogen)	1:500
Phalloidin 488 (Invitrogen)	1:500
Alexa 488 anti-mouse (Invitrogen)	1:500
Alexa 488 anti-rabbit (Invitrogen)	1:500
Cy3 anti-mouse (Jackson Immunoresearch)	1:500
Cy3 anti-rabbit (Jackson Immunoresearch)	1:500

Table 2.

2.15 Western Blot

Protein lysates were prepared by homogenizing embryos in ice cold MK's modified lysis buffer supplemented with protease inhibitors. Embryos were homogenised by pipetting up and down. Homogenates were then cleared by centrifugation at 15000g for 15-30min at 4°C. Protein lysates (usually ½-1 embryo equivalents) were run on an SDS-page gel and then blotted onto a PVDF membrane. Membranes were then blocked in 5% milk in TBSTw (1xTBS buffer + 0.1% Tween-20). Blots were incubated with primary antibodies (HA-rabbit: Invitrogen, actin-rabbit: Invitrogen) in 5% milk overnight at 4°C. Visualization was performed using HRP-conjugated antibodies (Santa Cruz Biotechnology anti-rabbit, mouse and goat) and detected using the Lumisensor chemiluminescent reagent kit (Genscript).

2.16 Casein Zymography

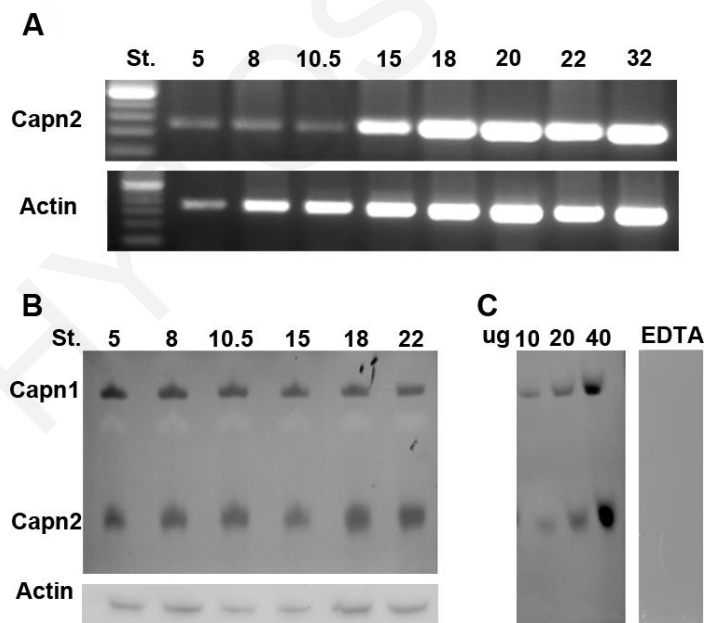
Casein zymography was performed on *Xenopus* protein extracts as previously described (Raser et al., 1995) with minor modifications. Briefly, the non-denaturing casein polyacrylamide gels were pre-run for 30 min on ice. Lysates were loaded into the gel and run for 1.5 h at 130V on ice. Afterwards, the gel was incubated at RT in Calpain activation buffer containing 1-4 mM calcium and 10 mM dithiothreitol O/N. For negative control, the gel was incubated in the same buffer without calcium and with the addition of 1mM EDTA. Finally the gel was stained with Coomassie blue.

3. Results

3.1 Calpain2 function during *Xenopus* development

3.1.1 Expression pattern of Calpain2 during *Xenopus* development

The temporal expression pattern of Calpain2 was examined by RT-PCR from blastula (stage 5) to tadpole embryos (stage 32). Calpain2 mRNA was detected in blastula stages and it continued to be expressed throughout development (**Figure 49A**), indicating that Calpain2 is a maternal gene and is expressed throughout development. In addition, Calpain2 protein activity was examined by casein zymography. Although casein zymography is an activity assay, it does not exactly reflect Calpain activation *in vivo* since calcium is added in the reaction buffer, but it correlates well with the protein levels (Raser et al., 1995). This technique allows the separation of Calpain2 (**Figure 49B, lower band**), from Calpain1 (**Figure 49B, upper band**) due to their different mobility on gel (Raser et al., 1995). Calpain2 and Calpain1 proteins were detected from blastula to tailbud stages, indicating that Calpain proteins are maternal proteins and are present throughout development in agreement with the data from the RT-PCR. The sensitivity of the method was tested by loading different amounts of the same sample and checking for the proportional increase in the brightness of the clearing band (**Figure 49C, left gel**). As expected, the activity of both Calpains was inhibited by adding EDTA to the reaction buffer (**Figure 49C, right gel**).



(A) RT-PCR was performed using specific primers for Calpain2 at different stages of development. Actin was used as a loading control. (B) Casein zymography analysis shows the activity of Calpain1 (upper band) and Calpain2 (lower band) at different stages of development (left top gel). Western blot of actin was used as a loading control (left bottom gel). (C) Various amounts (10 to 40 µg) of whole-embryo lysates were loaded on to the gel to assess the method sensitivity (middle gel). As a negative control, a gel loaded with 20 µg of lysate was incubated in a noncalcium proteolysis buffer containing 1mM EDTA.

Figure 49. Temporal expression of Calpain2 during *Xenopus* development

The spatial expression pattern of Calpain2 was examined via Whole Mount in-Situ hybridization (WISH). In cleavage stage embryos, Calpain2 mRNA accumulated primarily in the animal hemisphere (**Figure 50A**) and the same localization was maintained during mid-blastula (**Figure 50B**). At gastrula stages, the Calpain2 transcript was detected in both the ectoderm and mesoderm (**Figure 50C**), in agreement with a previous analysis of distribution of Calpains in *Xenopus* performed by immunohistochemistry (Moudilou et al., 2010). As neurulation proceeds, higher expression could be seen in the neural plate (**Figure 50D**). At tailbud stages (stage 22), there was strong expression in the spinal cord, the brain and the eye (**Figure 50E**). Cross-section of a WISH-stained tailbud embryo imaged under fluorescence microscopy showed clear expression in the neural tube and somites and weak staining in the notochord (**Figure 50F**). A similar distribution of Calpain2 was reported in E8.5-11.5 mouse embryos (Raynaud et al., 2008). At tadpole stages, Calpain2 mRNA was detected in the central nervous system, the otic vesicle, the cement gland, the branchial arches, the somites and the eyes. Head cross sections revealed that Calpain2 mRNA is enriched in the neural olfactory placode, the cement gland, the neural tube the eye and the archenteron floor (**Figure 50G**). These data show that Calpain2 mRNA is detected in morphogenetically active tissues such as the mesoderm and the neuropithelium suggesting a role of Calpain2 in morphogenetic movements during *Xenopus* development.

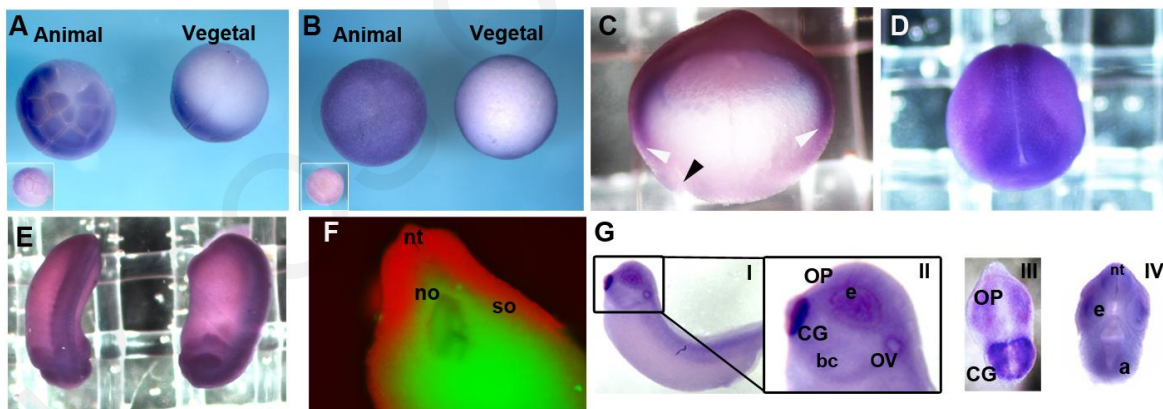


Figure 50. Spatiotemporal expression pattern of Calpain2 during *Xenopus* development.

(A) Animal (left) and vegetal (right) view of a stage 5 embryo. Control hybridization with the sense probe is shown in the inset. (B) Animal (left) and vegetal (right) view of a stage 9 embryo. Control hybridization with the sense probe is shown in the inset. (C) Sagittal section of a stage 10.5 embryo, apical to the top, dorsal to the left. (D) Dorsal view of a stage 16 embryo, anterior to the bottom. (E) Dorsal (left) and lateral (right) view of a stage 22 embryo, anterior to the bottom. (F) Cross-section view, dorsal to the top, of a WISH-stained tailbud embryo visualized by fluorescent microscopy (WISH-staining in red; background fluorescence in green). (G) WISH for Calpain2 of stage 32 embryos. (I) Calpain2 mRNA is detected in the spinal cord, somites, eye, cement gland and otic vesicle, olfactory placode and cement gland. (II) Zoomed of head region from I. (III) Front view of anterior head cross sections. Calpain2 is detected at the cement gland and the olfactory placode. (IV) Calpain2 mRNA is detected at the archenteron floor in posterior head cross sections. Abbreviations: a, archenteron e, eye; OP, Olfactory Placode; OV, Optic Vesicle; bc, branchial arches; so, somites; no, notochord; nt, neural tube; CG: Cement Gland.

3.1.2 Calpain2 localization in *Xenopus* embryos

In the absence of commercially available antibodies able to discern the different Calpain isoforms in *Xenopus* embryos, immunofluorescence analysis was performed on sections of embryos injected with an HA-tagged Calpain2 mRNA to study its subcellular localization. In the dorsal mesoderm of a stage 12 embryo, HA-Calpain2 was strongly localized at the plasma membrane and presumptive Golgi-ER complex, while a weaker signal was detected in the cytoplasm (**Figure 51A**), in agreement with the previously reported localization of Calpain2 in cell lines (Hood et al., 2004; Shao et al., 2006). In the prospective neurectoderm at early gastrula stage, HA-Calpain2 distribution appeared diffuse in the cytoplasm with only a weak signal at the membrane (**Figure 51B**). At neurula stage, Calpain2 was strongly localized at the membrane in neural ectodermal cells (**Figure 51C**). These differences in cellular localizations may reflect different states of activation of Calpain2, as previously observed in cell lines (Wells et al., 2005). The changes in Calpain2 localization temporally coincide with the periods of active morphogenetic movements in the mesoderm and neurectoderm respectively, suggesting again a possible involvement of Calpain2 in morphogenesis. In addition the changes of Calpain2 localization between the cytosol and the membrane might be correlated with intracellular calcium levels as it has been shown previous for Calpain2 and other calcium activated proteins (Sheldahl et al., 2003; Suzuki et al., 2004).

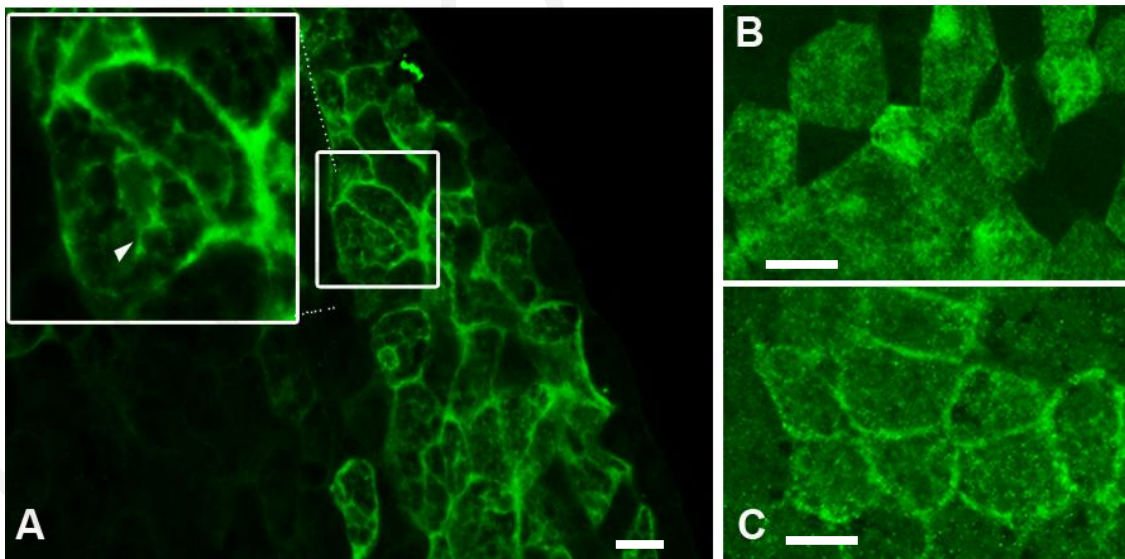


Figure 51. Localization of exogenous Calpain2.

(A) Cross-section through the dorsal mesoderm of a stage 12 embryo ectopically expressing HA-Calpain2 and stained with an anti-HA antibody. A high-magnification view of the boxed region is shown in the inset. The white arrowhead indicates the presumptive Golgi-ER complex. (B) HA-Calpain2 localization in ectodermal cells of a stage 9 embryo. (C) HA-Calpain2 localization in neural ectodermal cells of a stage 13 embryo. Scale bars = 20 μ m

3.1.3 Blockage of Calpains function with a Calpain specific inhibitor

To investigate the specific role of Calpains during *Xenopus* development, embryos were treated with a reversible Calpain inhibitor (Calpain inhibitor III, CI3) for different lengths of time during development. The fact that CI3 is a reversible inhibitor, allowed us to pinpoint the major developmental stages in which Calpain activity is required by removing the inhibitor at different times. Embryos treated at pre-gastrula stages with 100 μ M of inhibitor showed delays in blastopore closure, indicating that Calpain function is necessary for gastrulation (**Figure 52A**). Furthermore, removal of the inhibitor at stage 8 (pre-gastrula) resulted in embryos which were completely normal (data not shown), suggesting that Calpain activity is not required during blastula stages. Most of the embryos treated with CI3 died at gastrula and neurula stages. Surviving embryos displayed severe deformities at tadpole stages with very short and dorsally bent axes, complete loss of anterior structures and spina bifida stemming from failure of blastopore closure (**Figure 52B**). Removal of the inhibitor at late gastrula stages (stages 12) significantly improved the phenotype tadpole embryos (**Figure 52B**). This suggests that Calpain2 function is necessary both during gastrulation and neurulation. Embryos treated with the inhibitor at stage 11 onwards gastrulated normally but NTC was markedly delayed (**Figure 52C**), leading to shorter tailbuds with smaller eyes, kinked tails, reduced pigmentation and anencephaly (**Figure 52D**), in agreement to the rescue phenotype when the inhibitor was removed before the beginning of neurulation. Quantification of the phenotypes at gastrula, neurula and tadpole embryos strengthens the above observations. At the end of gastrulation ~76% of embryos treated at pre-gastrula stages with 100 μ M of inhibitor showed delays in blastopore closure while this phenotype was partially rescued when the inhibitor was removed at stage 10.5 and was absent from embryos treated at stage 11 with CI3 inhibitor (**Figure 53A**). At neurula stage 40% of embryos treated with CI3 from blastula stages initiated neurulation with open blastopore, and the remaining embryos displayed NTC defects. Removal of the CI3 inhibitor at stage 10.5 rescued the neurulation phenotypes. Treatment of embryos with CI3 from stage 11 onwards induced NTC phenotype in 98% of the embryos, (**Figure 53B**). By tadpole stages, 70% of the embryos treated from blastula stages with 100 μ M CI3 died (**Figure 53D**). The remaining embryos showed severe phenotypes as describe above. These phenotypes were clearly rescued by the removal of the Calpain inhibitor. 71% and ~48% of complete phenotype rescue at tailbud stage was observed when the inhibitor was removed at stage 10.5 and 12, respectively (**Figure 53C**). Moreover, removal of the inhibitor at stage 10.5 and 12 rescued the reduced dramatically the number of dead embryos (**Figure 53D**).

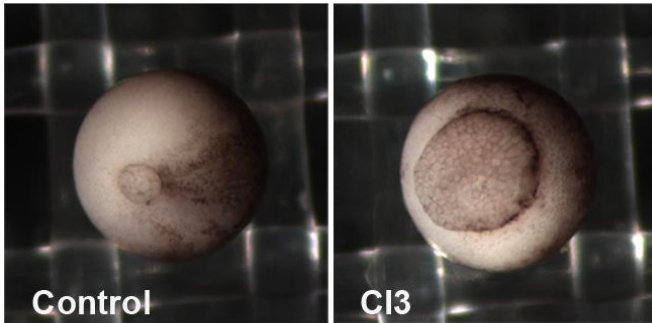
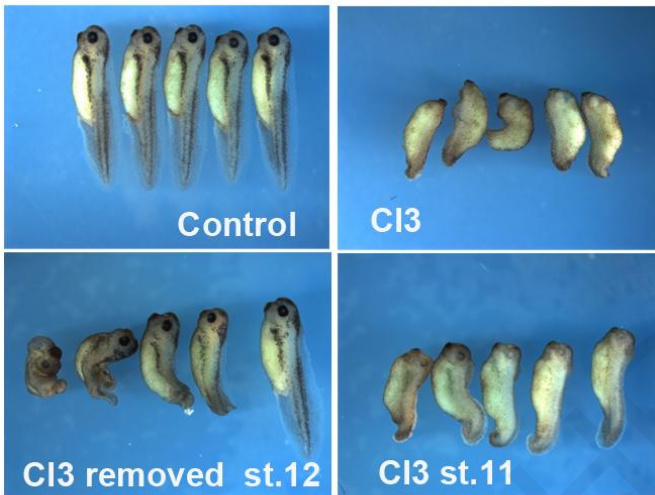
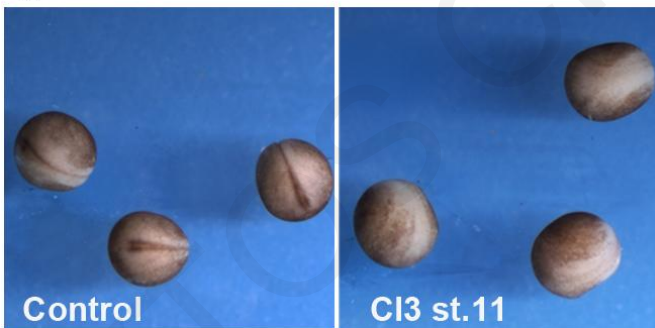
A**B****C**

Figure 52. Inhibition of Calpains by CI3 causes severe delays in blastopore and NTC.

(A) Vegetal view of a stage 12 control embryo (left) and an embryo treated with 100 μ M CI3 from pre-gastrula stages (right). CI3-treatment severely delays blastopore closure. (B) Tailbuds of embryos treated with CI3 at different times of development and rescued by removal of the inhibitor. Embryos in which the inhibitor was added at pre-gastrula stages and kept for the whole course of development display a severe phenotype, with shorter and bent AP axis and loss of anterior structure. Embryos in which the inhibitor was removed at stage 12 and replaced with fresh 0.1X MMR display a range of overall less severe phenotype, with normal heads but shorter and bent AP axis and some spina bifida phenotype. Embryos treated with CI3 from stage 11 onwards appear shorter, with reduced eyes and overall pigmentation. (C) Dorsal view of stage 18 control embryos (left) and embryos treated with 100 μ M CI3 from stage 11 (right). The addition of the inhibitor at this stage causes a significant delay in NTC.

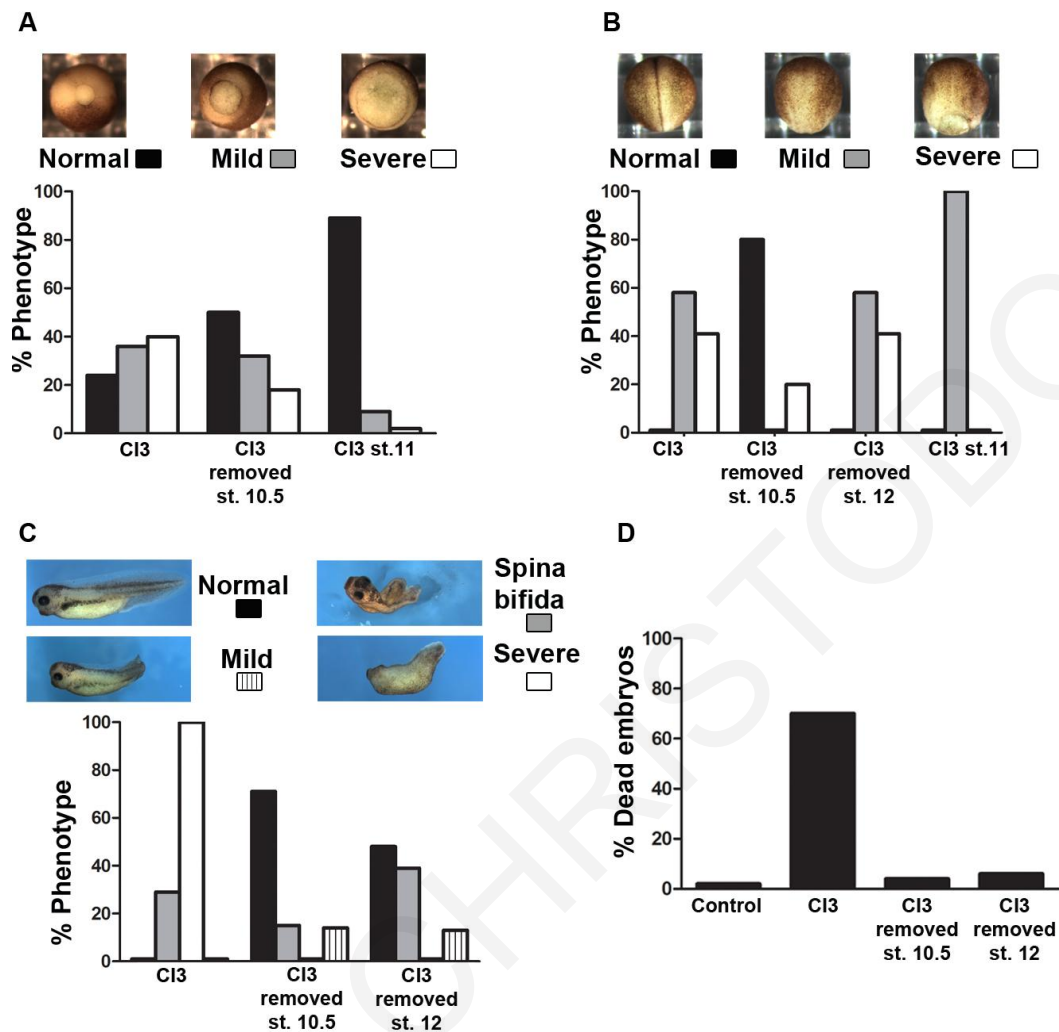


Figure 53. Quantification of phenotypes induced after treatment of embryos with CI3.

(A-D) Scoring of the phenotypes of embryos treated with the inhibitor from gastrula stages onwards (n=73), rescued at stage 10.5 (n=44), rescued at stage 12 (n=55) and treated from stage 11 (n=46). Graphs indicate the percent of embryos that display the phenotypes as depicted in the images above each graph. Percentages are calculated on surviving embryos only. (A) Delays in blastopore closure are assessed in embryos at stage 12. (B) Delays in NTC are scored in embryos at stage 18. (C) The range of phenotypes observed at tailbud stages are classified in mild (normal head structure, shorter AP axis), severe (very short and deformed embryos, completely lacking head structure) and spina bifida. (D) Death rates of embryos treated with CI3 from gastrula stages onwards, rescued at stage 10.5 and rescued at stage 12.

3.1.4 Blockage of Calpain2 function with a dominant negative construct

Given the impossibility to determine the time the inhibitor takes to permeate the embryo and to role out its possible toxic effect during early development, we generated a dominant-negative form of *Xenopus* Calpain2 by mutating the active site Cystein 105 into Serine (Calpain2C105S). This mutation is reported to inactivate the enzyme, without affecting its overall structure or binding capacity (Arthur et al., 1995; Masumoto et al., 1998). Injection of 1ng Calpain2C105S at the 2-cell stage caused a significant delay in blastopore closure (**Figure 54A**), as observed in embryos treated with CI3. At tadpole stage, Calpain2C105S-injected embryos appeared severely

deformed, shorter, dorsally bent and some displayed anencephaly (**Figure 54B**), again resembling CI3-treated embryos.

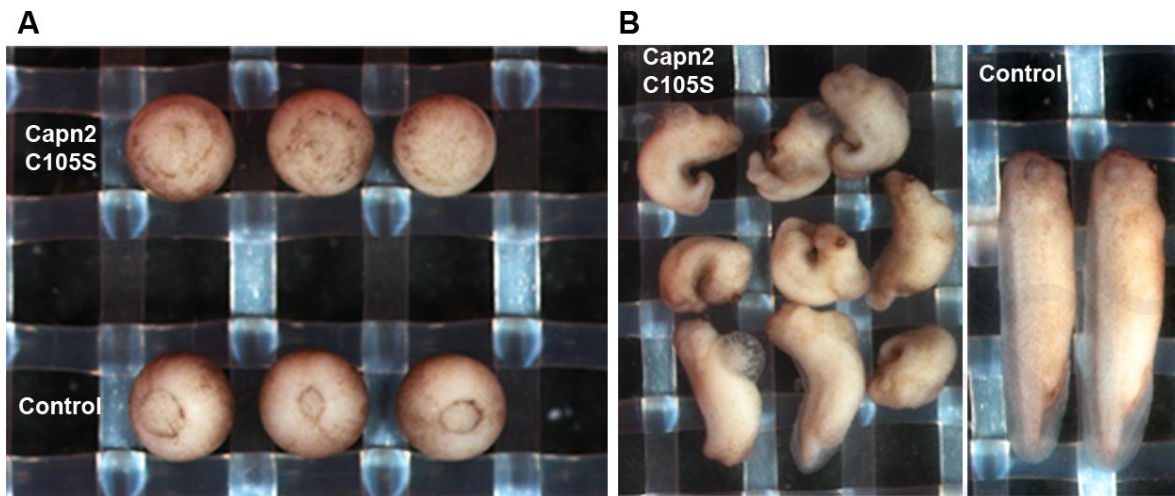


Figure 54. Calpain2 dominant negative induces phenotype similar to the phenotype induced by CI3.

(A-B) Embryos were injected at 2 blastomeres at 2-cell stage with 1ng Calpain2C105S. (A) Embryos injected with Calpain2C105S show a marked delay in blastopore closure at stage 12 (top embryos) compared to controls (bottom embryos). (B) Tailbuds of embryos injected with Calpain2C105S (left image) are shorter, dorsally-bent and lacking head structures. Some severe cases display spina bifida. Controls are shown to the right.

3.1.5 Downregulation of Calpain2 with a specific Calpain2 specific Morpholino induce similar phenotypes with CI3 treatment

Overall, the previous experiments suggested a crucial role for Calpains during gastrulation and neurulation. However, although CI3 is one of the most specific calpain inhibitors currently available, it is still reported to inhibit both Calpain1 and 2 due to their high sequence identity. For the same reason, the possibility that Calpain2C105S may also block other highly homologous Calpain isoforms can not be excluded. Given the fact that disruption of Calpain2 gene in mice led to embryonic lethality (Dutt et al., 2006; Takano et al., 2011), whereas knockout for Calpain1 resulted in fertile adult mice with reduced platelet aggregation (Azam et al., 2001), it was decided to selectively block Calpain2 by morpholino antisense oligonucleotide (MO). Embryos were injected with 50-70ng (total) of Calpain2 MO either at 1-cell stage or 2 out of 2 blastomeres at 2-cell stage and monitored during development. Western blotting analysis of 50ng MO-injected embryos showed undetectable protein levels of mRNA-injected HA-tagged Calpain2 at stage 13 (**Figure 55A**). In the absence of an available *Xenopus* Calpain2 specific antibody to examine endogenous Calpain2 downregulation as a result of MO injection, casein zymography analysis was used. Casein zymography revealed that only a slight reduction in endogenous Calpain2 levels was observed at stage 13 following the injection of 50ng MO (not shown), but a ~40% was observed later at stage 19 (**Figure 55B**).

A ~50% downregulation of activity at stage 13 was achieved by increasing the amount of injected MO to 70ng (**Figure 55B**). The discrepancy observed in the amount of downregulation between HA-Calpain2 and endogenous Calpain2 is probably due to the presence of stable maternal protein, since examination of the EST database did not reveal the presence of any pseudoalleles.

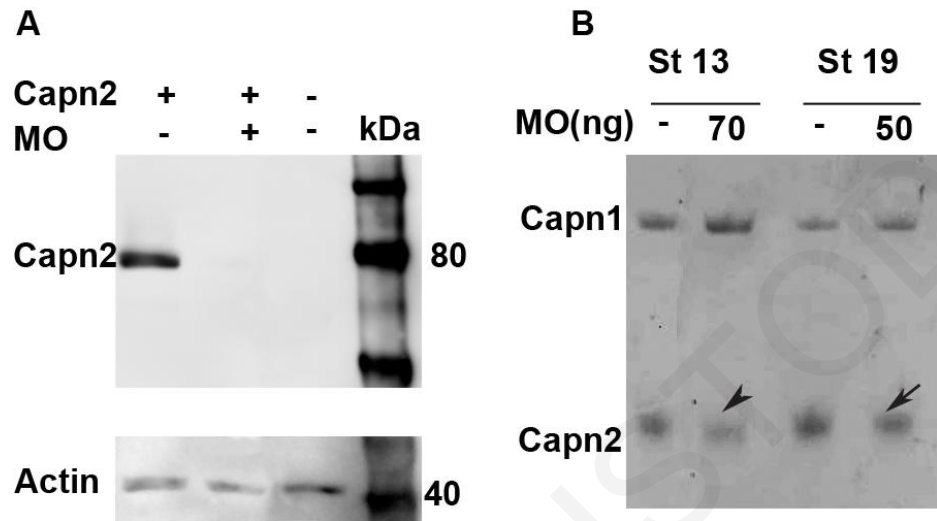


Figure 55. Characterization of Calpain2 MO.

(A) Western blot analysis detecting HA-tagged Calpain2 in lysates of stage 13 embryos. mRNA (200pg) encoding HA-Calpain2 is co-injected with or without MO (50ng). This amount of MO completely blocks the translation of HA-Calpain2. (B) Casein zymography analysis showing endogenous Calpain1 (top) and Calpain2 (bottom) activities in lysates of MO-injected embryos. Injection of 50ng MO causes a 37% reduction in Calpain2 expression at stage 19 (arrow). Injection of 70ng MO causes a 45% reduction in Calpain2 expression at stage 13 (arrowhead). Densitometry analysis was performed using ImageJ software.

80% of embryos injected with 70ng MO showed a slight delay in blastopore closure during gastrulation (**Figure 56A&E**), but in all cases the blastopore eventually closed. This phenotype is clearly milder than the one observed in CI3-treated embryos. This is not surprising since a relatively late downregulation of Calpain2 by MO was shown, whereas the inhibitor efficiently blocked protein activity from early stages. During neurulation, all MO-injected embryos presented a similar phenotype to embryos treated with CI3 from stage 11, showing a marked delay in NTC (**Figure 56B&E**). Particularly, anterior NTC was more severely affected than the posterior neural tube which eventually closed (**Figure 56C**). At tailbud stage, MO-injected embryos displayed a range of developmental abnormalities (**Figure 56D**) that were scored based on their severity (**Figure 55F**). ~24% of the embryos displayed a very severe phenotype, with much shorter AP axis and complete loss of head structures (anencephaly). ~39% showed a short and dorsally bent body axis and eye reduction, whereas ~33% had a short axis and eye reduction (**Figure 56F**). The overall phenotype caused by 70ng MO injections was fully rescued by co-injecting 500pg mRNA of HA-Calpain2R (lacking the 5'UTR region recognized by the MO)

demonstrating the specificity of the MO (**Figure 56D**). Injection of 70ng control MO did not elicit any abnormal phenotype (not shown) providing further evidence that the phenotype observed in the morphants was specific. Overall, the phenotypes of the Calpain2 MO-injected embryos resembled those observed in CI3-treated and Calpain2C105S expressing embryos suggesting that the phenotypes induced by the CI3 inhibitor stem from blockage of Calpain2 function.

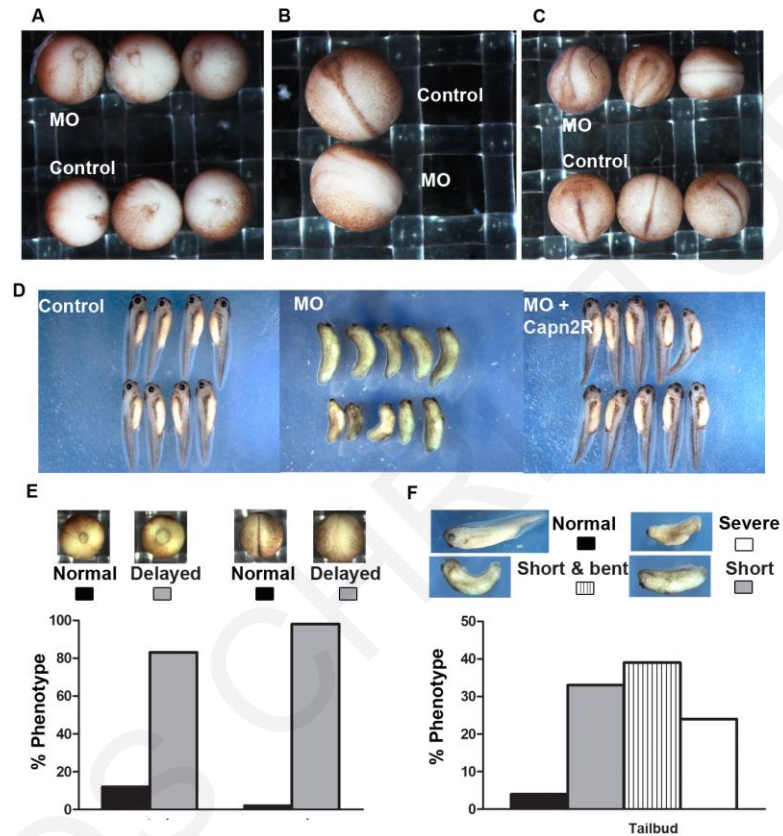


Figure 56. Phenotypes induced after downregulation of Calpain2 with Calpain2 MO.

(A) Vegetal view of stage 12.5 control embryos (bottom) and embryos injected with 70ng MO at 1-cell stage (top). MO-injected embryos show mild delays in blastopore closure. (B) Dorsal view of a stage 18 control embryo (top) and an embryo injected with 50ng MO at 1-cell stage (bottom). The MO-injected embryo show marked delays in NTC. (C) Dorsal & anterior views of stage 20 embryos injected with the MO as in B. At this stage, caudal neural folds appear to be fused in the MO-injected embryos (top, third embryo to the right) as in controls (bottom, embryo in the middle). However, anterior neural tube is still open in MO-injected embryos (top, first and second embryos from the left) whereas it is completely closed in controls (bottom, first and third embryos). (D) Tadpole control embryos, embryos injected with 70ng MO at 1-cell stage and embryos in which the same amount of MO was co-injected with 500pg Calpain2R. MO injections cause shortening of the AP axis and head malformations. The phenotype is successfully rescued by Calpain2R. (E) Delays in blastopore closure and during neurulation are scored in embryos (injected as in A) at stage 12 and 18, respectively (n=71). Graphs indicate the percentage of embryos that display the phenotypes as depicted in the images above each graph. (F) Tadpoles embryos injected with the MO as in A are scored for their phenotypes. They were classified in short (shorter AP axis), short & bent (shorter and dorsally curved AP axis) and severe (very short and deformed embryos, completely lacking head structures). Graphs indicate the percentage of embryos that display the phenotypes as depicted in the images above each graph (n= 46).

3.1.6 Calpain2 function during gastrulation

I. Blockage of Calpain2 function does not affect mesoderm specification

To exclude the possibility that the gastrulation defects we observed in embryos treated with the Calpain inhibitor are due to defects in mesoderm induction, whole mount *in situ* hybridization for the pan-mesodermal marker *Brachyury* (*Xbra*) was performed. The intensity of *Xbra* staining at stage 11 was similar between treated and untreated embryos (**Figure 57A**), suggesting that CI3 does not affect mesoderm induction. At stage 12, in control embryos *Xbra* staining revealed a tight ring around the yolk plug and a long, narrow notochord. In contrast, in treated embryos *Xbra* formed a larger ring around the yolk plug in agreement with an impairment of blastopore closure and stained a short and broad notochord (**Figure 57B, insets top left**). Sagittal sections of *Xbra*-stained embryos confirmed that in CI3-treated embryos the chordal mesoderm failed to elongate suggesting inhibition of CE and/or mesoderm migration (**Figure 57B**). *In situ* hybridization for *Chordin* (*Chrd*), a dorsal marker expressed in the gastrula organizer and in the notochord at later stages, showed no difference in its expression level and localization at stage 10.5 in CI3-treated and untreated embryos (**Figure 57C**), indicating that D/V patterning was not affected. These data lead to the conclusion that blockage of Calpain2 activity does not affect the levels of expression of mesodermal markers but alters their localization, suggesting that the gastrulation defects observed in CI3-treated embryos are not due to defective mesodermal specification, but probably to perturbed movements of mesodermal cells.

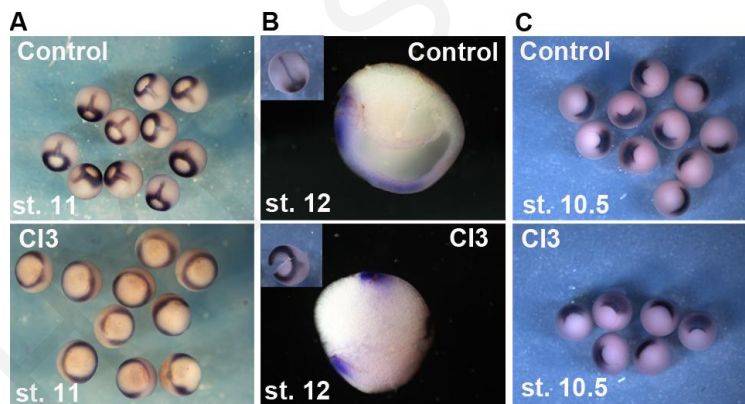


Figure 57. Expression of mesodermal markers after blockage of Calpain function.

(A-C) WISH showing the expressions of mesodermal markers *Xbra* (A&B), and *Chrd* (C) in embryos treated with CI3 from 2-cell stage onwards. Inhibition of Calpains does not affect the expression and localization of *Xbra* and *Chrd* at early gastrula stages (A&C). (B) Sagittal sections of *Xbra*-stained embryos at stage 12 showed a shorter notochord in CI3-treated embryos compared to controls.

II. Calpain2 function is necessary for mesoderm convergent extension and affects mesoderm migration

The first phenotype induced by treatment of embryos with CI3 inhibitor is failure of blastopore closure during gastrulation. Blastopore closure is a complex process and several morphogenetic movements can influence it including CE and mesoderm migration (Stylianou and Skourides, 2009; Wallingford et al., 2002). In an effort to better understand the underlying mechanism responsible for the phenotype induced by Calpain2 inhibition, the role of Calpain2 on CE was examined, using the well established animal cap elongation assay. Animal caps were dissected from CI3-treated and control embryos at stage 8 and subsequently induced with activin. While control explants elongated normally, those excised from CI3 treated embryos (50-100 μ M CI3) remained almost completely round (**Figure 58A**) indicating that CE was severely impaired. Knockdown of Calpain2 by MO-injection blocked animal cap elongation, although not completely as in CI3-treated caps (**Figure 58B**). This is most likely because the MO does not completely downregulate Calpain2 during gastrula stages previously observed by casein zymography (**Figure 55B**) and confirmed by the mild phenotype observed during gastrulation in MO-injected embryos (**Figure 56A**).

To assess whether Calpain activity is also required for mesoderm migration, cell movements of dissociated activin-treated caps, plated on fibronectin-coated cover slips were analyzed. Mesodermal cells adhered, spread and began migrating normally in the presence of the inhibitor. However time-lapse recordings showed that CI3-treated cells moved significantly slower than controls (**Movie 1**). Indicative cell traces of controls and CI3 treated cells are shown in **Figure 58C**. Migration rates were calculated and showed an overall 45% reduction for treated cells compared to controls (**Figure 58D**). Calpain activity is thus not strictly required for mesoderm migration but it modulates migration rates.

Overall, these data show that Calpain inhibition by CI3 completely blocks mesoderm CE and modulates mesoderm migration. This suggests that both defects are likely responsible for the failure of blastopore closure during gastrulation, although impairment of CE seems to be the major determinant.

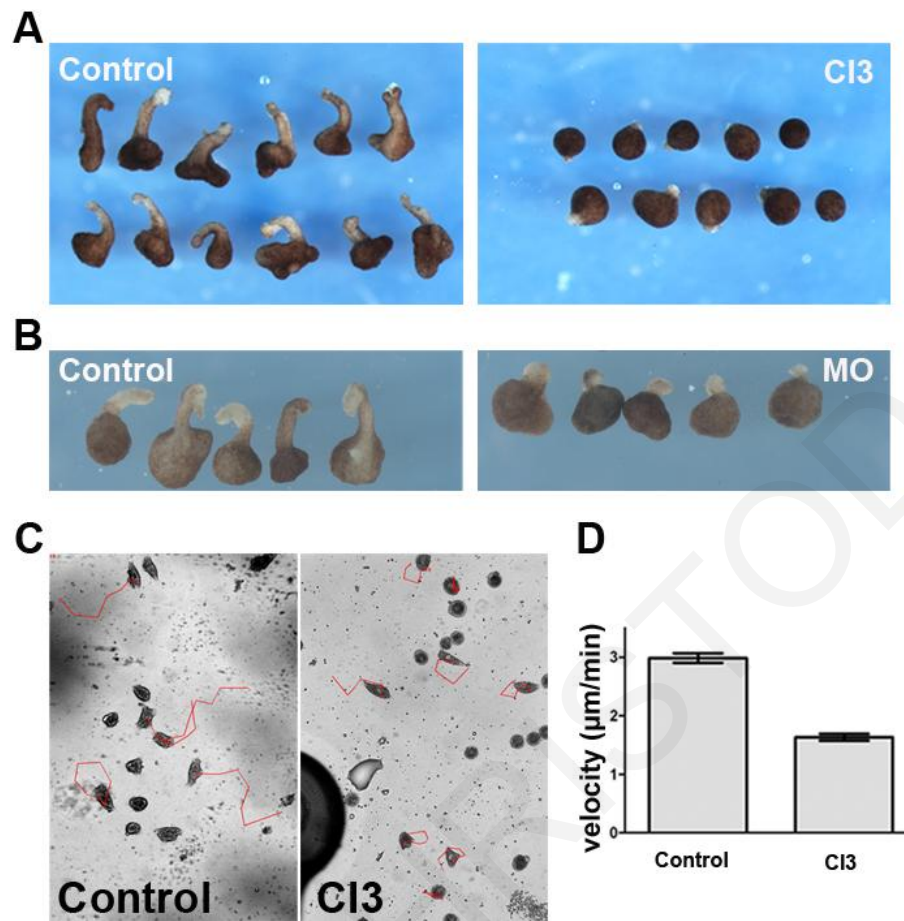


Figure 58. Calpain2 function is indispensable for Convergent Extension and is implicated in mesoderm migration.

(A) 50 μM CI3 inhibitor completely blocks the activin-induced elongation of animal caps explants in 3 independent experiments. (B) Injection of 70ng of Calpain2 MO impairs the activin-induced elongation of animal caps explants. (C) Cell traces from Control and CI3 treated mesodermal cells derived from activin-treated dissociated caps and plated on fibronectin coated coverslip. (D) Migration rates of CI3-treated or untreated mesodermal cells derived from activin-treated dissociated caps (values shown are means \pm SEM., n=25).

3.1.7 Calpain2 function during Neurulation

I. Calpain2 downregulation leads to defective Neural Tube Closure without affecting neural markers expression.

As discussed above, both CI3 treatment as well as Calpain2 MO injections resulted in defects of NTC. Time-lapse recordings of MO-injected embryos (1 out of 2 blastomeres) revealed a marked delay in NTC, with the anterior neural plate remaining open at stage 18 (**Movie 2**). The phenotype could be successfully rescued by co-injecting Calpain2R mRNA with the MO, as shown by a normal movement of the neural ectoderm towards the midline, as in controls (**Figure 59A and Movie 3**). MO injection in one dorsal blastomere at the 4-cell stage to target the neural plate was sufficient to cause the same severe delay in NTC (**Figure 59B**), suggesting that Calpain2 function is required for the shaping of the neural plate. Furthermore, the expression and localization of the pan-neural marker *Sox2* was examined by RT-PCR and *in situ* hybridization. While the localization of this marker denoted a wider neural-plate region in the MO-injected side (**Figure 59C**), its expression level was unaffected in MO-injected embryos (**Figure 59D**). Quantification of the width of *Sox2* expression confirmed that the neural plate in MO-injected sides was significantly wider than in the uninjected sides (**Figure 59 E&F**). Coinjection of Calpain2R mRNA with MO decreased the width of the *Sox2* expression domain (**Figure 59F**), confirming once again the specificity of the Calpain2 MO. *In situ* hybridization for the lateral neural plate marker *Pax3* at stage 18 showed that its expression was not affected while it was shifted laterally in the injected side (**Figure 59G**), again indicating a delay in NTC. In some MO-injected embryos, *Pax3* expression at tadpole stages revealed that anterior neural folds that failed to fuse (**Figure 59H**). Overall, these data suggested that the defective NTC observed in embryos in which Calpain2 had been downregulated is not due to neural specification defects as shown by the normal expression of *Sox2* and *Pax3*

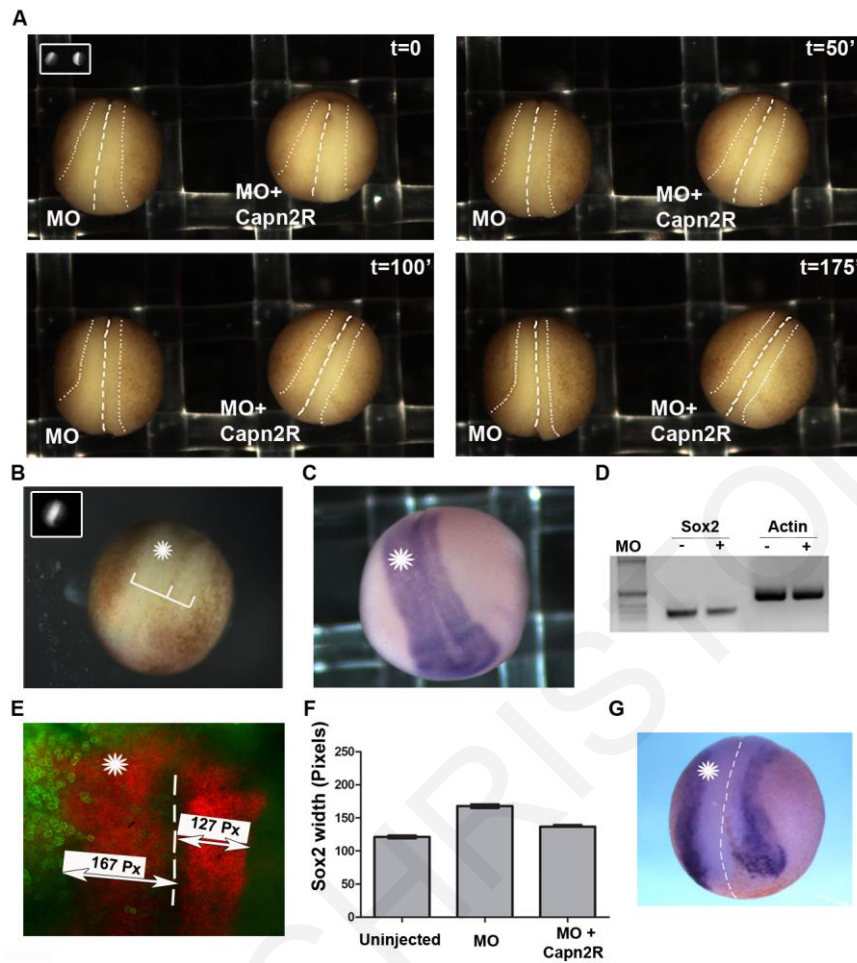


Figure 59. Downregulation of Calpain2 by MO affects cell movements during Neural Tube Closure.

(A) Stills from a 175 minute time-lapse movie of an embryo injected at 1 out of two blastomeres with 30ng MO (left embryo in each frame) and an embryo in which the same amount of MO was co-injected with 300pg Calpain2R mRNA (right embryo in each frame). White dashed lines outline the width of the neural plate. Time (t) in minutes is shown at the top right of each frame. The injected side of the embryo is shown by FITC fluorescence in the top left inset in the first frame. (B) Targeted injection of 20ng MO at 1 dorsal blastomere at 4-cell stage is sufficient to cause the severe delay in neural plate movement. The injected side is visualized by FITC fluorescence (inset) and indicated by an asterisk. White lines show the width of the neural plate. (C) WISH for neural marker *Sox2* in a stage 16 embryo co-injected with 20ng MO and 50pg mGFP at 1 dorsal blastomere at 4-cell stage. The injected side is marked by an asterisk. (D) RT-PCR analysis shows that *Sox2* expression is not affected by MO-injection in XBF2-induced animal caps. *Sox2* expression levels have been calculated using ImageJ and normalized against the loading control. (E) High magnification of the neural plate of a *Sox2*-stained embryo injected as in C and subsequently stained with an anti GFP antibody and visualized by fluorescent microscopy. mGFP staining (green) identifies the injected side (asterisk). *Sox2* staining is shown in red. The width of *Sox2* staining is measured using ImageJ software. (F) Quantification of the width of *Sox2* expression. The width was measured as described in F. As shown by the graph, the width of *Sox2* expression is significantly wider in the MO-injected sides than in the uninjected ones. Co-injection with 250pg Calpain2R clearly rescues the phenotype (values shown are means \pm s.e.m., n=15). (G) WISH for the neural fold marker *Pax3* in a stage 18 embryo injected as in C.

II. Calpain2 function is necessary for neural folds elevation and anterior Neural Tube Closure

The above results show that Calpain2 function is necessary for NTC. Thereafter Calpain2 morphant neurula embryos were examined carefully. Cross sections of neurula embryos injected with 40pg Calpain2 MO at 1 dorsal blastomere at the 4 cell stages show failure of neural fold elevation in the morpholino injected site (**Figure 60A**). This phenotype was rescued by coinjection Calpain2R mRNA with the Calpain2 MO (**Figure 60A**). Cross sections of late neurula stage 19 embryos, show that the neural folds are fused and the neural tube is correctly formed in control embryos, whereas the neural tube remains open in unilaterally Calpain2 MO-injected embryos (**Figure 60B**). Failure of neural fold elevation in morphant embryos was confirmed by phalloiding staining of stage 16 unilaterally morpholino injected embryos. In these embryos, phalloiding staining indicated failure of neural fold elevation in morphant side of the embryos, as shown by the defective hinge point formation (**Figure 60C**). At tailbud stage the neural tube is formed and is covered by the epidermis in controls, however in morphant embryos the anterior neural tube fails to close at the MO-injected side, while posterior NTC is delayed but is eventually completed (**Figure 60D, D'**). Cytokeratin is a marker of the epidermis. Cytokeratin staining of unilaterally injected tailbud embryos confirms that the anterior neural plate at the injected side remains exposed (**Figure 60E, E'**).

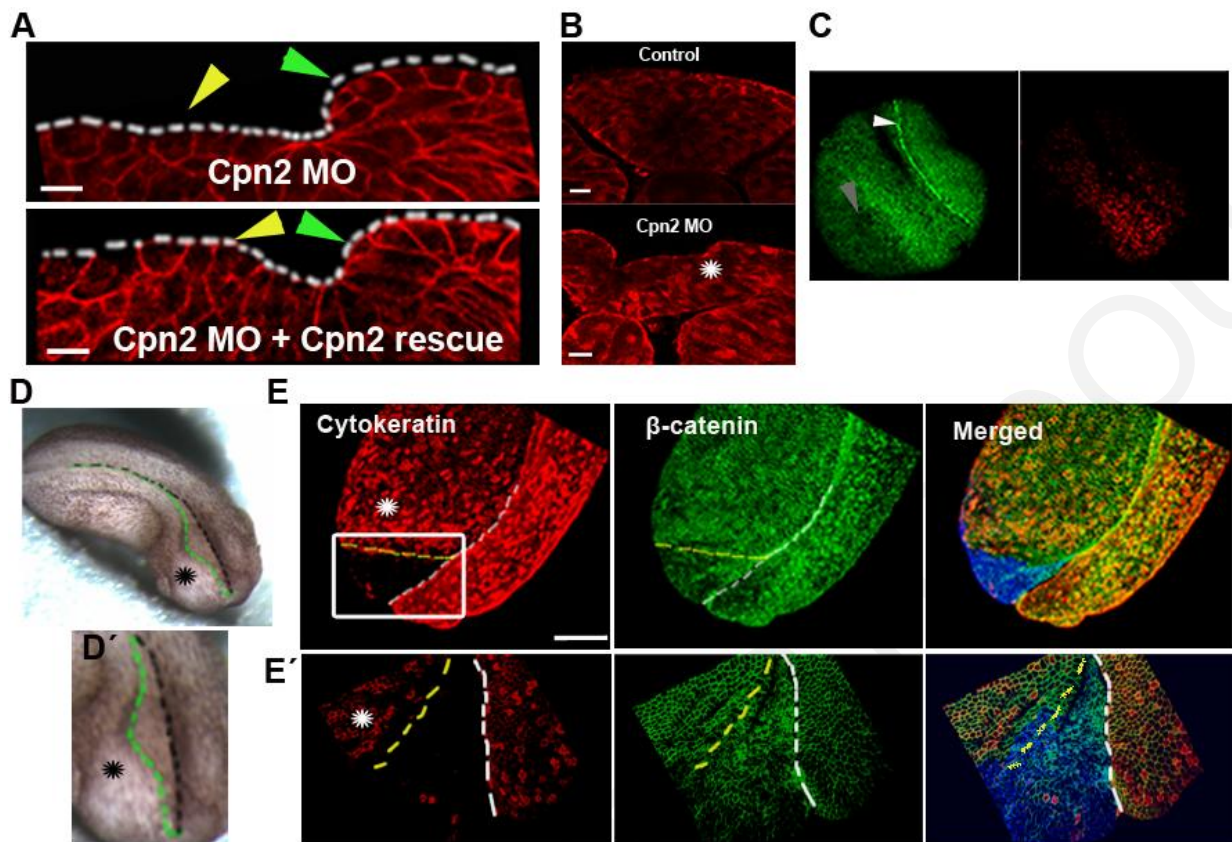


Figure 60. Calpain2 downregulation results in defective neural fold formation and anterior Neural Tube Defects.

(A) Cross sections of stage 16 embryos injected at 1 dorsal blastomere at 4 cell stage with Calpain2 MO or with Calpain2 MO + Calpain2R mRNA and stained for β -catenin. Green arrowheads show the uninjected side and yellow arrowheads indicate the injected side. Scale bar = 20 μ m (B) Cross sections of stage 19 control and morphant embryos stained for β -catenin. Scale bar = 20 μ m (C) Dorsal view, maximum intensity profile image of a stage 16 stage embryo injected with 40ng Calpain2 MO + histone GFP at 1 dorsal blastomere at 4 cell stage. Injected side is indicated by GFP signal (red). Phalloidin staining (green) reveals the formation of hinge point at the uninjected side (white arrowhead) while hinge point fails to form at the MO injected side (grey arrowhead). (D) Dorsal view of a tailbud embryo injected with 40ng Calpain2MO at 1 dorsal blastomere at the 4 cell stage. D') High magnification image of the anterior part of the embryo shown in D. Black lines indicate the midline at the uninjected side and green lines indicate the margins of epidermis at the injected site. (E) Dorsal view of tailbud morphant embryo stained with cytokeratin and β -catenin. MO injected side is indicated by GFP signal (blue). White lines show the midline and green lines show the margins of the epidermis at the injected site. E') Magnified images of the anterior part of the embryo shown in E. Scale bar = 500 μ m

III. Calpain2 is implicated in neural convergent extension

NTC is driven by two major morphogenetic movements, CE and AC. CE is linked with caudal NTC and AC with rostral NTC. As seen before, in Calpain2 morphant neurula embryos, posterior NTC is delayed but finally completed, while anterior NTC fails to complete. These suggest that Calpain2 activity might be necessary for both CE and AC during neurulation. As it has been shown above, Calpain2 activity is essential for mesoderm CE. Thereafter, it was decided to first examine the role of Calpain2 in neural CE and address its role in AC later on. We set to determine if Calpain2 is indeed necessary for neural CE by using XBF2-injected ectodermal

explants (animal caps). XBF2 expression induces neural fate without inducing mesoderm. These explants undergo CE leading to different degrees of elongation (Mariani and Harland, 1998; Wallingford and Harland, 2001). As expected, 50% of XBF2-injected controls showed a mild elongation and 40% strong elongation (**Figure 61A&D**). Co-injection of MO significantly inhibited explant elongation (**Figure 61B**), with 50% of the caps showing no elongation at all (**Figure 61D**). In explants treated with 50 μ M CI3, CE was completely blocked and the caps remained completely round (**Figure 61C&D**). In addition, the role of Calpain2 in neural CE was examined in neural plate explants that contained the underlying mesoderm (Borchers et al., 2006; Elul and Keller, 2000). Calpain2 MO also significantly inhibited the elongation of these explants that better reflect the *in vivo* situation (**Figure 61E&F**). Images of the elongating explants were taken every 2 hours and the change in length was measured. While control explants exponentially elongate over time, MO-injected explants initially elongated but began to gradually reach a plateau after 2 hours (**Figure 61E**). Additionally, MO-injected explants remained wider than controls and neural fold elevation was defective (**Figure 61F**). In conclusion, these results show that Calpain2 downregulation inhibits CE movements in both neuralized ectodermal explants and in neural plate explants, confirming that at least in part the observed NTC defects in both morphants and CI3 treated embryos stem from defects in CE movements.

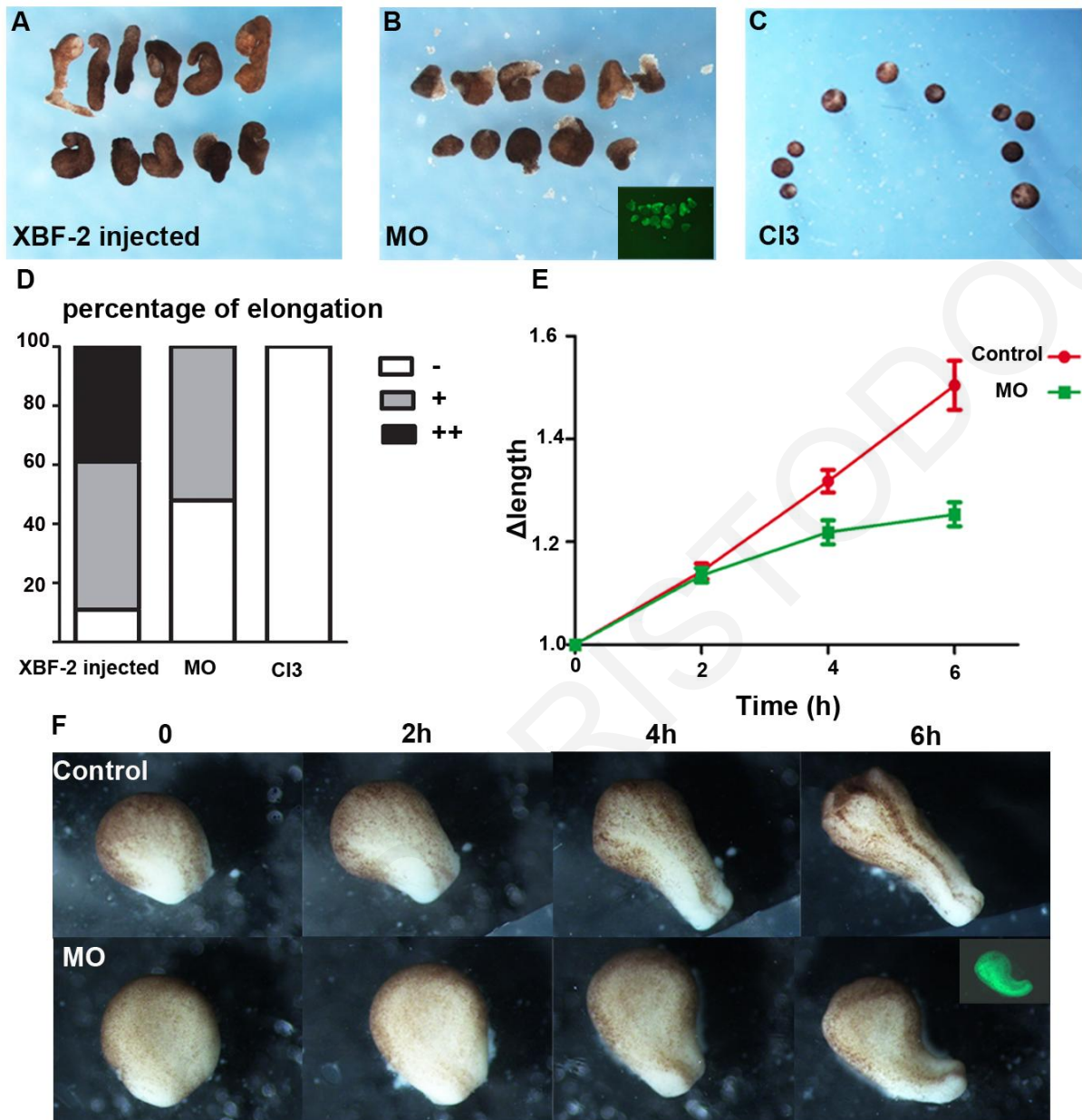


Figure 61. Downregulation of Calpain2 expression by MO inhibits neural Convergent Extension.

(A-C) Neural convergent extension was analyzed in XBF2-injected animal caps. One-cell stage embryos were injected with 100pg XBF2 either alone (A) or co-injected with 70ng MO (B) or treated with 50 μ M CI3 (C). The inset in B shows MO presence in the explants as shown by FITC fluorescence. (D) Percentage of elongated explants from the experiment described in A-C. Explants with different degrees of elongation were grouped according to their length to width ratio (LWR). Black indicates a strong elongation (LWR >2), gray a mild elongation (LWR=1.2-2) and white no elongation (LWR=1-1.2), (XBF-2 injected, n=26; MO, n=23; CI3, n=24). (E-F) Neural convergent extension was analyzed in neural plate explants. (F) Neural plate explants excised from stage 12-12.5 control (top panel) or MO-injected (bottom panel) embryos were left to elongate. The time (in hours) at which each picture was taken is indicated above. The inset of the last image in the bottom panel shows FITC fluorescence. (E) The graph shows the change in length (Δ length) over time in control (red) and MO-injected (green) neural explants that were prepared as in F. The lengths were measured using ImageJ software. The plotted data are means \pm s.e.m (n=10). Abbreviations: LWR, length to width ratio.

3.1.8 Elucidating the involvement of Calpain2 in Convergent Extension

Since Calpain2 inhibition abolishes CE movements in both mesodermal and neural tissues without affecting mesoderm or neural specification, we wanted to further probe the mechanism behind this effect. One possibility is that Calpain2 activity is required for adherens junction turnover and remodeling, which is in turn required for cell intercalation. Adherens junction molecules have been identified as Calpain targets in different cell lines (Benetti et al., 2005; Jang et al., 2009; Rios-Doria et al., 2003) and it is also known that both overexpression and loss of cadherins interferes with CE movements (Niessen et al., 2011). To explore this possibility we decided to examine the effects of Calpain2 inhibition on mesoderm radial intercalation, another intercalative activity that requires adherens junction remodeling and turnover. Open-faced Keller explants were excised at stage 10.5 and plated on fibronectin-coated coverslips. The tissue architecture of the mesendodermal sheet in such explants mimics the architecture of the mesendodermal mantle in whole embryos. These explants initially contain multiple layers of cells but when placed on fibronectin they thin into a monolayer via radial intercalation as the mesendoderm migrates out from the axial mesoderm (Davidson et al., 2002b). Remarkably radial intercalation was unaffected in the presence of the CI3 inhibitor (**Figure 62**) with the mesendoderm thinning into a monolayer suggesting that adherens junction turnover is not significantly affected under these conditions. It is thus unlikely that the mechanism through which Calpain inhibition blocks CE movements is via inhibition of adherens junction remodeling.

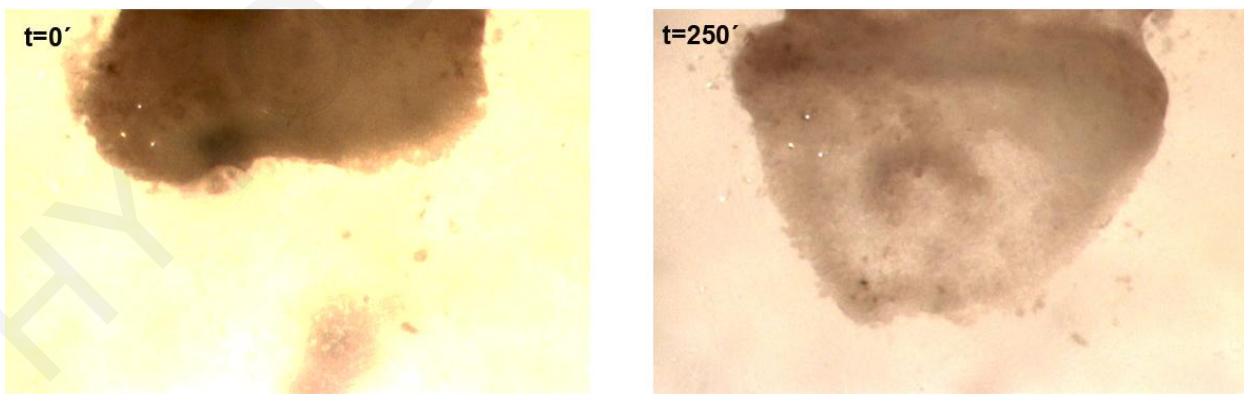


Figure 62. Radial intercalation is unaffected in Keller explants treated with CI3.

Keller explants were excised at stage 10.5. The explants were subsequently plated into fibronectin-coated chambered coverslips in DFA in the presence of 50 μ M CI3. Still frames from a time lapse movie at 0 and 250 minute, are showing that the mesodermal cells have been successfully radially intercalated towards the substrate. From multiple cell layers, the mesoderm thins and spreads after 250 minutes.

Another possible mechanism through which Calpain2 could affect CE is via modulation of the PCP pathway. It is known that during CE, cells acquire an elongated bipolar shape and form protrusions predominantly oriented along their long axis. This polarized morphology promotes M/L cell intercalation that ultimately leads to narrowing of the M/L axis (convergence) and elongation of the A/P axis (extension) (Keller et al., 2003). To investigate whether inhibition of Calpain activity influences the polarized behavior and motility of these cells, we analyzed cell shape and motility in mGFP-injected DMZ explants in the absence and presence of CI3. The explants were dissected at stage 10.5 and time-lapse recordings were generated over 10 minutes (**Movies 4&5**). While in control explants movements appeared directional and coordinated (**Movie 4 and Figure 63A**), in CI3-treated explants cell movements were impaired and the protrusive activities of the cells appeared randomized (**Movie 5 and Figure 63B**). Examining still frames from these time-lapse sequences, we could analyze the morphology and orientation of individual cells. As shown in **Figure 63C**, the majority of the cells in control explants showed the typical elongation and was oriented perpendicular to the anterior–posterior axis. In CI3-treated explants, however, the overall tissue polarity was disrupted and some cells also failed to acquire the typical bipolar shape and remained more round (**Figure 63C**). These observations were confirmed by plotting the LWR of each cell against the angle of its long axis (**Figure 63D**). The circular diagram clearly showed that control cells are mediolaterally polarized, whereas cells in CI3-treated explants are randomly oriented (**Figure 63D**). Furthermore 52% of CI3 treated cell did not significantly elongate ($LWR < 2$), whereas only 19% of control cell remained round. Overall, these data suggest that blockage of Calpain2 activity does not lead to a significant defect of adherens junction turnover and that CE defects are likely due to loss of proper cell polarity and cell shape changes required for this movement.

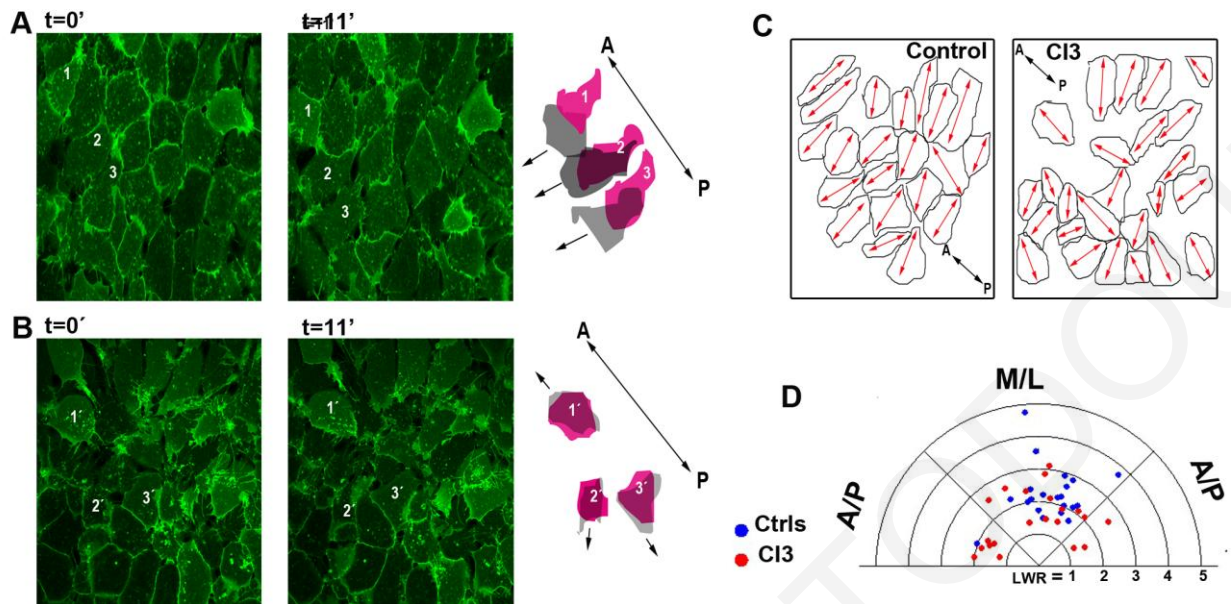


Figure 63. Inhibition of Calpains affects the morphology and motility of mesodermal cells.

Still frames from time-lapse movies of control (A) and CI3-treated (B) DMZ explants. mGFP was used as a lineage tracer. Time (t) in minutes is shown at the top left of each frame. Outlines of randomly chosen cells (1,2,3 in control explants and 1', 2', 3' in CI3-treated explants) are shown to the right of each panel. They were drawn from the first (pink) and last (gray) frames of the movie and superimposed. Black arrows indicate the direction of migration for each cell. The black double arrow head represents the orientation of the antero-posterior (AP) axis. Cells in CI3-treated explant show alteration in morphology, orientation and motility. (C) Outlines of cells from an intermediate frame were traced and their long axes indicated with red arrows. The black double arrow head represents the orientation of the AP axis. In control explants, the cells are polarized along the medio-lateral axis. In CI3-treated explants, some cells show identical polarization axis but the overall tissue polarity is disrupted. (D) Circular diagram of LWR versus the angle of the long axis of each of cells in A and B. Controls cells are clustered mediolaterally. Cells in CI3 treated explants are distributed randomly. Circular diagram prepared using Oriana 4.01 software.

3.1.9 Calpain2 function is necessary for Apical Constriction during *Xenopus* Development

I. Calpain2 function is indispensable for anterior Neural Tube Closure through its involvement in Apical Constriction

The necessity of Calpain2 function in CE explains the delayed posterior NTC but it cannot explain the anterior NTDs phenotype (open anterior neural tube, anencephaly). Therefore we set to determine the affected mechanism behind the blockage of rostral NTC. One possibility is that Calpain2 downregulation in neural tube cells leads to impairment of primary cilia formation and function, a defect well documented to elicit rostral NTDs (Bay and Casparly, 2012; Wallingford, 2006). To examine the status of neural tube primary cilia IF against acetylated tubulin in cross sections of stage 20 morphant embryos was performed. Acetylated tubulin staining revealed that the formation and length of neural primary cilia is not affected in morphant cells when compared with control cells (**Figure 64**). This excludes the possibility that the anterior NTDs elicited in Calpain2 morphants are due to defective formation of neural primary cilia.

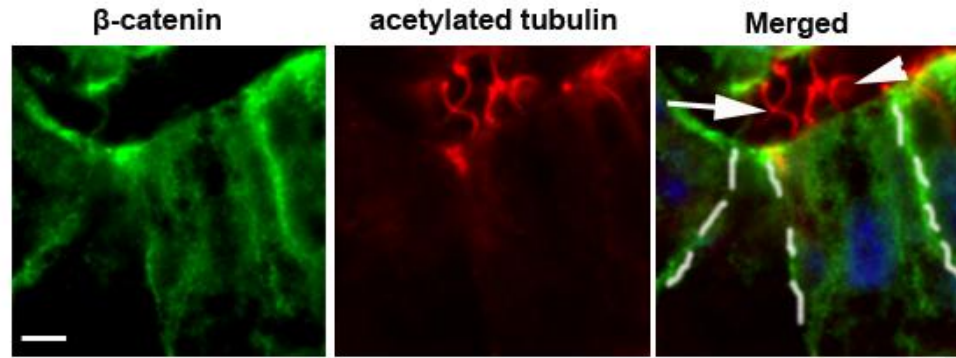


Figure 64. Calpain2 function is not necessary for neural tube primary cilia formation.

Maximum intensity profile image of cross sections from a tailbud embryo injected at 1 dorsal animal blastomere at 16 cell stage showing cells of the neural tube. Sections are stained with β -catenin (green) and acetylated tubulin (red). Blue color shows GFP signal which indicates Calpain2MO positive cells. White lines show the boundaries of an uninjected and a morphant cells. Primary neural cilia are projecting both from control (arrow) and the morphant cell (arrowhead). Scale bar: 5 μ m

Apical Constriction (AC) is the major morphogenetic movement linked with anterior NTDs. Specifically during neurulation, AC drives the conversion of neuroepithelial cells from columnar to wedge shaped driving the elevation and the bending of the neural folds (Sawyer et al., 2010). To examine if AC is impaired in Calpain2 morphants, embryos were unilaterally injected with the Calpain2 MO and allowed to develop to stage 16. Subsequently embryos were fixed and stained using a β -catenin antibody. As shown Calpain2 morphant neuroepithelial cells do not undergo AC failing to acquire the characteristic wedge shape of apically constricted cells (**Figure 65A, A'**). In order to explore if AC inhibition is cell autonomous 20ng Calpain2MO were injected at 1 dorsal blastomere at the 16 cell stage. This allowed the presence of neighboring Calpain2 morphants and control cells in the neuroepithelium. Cells positive for FITC-Calpain2 MO show impaired AC, while neighboring cells negative for Calpain2MO are apically constricted, suggesting that the phenotype is cell autonomous (**Figure 65B**). The phenotype is rescued by coexpression of Calpain2R mRNA with Calpain2MO (**Figure 65C**), showing that the defects in AC are specific for Calpain2 downregulation. In order to quantify the effects of Calpain2 downregulation on cell shape we measured the apical surface area/cell perimeter ratio and the cell height in controls, Calpain2 morphants and rescued cells. The mean ratio of the apical surface area/perimeter ratio in morphant cells was approximately 5 times higher than in control cells, and was partially rescued when the MO was coinjected with Calpain2R mRNA (**Figure 65D**). In addition cell height was also significantly affected in Calpain2 MO-injected cells, with almost a 2 fold decrease in the cell length of morphant cells compared to controls and this phenotype could also be partially rescued (**Figure 65E**).

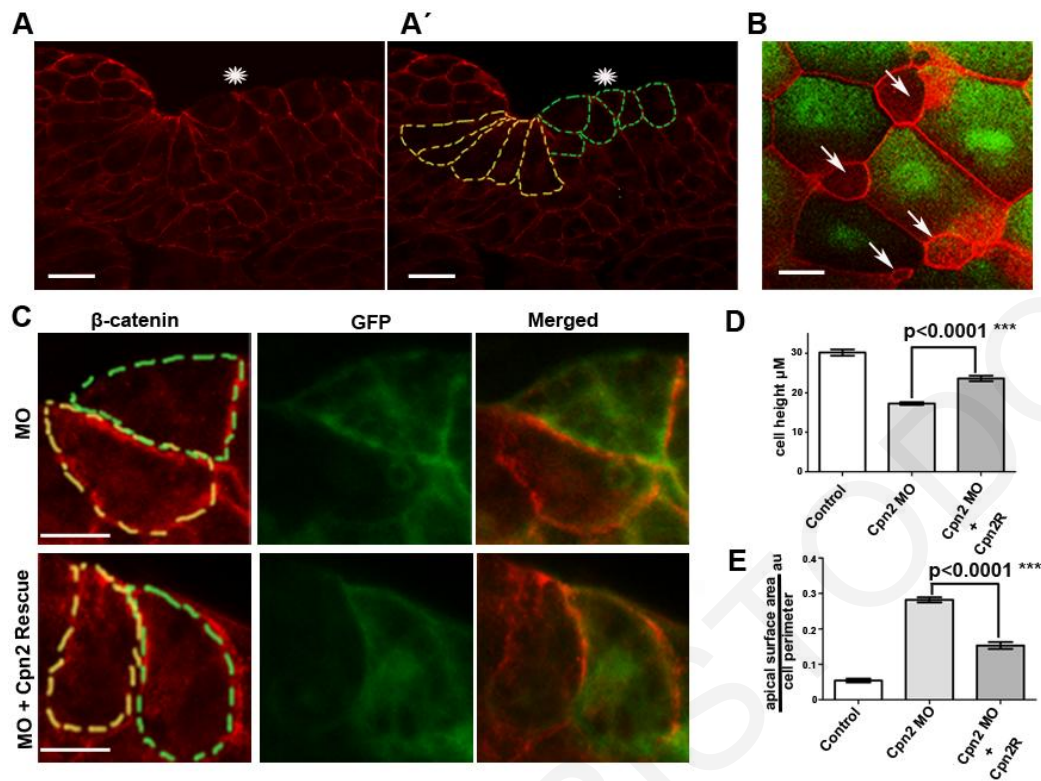


Figure 65. Calpain2 downregulation leads to defective Apical Constriction.

(A, A') Cross section of a neurula stage embryo injected at 1 dorsal blastomere at the 4-cell stage with 40ng Calpain2 MO and stained with β -catenin. Injected side is indicated by an asterisk. β -catenin staining was used to trace the cortices of superficial cells (A'). Scale bar = 20 μ M (B) Dorsal view of neuroepithelial cells stained for β -catenin. GFP signal shows the Calpain2 morphant cells. Scale bar = 5 μ M (C) Images showing representative morphant and rescued neuroepithelial cells. Cell cortices are delineated by β -catenin staining. GFP signal indicates the MO positive cells. Scale bar = 10 μ M (D) Mean apical surface area/perimeter ratio of Calpain2MO and Calpain2MO + Calpain2R neuroepithelial cells (n=40, mean \pm SEM) (E) Mean cell height of control, Calpain2MO and Calpain2MO + Calpain2R neuroepithelial cells (n=40, mean \pm SEM)

II. Calpain2 temporal and spatial localization is in agreement with a role in Apical Constriction

The blockage of AC in Calpain2 morphants led us to examine the localization of this protein. Several proteins involved in AC display enrichment at the apical region of epithelial cells (Haigo et al., 2003; Kinoshita et al., 2008; Nishimura and Takeichi, 2008). We thus examined the localization of Calpain2 pre and post AC in the *Xenopus* neuroepithelium, a tissue in which Calpain2 mRNA levels are enriched and Calpain2 shows increased activity (**Figure 50D, 51C**). In this tissue, AC begins at stage 13+ and by stage 17 the cells acquire the characteristic elongated wedge shape (Lee et al., 2007). In the absence of a specific antibody against the endogenous *Xenopus* Calpain2, we examined the localization of ectopically expressed HA-Calpain2. During the initial stages of AC, exogenous Calpain2 localizes at the apical membrane and at cell-cell junctions where is co-localizes with C-Cadherin (**Figure 66**). At later stages, in apically constricted cells, Calpain2 is enriched at the apical surface of neuroepithelial cells,

resembling the localization of other key regulators of AC providing additional support for a specific role in this process (**Figure 66**). These results show that the localization as well as the spatial and temporal expression pattern of Calpain2 are in agreement with its role in AC during neurulation.

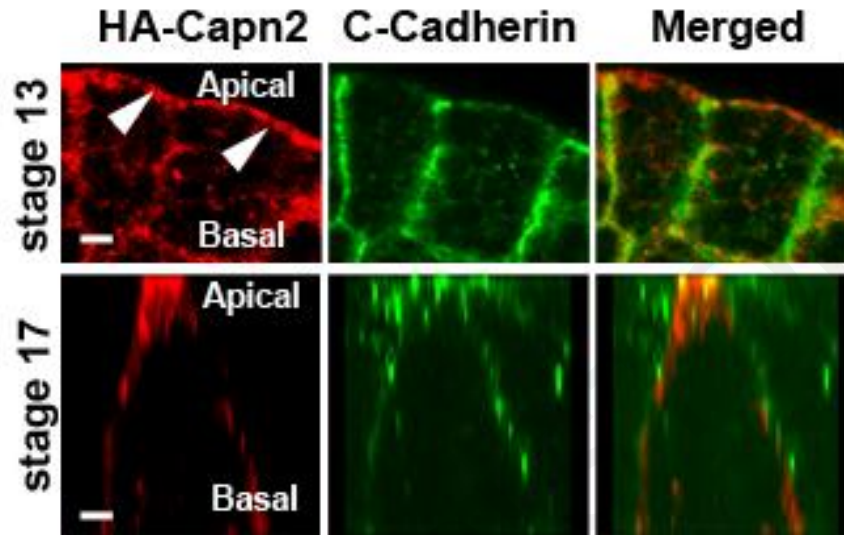


Figure 66. Calpain2 localization in neuroepithelial cells pre and post Apical Constriction.

X-Z projection from z-stack images of a neuroepithelial cells from stage 13 and 17 embryos, expressing HA-Calpain 2 and stained for HA (red) and C-Cadherin (green). Scale bar = 5 μ M..

III. Calpain2 regulates Apical Constriction independently of tissue context

AC is a process conserved among different organisms and tissues (Sawyer et al., 2010). In addition to its role during neurulation, it has been shown that AC drives the formation of organs such as the gut, the cement gland, the eye and is implicated in the formation of all placodes (Chung et al., 2010; Lee et al., 2007; Llimargas and Casanova, 2010; Plageman et al., 2011). Key regulators of AC are generally expressed in all epithelial tissues undergoing this morphogenetic movement (Lee et al., 2009). Examination of Calpain2 expression in *Xenopus* revealed elevated expression in tissues where AC is taking place. Specifically, in tadpoles Calpain2 mRNA was detected in the eye, the olfactory placode, the otic vesicle, and the cement gland (**Figure 50G**). Calpain2 mRNA was also detected in the archenteron floor (**Figure 50G**), another tissue where the importance of AC has been previously documented (Chung et al., 2010). In conclusion, both Calpain2's spatial and temporal expression are consistent with a role in AC independently of tissue context.

We have so far considered the role of Calpain2 in AC of neuroepithelial cells. In order to investigate if Calpain2's implication in AC is tissue dependent, loss of function experiments were carried out to examine the role of Calpain2 in other morphogenetically active epithelial tissues.

Specifically, the role of Calpain2 was addressed during gut, cement gland and olfactory placode formation taking advantage of the precise temporal control afforded by the Calpain inhibitor III (CI3).

Stage 20 embryos were treated with 100 μ M CI3 inhibitor and allowed to develop to stage 46. The gut of CI3-treated embryos displayed severe deformities and failed to coil normally compared to sibling control embryos (**Figure 67A**), suggesting that Calpain activity is important for proper gut formation. To verify this result, we performed injections of Calpain2MO specifically targeting the archenteron floor. To quantify the effect of Calpain2 downregulation on the morphology of this tissue, we measured the angle at which the two sides of the epithelium intersect in stage 32 embryos (**Figure 67B,C**). In control embryos, this angle was 80° (n=20), in agreement with previously published data (Chung et al., 2010). In morphants, this angle was significantly greater, at 141° (n=20) (**Figure 67C**). This suggested failure of AC in the cells of the gut epithelium and consequently reduced bending of the archenteron floor. IF against ZO1 in cross sections of stage 32 embryos revealed that the apical surface of the cells in the archenteron floor is larger in Calpain2 morphants compared to control embryos, as shown from the distance between the tight junctions (**Figure 67B**). AC is also important for the formation of the cement gland (Lee et al., 2007). To assess the involvement of Calpain2 in the formation of the cement gland, sibling embryos allowed to develop to stage 18 and were then treated with 100 μ M CI3 and allowed to develop to stage 26. AC at the cement gland starts at stage 19 and is completed by stage 26 (Lee et al., 2007). After phalloidin staining, 3D images of control and CI3 treated embryos revealed that the formation of the cement gland was severely impaired by the inhibition of Calpain2 (**Figure 67D**). Quantification of the cell surface area of cement gland epithelial cells from control and CI3 treated embryos revealed that the defect was due to impaired AC (**Figure 67E**).

Finally we analyzed the possible involvement of Calpain2 in the formation of the olfactory placode, showing the necessity of Calpain2 activity in AC driven morphogenesis in another tissue. Sibling embryos were allowed to develop to stage 29. At this stage embryos were treated with 100 μ M CI3. Then embryos were allowed to develop to stage 37, fixed and stained with phalloidin. 3D presentation of Z-stack images shows the formation of the olfactory pit cavity in control embryos, while in CI3 treated embryos the cavity failed to form (**Figure 67F**). This failure is due to the blockage of AC in CI3 treated embryos, as shown from the difference of the cell surface area of control and CI3 treated cells in the olfactory epithelium (**Figure 67G**). Overall, these data suggest that Calpain2 is a general regulator of AC independently of tissue context.

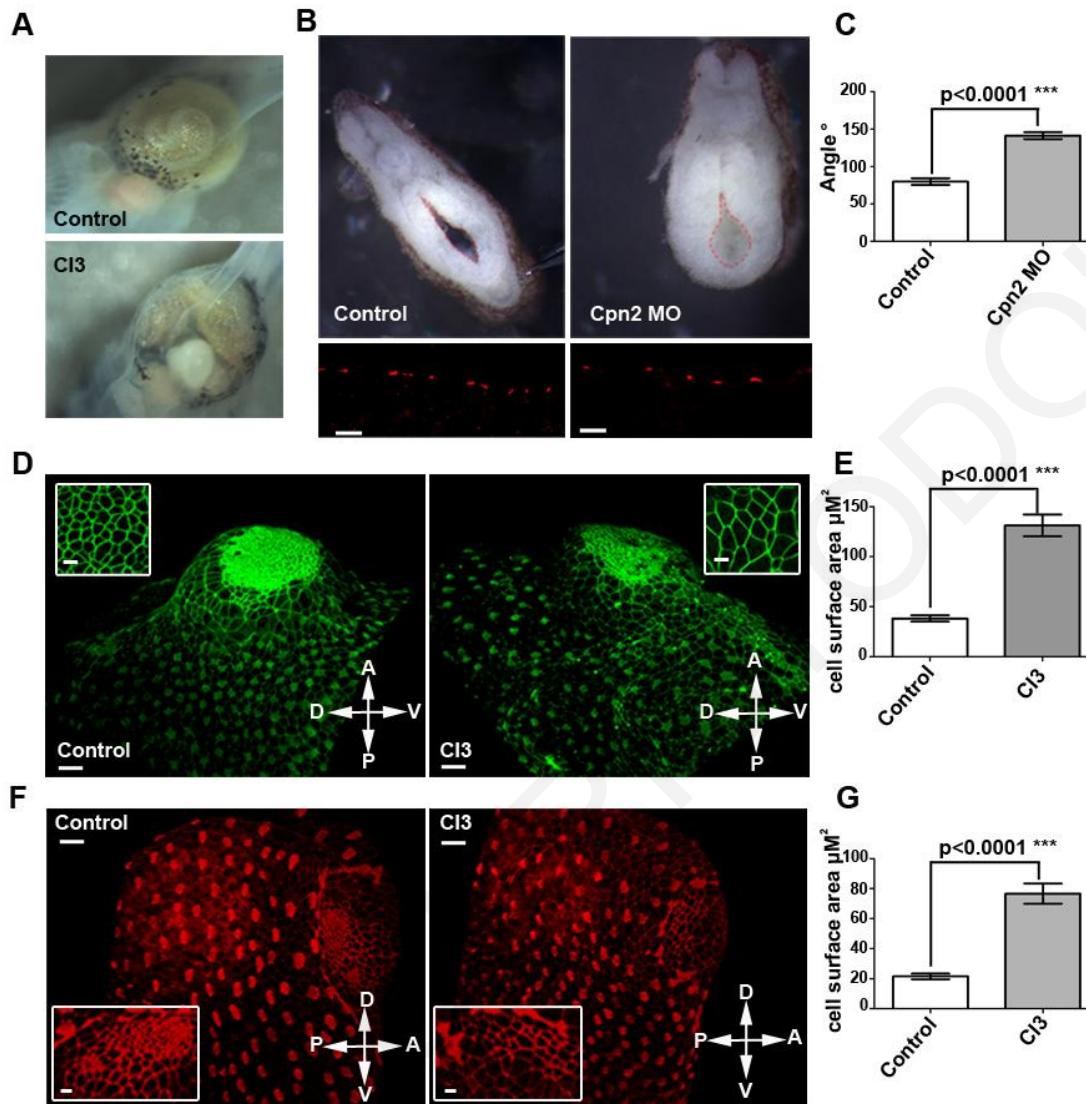


Figure 67. Calpain2 regulates Apical Constriction independently of tissue context.

(A) Stage 44 control and CI3 treated embryo. CI3 treatment causes gut malformations. (B) Cross sections of stage 32 control and Calpain2 MO injected embryo. Lines show the archenteron cavity. ZO-1 staining of sections (red). Scale bar = 10 μm . (C) Mean angle of the archenteron floor of Control and Calpain2 morphant embryos (n=20, mean \pm SEM). (D) 3D presentation of Z-stack images of control and CI3 treated embryos. Scale bar = 50 μm . Insets are magnified areas of the cement gland epithelium. Scale bar = 10 μm . (E) Mean cell surface area of Control and CI3 treated cement gland epithelial cells (n=30, mean \pm SEM). (F) 3D presentation of Z-stack olfactory placode images of control and CI3 treated embryos. Scale bar = 50 μm . Insets are zoomed images of the olfactory pit epithelium. Scale bar = 5 μm (G) Quantification of the cell surface area of Control and CI3 treated olfactory epithelial cells (n=25, mean \pm SEM). (A:Anterior, P:Posterior, D: Dorsal, V:Ventral).

IV. Calpain2 downregulation affects Apical Constriction but does not affect apicobasal polarity

In order to rule out that defects in AC observed in Calpain2 morphants stem from general defects in apicobasal polarity and/or tight junction assembly, the localization of apicobasal polarity markers ZO-1, aPKC, Par6 and cortactin was examined in morphant embryos with IF. The localization of the tight junction marker ZO-1 was unaffected in morphant neuroepithelial cells which fail to undergo AC. (**Figure 68A, A'**). This shows that the formation of tight junctions is

unaffected after Calpain2 downregulation. The localization of both α PKC and Par6 was unaffected in Calpain2 morphant cells (**Figure 68B, C**).

We went on to examine the localization of cortactin, a known substrate of Calpain2 (Perrin et al., 2006), which is implicated in AC through its binding to Dynamin 2 (Chua et al., 2009). As shown cortactin localizes to tight junctions and at the apical cell surface both in control and Calpain2 morphant cells (**Figure 68D**). These data indicate that Calpain2 downregulation affects AC in neuroepithelial cells without affecting apico-basal polarity, tight junction assembly and localization of tight junction proteins implicated in AC.

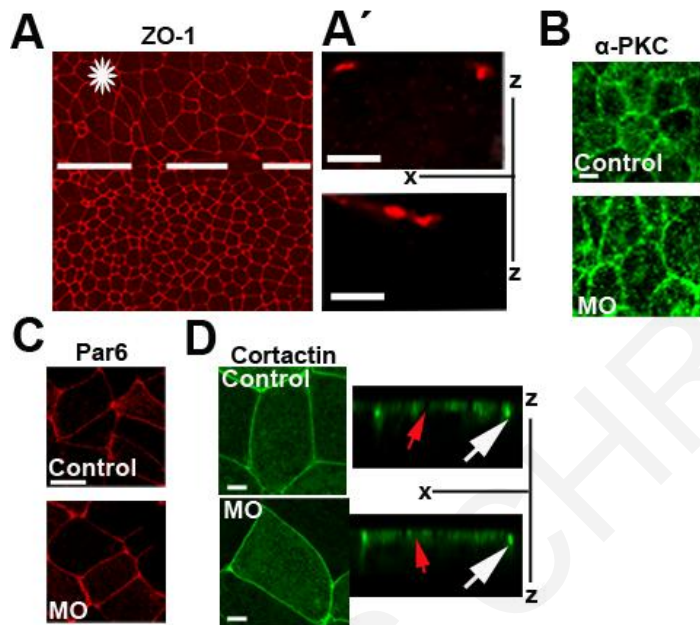


Figure 68. Calpain2 function is dispensable for establishment of apicobasal polarity

(A) Dorsal view maximum intensity projection image of the neuroepithelium from an embryo injected at 1 dorsal blastomere at the 4-cell stage with 40ng of Calpain2 MO and stained for the tight junction marker ZO-1. Injected side is indicated with an asterisk. Scale bar = 10 μ M (A') X-Z projections of morphant and control cell. Scale bar=5 μ M.

(B) Neuroepithelial cells from embryos injected unilaterally with Calpain2 MO and stained for α PKC. Scale bar=10 μ m. (C) Neuroepithelial cells from embryos injected 2 out of 2 with HA-Par6 mRNA and 1 out of 4 with Calpain2 MO. The embryos were stained for HA. Scale bar= 20 μ m (D) Dorsal view of stage 13 neuroepithelial control and Calpain2 morphant cells expressing Cortactin-GFP. X-Z projections of stage 13 control and CALPAIN2 morphant cells expressing Cortactin-GFP. Red arrows indicate the tight junctions and white arrows show the apical surface of the cells. Scale bar = 5 μ m.

V. Calpain2 function is necessary for Shroom3, Lulu and GEF-H1 induced AC

Calpain2 is implicated in CE of mesodermal and neural tissues as shown above. During NTC, CE and AC take place simultaneously. In order to exclude the possibility that the AC defects elicited by Calpain2 downregulation are indirect due to defects in CE or tissue specification issues, we examined the requirement of Calpain2 function in ectopically induced AC. Ectopic expression of a number of molecules is sufficient to induce AC in epithelial cells, among these Shroom3, Lulu and GEFH1 (Chu et al., 2013; Haigo et al., 2003; Itoh et al., 2014). Therefore, in order to position Calpain2 in the signaling pathway regulating AC(AC), the effect of Calpain2 downregulation in AC induced by these molecules was examined. Injections of Shroom3, Lulu-GFP and GEF-H1 at the one dorsal blastomere of a 4 cell stage embryo revealed that cells expressing these molecules

3.1.10 Calpain2 activation mechanisms in *Xenopus*

It is known from *in vitro* studies and crystallography data that Calpains display a strict Ca^{2+} requirement for their activity. In the absence of Ca^{2+} , Calpains are predominantly found in the cytoplasm in an inactive form. In the presence of Ca^{2+} , Calpains translocate to the plasma membrane and become activated (Suzuki et al., 2004). This was confirmed by treating stage 9 embryos expressing HA-Calpain2 with the Calcium ionophore Ionomycin. Ionomycin treatment leads to a dramatic translocation of Calpain2 from the cytosol to the plasma membrane (**Figure 70**). Therefore, the localization of Calpain2 can be used to infer the activation status of Calpain2.

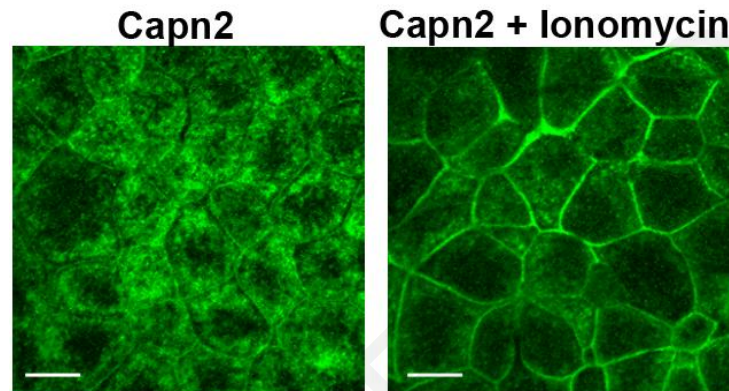


Figure 70. Calpain2 is activated after increase of intracellular Calcium in *Xenopus* embryos. HA-Calpain localization in control stage 9 embryos (left) and stage 9 embryos treated with Ionomycin

The existence of a calcium-mediated pathway that is activated by specific Wnt proteins (Wnt4, Wnt5a, Wnt11) has been described in *Xenopus*. Wnt/ Ca^{2+} it is known to be important for the regulation of CE and AC through the activation of several calcium-dependent proteins (Choi and Sokol, 2009; Kuhl et al., 2000a; Kuhl et al., 2000b; Sheldahl et al., 1999). This raised the possibility that Calpain2 is activated downstream of this pathway. Therefore initially we examined if Calpain2 is activated downstream of the Wnt/ Ca^{2+} signaling pathway via expression of Wnt5a. HA-Calpain2 mRNA was microinjected in *Xenopus* embryos either alone or with Wnt5a. Animal caps were excised at stage 9 and stained with an anti-HA antibody. Cell-boundaries were visualized with a C-cadherin antibody. HA-Calpain2 was present throughout the cytoplasm in the absence of exogenous Wnt5a signaling. Following co-injection of Wnt5a, HA-Calpain2 translocated to the plasma membrane (**Figure 71A**). Fluorescence-intensity profiles for HA-Calpain2 and C-cadherin were generated, showing that C-cadherin and Calpain2 clearly co-localized at membrane regions only in the presence of exogenous Wnt5a (**Figure 72B**).

To further address the role of Calpain2 as an effector of the Wnt/ Ca^{2+} pathway, we assessed CE in activin-induced caps from control embryos and embryos injected with Wnt5a alone or co-

injected with Calpain2 dominant negative (Calpain2C105S). In agreement with previously published data, injection of Wnt5a inhibited the elongation of these explants, confirming the role of the Wnt/Ca²⁺ signaling pathway in regulating CE (Moon et al., 1993; Torres et al., 1996; Yamanaka et al., 2002). Remarkably, co-expression of Calpain2C105S dominant negative clearly reversed the inhibitory effect of Wnt5a on cap elongation (**Figure 72C**), suggesting that Wnt5a blocks CE in part through excessive activation of endogenous Calpain2. Overall these results identify Calpain2 as a new calcium-sensitive enzyme that via activation through the Wnt/Ca²⁺ can modulate CE and AC driven morphogenetic movements.

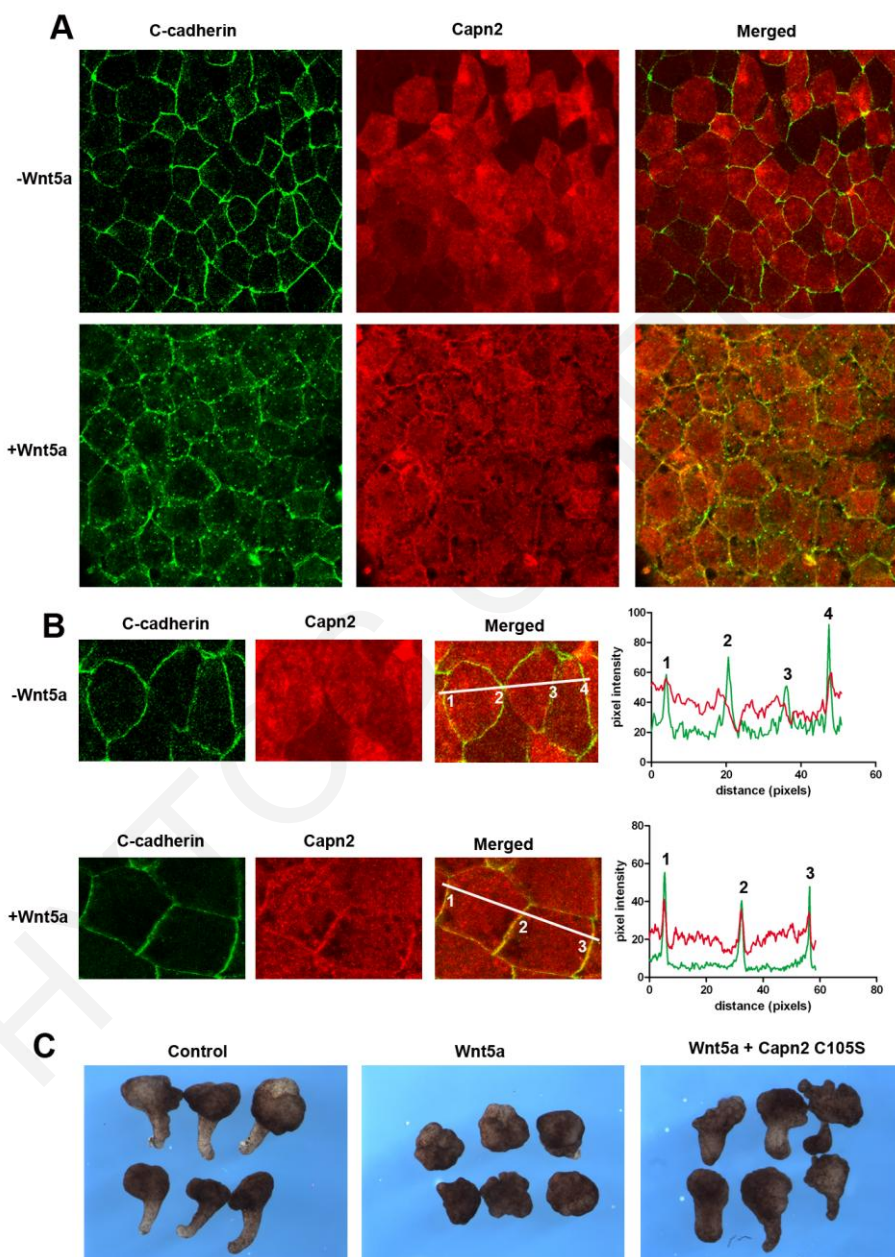


Figure 71. Calpain2 acts downstream of the Wnt/Ca²⁺ pathway.

Figure 71. Calpain2 acts downstream of the Wnt/Ca²⁺ pathway.

(A) Ectodermal cells from embryos injected with 200pg HA-Calpain2 alone (top panels) or co-injected with 500pg Wnt5a (bottom panels) are double stained for C-cadherin (green) and HA-Calpain2 (red). Plasma membrane can be visualized in both top and bottom panels by C-cadherin staining. In the absence of Wnt5a (top panel) Calpain2 is mainly diffused in the cytoplasm, whereas in the presence of Wnt5a there is a clear increase in its membrane localization. (B) Co-localization studies in individual groups of cells in the absence (top panel) or presence of Wnt5a (bottom panel). Fluorescence-intensity profiles are shown to the right and represent the areas marked by the white line. Numbering represents membrane regions. Only in the presence of Wnt5a C-cadherin and Calpain2 show clear colocalization at membrane regions, as determined by fluorescence-intensity overlap. Pixel intensity profiles were generated using ImageJ software. (C) Injection of 100pg Wnt5a blocks the activin-induced elongation of animal caps explants. Co-injection of 1ng Calpain2 C105S reverses the inhibition of elongation caused by Wnt5a

It has been previously shown that the multifunctional protein Dishevelled (Dsh), known to be a key activator of both canonical Wnt and PCP pathways, also functions in the Wnt/Ca²⁺ by activating intracellular calcium flux and promoting the translocation to the membrane of two Ca²⁺-sensitive enzymes, PKC and CamKII (Sheldahl et al., 2003). We therefore set to determine if Calpain2 localization to the membrane is mediated by Dsh, by using a well characterized dominant negative mutant of Dsh, Xdd1 (Sokol, 1996). Calpain2 localization to the membrane in neural ectodermal cells of a stage 13 embryo was clearly reduced in Xdd1-injected embryos (**Figure 72**). This result suggests that Calpain2 is activated downstream of the Wnt/Ca²⁺ in a Dsh dependent manner.

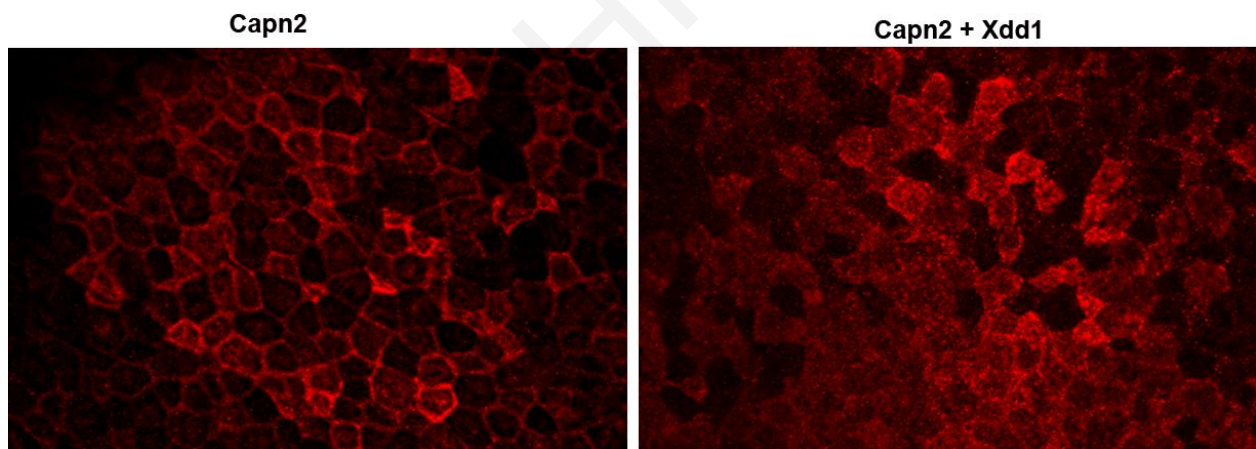


Figure 72. Calpain2 activity is dependent on Dishevelled.

Ectodermal cells of stage 13 embryos injected with 200pg HA-Calpain2 alone or co-injected with 1ng Xdd1 stained with anti-HA antibody.

3.2 Live imaging of actin and Calcium dynamics during Neural Tube Closure

3.2.1 AC is driven by pulsed contraction of a transient apical contractile actin network

AC of neuroepithelial cells contributes to the bending and fusion of neural folds during NTC (Suzuki et al., 2012). Several studies have shown that regulators or members of the actomyosin complex are necessary for proper AC of neuroepithelial cells in vertebrates, and defects of the actomyosin complex results in NTDs (Wallingford, 2005). Data from EM studies suggest that in vertebrates a circumferential actomyosin complex drives AC according to a purse string like model (Martin and Goldstein, 2014). In contrast, live imaging in *Drosophila* revealed that AC in invertebrates is driven by contractions of a medioapical actomyosin complex in a ratchet like mechanism, during which the medioapical actomyosin complex exerts forces on discrete cortical junctions (Martin et al., 2009). However to our knowledge the dynamics of the actomyosin complex during AC have not been documented live in any vertebrate system. We therefore decided to record the actin dynamics of neuroepithelial cells during NTC in *Xenopus*. To do this we injected Utrophin-GFP mRNA at the 2 dorsal blastomeres of 4 cell stage embryos to target the neural plate, allowed them to develop to stage 14 and subsequently imaged the neural plate (**Figure 73A**). During NTC we observed the transient appearance of a highly dynamic apical actin pool in neuroepithelial cells (**Figure 73A-B, Movie 6**). Apical actin enrichment occurred cell autonomously in the majority of cells (84%, n=150) and occasionally in groups of 2-5 cells (16%, n=150) (**Movie 6**). Simultaneous tracking the cell surface area revealed that apical actin enrichment takes place just before cells begin to constrict (**Figure 73B**), leading to $16,96 \pm 0.84$ % (Mean \pm SEM, n=50) reduction of the apical cell surface within one minute from the appearance of apical actin enrichment (**Figure 73C**). Quantification of the apical cell surface area and apical Utr-GFP intensity over time also revealed that AC during NTC occurs in a stepwise fashion, where the surface area of individual cells is initially reduced (contraction pulse) followed by a slight increase and stabilization (stabilization step) (**Figure 73D**).

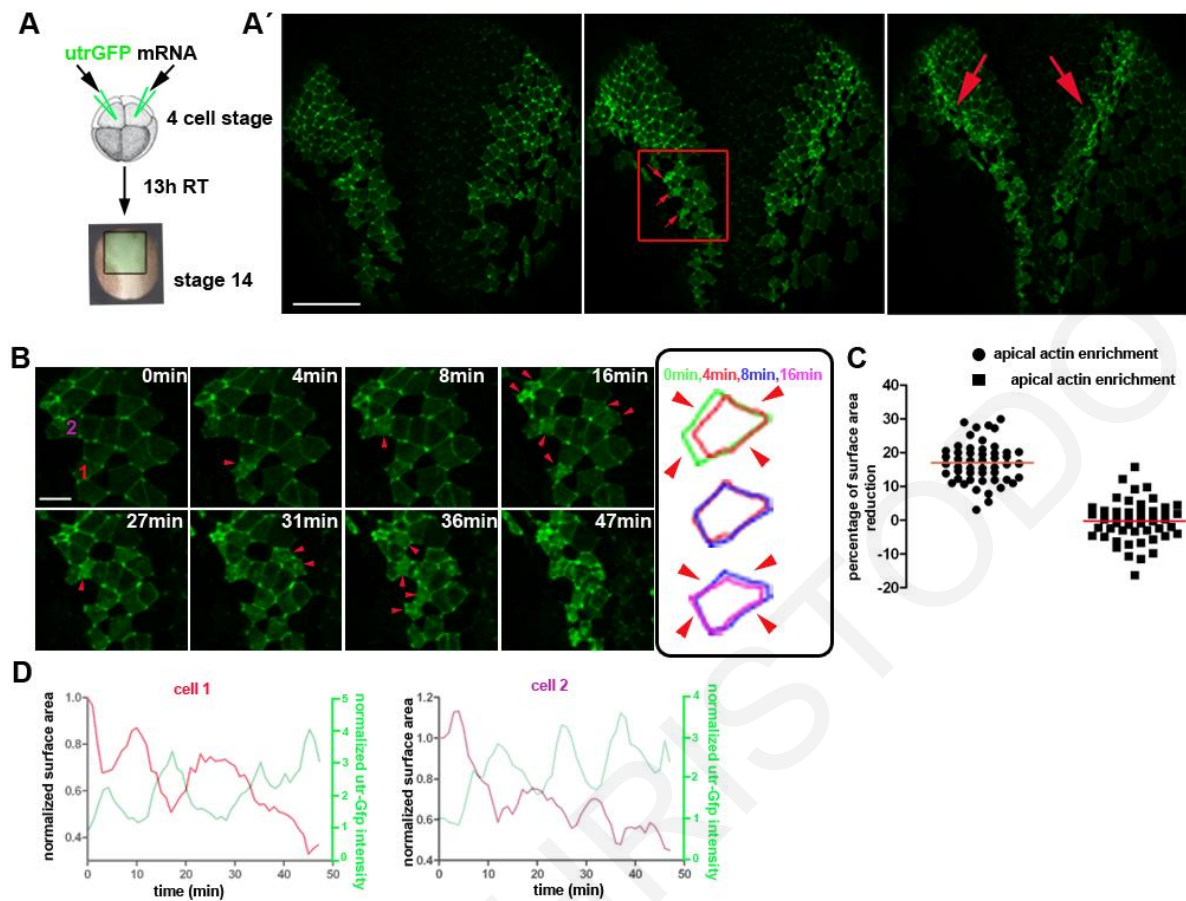


Figure 73. Dynamics of apical actin network during Apical Constriction of neuroepithelial cells.

(A) Experimental strategy for imaging actin dynamics during NTC. (A') Stills from a time lapse recording showing actin dynamics during NTC. Red arrows indicate cells displaying apical actin enrichment. Scale bar: 100 μ m. (B) Close up of region bound by red box in A'. (B') Schematic showing the boundaries of an individual cell at different time points. Apical cell surface is reduced after apical actin enrichment events. Scale bar: 20 μ m. (C) Cell surface area change over a period of 1 min in the absence and presence of apical actin enrichment. (D) Normalized apical cell surface area and apical utr-GFP intensity over time of cell two representative cells. AC occurs in a stepwise fashion initiated by pulsed contractions (reduction of surface area), followed by stabilization steps. Increase of apical utr-GFP intensity is also pulsed and coincides with contraction pulses.

Expression of Lulu-GFP, GEF-H1 and Shroom3 in ectodermal cells of gastrula embryos induce AC as described above. When the surface area of a cell expressing GEF-H1 was tracked over time it became clear that AC is driven by constriction pulses followed by stabilization steps in agreement with studies (Figure 73A-C) in agreement with neuroepithelial cell's behavior. Similar results were obtained from quantification of the cell surface area of ectodermal cells expressing Lulu-GFP (Figure 73D) and Shroom3 (data not shown).

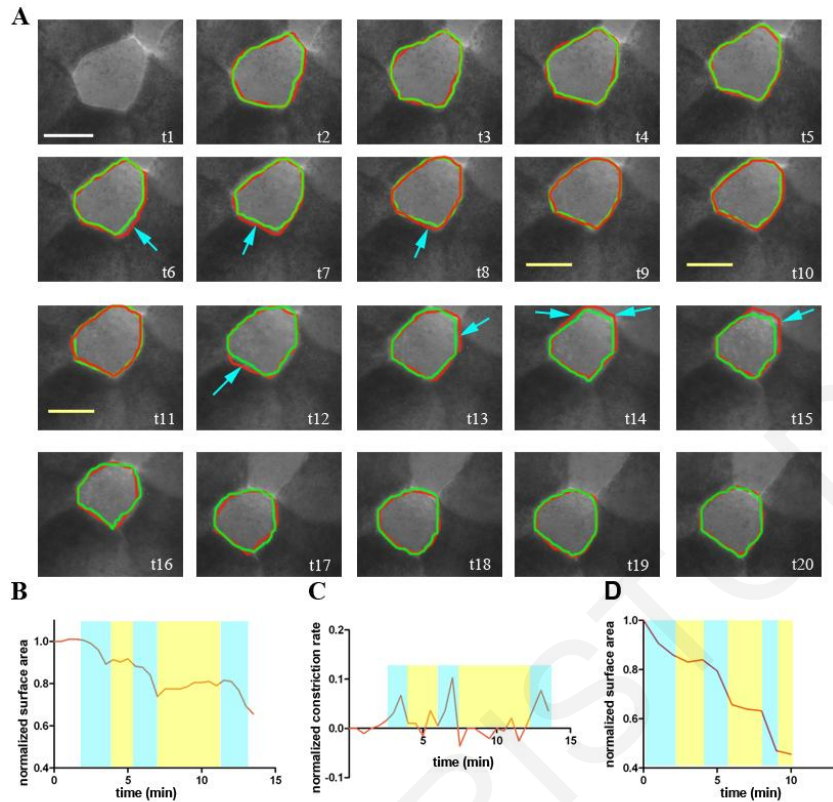


Figure 74. Pulsed contractions followed by stabilization steps drive ectopically induced Apical Constriction.

(A) Stills from a time lapse recording of representative ectodermal cell of a gastrula *Xenopus* embryos injected with 20pgGEFH1 mRNA + 80pg mem-cherry. Frames were taken every 30 seconds. Red cortices indicate the cell surface area of the previous time point. Green cortices indicate the cell surface of each time point. Blue arrows indicate constriction pulses and yellow lines indicate the stabilization step. Scale bar = 10 μ m (B) Quantification of the normalized cell surface area over time of a representative cell expressing HA-GEF-H1. (C) Quantification of the normalized cell surface area change (constriction rate) over time of a representative cell expressing HA-GEF-H1. Positive events represent the constriction pulses. (D) Quantification of the normalized cell surface area during time of a representative cell expressing Lulu-GFP. Blue highlight denotes constriction pulses and yellow indicate the stabilization phase

Tracking contraction events from time lapse recordings also reveals that these events are both cell autonomous and asynchronous similar to the actin enrichment events (**Figure 75, Movie7**). In addition maximal contraction is always observed during the maxima of apical actin intensity suggesting a cause and effect relationship leading to the conclusion that AC in vertebrates is likely driven by contractions of this apical pool of actin similar to what has been described in invertebrates (**Figure 74D, Movie 8**). If this apical actin network is in fact contractile and responsible for the contraction pulses it would be expected to exert forces on cell-cell junctions inducing their displacement (Lang et al., 2014). Indeed the appearance of the apical actin network is concomitant with apical junction displacement providing further evidence that this is a contractile network driving the contraction pulses (**Figure 76**). Overall these data show that AC

during NTC closure occurs through discrete cell autonomous and asynchronous contraction pulses which appear to be driven by transient apical actin polymerization events.

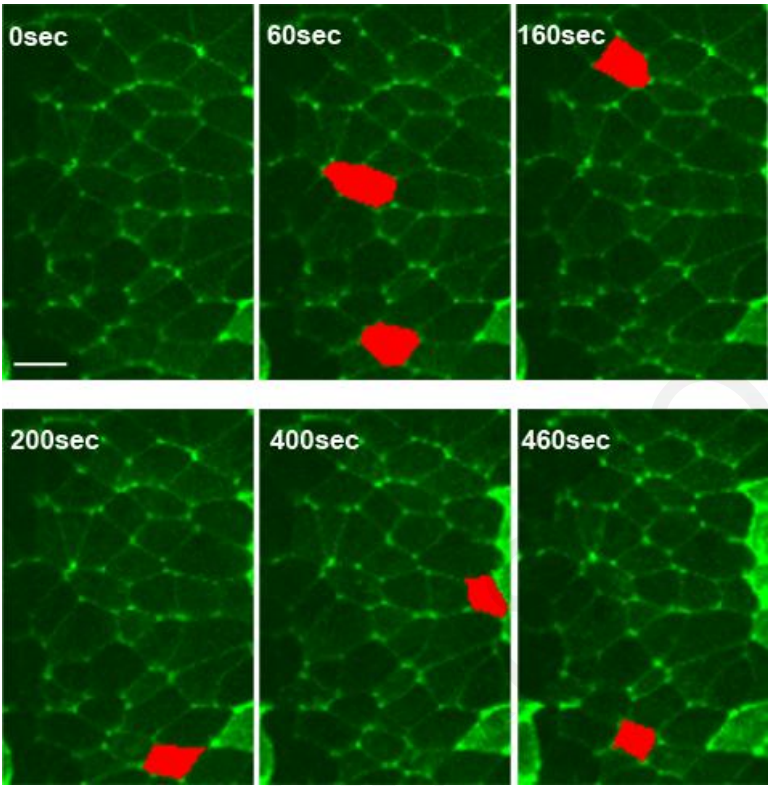


Figure 75. Contraction pulses of neuroepithelial cells undergoing Apical Constriction are cell autonomous and asynchronous.

Stills frames from a time lapse recording of an embryo expressing utr-GFP during NTC. Initiation of contraction pulses was color coded (red). Contraction pulses of neuroepithelial cells are cell autonomous and asynchronous, scale bar: 20µm.

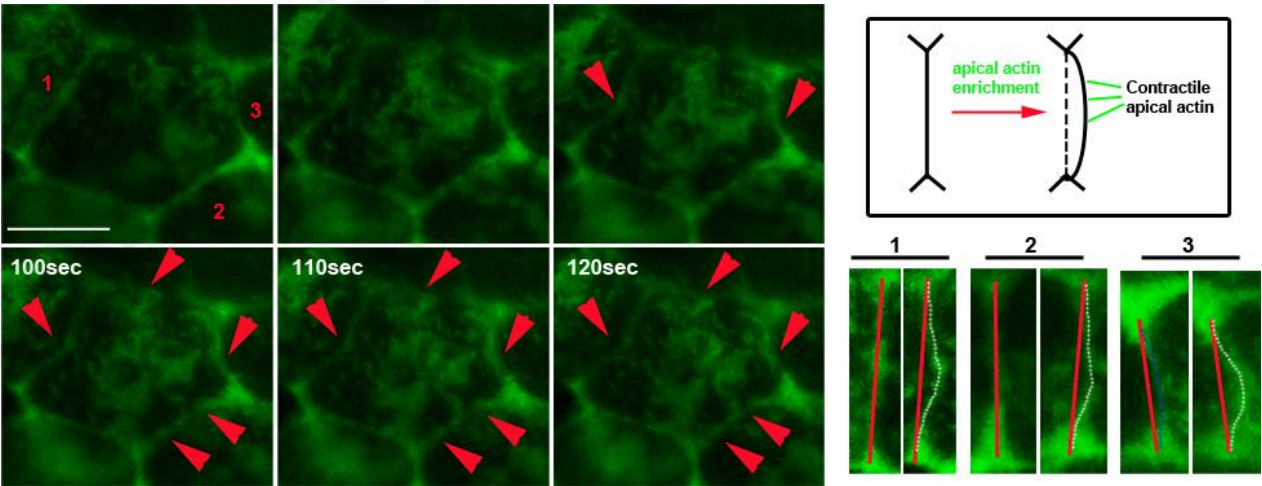


Figure 76. The apical actin network in neuroepithelial cells is contractile.

High resolution stills from a time lapse sequence showing a cell with apical actin enrichment. Cell-cell boundaries are initially straight and are gradually displaced inward at different time points (red arrowheads). Apical actin exerts forces on apical cell junctions driving their displacement. Scale bar :10µm

3.2.2 Mediolateral junction shrinkage contributes to apical cell surface area reduction during Neural Tube Closure

As shown above time lapse recordings during NTC, revealed that a subset of cells is actively undergoing surface area reduction driven by apical actin contraction (**Movie 6**). Quantification of the surface area of small regions within the neural plate which do not display any contraction pulses and apical actin contraction during the recorded period revealed that the surface area of such regions is also reduced over time (~5% in 10 minutes). We then asked how this reduction is accomplished, in the absence of detectable contraction pulses. Further analysis of such recordings showed that the mediolateral (M/L) cell junctions of approximately 30% of cells within a representative region shrink over time (**Figure 77A**), in agreement with a previous study (Nishimura et al., 2012). This is a clearly polar event and quantification of (M/L) and anteroposterior (A/P) junction length over time from representative cells indicates that M/L junction's length is reduced while A/P junction length is constant with slight fluctuations (**Figure 77B**). Quantification of apical cell surface area over time of individual cells shows that M/L junction shrinkage coincides with cell surface area reduction as expected (**Figure 77B**). M/L junction's length is reduced 27.46 ± 1.95 % (Mean \pm SEM, n=38) in a period of 10 minutes while A/P junction's length showed -0.58 ± 1.77 % reduction (Mean \pm SEM, n=35) over the same time period (**Figure 77C**). M/L junction shrinkage leads to 14.59 ± 2 % reduction of the apical cell surface area over a period of 10 minutes (Mean \pm SEM, n=19) (**Figure 77C**). These results suggest that surface area reduction in the absence of apical actin driven AC is stemming from M/L junction shrinkage. Both M/L junction shrinkage and cell autonomous and asynchronous contraction pulses occur simultaneously during NTC, both contributing to the overall reduction of apical cell surface area (**Figure 77D, Movie9**).

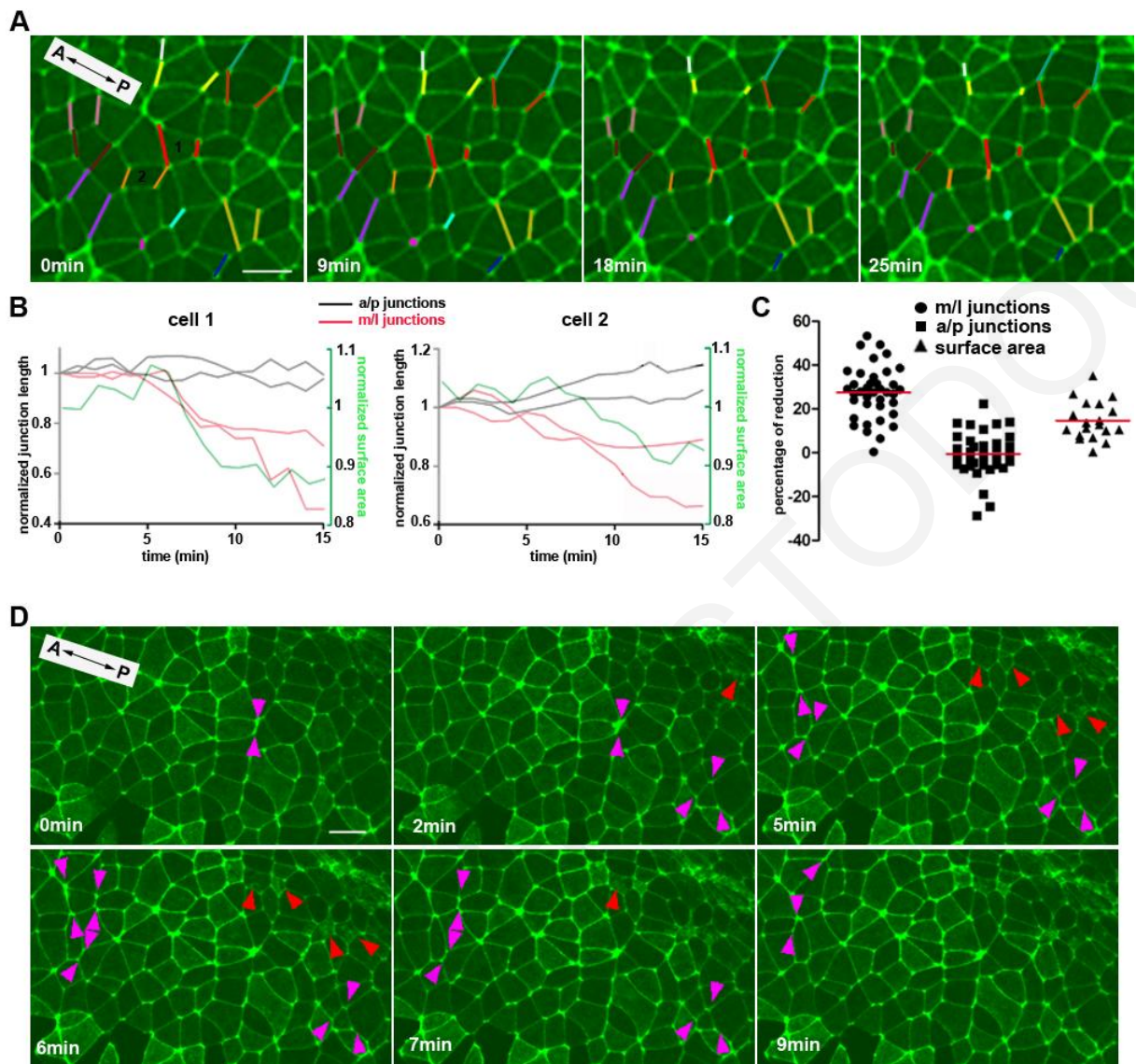


Figure 77. Two distinct processes contribute to apical surface reduction during Neural Tube Closure.

(A) Stills from a time lapse sequence of a representative region within the neural plate of an embryo expressing *utr-GFP*. Several junctions (color coded) oriented parallel to the mediolateral axis of the neural plate shrink over time. (B) Normalized junction length and normalized surface area of indicated cells from A over time. M/L junction length (red lines) is reduced over time, while A/P junction length (black lines) remains constant (cell 1) or display a slight increase (cell 2). Surface area reduction (green line) coincides with shrinking of M/L junctions. (C) Quantification of M/L, A/P junction and apical cell surface reduction over a 10 minute period. (D) Stills from a time lapse sequence of a representative region within the neural plate of an embryo expressing *utr-GFP*. Purple arrowheads indicate M/L junction shrinkage events. Red arrowheads indicate AC events driven by the enrichment of an apical actin network. Scale bars: 20 μ m

3.2.3 Asynchronous and Cell autonomous Calcium flashes are generated during Apical Constriction

As shown above, both the assembly of the apical actin network and AC in the neural plate are pulsed. How is this pulsed contraction of actomyosin is triggered or regulated is not well understood. The role of Ca^{2+} in muscle contraction is well documented (Szent-Gyorgyi, 1987) and studies using pharmacological inhibitors have previously implicated Ca^{2+} signaling in neural tube morphogenesis (Smedley and Stanisstreet, 1986). Furthermore, elevation of intracellular Ca^{2+} has been linked with AC during wound healing and *Drosophila* development (Antunes et al., 2013; Hunter et al., 2014). We thus decided to image Ca^{2+} levels during NTC, using GECO-RED a genetically coded Ca^{2+} indicator (Zhao et al., 2011). The 2 dorsal blastomeres of 4 cell stage embryos were injected with mRNAs encoding membrane-GFP and GECO-RED (**Figure 78A**). Subsequently embryos were allowed to develop to stage 14 and imaged during NTC (**Figure 78B**). Live imaging revealed that despite the lack of frequent Ca^{2+} waves during this process, individual cells in the neural plate frequently display rapid transient Ca^{2+} level increases (**Figure 78B, Movie 10**). The majority of these Ca^{2+} flashes are cell autonomous and asynchronous (**Figure 78C, D**), similar to the contraction pulses and apical actin enrichment events described above. Synchronized Ca^{2+} flashes were also present but occurred with lower frequency in 2-5 neighboring cells or in a larger groups of cells (**Figure 78C, D, n=150**). The typical Ca^{2+} flash is short lived ($26 \pm 3\text{sec}$, $n = 80$ events, 3 embryos) and unlike Ca^{2+} waves reported to take place during mesoderm CE (Wallingford et al., 2001). Ca^{2+} flashes increase gradually as NTC progresses becoming extremely frequent during late stages of NTC and their frequency correlates well with the closure velocity of the neural tube (**Figure 78E**).

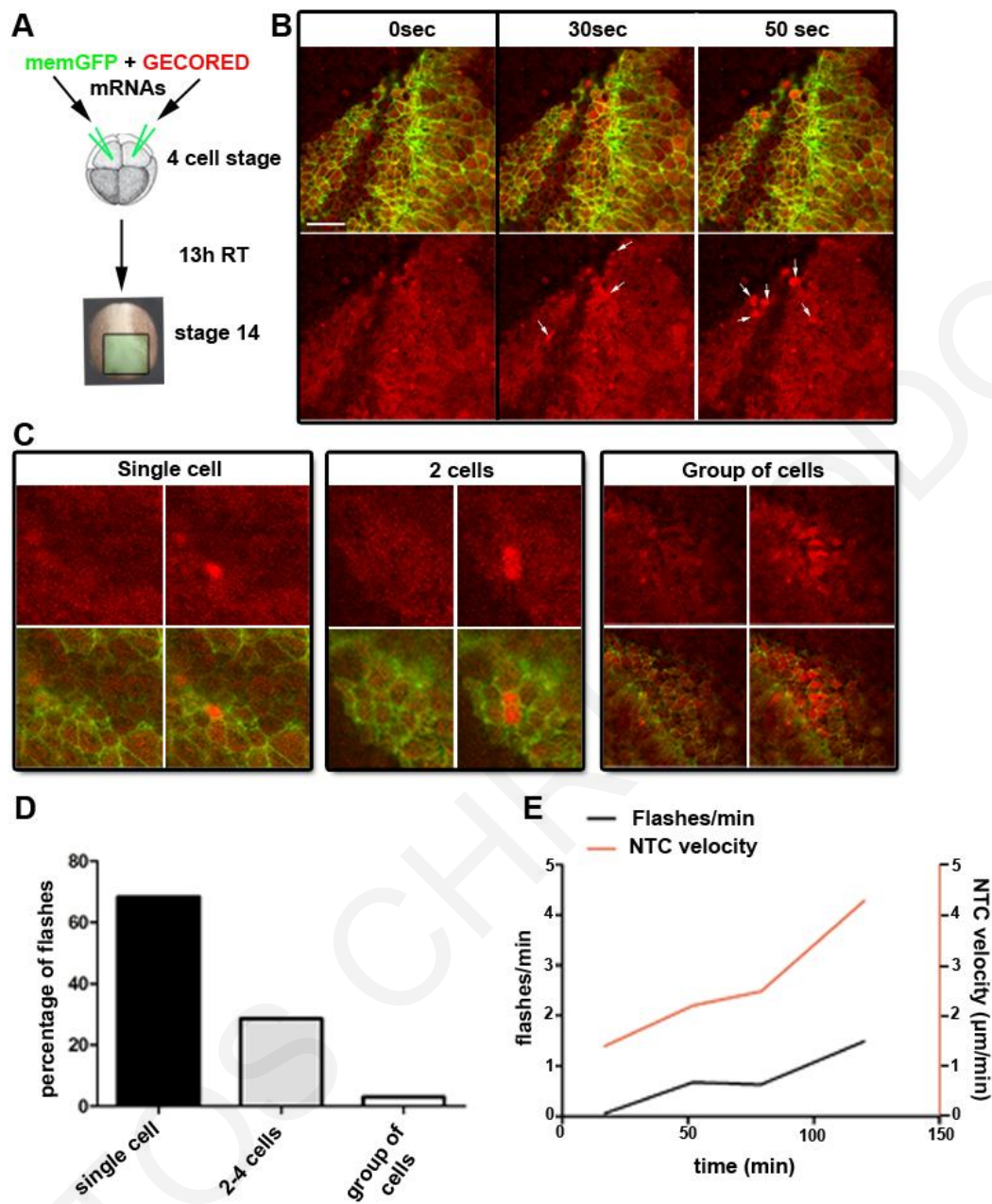


Figure 78. Cell autonomous Calcium flashes take place during neurulation and their frequency correlates with the speed of Neural Tube Closure.

(A) Experimental strategy for imaging Ca^{2+} dynamics during NTC (B) Stills from a time lapse recording of anterior NTC from an embryo expressing mem-GFP (green) and GECO-RED (red). Arrows show Ca^{2+} flashes at different time points. Scale bar: $50\mu\text{m}$ (C) Examples of single cell, two cell and multiple cell Ca^{2+} flashes. (D) Quantification of number of Ca^{2+} flashes occurring in single cells, small group of cells (2-4) or in larger groups of cells ($n=150$). (E) Graph showing Ca^{2+} flash frequency and NTC speed over time.

The fact that the majority of Ca^{2+} flashes are cell autonomous and asynchronous similar to apical actin driven contraction pulses and correlate well with the speed of NTC suggests that these transients may have a direct role in AC. However, Ca^{2+} transients may also be secondary events to constriction. To distinguish between these two possibilities we simultaneously tracked cell cortices (mem-GFP) and Ca^{2+} levels (GECO-RED) of neuroepithelial cells. In all cases, Ca^{2+} flashes precede the initiation of apical cell surface reduction showing that Ca^{2+} flashes are not elicited by cell contraction but are likely triggering these events (**Figure 79A, Movie 10-11**). Tracking the apical cell surface for one minute after a Ca^{2+} flash and without a Ca^{2+} flash, revealed that the mean apical cell surface reduction after a Ca^{2+} flash is $16,41 \pm 1,22$ % (Mean \pm SEM, n =65 cells, 3 embryos) while mean apical cell surface reduction without a flash is $-0.41\% \pm 0.67$ (Mean \pm SEM, n=65 cells, 3 embryos) (**Figure 79B**). Simultaneous tracking of the cell surface area and Ca^{2+} levels in cells undergoing more than one contraction pulse, demonstrate that Ca^{2+} flashes occur just before the contraction pulse but never during the stabilization step for all cells examined (n=20 cells) (**Figure 79C-D, Movie 11**).

These data suggest that Ca^{2+} flashes are an integral part of AC in neuroepithelial cells and that contraction pulses are triggered by transient Ca^{2+} elevation. Ectopic expression of a number of molecules including Lulu has been shown to be sufficient for ectopic AC induction in epithelial cells (Chu et al., 2013; Haigo et al., 2003; Itoh et al., 2014). We thus asked if ectopic induction of AC would elicit ectopic Ca^{2+} flashes. Monitoring of intracellular Ca^{2+} levels during Lulu induced AC in gastrula stage embryos revealed that cell autonomous Ca^{2+} flashes are in fact generated ectopically in actively constricting cells expressing Lulu-GFP (**Figure 79E, Movie12**) and that they precede contraction pulses (**Figure 79F**). No cell autonomous Ca^{2+} flashes were observed in GFP negative cells of Lulu-GFP injected embryos. Overall these data suggest that Ca^{2+} transients are responsible for the pulsed contraction events observed during AC.

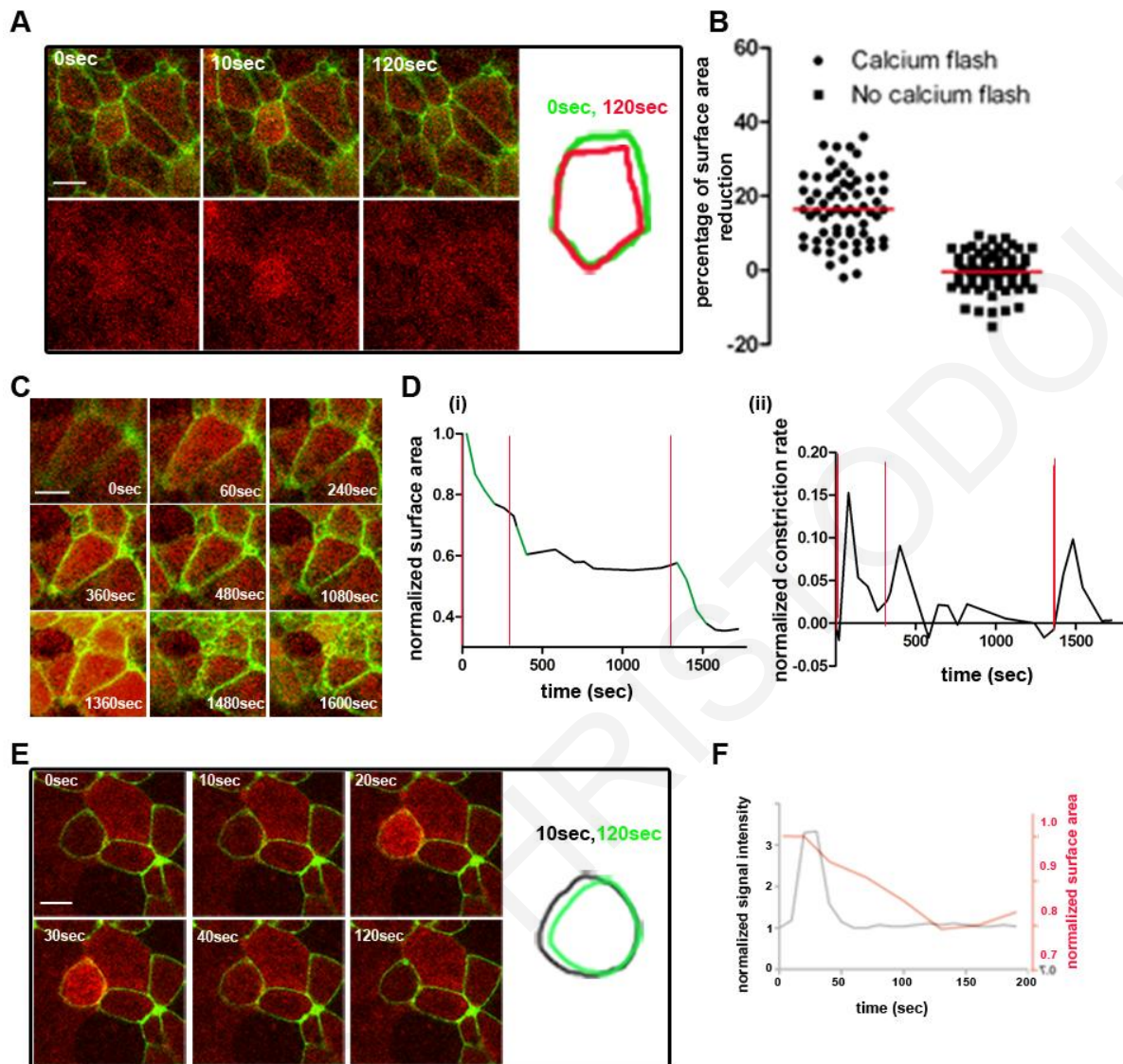


Figure 79. Calcium flashes precede contraction pulses.

(A) Stills from a time lapse recording of a neuroepithelial cell expressing GECO-RED (red) and mem-GFP (green). Cell cortices at 0sec (green) and 120sec (red). (B) Apical cell surface reduction of neuroepithelial cells which display a Ca^{2+} flash and ones that do not over a period of one minute ($n=65$). (C) Stills from a time lapse recording showing a representative neuroepithelial cell expressing GECO-RED (red) + mem-GFP (green). During the recording this cell displays 3 Ca^{2+} flashes. (D) Graph showing the apical cell surface area (i) and constriction rate (ii) with simultaneous tracking of the Ca^{2+} flashes (red lines) of the cell in C over time. Ca^{2+} flashes precede the contraction pulses. (E) Stills from a time lapse recording of a representative cell of a stage 9 embryo, expressing Lulu-GFP (green) + GECO RED (red) Scale bar = $20\mu\text{m}$. (F) Quantification of GECO-RED signal intensity over time (black line) with cell surface area over time (red line). Ca^{2+} flash precedes surface area reduction. Scale bars: $10\mu\text{m}$

3.2.4 The asynchrony and the autonomy of the calcium flashes are necessary for proper morphogenesis

As described above asynchronous and cell autonomous Ca^{2+} transients lead to asynchronous and cell autonomous pulsed contractions rather than continuous synchronized contraction of all the cells. In an effort to address the role of asynchronous and cell autonomous Ca^{2+} pulses on tissue morphogenesis and AC Lulu expressing embryos were treated with Thapsigargin (THA), an inhibitor of the sarco/endoplasmic reticulum Ca^{2+} ATPase. Use of THA leads to the depletion of Ca^{2+} stores and an increase of cytosolic Ca^{2+} levels (Dakin et al., 2005). As expected, THA treatment lead to an increase of the baseline cytosolic Ca^{2+} levels in the outer epithelium of the embryo (**Figure 80A**). Imaging AC in the presence of THA revealed an increased rate of constriction of Lulu positive cells (**Figure 80B, Movie13**), while control cells failed to respond (data not shown), suggesting that only cells in which the polarity of key molecules is properly established can apically constrict in response to elevated Ca^{2+} . Another consequence of THA treatment was the elimination of Ca^{2+} flashes. Cells were constricting without the appearance of calcium flashes (**Movie 14**). Quantification of the cell surface area over time from representative Lulu expressing cells from control and THA treated gastrula embryos revealed that in treated embryos cells undergo AC via continuous and synchronized contraction (**Figure 80C**). This might be a consequence of the steady increase of intracellular Calcium concentration after THA treatment. These data suggest that cytosolic Ca^{2+} levels are linked with the rate of constriction and that the pulsed asynchrony displayed by cells undergoing AC is stemming from the asynchronous and cell autonomous Ca^{2+} transients. What is the reason behind the asynchrony and cell autonomy of contraction if faster constriction can be achieved via continuous and non-cell autonomous contraction? Are they necessary for proper morphogenetic movements? In order to address these questions neurula stage embryos were treated with THA. Treated embryos displayed severe NTC defects, with defective hinge point formation and wider neural plates compared with control embryos (**Figure 81A, A'**). Imaging of the neural plates of control and treated embryos revealed that despite a similar average constriction index between the two (same average surface area of neuroepithelial cells in control and THA treated embryos) (**Figure 81B**) in treated embryos the spatial distribution of the extent of constriction was disrupted. In control embryos when the degree of constriction is plotted along the left to right axis of the embryo three areas of elevated constriction become evident two at the hinge points and one at the center of the neural plate. In the presence of THA this "constriction patterning" is disrupted and elevated

constriction foci become random as shown in the graph (**Figure 81C,C'**). These results suggest that asynchronous and cell autonomous constriction pulses are necessary for the correct temporal and spatial distribution of AC and as a result correct morphogenesis of the neural tube.

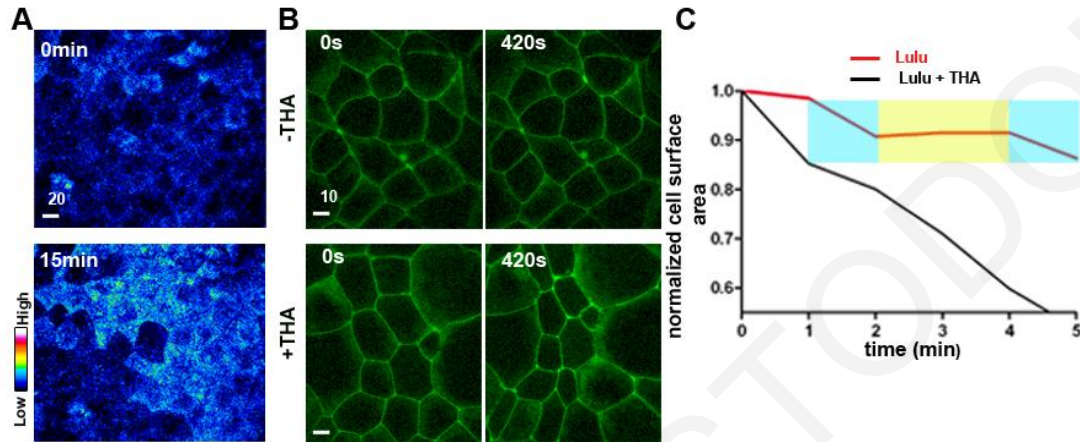


Figure 80. Elevation of intracellular Calcium levels leads to increase Apical Constriction rate and results in continuous rather than pulsed constriction.

(A) Intensity coded images of GECO-RED expressing gastrula embryo treated with Thapsigagin (THA). THA treatment results in intracellular Calcium increase as it is depicted by GECO-RED intensity at 0 and 15 minutes after treatment. (B) Stills from a time lapse recording of gastrula embryos expressing Lulu-GFP with and without THA treatment. Imaging started 15 minutes after THA treatment. Images were taken at 30 second intervals. (C) Cell surface area over time of representative Lulu expressing cells from control and THA treated gastrula embryos. Blue highlight denotes constriction pulses and yellow the stabilization step.

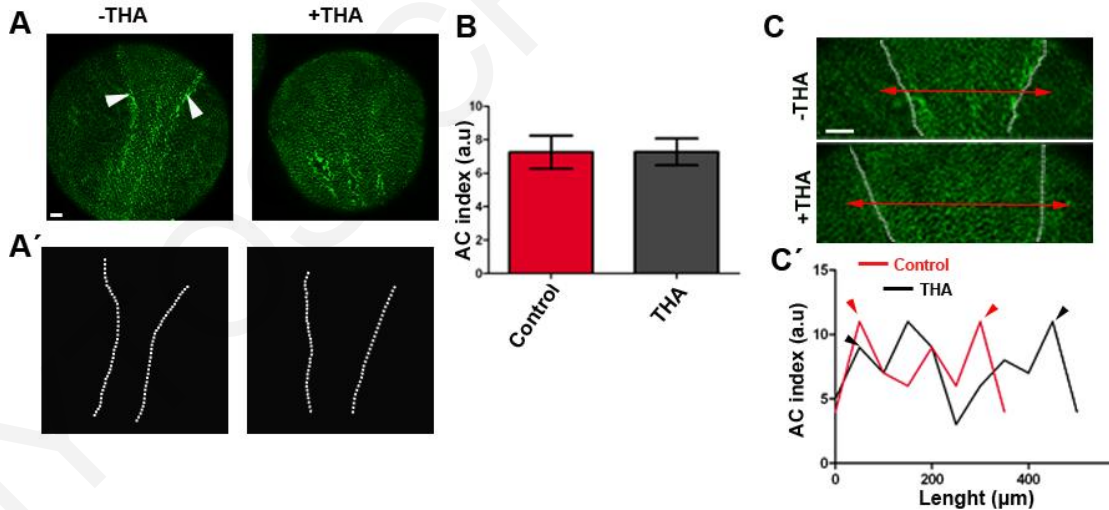


Figure 81. The autonomy and the asynchrony of contraction pulses are both necessary for proper morphogenesis.

(A) Stage 15 embryos stained with phalloidin in the absence and in the presence of THA. White arrowheads show the formation of hinge points in control embryos. Scale bar = 100µm (A') Margins of the neural plate in control and THA treated embryos. (B) Quantification of the mean AC index within the neural plate in control and THA treated embryos (n= 10 measurements from 2 different embryos, mean ± SEM). (C) Stage 15 control and THA treated embryos stained with phalloidin. Scale bars = 100µm (C') Quantification of the AC index (number of cells within a 50µm diameter circle) along the left to right axis of the embryo (red line in E). Arrowheads mark the neural folds.

3.2.5 Restriction of Calcium flashes via gap junction regulation

An important question that becomes apparent is how do the Ca^{2+} flashes observed in cells undergoing AC remain contained within each cell. One possibility is that the gap junctions close transiently to allow cell autonomous intracellular Ca^{2+} flashes preventing their propagation to neighboring cells. As mentioned above although no cell autonomous Ca^{2+} flashes were observed in control embryos of gastrula stage embryos occasional tissue level Ca^{2+} waves were observed in both uninjected and Lulu-GFP injected embryos. To examine the possibility of transient gap junction's regulation in cells undergoing AC, Ca^{2+} wave propagation in cells undergoing AC and neighboring control cells was monitored. To achieve this we injected GECO-RED mRNA in 2 blastomeres at the 2 cell stage and at the 4 cell stage we injected Lulu-GFP mRNA in one blastomere. In the provided time lapse recording (**Movie 15**) several Lulu positive cells are visible (red membrane staining) primarily at the right area of the frame surrounded by Lulu negative cells. During the first few frames a number of cell autonomous Ca^{2+} flashes can be seen in lulu positive cells while towards the end of the recording a strong tissue level Ca^{2+} wave can be seen propagating through the ectoderm however wave propagation appears to be limited to the lulu negative regions of the embryo with lulu positive cells failing to respond even when surrounded by responding control cells (**Movie 15, Figure 82A**). Quantification of the GECO-RED signal intensity in control cells and cells expressing Lulu GFP revealed that the basal levels of Ca^{2+} are higher in cells expressing Lulu GFP and confirmed that the majority of these cells fail to respond to the Ca^{2+} wave (**Figure 82B**). There are several studies supporting that increase of intracellular Ca^{2+} might lead directly or indirectly to closure of gap junctions leading to cell uncoupling (Oshima, 2014). Our results suggest that increased Ca^{2+} levels within cells undergoing AC may lead to the closure of gap junctions effectively uncoupling them from both the surrounding tissue and their apically constricting neighbors in order to permit asynchronous and cell autonomous constriction to take place.

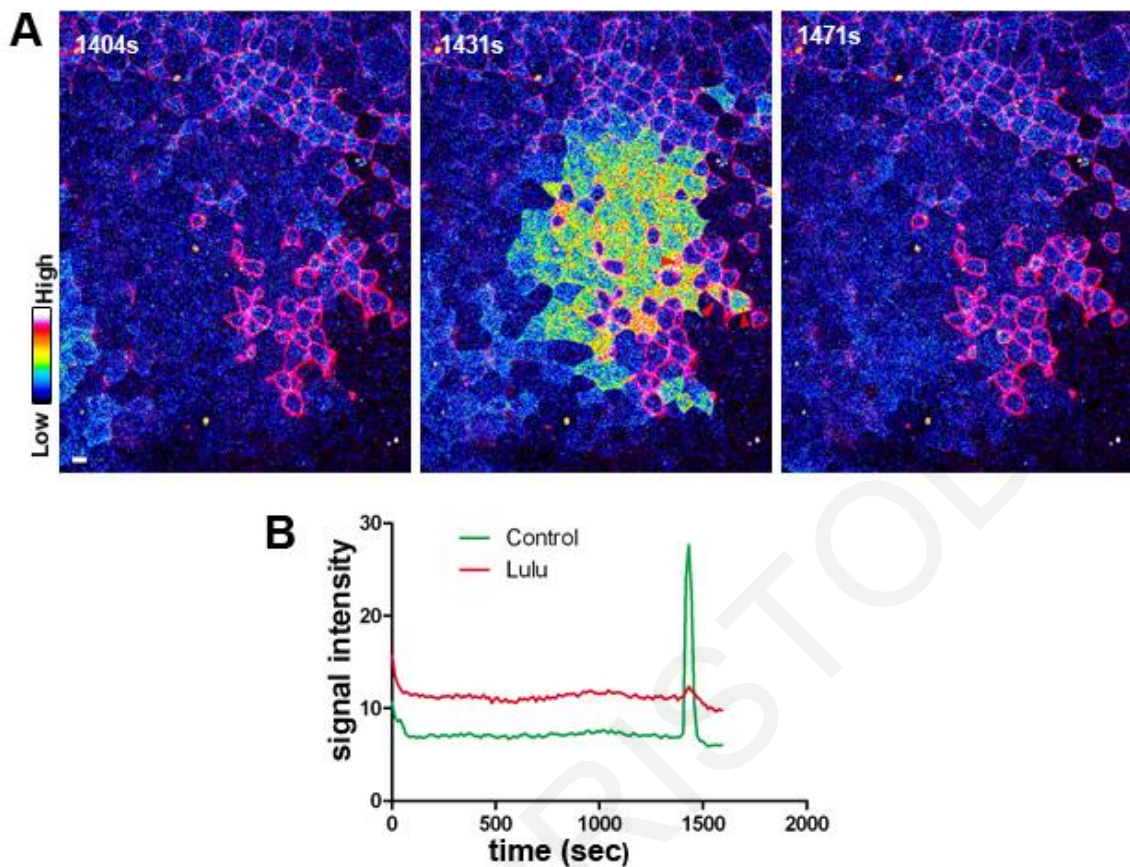


Figure 82. Cells undergoing Apical Constriction fail to transmit Calcium waves.
 (A) Stills from a time lapse recording of a stage 11.5 embryo expressing Lulu-GFP (purple) + GECO-RED (intensity coded) during the generation of a Ca^{2+} wave. Scale bars=20 μm (B) GECO-RED signal intensity over time including the Ca^{2+} wave in regions expressing LULU-GFP and control regions. Ca^{2+} wave initiates at 1430 sec.

3.2.6 Calpain2 function is necessary for the stabilization step during Apical Constriction

Our data implicate Calpain2 function in AC independently of tissue context. In an effort to better understand the mechanism behind Calpain2's involvement in AC we carried out live imaging of Lulu-GFP expressing ectodermal cells from early gastrula embryos in the presence and absence of the CI3 inhibitor. In both cases cells were imaged immediately after cell division was completed to ensure that CI3 treated and controls were at the same stage in the cell cycle. This was done to avoid differences in constriction rates when cells undergoing mitosis. During mitosis the cytoskeleton is remodeled and it's impossible for a cell to continue AC. As described above cells expressing Lulu-GFP undergo AC with constriction pulses followed by stabilization steps (**Figure 74**). When Lulu expressing cells in CI3 treated embryos were imaged, AC was visibly impaired as expected (**Figure 83A,B, Movie 16**). Quantification of the cell surface area over time from 20 different cells confirms this (**Figure 83C**). Quantification of the constriction rate from 20

cells revealed that positive events representing contraction pulses are taking place in both control and CI3 treated Lulu expressing cells. However cells from CI3 treated embryos unlike controls displayed frequent negative events (cell surface increases after the constriction pulse) suggesting that blockage of Calpain2 function leads to defects in the stabilization step (**Figure 83D**).

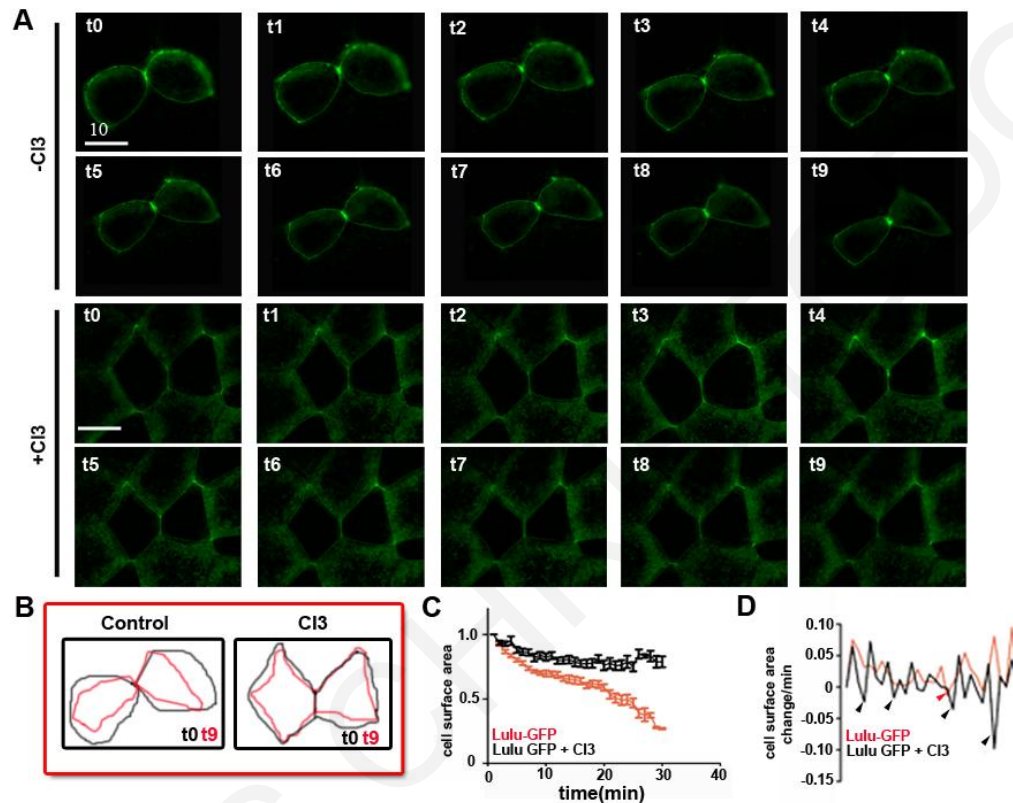


Figure 83. Calpain2 function in Lulu induced Apical Constriction.

Effect of CI3 treatment in Lulu induced apical constriction (A) Stills from time lapse recordings of representative cells expressing Lulu-GFP + mem-Cherry. Images were taken at 1 minute intervals. Scale bar = 10 μ m (B) Cell cortices of cells expressing Lulu-GFP at t0 and t9. (C) Normalized cell surface area over time (n=20, mean \pm SEM for each time point). (D) Normalized cell surface area change over time (n=20, mean for each time point) Arrowheads indicate stretching events.

To examine if Calcium flashes are affected in the absence of Calpain2 function we co-injected Lulu-GFP with GECO-RED mRNA and treated embryos with CI3. Imaging of Ca²⁺ levels in LuLu-GFP expressing cells of gastrula embryos revealed that Ca²⁺ flashes occur normally in the presence of CI3 (**Figure 84, Movie 17**) and trigger contraction pulses just like in control embryos.

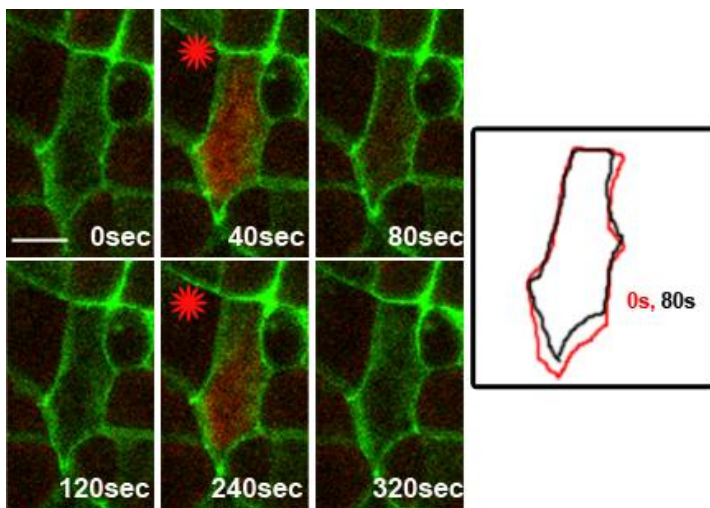


Figure 84. Calcium flashes in CI3 treated embryos.

Stills from a time lapse recording of representative cell from gastrula embryo expressing Lulu-GFP (green) + GECO RED (GFP) and treated with CI3. Red stars mark the frames where Ca^{2+} flashes take place scale bar: $20\mu\text{m}$. Inset: Tracking of the cell cortex shows that after a Ca^{2+} flash, a contraction pulse takes place.

The above results suggest that Calpain2 is implicated in AC and specifically in the stabilization step. To further analyze this observation, the pulse magnitude, the number of pulses per minute and the number of stretching events per minute in control and treated embryos were quantified. This analysis shows that the pulse magnitude is not significantly affected by Calpain2 inhibition (**Figure 85A**), and the number of pulses per minute are only slightly reduced (**Figure 85B**). This indicates that blockage of Calpain2 function leads to mild changes in the frequency of contraction pulses and has no effect on the contraction pulse magnitude. The lack of a contraction defect is in agreement with the data presented before suggesting that Calpain inhibition does not disrupt the formation of the actomyosin complex. Quantification of the stretching events per minute however revealed that the number of stretching events was significantly higher in the presence of CI3 (**Figure 85C**), confirming that defects in AC when Calpain2's function is defective are primarily stemming from a requirement of Calpain2 activity for the stabilization step.

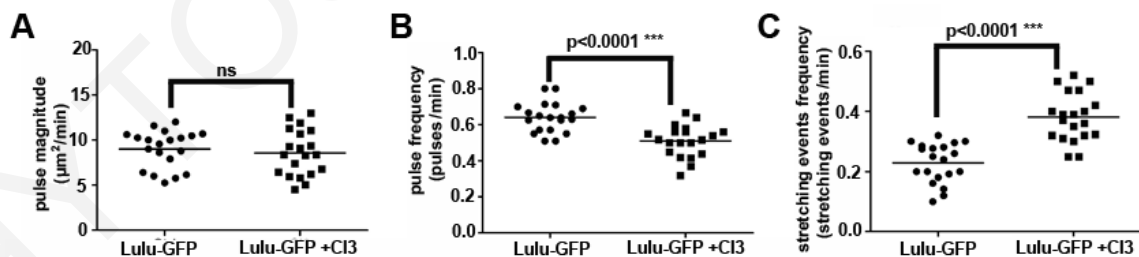


Figure 85. Calpain2 activity is necessary for the stabilization step during Apical Constriction.

(A) Quantification of the pulse magnitude of cells expressing Lulu-GFP in control and CI3 treated embryos ($\mu\text{m}^2/\text{min}$, $n=20$). (B) Quantification of the pulse frequency of cells expressing Lulu-GFP in control and CI3 treated embryos (number of constriction pulses /minute, $n=20$). (C) Quantification of the stretching events of cells expressing Lulu-GFP in control and CI3 treated embryos (events with the cell surface area expansion/min, ($n=20$)).

4. Discussion

In the present study, we investigate the role of the calcium regulated cysteine protease Calpain2 during *Xenopus laevis* development. In addition we study actin and calcium dynamics during NTC in respect to their role in AC. Specifically, we demonstrate that Calpain2 expression and activity are under strict spatiotemporal regulation and that Calpain2 function is important CE of both neural and mesodermal tissues regulating cell polarity. Furthermore, we show that Calpain2 activity is necessary for AC independently of tissue context and that Calpain2 function is necessary specifically for the stabilization step. We next show that Calpain2 is activated by the Wnt/Ca²⁺ pathway in a Dishevelled depended manner.

Subsequently, we show that AC in *Xenopus* is driven by cell autonomous and asynchronous pulsed contractions which are followed by stabilization steps. Imaging of actin dynamics demonstrates that contraction pulses are driven by the contraction of a transient apical actin network. We also show that these pulsed contraction events are elicited by cell autonomous and asynchronous Ca²⁺ flashes which are an integral part of AC. Pharmacological elevation of cytosolic Ca²⁺ levels leads to synchronous and continuous AC resulting in the failure of NTC suggesting that asynchronous pulsed contractions are essential for the correct spatial regulation of tissue contraction that shapes tissues and organs.

4.1 Calpain2 expression

We initially analyzed Calpain2 temporal expression at both the mRNA and protein levels by RT-PCR and casein zymography, respectively. Both methods revealed that Calpain2 is a maternal protein expressed throughout development. We also examined its spatial distribution by *in situ* hybridization. In pre-gastrula and gastrula stages, Calpain2 localizes asymmetrically along the animal-vegetal axis, with a broad staining detected mainly at the animal pole. Similar asymmetrical distributions in early embryos have been previously reported for some maternal mRNAs (Lee et al., 2009; Rebagliati et al., 1985; Schroeder and Yost, 1996; Weeks and Melton, 1987). During gastrulation, the protease is expressed predominantly in the ectoderm and mesoderm. This is in agreement with a previous analysis of distribution of Calpains in *Xenopus* performed by immunohistochemistry (Moudilou et al., 2010). As development proceeds, increased levels of Calpain2 are detected in the neural tube, brain, neural crest, otic vesicle, branchial arches, eyes, olfactory placode and archenteron floor. A similar distribution of Calpain2

was reported in E8.5-11.5 mouse embryos (Raynaud et al., 2008). Overall, Calpain2 appears elevated in tissues that undergo intense morphogenesis.

4.3 Calpain2 function during *Xenopus* morphogenesis

We investigated Calpain2 function during embryogenesis using a reversible Calpain inhibitor, an active-site Calpain2 dominant negative and a morpholino antisense nucleotide designed to specifically block Calpain2 translation. Using these approaches, we provide evidence that Calpain2 function is essential during *Xenopus* gastrulation and neurulation, regulating mesoderm migration, CE movements and AC. Embryos treated with the inhibitor at gastrula stages show delayed mesoderm involution and ultimately fail to close the blastopore, resulting in shorter embryos and spina bifida. Similar results were obtained when Calpain2C105S was used to block endogenous Calpain2. We show that both mesoderm CE and mesoderm migration are impaired in CI3-treated embryos, but the expression of mesodermal markers is unaffected.

At the moment we cannot exclude the possibility that the observed phenotype may result from the concomitant inhibition of Calpain1, since the inhibitor used could block both Calpain1 and Calpain2 activities and also the Calpain2C105S dominant negative could potentially inhibit both Calpains given their high sequence identity. Considering that disruption of Calpain2 gene in mice resulted in early embryonic lethality (Dutt et al., 2006)(Takano et al., 2011), whereas knockout mice for Calpain1 presented only mild defects in platelet aggregation (Azam et al., 2001), it is likely that blockage of Calpain2 is the main factor in determining the phenotype we observed. Furthermore, although the CI3 inhibitor is reported to be specific for Calpains 1 and 2, we cannot exclude a partial inhibition of Calpain8, a tissue-specific Calpain that shares 52% of amino acid sequence identity with Calpain2 and has also been shown to be involved in CE movements (Cao et al., 2001). However, the spatial and temporal expressions of Calpain8 described in the same study are not in agreement with a role in CE or NTC. Calpain8 mRNA is first detected at stage 10, localizes at the ventral side of the blastopore at gastrula stages and it is not detectable in the neural plate at neurula stages (Cao et al., 2001).

In addition to the defects in mesodermal morphogenesis, all three loss of function approaches also result in defects of NTC. This is a significant finding given the fact that NTDs are among the most common human birth defects but their molecular basis has not yet been fully addressed (Wallingford, 2005; Wallingford, 2006). Targeting the neural plate with the Calpain2 MO allowed us to specifically downregulate Calpain2 in neural tissues. The morphants show a marked delay in NTC, in agreement with the CI3 inhibitor treatment suggesting that Calpain2 is

necessary for this process. Since Calpain2 MO inhibits neural convergent extension in both BF2-induced animal caps and in neural explants it appears that, at least in part, the delay in NTC observed in Calpain2 morphants is due to problems with CE. Calpain2 downregulation in neural tissues results also in anterior NTDs, a phenotype linked with AC. As we show Calpain2 function is necessary for proper AC of neuroepithelial cells, but it is also implicated in AC driven organogenesis.

4.4 Mechanism of Calpain2 involvement in convergent extension and Apical Constriction

We further investigated the possible mechanism behind Calpain2 requirement in CE and AC.

Our experiments using open-faced Keller explants suggest that loss of proper cell polarity, rather than inhibition of adherens junction turn over, is likely the cause of the defects in CE we observe when Calpain activity is downregulated. However new studies have shown that myosin mediated polarized junction remodeling is also essential for *Xenopus* mesoderm CE (Shindo and Wallingford, 2014). Therefore we cannot exclude an implication of Calpain2 in this process. Future work will be needed to examine the possible implication of Calpain2 in junction remodeling during CE.

During AC phases of actomyosin contractions and stabilization are repeated. After blockage of Calpain function we show that the stabilization phase is severely affected while the generation of pulses is slightly affected. On the other hand, the pulses magnitude was not affected. These data suggest that Calpain2 function is indispensable for the stabilization step during AC.

4.5 Regulation of Calpain2 activity during embryogenesis

It is known that *in vitro*, Calpain2 requires Ca^{2+} concentrations ($>500\mu\text{M}$) that are considerably higher than the physiological intracellular concentrations of Ca^{2+} (usually $< 1 \mu\text{M}$) (Goll et al., 1992). This ensures a tight regulation on Calpain2 activation, being achieved only after specific stimuli able to open calcium channels or to activate calcium release from intracellular stores (Leloup et al.; Shao et al., 2006). It is also known that translocation of Calpains to the plasma membrane usually correlates well with enzyme activation. Crystal structure analysis in combination with studies using calcium ionophore treatments in different cell lines suggest a two-step model for Calpain activation. First, the inactive cytoplasmic enzyme translocates to the plasma membrane in response to increased intracellular Ca^{2+} levels and subsequently it is activated in the presence of local Ca^{2+} and phospholipids (Gil-Parrado et al., 2003; Michetti et al., 1996; Molinari et al., 1994; Strobl et al., 2000; Suzuki et al., 2004). Indeed, it has been shown

that the domain III of Calpain's 1 and 2 displays higher affinity for phospholipids in the presence of Ca^{2+} (Tompa et al., 2001). Our results suggest that in addition to the regulation of its expression, Calpain2 activation is also regulated both temporally and spatially in the embryo. During gastrulation, Calpain2 localizes at the membrane in the dorsal mesoderm which is morphogenetically active, while it is found in the cytosol (presumably inactive) in the prospective neurectoderm. At neurula stages, Calpain2 becomes membrane bound in the neurectoderm concomitantly with the morphogenetic movements taking place in this tissue. The spatiotemporal activation of Calpain2 is in agreement with our data showing that calcium flashes take place during neural tube closure. Thus, there is an overall correlation of Calpain2 activation and calcium levels with morphogenetically active tissues and calcium dynamics in agreement with the role of Calpain2 in these processes based. A Calpain2 sensor similar to that described by Yang et al in 2011 would be useful in order to track Calpain2 activation *in vivo* during gastrulation and neurulation. For example such sensor can be used to determine when Calpain2 becomes activated during AC and how long does it remain active after a calcium flash. Such data will reveal if Calpain2 is activated during the contraction pulses and cleaves some molecules which are necessary for the stabilization step or if Calpain2 is activated after contraction pulses cleaving molecules implicated in the stabilization step.

Several groups have reported the importance of calcium signaling in the coordination of morphogenetic movements during early vertebrate development. The existence of a calcium-mediated pathway that is activated by some Wnt proteins (Wnt5a, Wnt4 and Wnt11) has been described in both zebrafish and *Xenopus* (Slusarski et al., 1997a; Slusarski et al., 1997b) and it is known to induce an increase in intracellular Ca^{2+} levels that in turn activate calcium dependent enzymes like calcineurin, CamKII and PKC (Kuhl et al., 2000a; Kuhl et al., 2000b; Sheldahl et al., 1999) thus modulating different events during morphogenesis.

Furthermore, rhythmic calcium intercellular waves have been observed in both *Xenopus* and in zebrafish (Gilland et al., 1999; Leclerc et al., 2006) and have been suggested to be a common regulatory mechanism in vertebrates. Specifically, in *Xenopus* such waves have been described in both the dorsal mesoderm and neural ectoderm of dorsal marginal zone explants (Wallingford et al., 2001) as well as in intact embryos (Leclerc et al., 2000). These are tissues known to be morphogenetically active and to undergo CE. It is still not known how the waves are generated. It has been shown that the Wnt/ Ca^{2+} is not responsible for their initiation, but it can only modulate their frequency. Interestingly, embryos in which the calcium waves have been blocked by pharmacological treatment (Wallingford et al., 2001) present phenotypes very similar to those we

observed following inhibition of Calpain activity. Our data as well as data in invertebrates now implicate also cell autonomous calcium transient in morphogenetic movements driven by cell autonomous cell shape changes (Antunes et al., 2013; Hunter et al., 2014).

Given the tight calcium-dependency of Calpains, we decided to investigate if Calpain2 is activated through the non canonical Wnt/Ca²⁺ pathway. We showed that in response to ectopic expression of Wnt5a, Calpain2 translocates to the plasma membrane, in agreement with a previous study in which Wnt5a induces calpain activation and stimulates axon growth in cortical neurons (Yang et al., 2011). We also found that Calpain membrane localization is dependent on Dishevelled, since expression of Xdd1 blocks Calpain2 activation in the neural plate. This is in agreement with a previous study that implicated Dishevelled in the Wnt/Ca²⁺ pathway by activating Ca²⁺ flux, PKC and CamKII (Sheldahl et al., 2003). Heterotrimeric G proteins are also known effectors of the Wnt/Ca²⁺ signaling and inhibition of their function results in blockage of PKC and CamKII membrane localization (Sheldahl et al., 1999; Slusarski et al., 1997a; Sheldahl et al., 2003). The exact connection between G proteins and Dishevelled is still unclear, although Dishevelled activation of the Wnt/Ca²⁺ pathway was shown to be independent of G proteins (Sheldahl et al., 2003). It will be interesting to investigate if Calpain2 membrane localization is also mediated through G proteins. Heterotrimeric G proteins, Wnt/Ca²⁺ pathway and Dishevelled have been implicated both in CE and AC. This strengthens our data showing that Calpain2 activation is through this pathway as Calpain2 is also implicated both in CE and AC.

4.6 The molecular mechanism controlling Calpain2 function in convergent extension

Since overactivation of the non canonical Wnt/Ca²⁺ pathway has been shown to inhibit CE movements, we decided to test if this blockage was at least partially due to Calpain2 activation. Indeed, expression of the dominant negative Calpain2 rescues the Wnt5a blockage of CE movements in animal cap assays, suggesting that Wnt5a activates Calpain2 as one of the downstream effectors responsible for CE blockage. Overall, we conclude that Calpain2 activity has to be precisely regulated during CE since both its inhibition and overactivation block this movement. This is not surprising since different molecules involved in CE movements are known to lead to the same morphogenetic defect when overexpressed or inhibited, indicating that their dose is absolutely crucial for proper morphogenesis (Borchers et al., 2006; Djiane et al., 2000; Wallingford and Harland, 2001; Wallingford et al., 2000).

It is possible that Calpain2 regulates morphogenesis cleaving a set of different substrates. Indeed several known Calpain substrates have been implicated in the regulation of adhesion and motility of different cell lines: protein kinases (PKC, FAK, and Src), phosphatases (calcineurin, PTP-1B), cytoskeleton-associated proteins (paxillin, α -actinin, and talin), adhesion molecules (β -integrins) and regulatory proteins (RhoA) (Wells et al., 2005). The future challenge will be to identify specific Calpain2 substrates during *Xenopus* development. A possible candidate substrate is calcineurin, since it has been shown that Calpain2 is able to cleave and activate this protein in cultured neurons and *in vivo* in the hippocampal region of mice during excitotoxic neurodegeneration (Wu et al., 2004). Calcineurin is a phosphatase that upon activation through Wnt/Ca²⁺ pathway dephosphorylates NF-AT transcription factor that can thus migrate into the nucleus and induce transcription of genes that regulate CE (Borchers et al., 2006; Saneyoshi et al., 2002). It is thus possible that Calpain2 could modulate CE movement by proteolytic cleavage of calcineurin. The phenotypes we observed by blocking Calpain2 activity closely resemble those obtained by inhibition/overactivation of NFAT (Borchers et al., 2006). Furthermore, it has been reported that Calpains are able to cleave adhesion molecules in different cell lines (Benetti et al., 2005; Jang et al., 2009; Rios-Doria et al., 2003). It is thus possible that Calpains modulate *Xenopus* morphogenetic movements by affecting cell-cell adhesion. However, our experiments using Keller explants on fibronectin seem to rule out this possibility as radial intercalation is not affected by CI3 treatment, suggesting that possible defects in junction remodeling (if present) are mild and cannot account for the severe CE defects.

A more intriguing possibility is that Calpain2 could modulate the PCP pathway. Indeed, Calpain2 has been reported to cleave RhoA *in vitro* and in cultured cells (Kulkarni et al., 2002). Our experiment in CI3-treated DMZ explants shows a disruption of the overall tissue polarity and impairment of cell-cell intercalation in a similar fashion of explants in which the activity of members of the PCP pathway have been altered (Tahinci and Symes, 2003; Tahinci et al., 2007; Wallingford et al., 2000). Several studies have suggested that Wnt/Ca²⁺ and PCP overlap at different levels in terms of function and signaling mechanisms (Elul and Keller, 2000; Elul et al., 1997; Ezin et al., 2003; Sheldahl et al., 2003; Shih and Keller, 1992) although it is still not clear how the two signaling pathways are integrated and coordinated to govern cellular movements. It is possible that Calpain2 modulates the cross-talk between the different Wnt pathways.

4.7 Molecular mechanism for Calpain2 involvement in Apical Constriction

As we have shown, cell autonomous calcium flashes are generated during vertebrate neural tube closure. Calpain2 is activated after binding to Calcium. In addition we have shown that Calpain2 is found in its active form during *Xenopus* neurulation. Therefore, Calpain2 could be activated by these calcium transients during neurulation regulating AC. Furthermore we have also shown that Calpain2 acts downstream of $\text{Wnt}/\text{Ca}^{2+}$ and overexpression of *Wnt5a* induce ectopic AC in *Xenopus* ectodermal cells. One possibility is that Calpain2 is activated through $\text{Wnt}/\text{Ca}^{2+}$ during neurulation regulating AC. In addition, mouse knock out of a known Calpain2 activator, the orphan G protein-coupled receptor display rostral NTDs (Matteson et al., 2008), which are correlated with defective AC.

Overall intracellular Calcium, $\text{Wnt}/\text{Ca}^{2+}$ and G-proteins are possible activators of Calpain2 during AC. Our proposed model is that Calpain2 is activated by Calcium transients, G proteins and *Wnt5a* during AC. Subsequently Calpain2 cleaves downstream molecules necessary for stabilization of apical cell surface.

Several molecules shown to be cleaved by Calpain-2 would be expected to be involved in AC including α -actinin, filamin, MARCKS, cortactin, vinculin and Tiam (Franco and Huttenlocher, 2005). Some of these proteins contribute to the formation of the actin meshwork and their cleavage could potentially be required for the stabilization step. Tiam on the other hand is a known activator of Rac and its knock out results in rostral NTDs (Yoo et al., 2012). Calpain2 cleavage inactivates Tiam (Woodcock et al., 2009). This leads to de-activation of Rac and a balance between Rho and Rac GTPases is critical for AC (Chauhan et al., 2011). Vinculin has also been shown to be cleaved by Calpain2 (Serrano and Devine, 2004). Vinculin is a cytoskeleton anchorage protein, and its knock out results in rostral NTDs (Xu et al., 1998). Importantly application of external force has been shown to coincide with vinculin accumulation at E-cadherin junctions where it potentiates the E-cadherin mechanosensory response while vinculin has also been shown to associate with VE-cadherin junctions and to control force-dependent remodeling (Huvneers et al., 2012; le Duc et al., 2010). Adherens junction remodeling and force sensing would be expected to play a crucial role in the stabilization step. In fact the sole other protein shown to be specifically involved in apical surface stabilization is the transcription factor twist. Two targets of twist, *Fog* and *T48* are believed to be responsible for the movement of adherens junctions toward the apical area of the cell via RhoGEF2 dependent myosin translocation (Kolsch et al., 2007; Leptin, 1999). It has therefore been proposed that that

twist may be involved in AC via stabilization of the apical surface through the promotion of the assembly of apical junctions. Calpain2 regulation of vinculin would thus be a plausible mechanism for apical junction assembly and remodeling required for apical surface stabilization.

4.8 Mechanisms driving apical cell surface reduction during Neural Tube Closure

Neurulation is a critical period in the development of all vertebrate embryos, during which the CNS is formed. NTDs are one of the most common human birth defects (Copp and Greene, 2010) and as a result delineation of the mechanisms driving NTC will lead to a better understanding of human NTDs. In this work we used live imaging combined with gain and loss of function approaches to explore AC, one of the fundamental morphogenetic movements that drive NTC.

Our work reveals that apical surface reduction of neuroepithelial cells is achieved via two distinct mechanisms: AC through discrete, cell autonomous contraction events and M/L junction shrinkage. Both processes take place simultaneously during NTC and contribute to the shaping of the tissue. M/L junction shrinkage results in polar surface area reduction and it is believed to drive tissue bending towards the midline helping to close the neural tube. Previous studies have shown that this process is regulated downstream of the PCP pathway.

Proposed model for Apical Constriction in neuroepithelial cells

The predominant model for AC during NTC prior to this work suggested that contraction of a circumferential actomyosin complex is responsible for the cell shape changes within the neural plate (Baker and Schroeder, 1967; Burnside, 1971; Schroeder, 1970). This is further supported by data showing that induction of AC in polarized epithelial cells promotes the formation of circumferential actomyosin complex with sarcomeric organization (Hildebrand, 2005). However in invertebrate models several lines of evidence suggest that a contractile pool of apical actin is responsible for AC (Martin and Goldstein, 2014). We now suggest that AC of neuroepithelial cells is similarly driven by transient, cell autonomous and asynchronous apical actin enrichment events. In agreement with our data, apical actin contractile filaments have been previously suggested to play a role in vertebrate AC during mouse lens formation (Lang et al., 2014). We show that transient apical actin polymerization events occur during the contraction pulse and we provide evidence that this actin pool is responsible for the apical surface reduction. Firstly, the appearance of this pool correlates with the initiation of apical surface reduction and maximal reduction is occurring when the intensity of this actin pool reaches its maximum. Secondly,

apical actin enrichment correlates with inward apical cell-cell junction displacement that leads to local bending of the cell-cell boundary. If a circumferential belt of contractile actomyosin was driving AC it would be expected that such deformations would be synchronous in each cell as the actomyosin ring would contract; however as we show these events are not synchronous and can be temporally resolved. This suggests that the apical actin network is responsible for the cell-cell junction displacement which results in apical surface reduction; however it is also possible that it is a result of the combination of contraction of both the apical actin and of a circumferential actomyosin belt. Separating the mechanical inputs of these two would be difficult since their molecular composition is very similar. However, it would be possible to use photoactivatable caged versions of molecules modulating actin dynamics (Ghosh et al., 2004). Such molecules could be locally uncaged to address the precise role of the apical actin pool.

4.9 Calcium flashes trigger cell autonomous contraction pulses

Our work suggests that contraction pulses during AC are driven by contraction of an apical actin pool and are elicited by Ca^{2+} flashes. Ca^{2+} signaling (through the Wnt/ Ca^{2+} pathway or in the form of Ca^{2+} waves) has been implicated in several morphogenetic events and cell shape changes that take place during embryogenesis. Interestingly, use of Ca^{2+} chelators in *Xenopus*, Chick and rat embryos, showed that Ca^{2+} is necessary for neural fold formation and NTC in vertebrates (Ferreira and Hilfer, 1993; Moran and Rice, 1976; Nagele et al., 1991; Smedley and Stanisstreet, 1986). However, these studies could not link Ca^{2+} directly with AC since these experimental approaches also lead to defects of Ca^{2+} depended cell-cell adhesion. Here we link Ca^{2+} levels directly to AC. We show that cell autonomous Ca^{2+} flashes are generated during NTC in *Xenopus* and that their frequency correlates with the closure rate of the neural tube. In addition, we establish that Ca^{2+} flashes occur just before apical cell surface narrowing suggesting that they trigger the contraction pulses and are ectopically induced when AC is induced ectopically. Taken together these results strongly suggest that calcium is a critical regulator of AC.

The mechanism behind the regulation of contraction pulses by calcium warrants further study. It has been established that Ca^{2+} influx leads to activation of RhoA during smooth muscle contraction (Sakurada et al., 2003) and endothelial cell spreading (Masiero et al., 1999). Apical accumulation of RhoA is necessary for proper AC and NTC (Kinoshita et al., 2008). RhoA leads to ROCK activation which has been shown to be necessary for the contraction pulses (Mason et al., 2013). Active ROCK phosphorylates myosin light chain, driving the contraction of actin

filaments. Moreover, Ca^{2+} levels may also regulate the actin cytoskeleton directly via Ca^{2+} regulated actin binding proteins such as Gelsolin (Antunes et al., 2013). The very transient nature of these events requires in vivo imaging and the parallel use of FRET sensors to establish how the activation states of molecules like Rho and ROCK are temporally modulated and how they influence this process. Combining these tools with pharmacological approaches to modulate calcium levels would provide information about how the activation of these molecules is regulated by cytosolic Ca^{2+} both spatially and temporally.

4.10 The asynchrony and autonomy of contraction pulses are both necessary for proper Apical Constriction driven morphogenesis

Of particular interest is the fact that Ca^{2+} flashes and the subsequent apical actin enrichment events are asynchronous and cell autonomous leading to cell autonomous and asynchronous contraction pulses. What are the reasons behind the cell autonomy and asynchrony of contractions and how do cells accomplish this? Use of THA leads to elevated Ca^{2+} levels in the tissue eliminating Ca^{2+} flashes. This leads to synchronized continuous contraction. Despite similar average constriction index in the neural plates of THA treated embryos compared to controls, THA treatment leads to failure of NTC. Examination of control embryos revealed that as previously described three areas of increased constriction are present, two at the left and right hinge points and a third in the medial hinge region. This patterned constriction is lost in THA treated embryos with foci of increased constriction found randomly distributed in the neural plate. The above suggest that cell autonomous pulses are a prerequisite in order to properly orchestrate the spatial and temporal distribution of constricting cells and loss of this regulation leads to defective morphogenesis. Support for this interpretation comes from work in *Drosophila*. Constitutive activation of myosin during *Drosophila* ventral furrow formation was also shown to promote continuous rather than pulsed AC. Although loss of pulsed constriction did not affect the mean constriction rate, it led to delays of invagination again suggesting that pulsed constriction is required for correct tissue morphogenesis (Vasquez et al., 2014). Given the importance of cell autonomous contractions during AC we then asked, how is this autonomy accomplished? Ca^{2+} waves are primarily propagated through gap junctions (Oshima, 2014). We show that Ca^{2+} flashes in constricting cells are not propagated to neighboring control cells and that tissue level Ca^{2+} waves are propagated by control cells but fail to elicit responses from constricting cells. These results suggest that actively constricting cells are effectively isolated from their neighbors likely via closure of their gap junctions. The mechanism behind this isolation of cells undergoing

AC is unclear; however gap junctions have been shown to be regulated by Ca^{2+} levels and close when intracellular Ca^{2+} levels are raised (Oshima, 2014). Our data suggest that constricting cells maintain elevated cytosolic Ca^{2+} levels, which may lead to GAP junction closure thus preventing Ca^{2+} transients from spreading.

4.11 Future Perspectives

I) The role of Ca^{2+} flashes in Apical Constriction

Our work has produced a number of significant findings which further our understanding of AC and the mechanism's through which it shapes tissues. At the same time this work opens up several new directions and brings up many questions which need to be addressed. We show that AC in vertebrates is a stepwise process driven by contraction pulses followed by stabilization steps. In addition we show that Ca^{2+} flashes trigger apical actin driven contraction pulses. On the other hand, we demonstrate that Calpain2 a calcium dependent protease is specifically involved in the stabilization step during AC. The latter suggests that Ca^{2+} flashes not only trigger contraction but in addition activate calcium dependent molecules required for the stabilization step. It would therefore be useful to use FRET sensors (CFP as a donor and YFP as an acceptor molecule) to simultaneously track Ca^{2+} levels and the activation status of several proteins during AC. Such experiments would allow sufficient temporal resolution which given the transient nature of these events is necessary in order to get a good idea of how different events are regulated. It would be possible for example to determine whether the activation of proteins implicated in the contraction pulse, such as RhoA takes place after the Ca^{2+} flash. This will directly link Ca^{2+} flashes and the contraction pulses. In addition comparing the activation status of proteins implicated in the stabilization step, such as Calpain2, in the presence and in the absence of Ca^{2+} flashes it would allow us to determine if the activation of these proteins is triggered by the Ca^{2+} flashes.

We have shown that the degree of AC is not affected after blockage of Ca^{2+} flashes with Thapsigargin (THA). However THA treatment blocks cell autonomous and asynchronous Ca^{2+} flashes leading to synchronous and continuous AC. It would be interesting to examine the effect of cytoplasmic calcium levels attenuation during AC. Use of Ca^{2+} chelators leads attenuated cytoplasmic calcium levels but also leads to defects in Ca^{2+} depended cell-cell adhesions. Therefore this approach cannot be used to specifically examine the role of intracellular Ca^{2+} in

AC. Use of molecules such as the IP₃ receptor inhibitor Xestospongine which blocks IP₃ induced Ca²⁺ release from internal stores, leads to attenuation of cytoplasmic calcium without affecting cell-cell adhesion. However when we tried to use Xestospongine in *Xenopus* embryos, Xestospongine failed to pass through the intact embryo epithelium. Therefore Xestospongine could be used in other organisms and tissues in which AC takes place, for example in *Drosophila* ventral furrow, in order to show the effect of Ca²⁺ depletion in AC.

II) Exploring the mechanism leading to GAP junction closure in Apically Constricting cells

The cell autonomy of Ca²⁺ flashes is responsible for the autonomy of the contraction pulses. We show that constricting cells have a mechanism to isolate themselves as Ca²⁺ flashes are not propagated to neighboring cells during Neural Tube Closure and in addition tissue level Ca²⁺ waves fail to be propagated by constricting cells. These results suggest that actively constricting cells keep gap junctions closed in order to isolate themselves from the surrounding cells and tissue. However more work will be required in order to determine the precise mechanism leading to gap junction closure and cell isolation during AC. One experiment that can be used to prove that gap junctions transiently regulated in AC is GAP-FRAP (Abbaci et al., 2007). In this experiment gap junction intercellular communications is assessed by bleaching a fluorescent molecule (for example calcein) within a cell and tracking of its recovery which is attributed to the movement of unbleached molecules from the neighboring cells through GAP junctions. One would expect that cells undergoing AC will show a slow recovery rate compared to control cells. We attempted to perform such experiments using several dyes, however the yolk within the cells of *Xenopus* embryos induce the aggregation of dyes leading to very slow or no movement of the dyes within the cells. GAP-FRAP experiments to examine gap junction communication in constricting cells can be performed in epithelial cell lines expressing connexins after ectopic induction of AC through the expression of molecules such as Shroom3 and Lulu.

Then the mechanism leading to GAP junction closure can be explored in more detail. Known mechanism regulating Gap junction gating is phosphorylation of connexins and elevated intracellular Calcium levels. Therefore examination of the phosphorylation status of connexins in constricted vs controls will address the possibility that phosphorylation of connexins is the mechanism regulating GAP junction closure during AC. However our data show that constricted cells display elevated Calcium levels pointing towards the possibility that elevated baseline Calcium levels in constricted cells is the reason behind the isolation of these cells.

Overexpression of inducible connexin construct within the neural plate of vertebrate embryos and live imaging of actin dynamics or examination of AC patterning will give further information regarding the necessity of gap-junction regulation during AC of neuroepithelial cells.

III) How does the mechanical interplay between cells regulate Apical Constriction patterning

It has been shown that mechanically cell coupling is necessary for generation of contraction pulses during AC driven morphogenesis (Solon et al., 2009). Contraction of a cell generates forces which are transmitted to neighboring cells inducing their contraction. We have shown that contraction pulses during neural tube closure are triggered by Ca^{2+} flashes. In addition Hunter et al. showed that tension gated Calcium channels are also involved in AC (Hunter et al., 2014). Therefore we hypothesize that Ca^{2+} flashes are induced by contraction of neighboring cells. In order to explore this hypothesis will have to laser ablate cells within the neural plate. This would release the tension within the tissue. If Ca^{2+} flashes don't take place after release of tension this would suggest that Ca^{2+} flashes are induced by tension produced after cell contraction.

Additionally of interest is the exploration of the mechanism through which cells in the neural plate communicate at the mechanical level. One mechanism through which cells sense such forces is through catenins, since force can induce conformational changes of these molecules (Kim et al., 2015). Generation of dominant negative catenins unable to change their conformation after exposure to tension will lead to force blind cells. This would be a great tool in order to explore the necessity of force in the generation of Ca^{2+} flashes and contraction pulses assuming this is how force sensing occurs in this context. Catenins interact with Vinculin which links adherens junctions with actin cytoskeleton. Application of force also induces conformational changes in Vinculin. Vinculin has been implicated in AC. Genetically coded Vinculin tension sensor has been generated (Grashoff et al., 2010). Live imaging using a Vinculin tension sensor during neural tube closure will provide data regarding the spatial and temporal generation of forces within the neural plate. Then this force pattern can be correlated with high AC pattern.

Another question is how this mechanosensing is translated into molecular pathways regulating the constriction pattern in the neural plate as well as in other tissues that undergo AC dependent morphogenesis. Mechanotransduction at extracellular matrix-cell interphase is achieved through integrins and the focal adhesion complexes (Ross et al., 2013). A recent study in our lab has revealed ligand independent but force dependent activation of integrin at cell-cell junctions.

Therefore the integrin mechanotransduction complex composed of integrins, FAK, Src and p130cas could also be responsible for the sensing of forces generated by contraction of neighboring cells into molecular pathways leading to actomyosin activation and contraction. Future plans include the exploring this possibility with preliminary data suggesting that this integrin based mechnosensory complex is in fact regulating mechanical cross talk between apically constricting cells at the neural plate.

References

- Abbaci, M., Barberi-Heyob, M., Stines, J. R., Blondel, W., Dumas, D., Guillemin, F. and Didelon, J. (2007). Gap junctional intercellular communication capacity by gap-FRAP technique: a comparative study. *Biotechnol J* **2**, 50-61.
- Alfandari, D., Ramos, J., Clavilier, L., DeSimone, D. W. and Darribere, T. (1996). The RGD-dependent and the Hep II binding domains of fibronectin govern the adhesive behaviors of amphibian embryonic cells. *Mech Dev* **56**, 83-92.
- Antunes, M., Pereira, T., Cordeiro, J. V., Almeida, L. and Jacinto, A. (2013). Coordinated waves of actomyosin flow and apical cell constriction immediately after wounding. *J Cell Biol* **202**, 365-79.
- Arthur, J. S., Elce, J. S., Hegadorn, C., Williams, K. and Greer, P. A. (2000). Disruption of the murine calpain small subunit gene, *Capn4*: calpain is essential for embryonic development but not for cell growth and division. *Mol Cell Biol* **20**, 4474-81.
- Arthur, J. S., Gauthier, S. and Elce, J. S. (1995). Active site residues in m-calpain: identification by site-directed mutagenesis. *FEBS Lett* **368**, 397-400.
- Azam, M., Andrabi, S. S., Sahr, K. E., Kamath, L., Kuliopulos, A. and Chishti, A. H. (2001). Disruption of the mouse mu-calpain gene reveals an essential role in platelet function. *Mol Cell Biol* **21**, 2213-20.
- Baker, C., Holland, D., Edge, M. and Colman, A. (1990). Effects of oligo sequence and chemistry on the efficiency of oligodeoxyribonucleotide-mediated mRNA cleavage. *Nucleic Acids Res* **18**, 3537-43.
- Baker, P. C. and Schroeder, T. E. (1967). Cytoplasmic filaments and morphogenetic movement in the amphibian neural tube. *Dev Biol* **15**, 432-50.
- Bay, S. N. and Caspary, T. (2012). What are those cilia doing in the neural tube? *Cilia* **1**, 19.
- Beck, C. W. and Slack, J. M. (2001). An amphibian with ambition: a new role for *Xenopus* in the 21st century. *Genome Biol* **2**, REVIEWS1029.
- Benetti, R., Copetti, T., Dell'Orso, S., Melloni, E., Brancolini, C., Monte, M. and Schneider, C. (2005). The calpain system is involved in the constitutive regulation of beta-catenin signaling functions. *J Biol Chem* **280**, 22070-80.
- Bertet, C., Sulak, L. and Lecuit, T. (2004). Myosin-dependent junction remodelling controls planar cell intercalation and axis elongation. *Nature* **429**, 667-71.
- Bhatt, A., Kaverina, I., Otey, C. and Huttenlocher, A. (2002). Regulation of focal complex composition and disassembly by the calcium-dependent protease calpain. *J Cell Sci* **115**, 3415-25.
- Blanchard, H., Grochulski, P., Li, Y., Arthur, J. S., Davies, P. L., Elce, J. S. and Cygler, M. (1997). Structure of a calpain Ca(2+)-binding domain reveals a novel EF-hand and Ca(2+)-induced conformational changes. *Nat Struct Biol* **4**, 532-8.
- Blankenship, J. T., Backovic, S. T., Sanny, J. S., Weitz, O. and Zallen, J. A. (2006). Multicellular rosette formation links planar cell polarity to tissue morphogenesis. *Dev Cell* **11**, 459-70.
- Blitz, I. L., Biesinger, J., Xie, X. and Cho, K. W. (2013). Biallelic genome modification in F(0) *Xenopus tropicalis* embryos using the CRISPR/Cas system. *Genesis* **51**, 827-34.
- Borchers, A., Fonar, Y., Frank, D. and Baker, J. C. (2006). XNF-ATc3 affects neural convergent extension. *Development* **133**, 1745-55.
- Borges, R. M., Lamers, M. L., Forti, F. L., Santos, M. F. and Yan, C. Y. (2011). Rho signaling pathway and apical constriction in the early lens placode. *Genesis* **49**, 368-79.
- Burnside, B. (1971). Microtubules and microfilaments in newt neuralation. *Dev Biol* **26**, 416-41.

- Cao, Y., Zhao, H. and Grunz, H.** (2001). XCL-2 is a novel m-type calpain and disrupts morphogenetic movements during embryogenesis in *Xenopus laevis*. *Dev Growth Differ* **43**, 563-71.
- Castelli, M., Boca, M., Chiaravalli, M., Ramalingam, H., Rowe, I., Distefano, G., Carroll, T. and Boletta, A.** (2013). Polycystin-1 binds Par3/aPKC and controls convergent extension during renal tubular morphogenesis. *Nat Commun* **4**, 2658.
- Chacon-Heszele, M. F., Ren, D., Reynolds, A. B., Chi, F. and Chen, P.** (2012). Regulation of cochlear convergent extension by the vertebrate planar cell polarity pathway is dependent on p120-catenin. *Development* **139**, 968-78.
- Chan, K. T., Bennin, D. A. and Huttenlocher, A.** (2010). Regulation of adhesion dynamics by calpain-mediated proteolysis of focal adhesion kinase (FAK). *J Biol Chem* **285**, 11418-26.
- Chauhan, B. K., Lou, M., Zheng, Y. and Lang, R. A.** (2011). Balanced Rac1 and RhoA activities regulate cell shape and drive invagination morphogenesis in epithelia. *Proc Natl Acad Sci U S A* **108**, 18289-94.
- Chen, J., Chang, S., Duncan, S. A., Okano, H. J., Fishell, G. and Aderem, A.** (1996). Disruption of the MacMARCKS gene prevents cranial neural tube closure and results in anencephaly. *Proc Natl Acad Sci U S A* **93**, 6275-9.
- Choi, S. C. and Sokol, S. Y.** (2009). The involvement of lethal giant larvae and Wnt signaling in bottle cell formation in *Xenopus* embryos. *Dev Biol* **336**, 68-75.
- Chu, C. W., Gerstenzang, E., Ossipova, O. and Sokol, S. Y.** (2013). Lulu regulates Shroom-induced apical constriction during neural tube closure. *PLoS One* **8**, e81854.
- Chua, J., Rikhy, R. and Lippincott-Schwartz, J.** (2009). Dynamin 2 orchestrates the global actomyosin cytoskeleton for epithelial maintenance and apical constriction. *Proc Natl Acad Sci U S A* **106**, 20770-5.
- Chung, M. I., Nascone-Yoder, N. M., Grover, S. A., Drysdale, T. A. and Wallingford, J. B.** (2010). Direct activation of Shroom3 transcription by Pitx proteins drives epithelial morphogenesis in the developing gut. *Development* **137**, 1339-49.
- Copp, A. J. and Greene, N. D.** (2010). Genetics and development of neural tube defects. *J Pathol* **220**, 217-30.
- Copp, A. J., Greene, N. D. and Murdoch, J. N.** (2003). The genetic basis of mammalian neurulation. *Nat Rev Genet* **4**, 784-93.
- Corrigall, D., Walther, R. F., Rodriguez, L., Fichelson, P. and Pichaud, F.** (2007). Hedgehog signaling is a principal inducer of Myosin-II-driven cell ingression in *Drosophila* epithelia. *Dev Cell* **13**, 730-42.
- Cortese, C. L., Boateng, L. R., Piazza, T. M., Bennin, D. A. and Huttenlocher, A.** (2011). Calpain-mediated proteolysis of paxillin negatively regulates focal adhesion dynamics and cell migration. *J Biol Chem* **286**, 9998-10006.
- Cousin, H., Abbruzzese, G., Kerdavid, E., Gaultier, A. and Alfandari, D.** (2011). Translocation of the cytoplasmic domain of ADAM13 to the nucleus is essential for Calpain8-a expression and cranial neural crest cell migration. *Dev Cell* **20**, 256-63.
- Dakin, K., Zhao, Y. and Li, W. H.** (2005). LAMP, a new imaging assay of gap junctional communication unveils that Ca²⁺ influx inhibits cell coupling. *Nat Methods* **2**, 55-62.
- Davidson, L. A., Ezin, A. M. and Keller, R.** (2002a). Embryonic wound healing by apical contraction and ingression in *Xenopus laevis*. *Cell Motil Cytoskeleton* **53**, 163-76.
- Davidson, L. A., Hoffstrom, B. G., Keller, R. and DeSimone, D. W.** (2002b). Mesendoderm extension and mantle closure in *Xenopus laevis* gastrulation: combined roles for integrin alpha(5)beta(1), fibronectin, and tissue geometry. *Dev Biol* **242**, 109-29.
- Dedieu, S., Mazeret, G., Poussard, S., Brustis, J. J. and Cottin, P.** (2003). Myoblast migration is prevented by a calpain-dependent accumulation of MARCKS. *Biol Cell* **95**, 615-23.

- Djiane, A., Riou, J., Umbhauer, M., Boucaut, J. and Shi, D.** (2000). Role of frizzled 7 in the regulation of convergent extension movements during gastrulation in *Xenopus laevis*. *Development* **127**, 3091-100.
- Dourdin, N., Bhatt, A. K., Dutt, P., Greer, P. A., Arthur, J. S., Elce, J. S. and Huttenlocher, A.** (2001). Reduced cell migration and disruption of the actin cytoskeleton in calpain-deficient embryonic fibroblasts. *J Biol Chem* **276**, 48382-8.
- Dutt, P., Croall, D. E., Arthur, J. S., Veyra, T. D., Williams, K., Elce, J. S. and Greer, P. A.** (2006). m-Calpain is required for preimplantation embryonic development in mice. *BMC Dev Biol* **6**, 3.
- Elul, T. and Keller, R.** (2000). Monopolar protrusive activity: a new morphogenic cell behavior in the neural plate dependent on vertical interactions with the mesoderm in *Xenopus*. *Dev Biol* **224**, 3-19.
- Elul, T., Koehl, M. A. and Keller, R.** (1997). Cellular mechanism underlying neural convergent extension in *Xenopus laevis* embryos. *Dev Biol* **191**, 243-58.
- Ezin, A. M., Skoglund, P. and Keller, R.** (2003). The midline (notochord and notoplate) patterns the cell motility underlying convergence and extension of the *Xenopus* neural plate. *Dev Biol* **256**, 100-14.
- Fernandez-Gonzalez, R., Simoes Sde, M., Roper, J. C., Eaton, S. and Zallen, J. A.** (2009). Myosin II dynamics are regulated by tension in intercalating cells. *Dev Cell* **17**, 736-43.
- Ferreira, M. C. and Hilfer, S. R.** (1993). Calcium regulation of neural fold formation: visualization of the actin cytoskeleton in living chick embryos. *Dev Biol* **159**, 427-40.
- Franco, S. J. and Huttenlocher, A.** (2005). Regulating cell migration: calpains make the cut. *J Cell Sci* **118**, 3829-38.
- Franco, S. J., Rodgers, M. A., Perrin, B. J., Han, J., Bennin, D. A., Critchley, D. R. and Huttenlocher, A.** (2004). Calpain-mediated proteolysis of talin regulates adhesion dynamics. *Nat Cell Biol* **6**, 977-83.
- Gammill, L. S. and Bronner-Fraser, M.** (2003). Neural crest specification: migrating into genomics. *Nat Rev Neurosci* **4**, 795-805.
- Gelbart, M. A., He, B., Martin, A. C., Thiberge, S. Y., Wieschaus, E. F. and Kaschube, M.** (2012). Volume conservation principle involved in cell lengthening and nucleus movement during tissue morphogenesis. *Proc Natl Acad Sci U S A* **109**, 19298-303.
- Gerhart, J., Danilchik, M., Doniach, T., Roberts, S., Rowning, B. and Stewart, R.** (1989). Cortical rotation of the *Xenopus* egg: consequences for the anteroposterior pattern of embryonic dorsal development. *Development* **107**, 37-51.
- Ghosh, M., Song, X., Mouneimne, G., Sidani, M., Lawrence, D. S. and Condeelis, J. S.** (2004). Cofilin promotes actin polymerization and defines the direction of cell motility. *Science* **304**, 743-6.
- Gil-Parrado, S., Popp, O., Knoch, T. A., Zahler, S., Bestvater, F., Felgentrager, M., Holloschi, A., Fernandez-Montalvan, A., Auerswald, E. A., Fritz, H. et al.** (2003). Subcellular localization and in vivo subunit interactions of ubiquitous mu-calpain. *J Biol Chem* **278**, 16336-46.
- Gilbert, S.** (2006). *Developmental Biology*. Sunderland, Massachusetts USA Sinauer Associates, Inc., Publishers.
- Gilland, E., Miller, A. L., Karplus, E., Baker, R. and Webb, S. E.** (1999). Imaging of multicellular large-scale rhythmic calcium waves during zebrafish gastrulation. *Proc Natl Acad Sci U S A* **96**, 157-61.
- Goll, D. E., Thompson, V. F., Li, H., Wei, W. and Cong, J.** (2003). The calpain system. *Physiol Rev* **83**, 731-801.

- Goll, D. E., Thompson, V. F., Taylor, R. G. and Zalewska, T.** (1992). Is calpain activity regulated by membranes and autolysis or by calcium and calpastatin? *Bioessays* **14**, 549-56.
- Gomez, G. A., McLachlan, R. W. and Yap, A. S.** (2011). Productive tension: force-sensing and homeostasis of cell-cell junctions. *Trends Cell Biol* **21**, 499-505.
- Grashoff, C., Hoffman, B. D., Brenner, M. D., Zhou, R., Parsons, M., Yang, M. T., McLean, M. A., Sligar, S. G., Chen, C. S., Ha, T. et al.** (2010). Measuring mechanical tension across vinculin reveals regulation of focal adhesion dynamics. *Nature* **466**, 263-6.
- Haigo, S. L., Hildebrand, J. D., Harland, R. M. and Wallingford, J. B.** (2003). Shroom induces apical constriction and is required for hinge point formation during neural tube closure. *Curr Biol* **13**, 2125-37.
- Hanna, R. A., Campbell, R. L. and Davies, P. L.** (2008). Calcium-bound structure of calpain and its mechanism of inhibition by calpastatin. *Nature* **456**, 409-12.
- Hardin, J. and Keller, R.** (1988). The behaviour and function of bottle cells during gastrulation of *Xenopus laevis*. *Development* **103**, 211-30.
- Harland, R. and Weintraub, H.** (1985). Translation of mRNA injected into *Xenopus* oocytes is specifically inhibited by antisense RNA. *J Cell Biol* **101**, 1094-9.
- He, B., Doubrovinski, K., Polyakov, O. and Wieschaus, E.** (2014). Apical constriction drives tissue-scale hydrodynamic flow to mediate cell elongation. *Nature* **508**, 392-6.
- Heasman, J.** (2002). Morpholino oligos: making sense of antisense? *Dev Biol* **243**, 209-14.
- Heasman, J.** (2006a). Patterning the early *Xenopus* embryo. *Development* **133**, 1205-17.
- Heasman, J.** (2006b). Patterning the early *Xenopus* embryo. *Development* **133**, 1205-1217.
- Heasman, J., Kofron, M. and Wylie, C.** (2000). Beta-catenin signaling activity dissected in the early *Xenopus* embryo: a novel antisense approach. *Dev Biol* **222**, 124-34.
- Hildebrand, J. D.** (2005). Shroom regulates epithelial cell shape via the apical positioning of an actomyosin network. *J Cell Sci* **118**, 5191-203.
- Hildebrand, J. D. and Soriano, P.** (1999). Shroom, a PDZ domain-containing actin-binding protein, is required for neural tube morphogenesis in mice. *Cell* **99**, 485-97.
- Hood, J. L., Brooks, W. H. and Roszman, T. L.** (2004). Differential compartmentalization of the calpain/calpastatin network with the endoplasmic reticulum and Golgi apparatus. *J Biol Chem* **279**, 43126-35.
- Hosfield, C. M., Elce, J. S., Davies, P. L. and Jia, Z.** (1999). Crystal structure of calpain reveals the structural basis for Ca²⁺-dependent protease activity and a novel mode of enzyme activation. *EMBO J* **18**, 6880-9.
- Huang, Y. and Wang, K. K.** (2001). The calpain family and human disease. *Trends Mol Med* **7**, 355-62.
- Hunter, G. L., Crawford, J. M., Genkins, J. Z. and Kiehart, D. P.** (2014). Ion channels contribute to the regulation of cell sheet forces during *Drosophila* dorsal closure. *Development* **141**, 325-34.
- Huttenlocher, A., Palecek, S. P., Lu, Q., Zhang, W., Mellgren, R. L., Lauffenburger, D. A., Ginsberg, M. H. and Horwitz, A. F.** (1997). Regulation of cell migration by the calcium-dependent protease calpain. *J Biol Chem* **272**, 32719-22.
- Huveneers, S., Oldenburg, J., Spanjaard, E., van der Krogt, G., Grigoriev, I., Akhmanova, A., Rehmann, H. and de Rooij, J.** (2012). Vinculin associates with endothelial VE-cadherin junctions to control force-dependent remodeling. *J Cell Biol* **196**, 641-52.
- Irvine, K. D. and Wieschaus, E.** (1994). Cell intercalation during *Drosophila* germband extension and its regulation by pair-rule segmentation genes. *Development* **120**, 827-41.
- Itoh, K., Ossipova, O. and Sokol, S. Y.** (2014). GEF-H1 functions in apical constriction and cell intercalations and is essential for vertebrate neural tube closure. *J Cell Sci* **127**, 2542-53.
- Jaffe, L. F.** (2008). Calcium waves. *Philos Trans R Soc Lond B Biol Sci* **363**, 1311-6.

- Jang, Y. N., Jung, Y. S., Lee, S. H., Moon, C. H., Kim, C. H. and Baik, E. J.** (2009). Calpain-mediated N-cadherin proteolytic processing in brain injury. *J Neurosci* **29**, 5974-84.
- Karner, C. M., Chirumamilla, R., Aoki, S., Igarashi, P., Wallingford, J. B. and Carroll, T. J.** (2009). Wnt9b signaling regulates planar cell polarity and kidney tubule morphogenesis. *Nat Genet* **41**, 793-9.
- Keller, R.** (2002). Shaping the vertebrate body plan by polarized embryonic cell movements. *Science* **298**, 1950-4.
- Keller, R., Davidson, L., Edlund, A., Elul, T., Ezin, M., Shook, D. and Skoglund, P.** (2000). Mechanisms of convergence and extension by cell intercalation. *Philos Trans R Soc Lond B Biol Sci* **355**, 897-922.
- Keller, R., Davidson, L. A. and Shook, D. R.** (2003). How we are shaped: the biomechanics of gastrulation. *Differentiation* **71**, 171-205.
- Keller, R. E.** (1980). The cellular basis of epiboly: an SEM study of deep-cell rearrangement during gastrulation in *Xenopus laevis*. *J Embryol Exp Morphol* **60**, 201-34.
- Keller, R. E.** (1981). An experimental analysis of the role of bottle cells and the deep marginal zone in gastrulation of *Xenopus laevis*. *J Exp Zool* **216**, 81-101.
- Kenwrick, S., Amaya, E. and Papalopulu, N.** (2004). Pilot morpholino screen in *Xenopus tropicalis* identifies a novel gene involved in head development. *Dev Dyn* **229**, 289-99.
- Kieserman, E. K. and Wallingford, J. B.** (2009). In vivo imaging reveals a role for Cdc42 in spindle positioning and planar orientation of cell divisions during vertebrate neural tube closure. *J Cell Sci* **122**, 2481-90.
- Kim, H. Y. and Davidson, L. A.** (2011). Punctuated actin contractions during convergent extension and their permissive regulation by the non-canonical Wnt-signaling pathway. *J Cell Sci* **124**, 635-46.
- Kim, T. J., Zheng, S., Sun, J., Muhamed, I., Wu, J., Lei, L., Kong, X., Leckband, D. E. and Wang, Y.** (2015). Dynamic visualization of alpha-catenin reveals rapid, reversible conformation switching between tension states. *Curr Biol* **25**, 218-24.
- Kinoshita, N., Sasai, N., Misaki, K. and Yonemura, S.** (2008). Apical accumulation of Rho in the neural plate is important for neural plate cell shape change and neural tube formation. *Mol Biol Cell* **19**, 2289-99.
- Klein, S. L., Strausberg, R. L., Wagner, L., Pontius, J., Clifton, S. W. and Richardson, P.** (2002). Genetic and genomic tools for *Xenopus* research: The NIH *Xenopus* initiative. *Dev Dyn* **225**, 384-91.
- Kolsch, V., Seher, T., Fernandez-Ballester, G. J., Serrano, L. and Leptin, M.** (2007). Control of *Drosophila* gastrulation by apical localization of adherens junctions and RhoGEF2. *Science* **315**, 384-6.
- Kuhl, M., Sheldahl, L. C., Malbon, C. C. and Moon, R. T.** (2000a). Ca²⁺/calmodulin-dependent protein kinase II is stimulated by Wnt and Frizzled homologs and promotes ventral cell fates in *Xenopus*. *J Biol Chem* **275**, 12701-11.
- Kuhl, M., Sheldahl, L. C., Park, M., Miller, J. R. and Moon, R. T.** (2000b). The Wnt/Ca²⁺ pathway: a new vertebrate Wnt signaling pathway takes shape. *Trends Genet* **16**, 279-83.
- Kulkarni, S., Goll, D. E. and Fox, J. E.** (2002). Calpain cleaves RhoA generating a dominant-negative form that inhibits integrin-induced actin filament assembly and cell spreading. *J Biol Chem* **277**, 24435-41.
- Lang, R. A., Herman, K., Reynolds, A. B., Hildebrand, J. D. and Plageman, T. F., Jr.** (2014). p120-catenin-dependent junctional recruitment of Shroom3 is required for apical constriction during lens pit morphogenesis. *Development* **141**, 3177-87.

- le Duc, Q., Shi, Q., Blonk, I., Sonnenberg, A., Wang, N., Leckband, D. and de Rooij, J.** (2010). Vinculin potentiates E-cadherin mechanosensing and is recruited to actin-anchored sites within adherens junctions in a myosin II-dependent manner. *J Cell Biol* **189**, 1107-15.
- Leckband, D. E., le Duc, Q., Wang, N. and de Rooij, J.** (2011). Mechanotransduction at cadherin-mediated adhesions. *Curr Opin Cell Biol* **23**, 523-30.
- Leclerc, C., Neant, I., Webb, S. E., Miller, A. L. and Moreau, M.** (2006). Calcium transients and calcium signalling during early neurogenesis in the amphibian embryo *Xenopus laevis*. *Biochim Biophys Acta* **1763**, 1184-91.
- Lee, C., Le, M. P. and Wallingford, J. B.** (2009). The shroom family proteins play broad roles in the morphogenesis of thickened epithelial sheets. *Dev Dyn* **238**, 1480-91.
- Lee, C., Scherr, H. M. and Wallingford, J. B.** (2007). Shroom family proteins regulate gamma-tubulin distribution and microtubule architecture during epithelial cell shape change. *Development* **134**, 1431-41.
- Lee, J. Y. and Harland, R. M.** (2007). Actomyosin contractility and microtubules drive apical constriction in *Xenopus* bottle cells. *Dev Biol* **311**, 40-52.
- Lee, J. Y. and Harland, R. M.** (2010). Endocytosis is required for efficient apical constriction during *Xenopus* gastrulation. *Curr Biol* **20**, 253-8.
- Leerberg, J. M., Gomez, G. A., Verma, S., Moussa, E. J., Wu, S. K., Priya, R., Hoffman, B. D., Grashoff, C., Schwartz, M. A. and Yap, A. S.** (2014). Tension-sensitive actin assembly supports contractility at the epithelial zonula adherens. *Curr Biol* **24**, 1689-99.
- Lei, Y., Guo, X., Liu, Y., Cao, Y., Deng, Y., Chen, X., Cheng, C. H., Dawid, I. B., Chen, Y. and Zhao, H.** (2012). Efficient targeted gene disruption in *Xenopus* embryos using engineered transcription activator-like effector nucleases (TALENs). *Proc Natl Acad Sci U S A* **109**, 17484-9.
- Leloup, L., Shao, H., Bae, Y. H., Deasy, B., Stolz, D., Roy, P. and Wells, A.** m-Calpain activation is regulated by its membrane localization and by its binding to phosphatidylinositol 4,5-bisphosphate. *J Biol Chem* **285**, 33549-66.
- Leloup, L., Shao, H., Bae, Y. H., Deasy, B., Stolz, D., Roy, P. and Wells, A.** (2010). m-Calpain activation is regulated by its membrane localization and by its binding to phosphatidylinositol 4,5-bisphosphate. *J Biol Chem* **285**, 33549-66.
- Leptin, M.** (1999). Gastrulation in *Drosophila*: the logic and the cellular mechanisms. *EMBO J* **18**, 3187-92.
- Leptin, M.** (2005). Gastrulation movements: the logic and the nuts and bolts. *Dev Cell* **8**, 305-20.
- Levayer, R. and Lecuit, T.** (2013). Oscillation and polarity of E-cadherin asymmetries control actomyosin flow patterns during morphogenesis. *Dev Cell* **26**, 162-75.
- Li, G. and Iyengar, R.** (2002). Calpain as an effector of the Gq signaling pathway for inhibition of Wnt/beta-catenin-regulated cell proliferation. *Proc Natl Acad Sci U S A* **99**, 13254-9.
- Lienkamp, S. S., Liu, K., Karner, C. M., Carroll, T. J., Ronneberger, O., Wallingford, J. B. and Walz, G.** (2012). Vertebrate kidney tubules elongate using a planar cell polarity-dependent, rosette-based mechanism of convergent extension. *Nat Genet* **44**, 1382-7.
- Llimargas, M. and Casanova, J.** (2010). Apical constriction and invagination: a very self-reliant couple. *Dev Biol* **344**, 4-6.
- Mariani, F. V. and Harland, R. M.** (1998). XBF-2 is a transcriptional repressor that converts ectoderm into neural tissue. *Development* **125**, 5019-31.
- Markova, O. and Lenne, P. F.** (2012). Calcium signaling in developing embryos: focus on the regulation of cell shape changes and collective movements. *Semin Cell Dev Biol* **23**, 298-307.
- Marsden, M. and DeSimone, D. W.** (2001). Regulation of cell polarity, radial intercalation and epiboly in *Xenopus*: novel roles for integrin and fibronectin. *Development* **128**, 3635-47.

- Martin, A. C.** (2010). Pulsation and stabilization: contractile forces that underlie morphogenesis. *Dev Biol* **341**, 114-25.
- Martin, A. C., Gelbart, M., Fernandez-Gonzalez, R., Kaschube, M. and Wieschaus, E. F.** (2010). Integration of contractile forces during tissue invagination. *J Cell Biol* **188**, 735-49.
- Martin, A. C. and Goldstein, B.** (2014). Apical constriction: themes and variations on a cellular mechanism driving morphogenesis. *Development* **141**, 1987-98.
- Martin, A. C., Kaschube, M. and Wieschaus, E. F.** (2009). Pulsed contractions of an actin-myosin network drive apical constriction. *Nature* **457**, 495-9.
- Masiero, L., Lapidos, K. A., Ambudkar, I. and Kohn, E. C.** (1999). Regulation of the RhoA pathway in human endothelial cell spreading on type IV collagen: role of calcium influx. *J Cell Sci* **112** (Pt 19), 3205-13.
- Mason, F. M., Tworoger, M. and Martin, A. C.** (2013). Apical domain polarization localizes actin-myosin activity to drive ratchet-like apical constriction. *Nat Cell Biol* **15**, 926-36.
- Masumoto, H., Yoshizawa, T., Sorimachi, H., Nishino, T., Ishiura, S. and Suzuki, K.** (1998). Overexpression, purification, and characterization of human m-calpain and its active site mutant, m-C105S-calpain, using a baculovirus expression system. *J Biochem* **124**, 957-61.
- Matteson, P. G., Desai, J., Korstanje, R., Lazar, G., Borsuk, T. E., Rollins, J., Kadambi, S., Joseph, J., Rahman, T., Wink, J. et al.** (2008). The orphan G protein-coupled receptor, Gpr161, encodes the vacuolated lens locus and controls neurulation and lens development. *Proc Natl Acad Sci U S A* **105**, 2088-93.
- McGreevy, E. M., Vijayraghavan, D., Davidson, L. A. and Hildebrand, J. D.** (2015). Shroom3 functions downstream of planar cell polarity to regulate myosin II distribution and cellular organization during neural tube closure. *Biol Open*.
- Menzies, A. S., Aszodi, A., Williams, S. E., Pfeifer, A., Wehman, A. M., Goh, K. L., Mason, C. A., Fassler, R. and Gertler, F. B.** (2004). Mena and vasodilator-stimulated phosphoprotein are required for multiple actin-dependent processes that shape the vertebrate nervous system. *J Neurosci* **24**, 8029-38.
- Michetti, M., Salamino, F., Tedesco, I., Averna, M., Minafra, R., Melloni, E. and Pontremoli, S.** (1996). Autolysis of human erythrocyte calpain produces two active enzyme forms with different cell localization. *FEBS Lett* **392**, 11-5.
- Moldoveanu, T., Gehring, K. and Green, D. R.** (2008). Concerted multi-pronged attack by calpastatin to occlude the catalytic cleft of heterodimeric calpains. *Nature* **456**, 404-8.
- Moldoveanu, T., Hosfield, C. M., Lim, D., Elce, J. S., Jia, Z. and Davies, P. L.** (2002). A Ca(2+) switch aligns the active site of calpain. *Cell* **108**, 649-60.
- Molinari, M., Anagli, J. and Carafoli, E.** (1994). Ca(2+)-activated neutral protease is active in the erythrocyte membrane in its nonautolyzed 80-kDa form. *J Biol Chem* **269**, 27992-5.
- Moon, R. T., Campbell, R. M., Christian, J. L., McGrew, L. L., Shih, J. and Fraser, S.** (1993). Xwnt-5A: a maternal Wnt that affects morphogenetic movements after overexpression in embryos of *Xenopus laevis*. *Development* **119**, 97-111.
- Moran, D. and Rice, R. W.** (1976). Action of papaverine and ionophore A23187 on neurulation. *Nature* **261**, 497-9.
- Morita, H., Nandadasa, S., Yamamoto, T. S., Terasaka-Iioka, C., Wylie, C. and Ueno, N.** (2010). Nectin-2 and N-cadherin interact through extracellular domains and induce apical accumulation of F-actin in apical constriction of *Xenopus* neural tube morphogenesis. *Development* **137**, 1315-25.
- Moudilou, E. N., Mouterfi, N., Exbrayat, J. M. and Brun, C.** (2010). Calpains expression during *Xenopus laevis* development. *Tissue Cell* **42**, 275-81.
- Muller, D. J., Hand, G. M., Engel, A. and Sosinsky, G. E.** (2002). Conformational changes in surface structures of isolated connexin 26 gap junctions. *EMBO J* **21**, 3598-607.

- Nagele, R. G., Bush, K. T., Lynch, F. J. and Lee, H. Y.** (1991). A morphometric and computer-assisted three-dimensional reconstruction study of neural tube formation in chick embryos. *Anat Rec* **231**, 425-36.
- Nakagawa, K., Masumoto, H., Sorimachi, H. and Suzuki, K.** (2001). Dissociation of m-calpain subunits occurs after autolysis of the N-terminus of the catalytic subunit, and is not required for activation. *J Biochem* **130**, 605-11.
- Nakajima, H. and Tanoue, T.** (2010). Epithelial cell shape is regulated by Lulu proteins via myosin-II. *J Cell Sci* **123**, 555-66.
- Nakajima, H. and Tanoue, T.** (2011). Lulu2 regulates the circumferential actomyosin tensile system in epithelial cells through p114RhoGEF. *J Cell Biol* **195**, 245-61.
- Nakajima, K. and Yaoita, Y.** (2015). Highly efficient gene knockout by injection of TALEN mRNAs into oocytes and host transfer in *Xenopus laevis*. *Biol Open*.
- Nakayama, T., Fish, M. B., Fisher, M., Oomen-Hajagos, J., Thomsen, G. H. and Grainger, R. M.** (2013). Simple and efficient CRISPR/Cas9-mediated targeted mutagenesis in *Xenopus tropicalis*. *Genesis* **51**, 835-43.
- Nandadasa, S., Tao, Q., Menon, N. R., Heasman, J. and Wylie, C.** (2009). N- and E-cadherins in *Xenopus* are specifically required in the neural and non-neural ectoderm, respectively, for F-actin assembly and morphogenetic movements. *Development* **136**, 1327-38.
- Nassar, D., Letavernier, E., Baud, L., Aractingi, S. and Khosrotehrani, K.** (2012). Calpain activity is essential in skin wound healing and contributes to scar formation. *PLoS One* **7**, e37084.
- Niessen, C. M., Leckband, D. and Yap, A. S.** (2011). Tissue organization by cadherin adhesion molecules: dynamic molecular and cellular mechanisms of morphogenetic regulation. *Physiol Rev* **91**, 691-731.
- Nieuwkoop, P. D. a. F., J.** (1994). Normal Table of *Xenopus laevis* (Daudin). New York: Garland.
- Nishimura, T., Honda, H. and Takeichi, M.** (2012). Planar cell polarity links axes of spatial dynamics in neural-tube closure. *Cell* **149**, 1084-97.
- Nishimura, T. and Takeichi, M.** (2008). Shroom3-mediated recruitment of Rho kinases to the apical cell junctions regulates epithelial and neuroepithelial planar remodeling. *Development* **135**, 1493-502.
- Nutt, S. L., Bronchain, O. J., Hartley, K. O. and Amaya, E.** (2001). Comparison of morpholino based translational inhibition during the development of *Xenopus laevis* and *Xenopus tropicalis*. *Genesis* **30**, 110-3.
- O'Connell, M. P., Fiori, J. L., Baugher, K. M., Indig, F. E., French, A. D., Camilli, T. C., Frank, B. P., Earley, R., Hoek, K. S., Hasskamp, J. H. et al.** (2009). Wnt5A activates the calpain-mediated cleavage of filamin A. *J Invest Dermatol* **129**, 1782-9.
- Oda, A., Druker, B. J., Ariyoshi, H., Smith, M. and Salzman, E. W.** (1993). pp60src is an endogenous substrate for calpain in human blood platelets. *J Biol Chem* **268**, 12603-8.
- Ono, Y. and Sorimachi, H.** (2012). Calpains: an elaborate proteolytic system. *Biochim Biophys Acta* **1824**, 224-36.
- Oshima, A.** (2014). Structure and closure of connexin gap junction channels. *FEBS Lett* **588**, 1230-7.
- Perrin, B. J., Amann, K. J. and Huttenlocher, A.** (2006). Proteolysis of cortactin by calpain regulates membrane protrusion during cell migration. *Mol Biol Cell* **17**, 239-50.
- Pfaff, M., Du, X. and Ginsberg, M. H.** (1999). Calpain cleavage of integrin beta cytoplasmic domains. *FEBS Lett* **460**, 17-22.
- Piccolo, S., Sasai, Y., Lu, B. and De Robertis, E. M.** (1996). Dorsoventral patterning in *Xenopus*: inhibition of ventral signals by direct binding of chordin to BMP-4. *Cell* **86**, 589-98.

- Plageman, T. F., Jr., Chauhan, B. K., Yang, C., Jaudon, F., Shang, X., Zheng, Y., Lou, M., Debant, A., Hildebrand, J. D. and Lang, R. A.** (2011). A Trio-RhoA-Shroom3 pathway is required for apical constriction and epithelial invagination. *Development* **138**, 5177-88.
- Plageman, T. F., Jr., Chung, M. I., Lou, M., Smith, A. N., Hildebrand, J. D., Wallingford, J. B. and Lang, R. A.** (2010). Pax6-dependent Shroom3 expression regulates apical constriction during lens placode invagination. *Development* **137**, 405-15.
- Raser, K. J., Posner, A. and Wang, K. K.** (1995). Casein zymography: a method to study mu-calpain, m-calpain, and their inhibitory agents. *Arch Biochem Biophys* **319**, 211-6.
- Rauzi, M., Lenne, P. F. and Lecuit, T.** (2010). Planar polarized actomyosin contractile flows control epithelial junction remodelling. *Nature* **468**, 1110-4.
- Rauzi, M., Verant, P., Lecuit, T. and Lenne, P. F.** (2008). Nature and anisotropy of cortical forces orienting Drosophila tissue morphogenesis. *Nat Cell Biol* **10**, 1401-10.
- Raynaud, F., Marcilhac, A., Chebli, K., Benyamin, Y. and Rossel, M.** (2008). Calpain 2 expression pattern and sub-cellular localization during mouse embryogenesis. *Int J Dev Biol* **52**, 383-8.
- Rebagliati, M. R., Weeks, D. L., Harvey, R. P. and Melton, D. A.** (1985). Identification and cloning of localized maternal RNAs from Xenopus eggs. *Cell* **42**, 769-77.
- Reverter, D., Strobl, S., Fernandez-Catalan, C., Sorimachi, H., Suzuki, K. and Bode, W.** (2001). Structural basis for possible calcium-induced activation mechanisms of calpains. *Biol Chem* **382**, 753-66.
- Rios-Doria, J., Day, K. C., Kuefer, R., Rashid, M. G., Chinnaiyan, A. M., Rubin, M. A. and Day, M. L.** (2003). The role of calpain in the proteolytic cleavage of E-cadherin in prostate and mammary epithelial cells. *J Biol Chem* **278**, 1372-9.
- Roffers-Agarwal, J., Xanthos, J. B., Kragtorp, K. A. and Miller, J. R.** (2008). Enabled (Xena) regulates neural plate morphogenesis, apical constriction, and cellular adhesion required for neural tube closure in Xenopus. *Dev Biol* **314**, 393-403.
- Rogers, S. L., Wiedemann, U., Hacker, U., Turck, C. and Vale, R. D.** (2004). Drosophila RhoGEF2 associates with microtubule plus ends in an EB1-dependent manner. *Curr Biol* **14**, 1827-33.
- Roh-Johnson, M., Shemer, G., Higgins, C. D., McClellan, J. H., Werts, A. D., Tulu, U. S., Gao, L., Betzig, E., Kiehart, D. P. and Goldstein, B.** (2012). Triggering a cell shape change by exploiting preexisting actomyosin contractions. *Science* **335**, 1232-5.
- Ross, T. D., Coon, B. G., Yun, S., Baeyens, N., Tanaka, K., Ouyang, M. and Schwartz, M. A.** (2013). Integrins in mechanotransduction. *Curr Opin Cell Biol* **25**, 613-8.
- Sakurada, S., Takuwa, N., Sugimoto, N., Wang, Y., Seto, M., Sasaki, Y. and Takuwa, Y.** (2003). Ca²⁺-dependent activation of Rho and Rho kinase in membrane depolarization-induced and receptor stimulation-induced vascular smooth muscle contraction. *Circ Res* **93**, 548-56.
- Saneyoshi, T., Kume, S., Amasaki, Y. and Mikoshiba, K.** (2002). The Wnt/calcium pathway activates NF-AT and promotes ventral cell fate in Xenopus embryos. *Nature* **417**, 295-9.
- Sawyer, J. K., Choi, W., Jung, K. C., He, L., Harris, N. J. and Peifer, M.** (2011). A contractile actomyosin network linked to adherens junctions by Canoe/afadin helps drive convergent extension. *Mol Biol Cell* **22**, 2491-508.
- Sawyer, J. K., Harris, N. J., Slep, K. C., Gaul, U. and Peifer, M.** (2009). The Drosophila afadin homologue Canoe regulates linkage of the actin cytoskeleton to adherens junctions during apical constriction. *J Cell Biol* **186**, 57-73.
- Sawyer, J. M., Harrell, J. R., Shemer, G., Sullivan-Brown, J., Roh-Johnson, M. and Goldstein, B.** (2010). Apical constriction: a cell shape change that can drive morphogenesis. *Dev Biol* **341**, 5-19.

- Schoenwolf, G. C. and Franks, M. V.** (1984). Quantitative analyses of changes in cell shapes during bending of the avian neural plate. *Dev Biol* **105**, 257-72.
- Schroeder, K. E. and Yost, H. J.** (1996). *Xenopus* poly (A) binding protein maternal RNA is localized during oogenesis and associated with large complexes in blastula. *Dev Genet* **19**, 268-76.
- Schroeder, T. E.** (1970). Neurulation in *Xenopus laevis*. An analysis and model based upon light and electron microscopy. *J Embryol Exp Morphol* **23**, 427-62.
- Selliah, N., Brooks, W. H. and Roszman, T. L.** (1996). Proteolytic cleavage of alpha-actinin by calpain in T cells stimulated with anti-CD3 monoclonal antibody. *J Immunol* **156**, 3215-21.
- Serrano, K. and Devine, D. V.** (2004). Vinculin is proteolyzed by calpain during platelet aggregation: 95 kDa cleavage fragment associates with the platelet cytoskeleton. *Cell Motil Cytoskeleton* **58**, 242-52.
- Shao, H., Chou, J., Baty, C. J., Burke, N. A., Watkins, S. C., Stolz, D. B. and Wells, A.** (2006). Spatial localization of m-calpain to the plasma membrane by phosphoinositide biphosphate binding during epidermal growth factor receptor-mediated activation. *Mol Cell Biol* **26**, 5481-96.
- Sheldahl, L. C., Park, M., Malbon, C. C. and Moon, R. T.** (1999). Protein kinase C is differentially stimulated by Wnt and Frizzled homologs in a G-protein-dependent manner. *Curr Biol* **9**, 695-8.
- Sheldahl, L. C., Slusarski, D. C., Pandur, P., Miller, J. R., Kuhl, M. and Moon, R. T.** (2003). Dishevelled activates Ca²⁺ flux, PKC, and CamKII in vertebrate embryos. *J Cell Biol* **161**, 769-77.
- Shih, J. and Keller, R.** (1992). Cell motility driving mediolateral intercalation in explants of *Xenopus laevis*. *Development* **116**, 901-14.
- Shindo, A. and Wallingford, J. B.** (2014). PCP and septins compartmentalize cortical actomyosin to direct collective cell movement. *Science* **343**, 649-52.
- Simoës Sde, M., Mainieri, A. and Zallen, J. A.** (2014). Rho GTPase and Shroom direct planar polarized actomyosin contractility during convergent extension. *J Cell Biol* **204**, 575-89.
- Sive, H. L., Grainger, R. M. and Richard, M. H.** (2010). Early Development of *Xenopus laevis*: A Laboratory Manual. Cold Spring Harbor: Cold Spring Harbor Laboratory Press.
- Slack, J. M.** (2006). Essential Developmental Biology: Blackwell Publishing.
- Slusarski, D. C., Corces, V. G. and Moon, R. T.** (1997a). Interaction of Wnt and a Frizzled homologue triggers G-protein-linked phosphatidylinositol signalling. *Nature* **390**, 410-3.
- Slusarski, D. C. and Pelegri, F.** (2007). Calcium signaling in vertebrate embryonic patterning and morphogenesis. *Dev Biol* **307**, 1-13.
- Slusarski, D. C., Yang-Snyder, J., Busa, W. B. and Moon, R. T.** (1997b). Modulation of embryonic intracellular Ca²⁺ signaling by Wnt-5A. *Dev Biol* **182**, 114-20.
- Smedley, M. J. and Stanisstreet, M.** (1986). Calcium and neurulation in mammalian embryos. II. Effects of cytoskeletal inhibitors and calcium antagonists on the neural folds of rat embryos. *J Embryol Exp Morphol* **93**, 167-78.
- Smith JC, W. J.** (2003). Patterning the *Xenopus* embryo: Oxford University Press.
- Smith, W. C. and Harland, R. M.** (1991a). Injected Xwnt-8 RNA acts early in *Xenopus* embryos to promote formation of a vegetal dorsalizing center. *Cell* **67**, 753-65.
- Smith, W. C. and Harland, R. M.** (1991b). Injected Xwnt-8 RNA acts early in *Xenopus* embryos to promote formation of a vegetal dorsalizing center. *Cell* **67**, 753-765.
- Solon, J., Kaya-Copur, A., Colombelli, J. and Brunner, D.** (2009). Pulsed forces timed by a ratchet-like mechanism drive directed tissue movement during dorsal closure. *Cell* **137**, 1331-42.
- Sorimachi, H., Hata, S. and Ono, Y.** (2010). Expanding members and roles of the calpain superfamily and their genetically modified animals. *Exp Anim* **59**, 549-66.

- Spray, D. C.** (2005). Illuminating gap junctions. *Nat Methods* **2**, 12-4.
- Staveley, B. E.** (2007). *Xenopus Development*, vol. 2013 (ed).
- Stoscheck, C. M., Gates, R. E. and King, L. E., Jr.** (1988). A search for EGF-elicited degradation products of the EGF receptor. *J Cell Biochem* **38**, 51-63.
- Strobl, S., Fernandez-Catalan, C., Braun, M., Huber, R., Masumoto, H., Nakagawa, K., Irie, A., Sorimachi, H., Bourenkow, G., Bartunik, H. et al.** (2000). The crystal structure of calcium-free human m-calpain suggests an electrostatic switch mechanism for activation by calcium. *Proc Natl Acad Sci U S A* **97**, 588-92.
- Stylianou, P. and Skourides, P. A.** (2009). Imaging morphogenesis, in *Xenopus* with Quantum Dot nanocrystals. *Mech Dev* **126**, 828-41.
- Su, L. T., Agapito, M. A., Li, M., Simonson, W. T., Huttenlocher, A., Habas, R., Yue, L. and Runnels, L. W.** (2006). TRPM7 regulates cell adhesion by controlling the calcium-dependent protease calpain. *J Biol Chem* **281**, 11260-70.
- Suzuki, K., Hata, S., Kawabata, Y. and Sorimachi, H.** (2004). Structure, activation, and biology of calpain. *Diabetes* **53 Suppl 1**, S12-8.
- Suzuki, M., Morita, H. and Ueno, N.** (2012). Molecular mechanisms of cell shape changes that contribute to vertebrate neural tube closure. *Dev Growth Differ* **54**, 266-76.
- Szent-Gyorgyi, A. G.** (1987). Muscle contraction: calcium in muscle activation. *Science* **238**, 223.
- Tada, M. and Concha, M. L.** (2001). Vertebrate gastrulation: calcium waves orchestrate cell movements. *Curr Biol* **11**, R470-2.
- Tada, M. and Heisenberg, C. P.** (2012). Convergent extension: using collective cell migration and cell intercalation to shape embryos. *Development* **139**, 3897-904.
- Tahinci, E. and Symes, K.** (2003). Distinct functions of Rho and Rac are required for convergent extension during *Xenopus* gastrulation. *Dev Biol* **259**, 318-35.
- Tahinci, E., Thorne, C. A., Franklin, J. L., Salic, A., Christian, K. M., Lee, L. A., Coffey, R. J. and Lee, E.** (2007). Lrp6 is required for convergent extension during *Xenopus* gastrulation. *Development* **134**, 4095-106.
- Takano, J., Mihira, N., Fujioka, R., Hosoki, E., Chishti, A. H. and Saïdo, T. C.** (2011). Vital role of the calpain-calpastatin system for placental-integrity-dependent embryonic survival. *Mol Cell Biol* **31**, 4097-106.
- Tompa, P., Emori, Y., Sorimachi, H., Suzuki, K. and Friedrich, P.** (2001). Domain III of calpain is a Ca^{2+} -regulated phospholipid-binding domain. *Biochem Biophys Res Commun* **280**, 1333-9.
- Torres, M. A., Yang-Snyder, J. A., Purcell, S. M., DeMarais, A. A., McGrew, L. L. and Moon, R. T.** (1996). Activities of the Wnt-1 class of secreted signaling factors are antagonized by the Wnt-5A class and by a dominant negative cadherin in early *Xenopus* development. *J Cell Biol* **133**, 1123-37.
- Ubbels, G. A., Hara, K., Koster, C. H. and Kirschner, M. W.** (1983). Evidence for a functional role of the cytoskeleton in determination of the dorsoventral axis in *Xenopus laevis* eggs. *J Embryol Exp Morphol* **77**, 15-37.
- Vasquez, C. G., Tworoger, M. and Martin, A. C.** (2014). Dynamic myosin phosphorylation regulates contractile pulses and tissue integrity during epithelial morphogenesis. *J Cell Biol* **206**, 435-50.
- Wallingford, J. B.** (2005). Neural tube closure and neural tube defects: studies in animal models reveal known knowns and known unknowns. *Am J Med Genet C Semin Med Genet* **135C**, 59-68.
- Wallingford, J. B.** (2006). Planar cell polarity, ciliogenesis and neural tube defects. *Hum Mol Genet* **15 Spec No 2**, R227-34.

- Wallingford, J. B., Ewald, A. J., Harland, R. M. and Fraser, S. E.** (2001). Calcium signaling during convergent extension in *Xenopus*. *Curr Biol* **11**, 652-61.
- Wallingford, J. B., Fraser, S. E. and Harland, R. M.** (2002). Convergent extension: the molecular control of polarized cell movement during embryonic development. *Dev Cell* **2**, 695-706.
- Wallingford, J. B. and Harland, R. M.** (2001). *Xenopus* Dishevelled signaling regulates both neural and mesodermal convergent extension: parallel forces elongating the body axis. *Development* **128**, 2581-92.
- Wallingford, J. B. and Harland, R. M.** (2002). Neural tube closure requires Dishevelled-dependent convergent extension of the midline. *Development* **129**, 5815-25.
- Wallingford, J. B., Niswander, L. A., Shaw, G. M. and Finnell, R. H.** (2013). The continuing challenge of understanding, preventing, and treating neural tube defects. *Science* **339**, 1222002.
- Wallingford, J. B., Rowing, B. A., Vogeli, K. M., Rothbacher, U., Fraser, S. E. and Harland, R. M.** (2000). Dishevelled controls cell polarity during *Xenopus* gastrulation. *Nature* **405**, 81-5.
- Wang, J., Hamblet, N. S., Mark, S., Dickinson, M. E., Brinkman, B. C., Segil, N., Fraser, S. E., Chen, P., Wallingford, J. B. and Wynshaw-Boris, A.** (2006). Dishevelled genes mediate a conserved mammalian PCP pathway to regulate convergent extension during neurulation. *Development* **133**, 1767-78.
- Wang, J., Mark, S., Zhang, X., Qian, D., Yoo, S. J., Radde-Gallwitz, K., Zhang, Y., Lin, X., Collazo, A., Wynshaw-Boris, A. et al.** (2005). Regulation of polarized extension and planar cell polarity in the cochlea by the vertebrate PCP pathway. *Nat Genet* **37**, 980-5.
- Weeks, D. L. and Melton, D. A.** (1987). A maternal mRNA localized to the animal pole of *Xenopus* eggs encodes a subunit of mitochondrial ATPase. *Proc Natl Acad Sci U S A* **84**, 2798-802.
- Wells, A., Huttenlocher, A. and Lauffenburger, D. A.** (2005). Calpain proteases in cell adhesion and motility. *Int Rev Cytol* **245**, 1-16.
- Williams, M., Yen, W., Lu, X. and Sutherland, A.** (2014). Distinct apical and basolateral mechanisms drive planar cell polarity-dependent convergent extension of the mouse neural plate. *Dev Cell* **29**, 34-46.
- Winklbauer, R.** (2009). Cell adhesion in amphibian gastrulation. *Int Rev Cell Mol Biol* **278**, 215-75.
- Winklbauer, R., Nagel, M., Selchow, A. and Wacker, S.** (1996). Mesoderm migration in the *Xenopus* gastrula. *Int J Dev Biol* **40**, 305-11.
- Woodcock, S. A., Rooney, C., Lontos, M., Connolly, Y., Zoumpourlis, V., Whetton, A. D., Gorgoulis, V. G. and Malliri, A.** (2009). SRC-induced disassembly of adherens junctions requires localized phosphorylation and degradation of the rac activator tiam1. *Mol Cell* **33**, 639-53.
- Wu, H. Y., Tomizawa, K., Oda, Y., Wei, F. Y., Lu, Y. F., Matsushita, M., Li, S. T., Moriwaki, A. and Matsui, H.** (2004). Critical role of calpain-mediated cleavage of calcineurin in excitotoxic neurodegeneration. *J Biol Chem* **279**, 4929-40.
- Xu, W., Baribault, H. and Adamson, E. D.** (1998). Vinculin knockout results in heart and brain defects during embryonic development. *Development* **125**, 327-37.
- Yamanaka, H., Moriguchi, T., Masuyama, N., Kusakabe, M., Hanafusa, H., Takada, R., Takada, S. and Nishida, E.** (2002). JNK functions in the non-canonical Wnt pathway to regulate convergent extension movements in vertebrates. *EMBO Rep* **3**, 69-75.
- Yang, G. Y., Liang, B., Zhu, J. and Luo, Z. G.** (2011). Calpain activation by Wingless-type murine mammary tumor virus integration site family, member 5A (Wnt5a) promotes axonal growth. *J Biol Chem* **286**, 6566-76.

- Yoo, S., Kim, Y., Lee, H. and Park, S.** (2012). A gene trap knockout of the Tiam-1 protein results in malformation of the early embryonic brain. *Mol Cells* **34**, 103-8.
- Zallen, J. A. and Wieschaus, E.** (2004). Patterned gene expression directs bipolar planar polarity in *Drosophila*. *Dev Cell* **6**, 343-55.
- Zhao, Y., Araki, S., Wu, J., Teramoto, T., Chang, Y. F., Nakano, M., Abdelfattah, A. S., Fujiwara, M., Ishihara, T., Nagai, T. et al.** (2011). An expanded palette of genetically encoded Ca²⁺(+) indicators. *Science* **333**, 1888-91.
- Zimmerman, U. J., Boring, L., Pak, J. H., Mukerjee, N. and Wang, K. K.** (2000). The calpain small subunit gene is essential: its inactivation results in embryonic lethality. *IUBMB Life* **50**, 63-8.
- Zolessi, F. R. and Arruti, C.** (2001). Apical accumulation of MARCKS in neural plate cells during neurulation in the chick embryo. *BMC Dev Biol* **1**, 7.
- Zou, J., Salarian, M., Chen, Y., Veenstra, R., Louis, C. F. and Yang, J. J.** (2014). Gap junction regulation by calmodulin. *FEBS Lett* **588**, 1430-8.

ANNEXES

I. Abbreviations

AC: Apical Constriction
A/P: Anteroposterior
CE: Convergent extension
CI3: Calpain Inhibitor III
CNS: Central Nervous System
DMZ: Dorsal Marginal Zone
D/V: Dorsoventral
GBE: Germband Extension
M/L: Mediolateral
NTC: Neural Tube Closure
NTDs: Neural Tube Defects
PCP: Planar Cell Polarity

II. Publications

Christodoulou N., and Skourides PA. 2014. Ca²⁺ flashes elicit pulsed contractions of an apical actin network to drive Apical Constriction during vertebrate Neural Tube Closure. *Cell Reports*, Under Review

Christodoulou N*, Zanardelli S*, and Skourides PA. 2013. Calpain2 protease: A new member of the Wnt/Ca(2+) pathway modulating convergent extension movements in *Xenopus*. *Dev Biol* **384**: 83-100.

Petridou NI, Stylianou P, **Christodoulou N**, Rhoads D, Guan JL, and Skourides PA. 2012. Activation of endogenous FAK via expression of its amino terminal domain in *Xenopus* embryos. *PLoS One* 7: e42577.

Antoniades I.*, Charalambous A.*, **Christodoulou N.** and Skourides P, Split-Inteins for Simultaneous, Site-Specific Conjugation of Quantum Dots to Multiple Protein Targets *in vivo*, *Journal of Nanobiotechnology*, 2011 Sep 15;9(1):37

Maria Andreou, Iro Eleftheriou, Anna Eleftheriou, **Neophytos Christodoulou**, Ioanna Antoniadis, Andriani Ioannou, Nicoletta Petridou, Panayiota Stylianou and Paris Skourides, Evaluation of total toxicity of effluents from several waste water treatment stations and major water sources of Cyprus using *Xenopus laevis* as a model organism, *Journal of Environmental Research And Development*, Vol. 6 No. 1, July-September 2011

*co-authors

III. Book contribution

Charalambous A., Andreou M., Antoniadis I., **Christodoulou N.**, Skourides P. *In vivo*, site-specific, covalent conjugation of Quantum Dots to proteins via split-intein splicing. Accepted in *Nanoparticles in Biology and Medicine. Methods and Applications*